Creepage Discharge Behaviour and Numerical Model Analysis at the Oil/Pressboard Interface with the Effect of Nano Composite Coating

著者	Jang　Kyunghoon
その他のタイトル	ナノコンポジットコーティングを効果を考慮した油/プレスボード界面における沿面放電挙動及び数値モデル解析
学位授与年度	平成28年度
学位授与番号	17104甲工第435号
URL	http://hdl.handle.net/10228/00006311

Doctoral Dissertation

Supervisor: Prof. Masayuki Hikita

Creepage Discharge Behaviour and Numerical Model Analysis at the Oil/Pressboard Interface with the Effect of Nano Composite Coating

ナノコンポジットコーティングの効果を考慮した油/プレスボ―ド界面における沿面放電挙動及び数値モデル解析

February 2017

Department of Engineering
Graduate School of Engineering

Kyushu Institute of Technology

Jang Kyunghoon

KYUSHU INSTITUTE OF TECHNOLOGY

ABSTRACT

DEPARTMENT OF ENGINEERING

Doctor of Philosophy

Creepage Discharge Behaviour and Numerical Model Analysis at the Oil/Pressboard Interface with the Effect of Nano Composite Coating

by Kyunghoon Jang

Electrical insulation has been described as the most important component of electrical equipment such as transformer, circuit breakers, vacuum interrupters and power cables. Above all, oil filled transformers are one of the basic elements of a power system. They are connected to a large number of customers via power transmission and distribution system. However, partial discharge and breakdown phenomenon by lightning surge has proved to be one of the major factors and weak point at the oil/pressboard (PB) interface. Besides, aged oil filled transformers are increasing trend, there is need for replacement of aged transformer. Especially, the life time of a transformer is mainly dependent on the life of solid insulation. To enhance competitiveness and cost reduction of transformer system, there is need for alternative conventional pressboard in terms of miniaturization and simplification of insulation structure in oil filled transformer. Besides, to improve of design electric field, dielectric strength as well as suppression of creepage discharge occurrence, there is necessary to improve the insulation performance to prevent discharge phenomena.

In this reason, a lot of work has been recently devoted to improve the dielectric properties of insulation by adding specific functional additives in to the solid polymer, GIS spacer as well as liquid oil. However, recently few studies have been focused on modifications of the insulating paper using various specific functional additives to improve dielectric and mechanical properties; it is because streamer propagation in oil is greatly affected by the presence of pressboard.

Above viewpoints, this research work suggest the new coating method on pressboard surface by thin solid layer coating such as epoxy resin, Teflon coating and silica/epoxy nanocomposite to study discharge phenomena and behavior in transformer composite insulation system. In experiment, five kinds of specimens are used with different coating materials using rod-plane and needle-bar electrode configuration. The creepage discharge properties of conventional pressboard in oil/pressboard composite insulation are compared with that of the solid layer coated pressboard newly in terms of discharge propagation length, discharge occurrence probability and dielectric properties. Besides, to clarify the effect of epoxy/silica nanocomposite, we investigated the creepage discharge behavior using epoxy/silica nanocomposite plate with different silica filler loading and different nano silica size.

Additionally, we investigated the creepage discharge behavior using COMSOL Multiphysics 2D model for simulation. In simulation, to understand the creepage discharge phenomena in composite insulation system depending on solid insulation parameters such as work function and permittivity, creepage discharge modelling and simulation have been investigated. The simulation is based on a system of coupled general expression of governing equations that contain the physics to model streamer development based on the hydrodynamic diffusion-drift including ionization, dissociation, charge recombination and electron attachment, combined with Poisson's equation in dielectric liquids. The governing equations for solid pressboard insulation are composed of Gauss's Law. All the results are reported and discussed.

Thesis Supervisor: Prof. Masayuki Hikita
Title: Professor, Department of Engineering

Contents

CHAPTER 4

CHAPTER 5

CHAPTER 6

CHAPTER 7

List of Figures

List of Table

Acknowledgements

First and foremost, I would like to express my deepest gratitude to Prof. Masayuki Hikita and Prof. Masahiro Kozako who were my thesis advisors for unwavering support and guidance during my Ph.D. studies. They are an outstanding professors and person and working with Prof. Hikita and Kozako has been a great privilege, great honor and a truly positive experience in Japan.

I also wish to thank my thesis committee members, Prof. Mitani, Prof. Komori and Prof. Toyoda for their valuable suggestions, guidance and encouragement that have substantially helped in my thesis.

Secondly, I would like to convey my honest appreciation to Prof. June-Ho Lee (Hoseo Univ.) and Se-Hee Lee (Kyungpook Univ.) for they guidance and encouragement that have substantially helped in my research work. Above all it has been a great honor to work with and learn on COMSOL MULTIPHYSICS from Prof. Se-Hee Lee and his students Su-Hun Kim and Jin-Hyun Choi.

Next, I would like to thank the Nissan Chemical Industry., LTD for their technical support of all the nano silica samples. I am thankful to all the members of the Nissan chemical research team.

A big thank you to my colleagues and friends who are Rajab during Ph.D. study, Impulse PD team Akahoshi and Kurachi for 3 years. And I would like to thank to convey my friends in Korea.

I would like to thank my family, Jang doosoo, Lee Suil and Jang Kyungtak, they have always been there to encourage and support me in what I have done, and they have made many sacrifices to give me the opportunities. And welcome back to Seoul, Korea for my cousin Minji Chang and her husband Jaisun Ihm :).

Symbols

Symbols used in thesis

Δ	Molecular ionization energy [J]
ε_0	Permittivity of vacuum or free space (8.854×10^{-12} F $\cdot$ m^{-1})
ε_r	Relative permittivity of a material
μ	Mobility of charge carrier [$m^2 \cdot s^{-1} \cdot V^{-1}$]
ρ	Mass density [$kg \cdot m^{-3}$]
σ	Electric conductivity [$S \cdot m^{-1}$]
τ_a	Electron attachment time constant [s]
α	Molecular separation distance [m]
C_p	Specific heat capacity of a material [$J \cdot kg^{-1} \cdot K^{-1}$]
D	Diffusion coefficient [$m^2 \cdot s^{-1}$]
$\vec{D}$	Electric displacement field vector [$C \cdot m^{-2}$]
$\vec{E}$	Electric field vector [$V \cdot m^{-1}$]
EA	Electron attachment rate [$mol \cdot m^{-3} \cdot s^{-1}$]
$f(\lvert\vec{E}\rvert)$	Electric field dependent function
$\vec{F}$	Total flux density vector [$mol \cdot m^{-2} \cdot s^{-1}$]
G	Generation rate term of particles [$mol \cdot m^{-3} \cdot s^{-1}$]
$G(\lvert\vec{E}\rvert)$	Generation rate term of particles that electric field dependent [$mol \cdot m^{-3} \cdot s^{-1}$]
h	Planck's constant [6.626×10^{-34} J $\cdot$ s]
I	Electric Current
I_1	Modified Bessel function of the first kind
$\overrightarrow{J_c}$	Conduction current density vector in a volume [$mol \cdot m^{-2} \cdot s^{-1}$] or on surface [$mol \cdot m^{-1} \cdot s^{-1}$]
$\overrightarrow{J_d}$	Displacement current density vector [$C \cdot m^{-1} \cdot s^{-1}$]
k	Boltzmann's constant [1.38×10^{-23} J $\cdot$ K^{-1}]
k_T	Thermal conductivity of a material [$W \cdot m^{-1} \cdot K^{-1}$]
K_d^0	Zero field dissociation rate constant [s^{-1}]
K_d	Dissociation rate constant [s^{-1}]
K_r	Recombination rate constant [$m^3 \cdot mol^{-1} \cdot s^{-1}$]
m^*	Effective electron mass [kg]
$\hat{n}$	Unit vector normal to the boundary

N	Density of particles in a volume [$\mathrm{mol} \cdot m^{-3}$] or on surface [$\mathrm{mol} \cdot m^{-2}$]
N_A	Avogadro's number (6.023×10^{23} mol^{-1})
q	Elementary charge (1.6022×10^{-19} C)
Q	Electrical power dissipation in a volume [$\mathrm{W} \cdot \mathrm{m}^{-3}$] or on surface [$\mathrm{W} \cdot \mathrm{m}^{-2}$]
t	time [s]
T	Absolute temperature [K]
$\vec{u}$	Velocity vector of a fluid [$\mathrm{m} \cdot \mathrm{s}^{-1}$]
v_i	Velocity of each charge carrier [$\mathrm{m} \cdot \mathrm{s}^{-1}$]
X	Relative mass density
W_a	Work function
V_a	Applied voltage

Abbreviations in thesis

AC	Alternating current
DC	Direct current
PD	Partial discharge
BDV	Breakdown voltage
PDIV	Partial discharge inception voltage
HV	High voltage
GND	Ground
IEEE	Institute of Electrical and Electronics Engineers
PMT	Photomultiplier tube
wt%	Weight percent
PB	Pressboard
NP	Neat pressboard or/and Neat epoxy
DP	Dry pressboard
EP	Epoxy coated pressboard
SP	Silica/epoxy composite coated pressboard or/and Silica/epoxy composite plate
TP	Teflon coated pressboard
I.I	Image Intensifier
P_d	Discharge occurrence probability
l_d	Discharge propagation length
R_z	10 point surface roughness
R_a	Average surface roughness

l_{dave}	Average discharge propagation length
V_{i}	Impulse voltage
S_{l}	Nano silica filler loading
k_1	10% discharge occurrence probability ratio
k_2	30% discharge occurrence probability ratio
k_3	Discharge propagation length ratio of epoxy silica nanocomposite coated PB
k_4	50% discharge occurrence probability ratio
k_5	Discharge propagation length ratio of epoxy/silica nanocomposite

CHAPTER 1

1.1 OIL FILLED TRANSFORMER

Electrical insulation has been described as the most important component of electrical equipment such as transformer, circuit breakers, vacuum interrupters and cables. Above all, oil filled transformers are one of the basic elements of a power system. They are connected to a large number of customers via power transmission and distribution system. And also large transformers are one of the basic elements of electric power system. When it comes to ageing and degradation process, large power transformers are a major concern to any electricity utility [1].

A large number of transformers working in power systems in many countries of the world have exceeded their technical lifetime. While designing, it is assumed that a transformer's technical lifetime is usually over 30 years. It is estimated that in Central Europe over 35% of power transformers have exceeded the age of 30, and about 20% have been working in the power system for over 35 years. The technical lifetime of a transformer depends mainly on the technical lifetime of oil-paper insulation. Especially, the life of a transformer is mainly dependent on the life of solid pressboard insulation of the winding paper. The pressboard decreases in tensile strength with the progress of aging and, at some point, can no longer withstand the short circuit stresses and with passing years the insulation used in the transformer undergoes ageing [3, 4].

Oil filled transformer as shown in Fig. 1.1 (a) and (b) basically adopts mineral oil and pressboard (PB) composite insulation system as an insulating medium which can be categorized into major insulation and minor insulation. It is because cellulose materials have excellent insulating capability in insulating oil as well as low cost and good performance. The major insulation consists of insulation at the region between different windings, between windings and the core limb/yoke and between leads and ground. In a large oil-immersed power transformer, the use of cellulose-based pressboard for electrical insulation is required in the gap between phase windings. Pressboard barriers that have higher dielectric strength compared to the mineral oil are important in dealing with the pre-breakdown events by increasing the partial discharge inception voltage (PDIV) [5, 6].

Many kinds of defects such as excessive moisture, high temperature and extremely concentrated electrical stress often lead to partial discharge (PD) [7]. On the other hand solid-liquid interface of oil filled transformer is considered as a

weak point giving rise to failure modes in the oil/pressboard composite insulation system, it is because creepage discharge tend to propagate along the interface between oil and pressboard and then leading to flashover and breakdown.

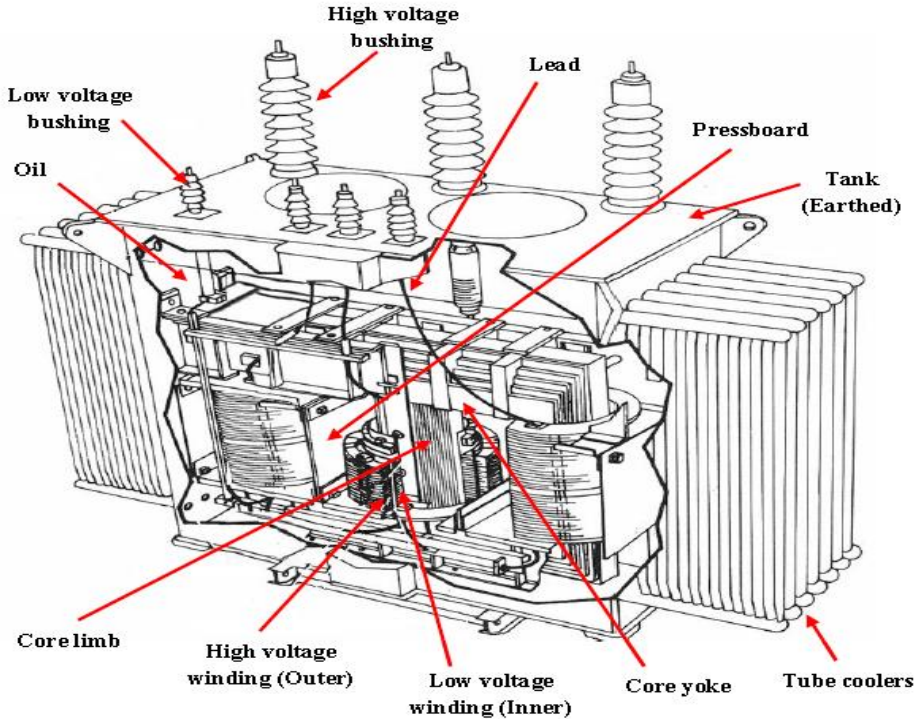

(a) Oil filled power transformer

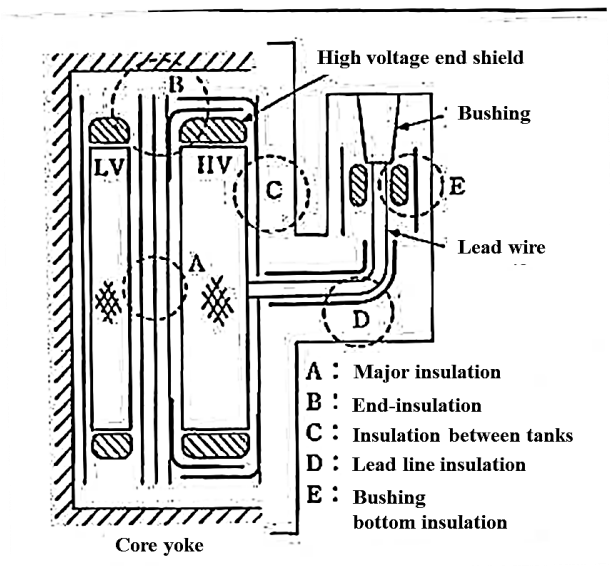

(b) Schematic of inner structure of oil filled transformer

Figure 1.1 Structure of oil filled transformer [1, 8]

1.2 RESEARCH MOTIVATION AND PROBLEM

Cellulose paper or pressboard and mineral oil are the main insulation materials used in oil filled transformer as a composite insulation system to protect the equipment from lightning surge. However, partial discharge and breakdown phenomenon by lightning surge has proved to be one of the major factors and weak point at the oil/pressboard interface. Besides, aged equipment is increasing rapidly. To enhance competitiveness and cost reduction of oil filled transformer, there is need for alternative conventional insulation, miniaturization, and simplification of insulation structure and improvement of design electric field. For above needs, the distance between insulation is narrowed, meaning that electric field and probability of discharge at oil/PB interface increases than designing condition. Thus, it is necessary to improve the dielectric property of conventional pressboard [1-9].

Figures 1.2 (a) and (b) show flashover failure along the mineral oil and pressboard interface. The creepage discharges tend to propagate along the interface between mineral oil and pressboard due to different permittivity. Despite advances in manufacturing and monitoring technologies, some unexpected faults and failures still occur. These are usually dielectric in nature, and often without any obvious cause [10].

Lightning impulse withstanding property is one of important characteristics in power apparatus to design of oil filled transformer; it is because the lightning impulse is a pure natural phenomenon. On the other hand, it is very difficult to predict the actual wave shape of a lightning disturbance. In addition, engineers want to predict the discharge initiation, development process in composite insulation system for upgrading the insulation design of power apparatus under lightning surge. Indeed, the conditions of the occurrence of discharges and the parameters influencing discharge development up to flashover are very useful for the design and dimensioning of high voltage components and systems such as insulators, spacers, bushings and circuit breakers envelopes. For these reasons, a lot of works have recently been devoted to improve the dielectric properties of insulating oil by adding specific functional additives into the oil [11, 12]. However, few studies have been focused on modifications of the insulating paper using various specific functional additives to improve dielectric and mechanical properties [13-16], it is because creepage discharge phenomena has been reported in many literatures that streamer propagation in oil is greatly affected by the presence of pressboard and other solid insulation [1, 17, 18-22]. Thus there is a growing interest in suppression of creepage discharge in oil filled transformer.

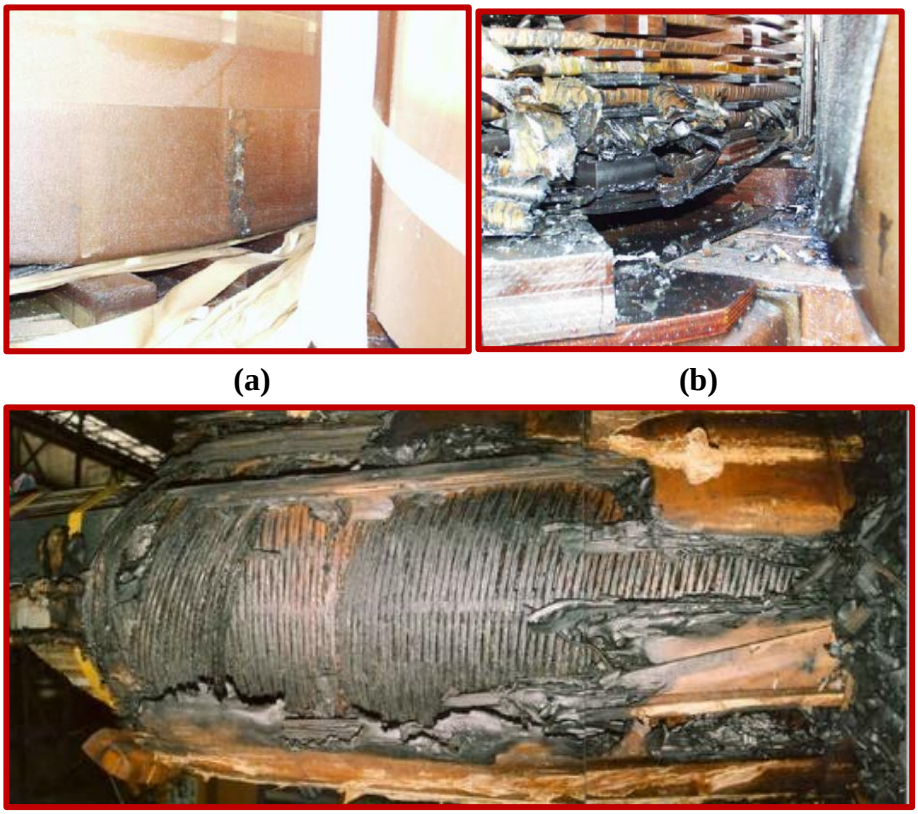

(a) **(b)**

(c)

Figure 1.2 Flashover failure of insulation (a) to (c) [1, 2]

1.3 RESEARCH OBJECTIVES AND CONTRIBUTIONS

The main objective of this research is to study the behavior and characteristics of creepage discharge at the oil/pressboard composite insulation system depending on solid layer coating materials on PB surface such as epoxy resin and epoxy/silica nanocomposite under standard lightning impulse voltage. Second objective is to investigate the effect of nano size silica on suppression of creepage discharge inception and discharge propagation process by silica/epoxy nanocomposite coating method.

The research has involved two kinds of approach such as experimental results and computer simulation studies. The experiments for creepage discharge observation at the oil/pressboard interface have been conducted in an oil chamber experiment setup. The creepage discharge characteristics of conventional

pressboard are compared with solid layer coated pressboard. A numerical analysis method in composite insulation system has been developed in the COMSOL Multiphysics 2D Model, a finite element analysis (FEA) software package to understand the creepage discharge behavior and mechanism. With respect to all these, contributions are followings:

1. The experimental work presented in this thesis contributes to a further understanding on the surface discharge behavior at the oil-pressboard interface dependent on surface condition, nano silica filer loading and different silica size.

2. This experiment results may assist in the prediction of discharge initiation and development in mineral oil for insulation design as well as upgrading for large power transformer and to allow study of their lifespan.

1.4 THESIS STRUCTURE

Chapter 1 discusses the problems and weak point in terms of partial discharge within large transformers associated with the oil/pressboard interface that motivates this research. The research objectives have been outlined.

Chapter 2 presents a review of the literature that is directly relevant to both the experimental work and numerical simulation model development that has been undertaken as part of this thesis.

Chapter 3 presents general electrohydrodynamics model in mineral oil in terms of ionization, dissociation, carrier recombination and carrier attachment due to extremely high electric field and temperature variation.

Chapter 4 explains about creepage discharge properties at the interface between oil and epoxy/silica nanocomposite coated pressboard under the applied standard lightning impulse voltage. In this chapter, the experimental set up (rod-plane electrode and needle-bar electrode) and method are indicated and the creepage discharge characteristics in terms of discharge occurrence probability, discharge propagation length and dielectric properties are compared with those of conventional pressboard and they have been discussed in this chapter.

Chapter 5 explains about the creepage discharge and dielectric properties of epoxy/silica nanocomposite plate with different filler loading and particle size to verify the effect of epoxy/silica nanocomposite on discharge suppression. In this research, the discharge occurrence probability, discharge propagation length and dielectric properties have been examined as a function of the voltage under standard lightning impulse voltage. The experimental preparation, setup and procedure are presented in detail.

Chapter 6 describes the numerical analysis method in composite insulation system quantitatively to understand the creepage discharge behavior and mechanisms depending on relative permittivity by epoxy/silica nanocomposite at short gap. Analysis model fully is coupled with governing equations based on the charge continuity equations for positive ions, negative ions and free electrons, along with the energy balance equation for a temperature and Poisson's equation for electric fields. The validation of the model using experimental results is discussed. In terms of simulation results, the role of electric field dependent molecular ionization on the streamer development is explained. In addition, the roles of electron attachment and other recombination process (ion-ion and ion-electron). Furthermore, the possibility of creepage discharge model for long gap distance in insulation oil is investigated.

Chapter 7 is the conclusions of this work, which is summarizing an important outcome obtained by an accomplishment of the present research. The chapter concludes with suggested future work to extend the theoretical work found in this thesis.

CHAPTER 2

Insulations of Oil Filled Transformer & Creepage Discharge Phenomena

2.1 MINERAL OIL

A petroleum-based mineral oil has been most often employed in the electrical insulation inside power transformers for more than a century for electrical equipment including transformers, circuit breakers and power cables. Mineral oil has an excellent performance as electrical insulation (electrical breakdown strength and thermal conductivity than gaseous insulators) and cooling medium [22, 23]. Unfortunately, as with all insulation, the failure of the liquid insulation can cause catastrophic damage to not only the power equipment, but also the surrounding environment. And also some problems such as scarcity and high price of mineral oil, sulfide-induced corrosion of copper lead to be conductive in liquid insulation, environmental pollution due to oil leakage, atmospheric pollution have been pointed out for practical use [22].

Mineral oils are obtained from crude petroleum extracted from the earth. Mineral insulating oil is a mix of hydrocarbons in the form of chain and ring molecules with small amounts of sulphur, nitrogen, oxygen and trace metallic elements [1, 23, 24]. Mineral oil is classified by the percentage content of the following three hydrocarbon groups, which are paraffinic ($C_{2n}H_{2n+2}$), naphthenic ($C_{2n}H_{2n}$) and aromatic (C_nH_n) as shown in Fig. 2.1 [23-26]:

- Paraffinic – straight and branched saturated hydrocarbons
- Naphthenic (cycloparaffins) – hexagonal ring of carbon-carbon single covalent bonds
- Aromatic – hexagonal ring modelled as alternating single and double carbon-carbon covalent bonds indicating delocalization of the carbon-carbon bonding electrons.

The paraffinic hydrocarbons are composed of straight and branched chains of carbon and hydrogen atoms, whilst the naphthenes have a saturated ring-like structure. The aromatics also have ring-like structure which is unsaturated that can be identified by double bonds between some of the carbon atoms [1]. In general, these mixtures determine the physical properties of transformer oil that make it an excellent electrical insulator and cooling medium such as high resistivity, high dielectric strength, high specific heat and thermal conductivity along with low viscosity and pour point as well as low density. The other important parameter for most transformer oils is the relative permittivity ε_{oil} that typically has a value of 2.2 [1-4, 23].

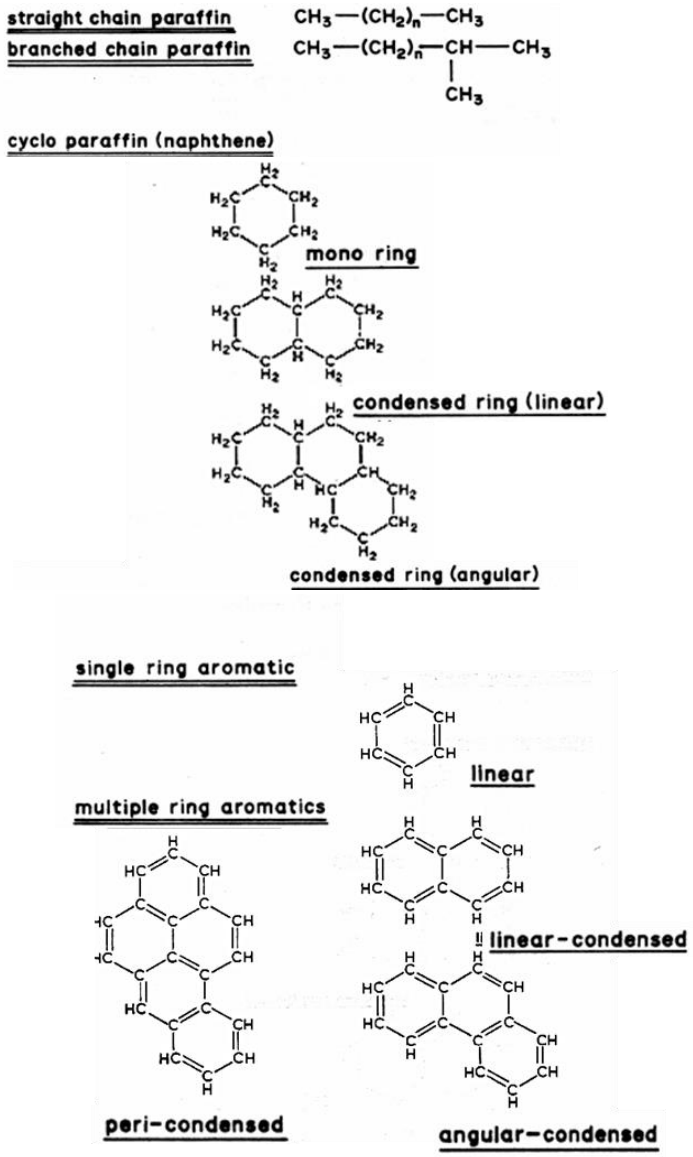

Figure 2.1 Molecular structures of hydrocarbon groups (paraffinic, naphthenic and aromatic) [1, 26]

2.1.1 THE EFFECT OF MOISTURE ON MINERAL OIL

Insulation oil is hydrophobic and oil and water do not readily mix but the real problem with moisture in oil is that, even in small amounts, it has a marked effect on the dielectric strength of the oil as shown in Fig. 2.2 [26]. The breakdown voltages for each oil sample were normalized with the corresponding dry oil value to account for the variation between different oil samples (60-88 kV). It is observed that the breakdown voltage remains almost unchanged when the relative moisture saturation is below 20%. Above that it decreases rapidly [27]. Guidelines are given for acceptable levels of moisture according to transformer category in the standard for insulating oils in electrical equipment which defines a minimum breakdown of 55 kV/mm and a maximum water content of 10 ppm for transformers rated at a minimum system voltage of 170 kV [1, 26].

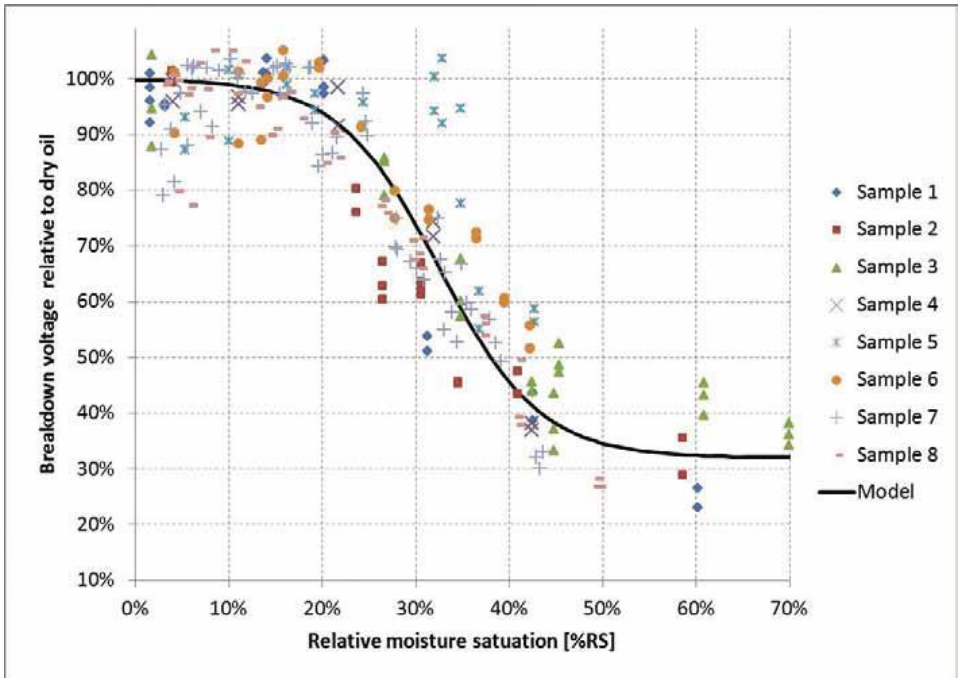

Figure 2.2 Measured dependency of the breakdown voltage on the relative moisture saturation with an approximative model fitted to the data. Each point corresponds to the average of six breakdown voltage measurements performed according to the IEC 60156 standard [26, 27]

2.2 CELLULOSE-BASED PRESSBOARD

Cellulose based insulation has been the preferred choice for the solid insulation in power transformers, In 1939, G. T. Kohan of Bell Telephone Laboratories in New York wrote an article in AIEE Transactions on cellulose as an insulating material for various electrical application: paper capacitors, paper-insulated power cables, oil filled cable [9]. Cellulosic insulation is used primarily in oil filled transformers from distribution to large power units covering a wide range from 10 kVA to 1500 MVA and from line voltage to 1000 kV. In terms of physical size, it ranges from the pole and pad mounted units on our streets to large substation units that can have several tons of cellulosic insulation immersed in 40,000 to 100,000 L (~10,000 to 30,000 gallons) of oil [9]. The insulation structure consists of not only the HV and LV insulation but also support structures, winding tubes, spacer blocks and formed items for end closing. These are illustrated in Fig. 2.3.

Electrical grade paper and pressboard are mostly made from wood pulp processed by the Kraft chemical process. The starting material is wood, both soft wood and hard wood. Wood is a natural composite material that is made up of flexible tubes of cellulose bound together by lignin, a brownish aromatic polymer that is mostly removed during the pulping process. A schematic representation of the fine structure of wood pulp is shown in Fig. 2.4 [9].

In general, fibres may consist of approximately 50-90% of carbohydrate group, i.e. cellulose (40-80%) and hemicelluloses (10-40%). Fibres may also consist of 5-25% of lignin [28, 29]. Specially, Hemicellulose molecules are the second major components that facilitate the hydrogen bonding process, but the mechanical strength is reduced if their quantity exceeds about 10% [17]. Another disadvantage of hemicelluloses is their ability to “hold on” to water which makes the paper/pressboard more difficult to dry out and thus, this signifies its dominant role in the hydrophilic behavior of the cellulose based solid insulation. Besides the significant hygroscopic nature of cellulose paper is obvious from the moisture sorption curves. Meanwhile, lignin is a component of wood that binds to cellulose fibres to strengthen the cell walls of plants and add further to their matrix rigidity [1, 17, 29].

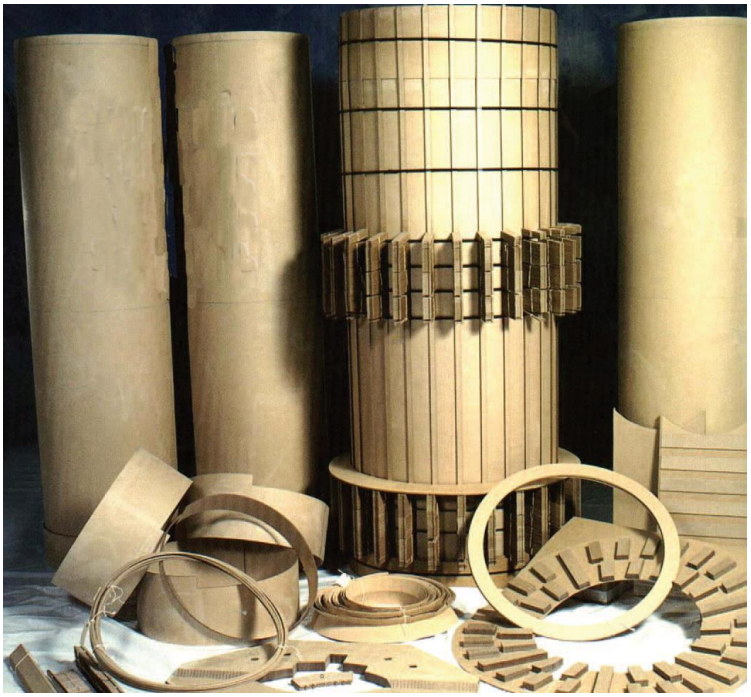

Figure 2.3 Formed items from pressboard [12]

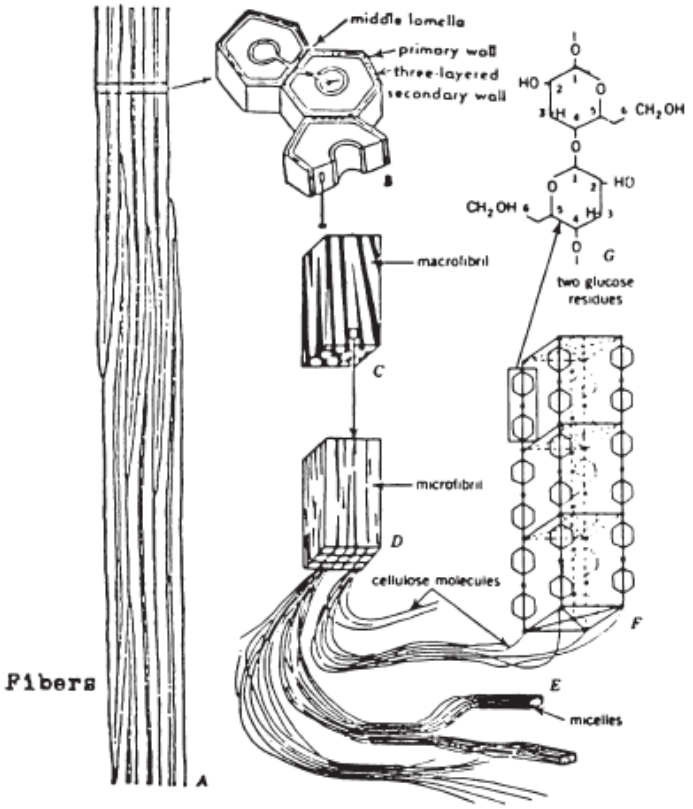

Fig 2.4 Micro to sub-micro structure of wood fibers [12]

Cellulose, the essential component of paper and pressboard is a polymer of glucose units linked to one another in a special manner as shown in Fig. 2.5. It may be represented simply as $[C_5H_{10}O_5]_n$, ignoring the extra atoms on the end groups. The number of glucose units (n) which form individual cellulose polymer chains for new electrical paper and pressboard is typically 1200. The length of the polymer chain is characterized by the number of links and this is the degree of polymerization [9, 30].

Figures 2.6 show fibrous, porous structure with non-homogeneous pressboard surface and numerous protrusions of cellulose fibers [1]. The pores diameter within the fibre structures of pressboard varies from 10 nm to 7μm. These pores provide paths for mineral oil and water to penetrate by diffusion and swelling mechanisms. Besides, the pores within the pressboard allow oil absorption during impregnation process [1, 31-33]. The ratio of fiber and oil changes as the material structure changes from a medium of bulk oil-pressboard composite toward the bulk oil medium. The porosity of pressboard can also result in impurities and small air bubbles within the oil being drawn into the pressboard. The material properties and geometry of pressboard thus lead to a complex oil-pressboard interface [33].

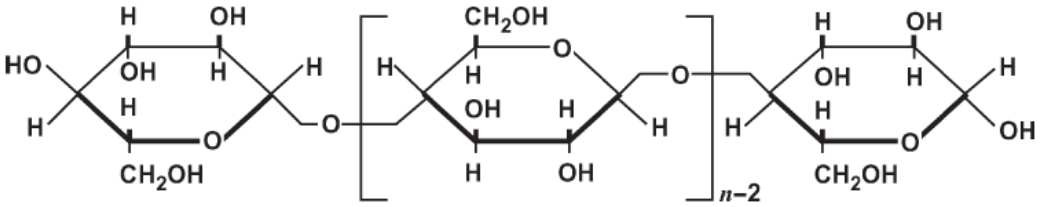

Figure 2.5 Cellulose polymers [12]

(a) Loose structure of cellulose fibres in pressboard [1]

(b) Numerous protrusions of cellulose fibers

Figure 2.6 Microscopic view of pressboard insulation [1]

2.2.1 THE EFFECT OF MOISTURE ON CELLULOSE-BASED PRESSBOARD

Cellulose based pressboard generally absorb moisture rapidly until reaches equilibrium according to the ambient conditions. At room temperature (20-25℃) cellulose can hold from 4 to 10% moisture in the relative humidity range of 30 to 70% typical on factory floors in winter and summer conditions [29]. The moisture level in insulation in a newly built transformer should be about 0.5%. This makes it mandatory to dry out scrupulously the insulation in electrical equipment. Wet insulation is a dielectric hazard in several ways:

- PD inception becomes significant above 3% moisture level and may result in gas bubbles and release of hydrogen,
- Progressed of paper degradation and aging process.

For regular Kraft paper the life would be lowered by half for every doubling of moisture content, though for upgraded paper the loss of life is not so drastic. From a temperature perspective, the temperature increases above 75 ℃ for the mechanical strength to decrease to half depending on the moisture content of the paper [29, 34].

Table 2.1 shows the creepage discharge on different pressboard condition in 30 mm gap distance [35]. The results can be deduced that the moisture content in pressboard plays a more critical role in creepage discharge at the oil-pressboard interface. On the other hand, moisture in pressboard bulk has been said to play important role in surface discharges [1]. Therefore, transformer insulation paper requires rigorous dry out before oil impregnation. Drying of the cellulose is required to reduce the moisture content, which if not completed can decrease the dielectric strength and accelerate aging [22].

Table 2.1 Creepage discharge on different pressboard condition [35]

	Dry virgin board	Wet virgin board (2.7-2.8 %)	Dry aged board	Wet aged board (2.8-2.9 %)
Surface breakdown voltage	46.9kV	40.2kV (14% reduction)	43.2kV (8% reduction)	38kV (19% reduction)
PDIV	38.8kV	27.4kV (29% reduction)	36.2kV (7% reduction)	24kV (38% reduction)

2.3 CREEPAGE DISCHARGE PHENOMENA AT THE OIL/PRESSBOARD INTERFACE

2.3.1 THE INFLUENCE OF SOLID INSULATION IN MINERAL OIL

Creepage Discharge phenomena has been reported in the literature that streamer propagation in mineral oil is greatly affected by the presence of pressboard and other kinds of solid insulation [1, 22, 36-37, 41, 42]. Especially, different insulation components or characteristics of oil-solid systems have been shown to have serious impact on discharge inception and propagation. They are the orientation of the oil-solid interface with respect to the dominant electric field direction and the permittivity difference between oil and pressboard as shown in Fig. 2.7 [22, 42]. And some researchers consider the electric filed distribution with/without presence of the solid insulation [42]. Figure 2.8 (a) shows the electric field distribution in the system without the presence of the insulating surface. The electric field magnitude has a maximum in the direction of the axis of the streamer. However, as seen in Figure 2.8 (b), when an insulating surface (relative permittivity $\varepsilon_r = 3.5$) is placed in the gap parallel and close to the axis of the streamer, the maximum field is no longer along the streamer axis, but points towards the insulating surface. The maximum field is also larger with the presence of the insulating surface. The streamer velocity in the presence of the insulator is also increased moderately compared to no presence of solid insulator [43].

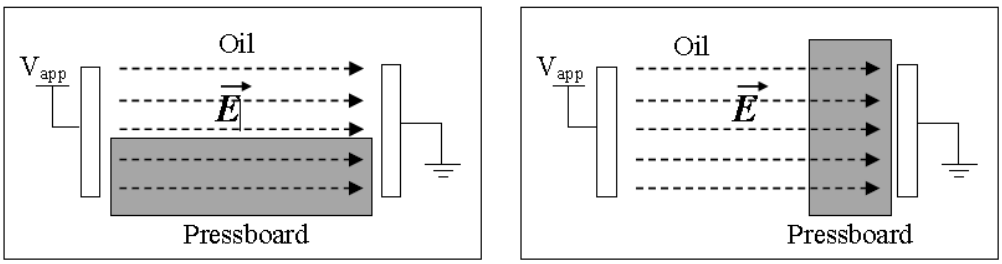

(a) Transformer oil-pressboard system where the Interface is oriented parallel to the dominant direction of the electric field.

(b) Transformer oil-pressboard system where the interface is oriented perpendicular to the dominant direction of the electric field.

Figure 2.7 General orientations of oil-pressboard interface with respect to dominant direction of electric field [1, 22]

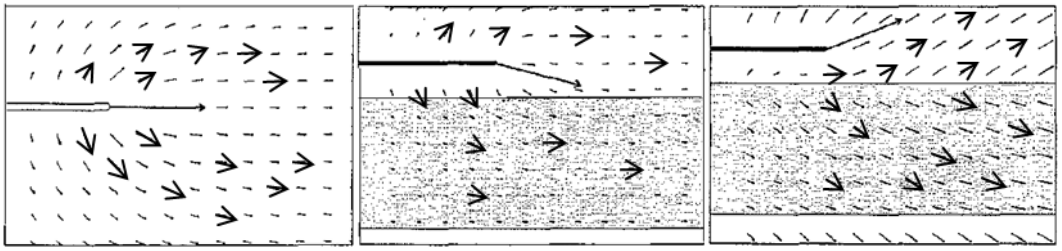

(a) (b) (c)

Figure 2.8 Vector plots of the electric field distribution for the streamer propagating (a) in air, (b) along an insulating surface and (c) electric field distribution when a layer of charge with density $\sigma = 50\mu C/m^2$ is applied to the dielectric surface [43].

Z. D. Wang *et al.*, [42] have reported the influence of discharge propagation length and PDIV with/without three kinds of solid insulation under AC voltage using needle-bar electrode configuration in Figure 2.9. As can be seen, in an open gap, the longest negative streamer is merely 6 mm, when the Perspex surface is present, the negative streamer channel can be as long as 26 mm, more than four times that in open gap. These results verify the promotion effect by presence of solid insulation on discharge.

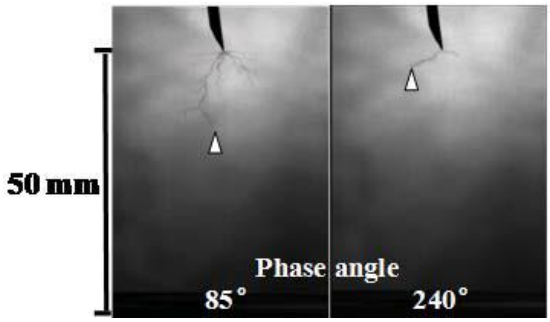

(a) In open gap

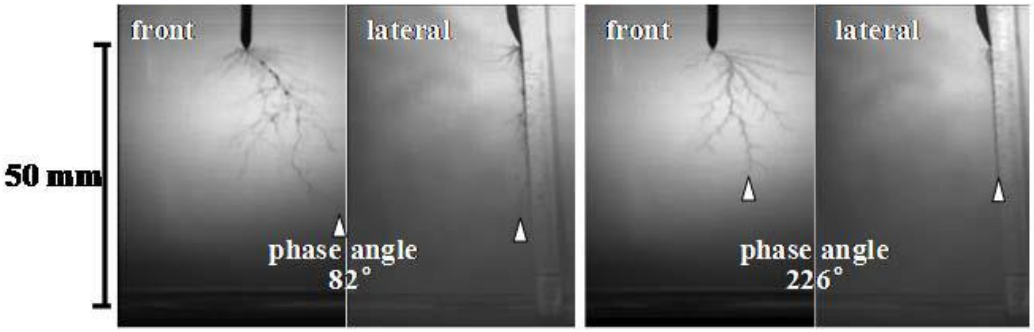

(b) On Perspex

Figure 2.9 Discharge propagation lengths in FR3 at 43 kV [42].

Figure 2.10 shows the breakdown process at the oil-pressboard interface in four distinct stages. The experiment was conducted by increasing the AC voltage gradually [1, 28, 44]. As seen in Fig. 2.10, the first event occurs at PDIV level. During this first stage, no visual activity has been observed but the occurrence of PD activity is known based on the monitoring data from the PD measurement system. As the voltage increases, the second stage occurs when a corona like event is visible at the needle tip. This stage is observed to occur at a voltage level that is above the PDIV level and lower than the flashover voltage, which is also called the sustained PD voltage range. Surface discharges can be sustained for long periods without surface flashover or breakdown as long as the voltage is within this range. Next, as the voltage is increased closer to the flashover voltage, the third stage occurs when streamers are observed from the ground bar electrode and distinct crackling is heard. Finally, as the voltage is increased further, a surface flashover occurs and causes electrical breakdown [1].

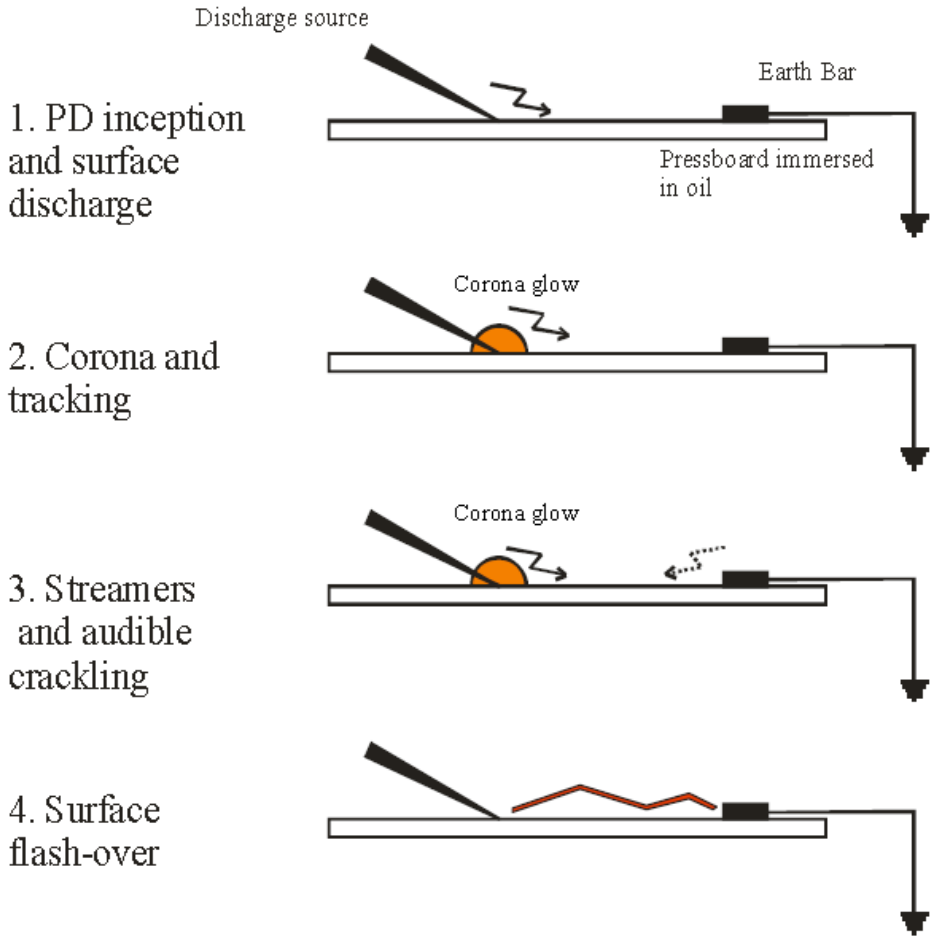

Figure. 2.10 Creepage discharge stages from discharge inception to breakdown [1, 26]

2.3.2 DISCHARGE PROPAGATION MODES

Discharge stopping length, average velocity and discharge shape characteristics including channel width and number of branches can offer additional information to help distinguish and understand various modes of streamer. In terms of the shape of streamer propagation, streamers are generally classified as slow and "bushy" for streamers emanating from the negative electrode or fast and "filamentary" for streamers emanating from the positive electrode [45]. The streamer velocity can vary from tens m/s to hundreds km/s. In terms of the velocity of streamer propagation, streamers are classified into different modes (1st, 2nd, 3d and 4th). However can be clearly divided, slow mode, fast mode and combination of fast and slow modes, similar to the classification of 2^{nd}, 3^{rd} and $3th+2^{nd}$ mode in depending on the electrodes geometry, applied voltage, polarity, molecular structure and hydrostatic pressure [46].

Z. D. Wang [47] have reported similar observation in Midel 7131 insulation oil without solid insulation as shown in Fig. 2.11 in which, as the propagation time increases, the streamer propagates at a constant speed of less than 3km/s for slow mode (a) ant that has relatively more branches. For fast mode, streamer propagates much faster at the speed from 5 km/s to 50 km/s and that has bright filamentary branches. On the other hand, for combination mode, streamer initiates at fast mode and then quickly changes into slow mode. At the beginning of this combination mode, only the filamentary branch with few ramified branches propagates at a high speed and then many small ramified branches start to grow around the main streamer branch, and the propagation speed falls into the slow mode propagation range. Figure 2.12 shows the shape evolution of slow streamer and fast streamer. In this case, the length of captured streamer is scattering due to the increasing velocity of fast streamers. Therefore unified streamer area, ratio of area to length (*width*) is deduced to compare the slow streamer and fast streamer with fairness. This *pseudo width* can indicate the branching or expanding of the streamer shape. It is found that the *pseudo width* of fast streamer and slow streamer follows the same relationship with applied voltage: the higher voltage, the more branches [47].

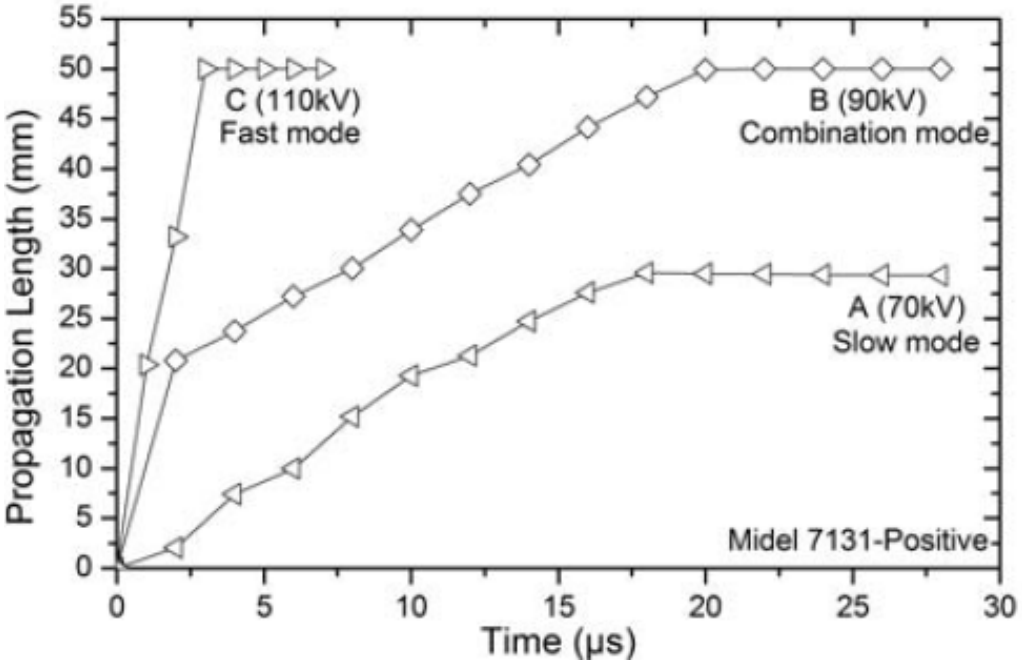

(a) Propagation length versus propagation time

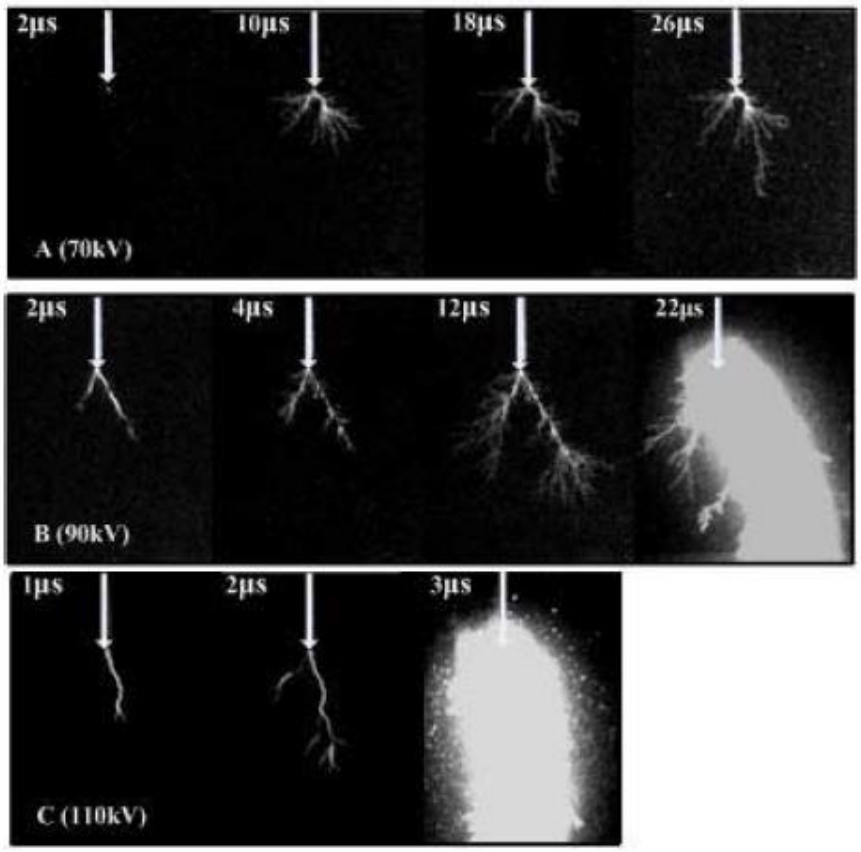

(b) Photographs of streamer propagation

Figure 2.11 Typical propagation modes in esters (Midel 7131, positive polarity, d=50 mm) [47]

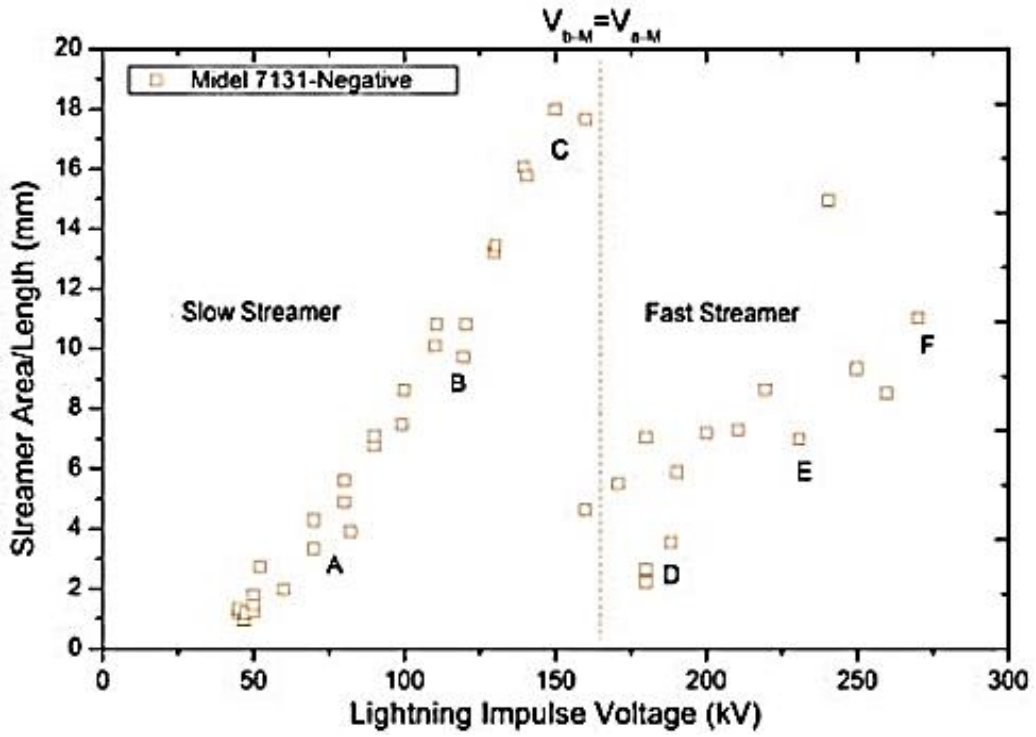

(a) Ratio of streamer area to length versus applied impulse voltage

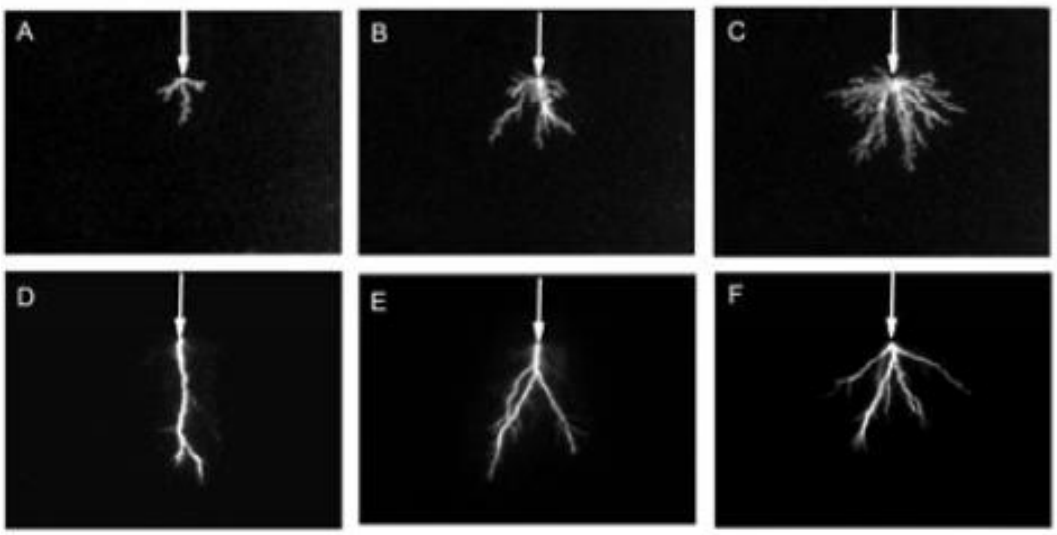

(b) Correlated streamer shape at different stages in (a)

Figure 2.12 Evolution of streamer shape along applied voltage (Midel 7131, negative polarity, d=50 mm) [47]

O. Kesaint and G. Massala [48] have reported the streamer average velocity with respect to the applied voltage in the transformer oil with and without pressboard as shown in Fig. 2.13. However, Lundgaard et al., [49] has also reported that slow velocity streamer propagation could change to a fast mode. The slow velocity streamer was found to cause weak darkening path on the pressboard surface, whilst the fast velocity has led to a burnt track on the pressboard surface, as shown in Fig. 2.14 [1].

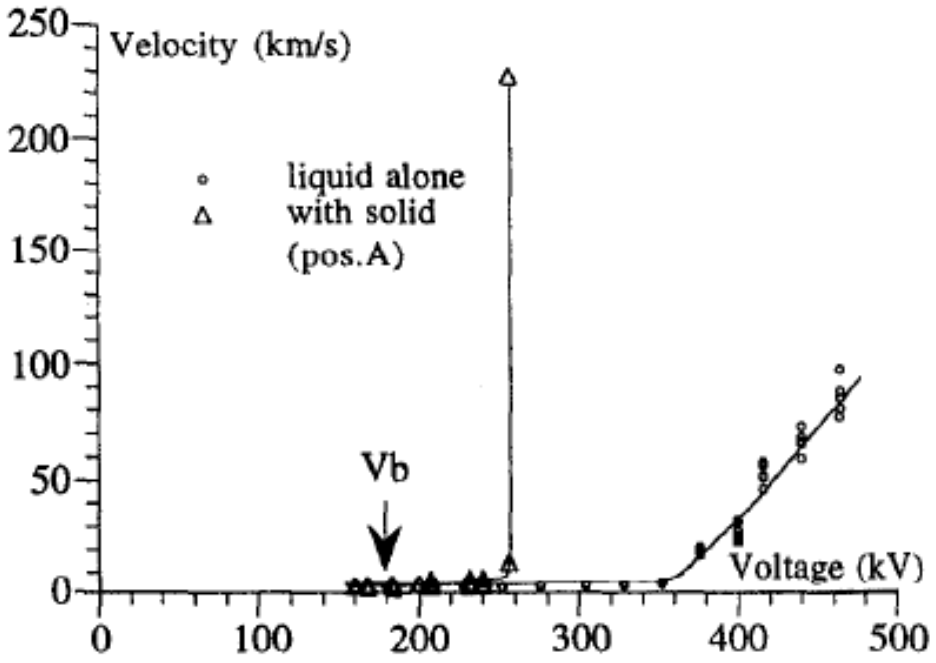

Figure 2.13 Average streamer velocity versus voltage in the liquid alone and with a solid parallel to the field (d=10 cm) [48]

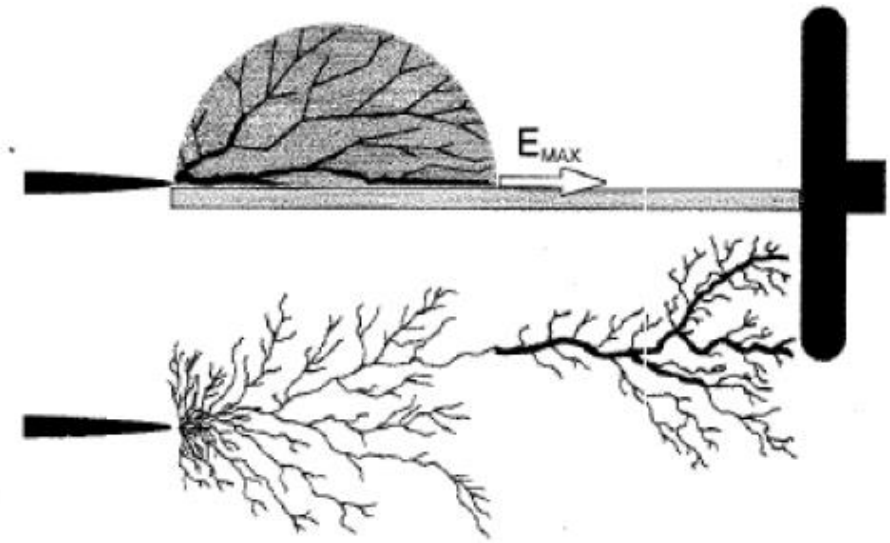

Figure 2.14 Positive streamer propagation along solid interface; Upper: the positive streamer model, Lower: actual tracks observed on pressboard surface [1]

The polarity effect in insulating oil in inhomogeneous electric fields manifests differences in discharge initiation, structure and propagation velocity of streamers. The physicochemical processes implicated in the development of streamers in each polarity can be succinctly explained as follows [47, 49]:

(1) In the vicinity of the positive electrode, either free electrons or electrons detached by field emission are accelerated towards the anode. Whereas the electrons rapidly drift to the anode, the positive ions essentially stand still. The liquid increases its temperature due to the interaction between the electrons and the fluid molecules. This local heating causes a low-density region, which becomes the origin of positive streamer branches. Inside this region, ionization of fluid molecules generates more free electrons which arrive at the anode. The remaining positive ions build a space charge representing the new, virtual tip. This pulsed process repeats periodically and the positive pre discharge propagates in the direction of the electric field until the inception conditions for subsequent stages are attained.

(2) The initiation process for negative streamers differs from the positive one. At sufficiently high fields, electrons are injected into the liquid and due to the interaction between the electrons and fluid molecules and the associated energy release, a low density region is formed. Whereas the positive streamer appears as a three stage process, only two propagation stages of the negative pre discharge could be observed whereby secondary modes can only be detected at large

electrodes gap. Depending on the growth rate of electric field, different structures can occur (leafless tree-top, frequently ramified or filamentary structure). Each mode has a typical minimum propagation velocity.

2.3.3 EFFECT OF RELATIVE PERMITTIVITY IN COMPOSITE INSULATION SYSTEM

At present, insulation in oil filled transformers consists of mineral insulating oil and solid insulation that is Kraft paper and pressboard. Cellulose materials have excellent insulating capability in mineral insulating oil and are low in cost. However the permittivity of pressboard is over twice that of oil. If this permittivity were reduced, the insulating distance in transformers can be decreased because uniform electric field distributions can be made in oil-paper-pressboard composite insulation systems [50]. Hence, a lot of researchers on creepage discharge for different material properties and modification of pressboard immersed in transformer oil [13, 14, 42, 50-52] as well as SF_6 gas condition for reduction permittivity by nanoparticles [42, 53-58]. Dielectric solid materials such as glasses, plastics and epoxy resin are characterized as having a compact structure and not being porous. These factors make them different when compared to the pressboard that is fibrous and porous form of solid insulation [1]. These factors suggest that the type of materials and surface roughness may offer different results in creepage discharge phenomenon [1].

David Ariza and Claire Pitois *et al.,* [51, 52] have reported the discharge inception probability, discharge propagation length and charge injected by conduction currents for negative polarity in mineral oil with different solid interfaces. The inception voltage for mineral oil without interface is the lowest in all the considered cases at about 13 kV as shown in Fig. 2.15. The inception voltage for the impregnated paper ($\varepsilon_r = 3.0$), PET ($\varepsilon_r = 3.0$) and PVDF ($\varepsilon_r = 8.0$) interfaces is nearly the same about 13.3kV despite of the differences in their relative permittivity and surface properties, whereas a significantly larger inception voltage is found for the PTFE ($\varepsilon_r = 2.1$) interface at about 15.5 kV. The discharge propagation length of low permittivity solid materials is also shorter than that of impregnated paper [52]. These results indicate that creepage discharge at the oil/solid interface depends on solid insulation properties and surface geometry. In addition, different discharge currents have also been observed. Hence, when considering the pressboard with a porous, fibrous and non-

homogenous surface structure, one can also hypothesise different results compared to other solid materials [1].

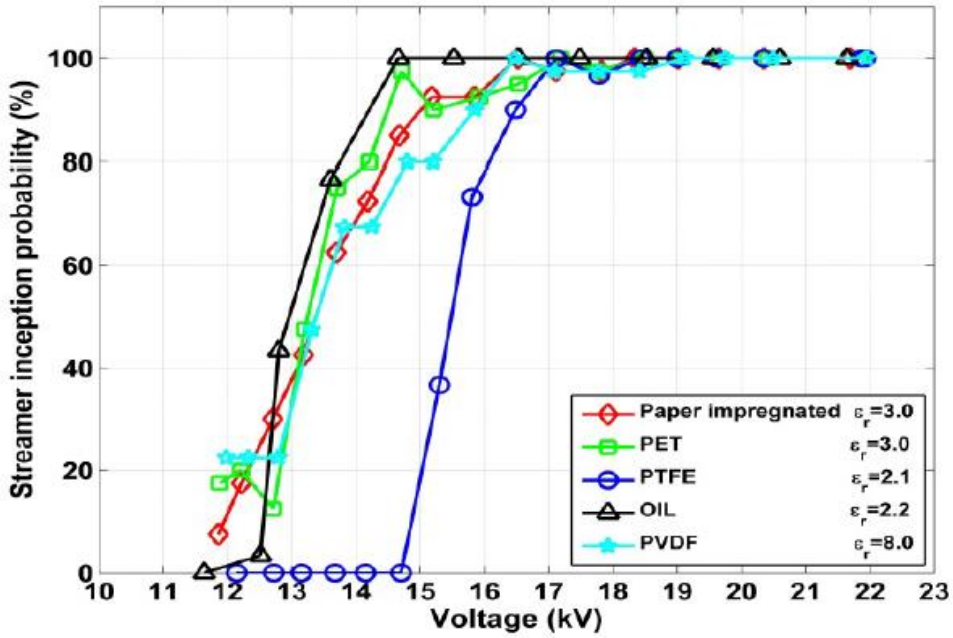

Figure 2.15 Streamer inception probability distribution function for point cathode in transformer oil with and without solid interface [51]

Figure 2.16 shows the liquid/solid interface with the protrusions and troughs on the solid surface that can be modelled in the figure as liquid and solid parts in series. The interface breakdown should be induced by a partial breakdown of the liquid part due to its lower dielectric strength, and factor K was introduced to describe the reduction of the creepage breakdown strength ΔU_s to the breakdown strength of open gap ΔU_O [42, 59].

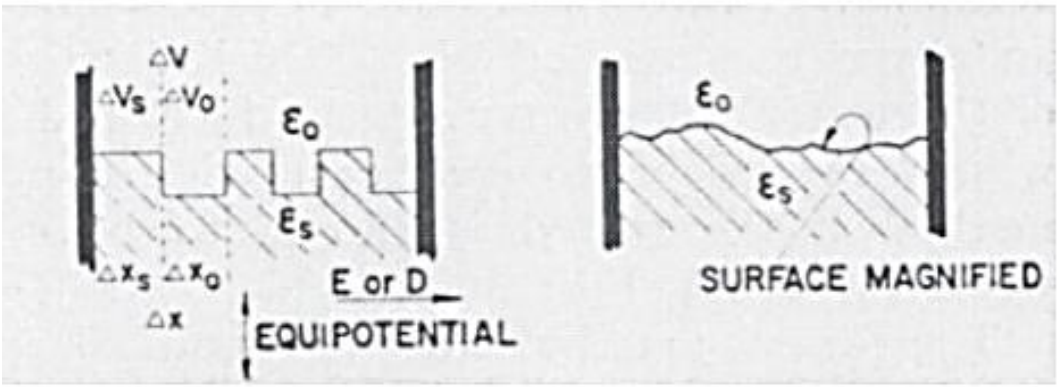

(a) Idealized series model (b) Actual condition

Figure 2.16 Equivalent series model to represent solid-liquid interface [59].

$$\mathrm{K} = \frac{\Delta U_s}{\Delta U_O} = 1 - \frac{\Delta x_s}{\Delta x_0} \cdot \left(1 - \frac{\varepsilon_o}{\varepsilon_s}\right) \qquad (2.1)$$

The limit of K can be deduced as:

$\lim_{\Delta x_s \to 0} \ K = 1$ and $\lim_{\Delta x_s \to \Delta x} \ K = \frac{\varepsilon_o}{\varepsilon_s}$

Therefore K should be larger than $\frac{\varepsilon_o}{\varepsilon_s}$ and less than 1 assuming that the liquid permittivity is smaller than that of solid materials, and it should vary with the combination of liquid and solid. The larger the permittivity mismatch between liquid and solid insulation, the more reduction in creepage discharge and breakdown strength [42, 59]. The supporting experimental evidences can be found in references [50- 52, 60, 61].

2.3.4 PERMITTIVITY AND POLARIZATION

The relative permittivity of a linear dielectric material describes the ability of tightly bound electrons in the material to be displaced from the positive nucleus under an applied electric field to form electric dipoles which results in a net electronic polarization. The greater the relative permittivity of a material, the greater the polarization charges that develops in a region where there is a local imbalance of dipoles, as shown in Fig. 2.17. This polarization charge is a source of electric field that affects electrodynamics in a system such as a composite liquid-solid insulation structure. The net polarization charge produces the polarization field:

$$\vec{P} = (\varepsilon_r - 1)\varepsilon_0 \vec{E} \qquad (2.2)$$

This is dependent on the electric field. A linear combination of the polarization field and the electric field in the form.

$$\begin{aligned} \vec{D} &= \varepsilon_0 \vec{E} + \vec{P} \\ &= \varepsilon_r \varepsilon_0 \vec{E}, \end{aligned} \qquad (2.3)$$

Results in the displacement field, which is a true measure of the total field from both free and polarization charges that can act upon free charge. Thus, the greater a material's relative permittivity ε_r, the greater the total force that acts upon free charge in a system [17].

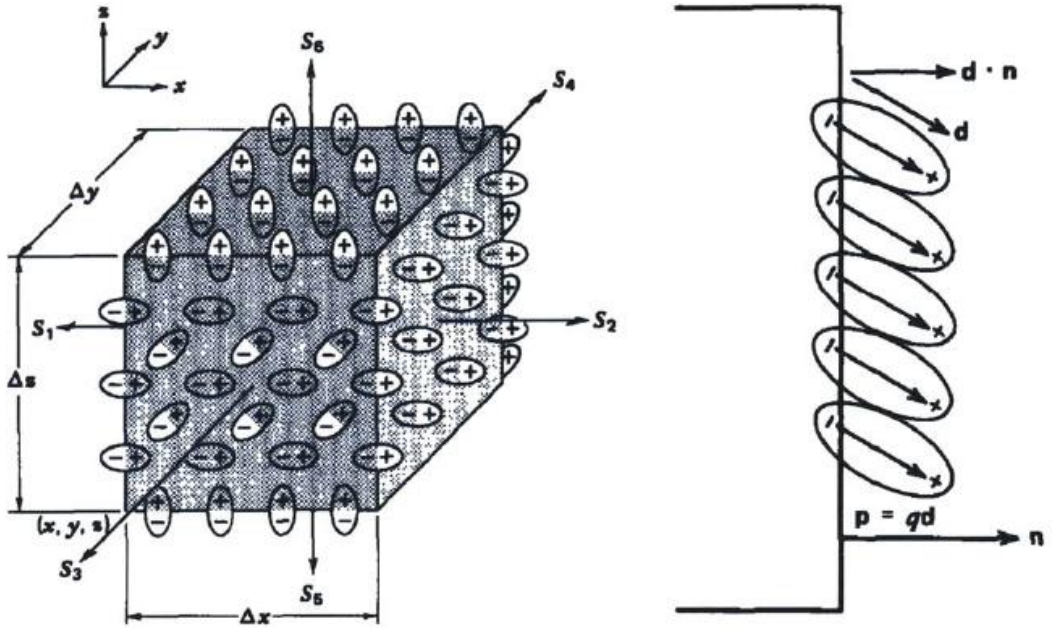

(a) (b)

Figure 2.17 (a) The net charge enclosed within a differential sized volume of dipoles has contributions only from dipoles that are cut by the surfaces. All totally enclosed dipoles contribute no net charge. (b) Only those dipoles within a distance $\vec{d} \cdot \vec{n}$ of the surface are cut by the volume. [17]

CHAPTER 3

Electrohydrodynamics

3.1 BASIC ELECTRODYNAMIC EQUATIONS

The fundamental equations of the electrodynamic model include Poisson's equation and the charge continuity equations. Eqn. 3.1 shows a form of Poisson's equation assuming that both a positive and a negative charge carrier exist in the system. Eqn. 3.2 and 3.3 show the general form of the charge continuity equations for both positive and negative charge carriers, respectively, assuming drift dominated charge transport [62].

$$-\nabla \cdot (\varepsilon \nabla \mathrm{V}) = \rho_+ + \rho_-, \quad \text{where } \vec{E} = -\nabla V \tag{3.1}$$

$$\frac{\partial \rho_+}{\partial \mathrm{t}} + \nabla \cdot \vec{J}_+ = G_{C+} + R_{C+} \tag{3.2}$$

$$\frac{\partial \rho_-}{\partial \mathrm{t}} + \nabla \cdot \vec{J}_- = G_{C-} + R_{C-} \tag{3.3}$$

In Poisson's equation, V represents the electric potential, ε represents the permittivity of the liquid, $\vec{E}$ is the electric field and ρ_+ and ρ_- represent the positive and negative charge densities, respectively. In the charge continuity equations, $\vec{J}_+ = \rho_+ \mu_+ \vec{E}$ and $\vec{J}_- = -\rho_- \mu_- \vec{E}$ represent the positive and negative drift current densities, where μ_+ and μ_- are the positive and negative charge mobility values in the liquid respectively, and G_{C+}, G_{C-}, R_{C+} and R_{C-} represent the generation and recombination terms for the positive and negative charge carriers. Mathematically, Poisson's equation describes the electric field distribution in an electrode system in the presence of free charge carriers, while the charge continuity equations describe how the distributions of free charge carriers are modified by the electric field. Therefore, these electrodynamic equations are coupled and must be self consistently solved. The electrodynamics model taking place in transformer oil or any other dielectric liquid during periods

of significant electrical stress, and then the next step in the process is the identification of sources and sinks of free charge carriers. The sources and sinks of free charge carriers can be broadly categorized as either being bulk effects or boundary effects. The injection of electrons from an electrode into the liquid via Fowler-Nordheim tunneling is an example of a boundary effect and such a source of charge would be accounted for by the setting of boundary and initial conditions for the charge continuity equations. The electric field dependent dissociation of weakly bonded neutral ion pairs in transformer oil under high electric field stresses is an example of a bulk charge generation effect and is accounted for by the generation terms of the charge continuity equations. The recombination of positive and negative ions to form neutral species is accounted for by the recombination terms of Eqn. 3.2 and 3.3.

3.2 CHARGE CARRIER GENERATION

3.2.1 CHARGE INJECTION BY ELECTRIC FIELD EMISSION

In generally, electrons are released from the metal electrode surface due to high electrostatic fields over $1\sim10\times 10^{8}\ \mathrm{V/m}$ as shown in Fig. 3.1. A theory to describe field emission was first developed by Fowler and Nordheim in 1928, hence the process of field emission is often referred to as Fowler-Nordheim field emission, of Fowler-Nordheim charge injection [62, 63]. Fowler and Nordheim's work involved the development of an equation to describe the electric field dependent current density in a vacuum, due to the quantum-mechanical tunneling of electrons from the metal through the potential barrier at the metal/vacuum interface. The level of electron tunneling, which takes place increases exponentially with the electric field level. This is due to the fact that as the field level increases the potential barrier at the metal/vacuum interface narrows, leading to an exponential increase in the probability of electrons tunneling through the barrier. The electron current was measured by Fowler and Nordheim. Electrons in the proximity of the Fermi level may have the probability of passing through the barrier – a phenomenon known as the "tunnel effect". The basic equation for the emission current by the influence of electric field can be expressed as follows:

$$J_{\mathrm{FE}} = \frac{e^3|\overrightarrow{E}|^2}{8\pi h\emptyset}\exp\left(-\frac{8\pi\sqrt{2m}\emptyset^{\frac{3}{2}}}{3he|\overrightarrow{E}|}\right) \tag{3.4}$$

Where, J_{FE} is the emitted current density, e is the magnitude of electron charge, $|\overrightarrow{E}|$ is the electric field, h is Planck's constant and $\emptyset$ is 4.5 eV. This equation is based on the potential energy distribution at the metal/vacuum interface. Figure 3.2 shows the mechanism of field emission from the metal surface, *W(x)* is potential barrier with applied field: $W(x) = -e|\vec{E}|x,\ x > 0$. This potential energy distribution is known as the "Triangular Barrier Approximation", which overestimates the potential barrier height at the metal/vacuum interface. This overestimation arises from the fact that the "Triangular Barrier Approximation" does not take into account the effects of image force barrier lowering caused by the presence of emitted charge in the vacuum. The one dimensional potential energy distribution, *W(x)*, external to the metal/vacuum interface taking into account the image force barrier lowering effects has the following form: $W(x) = -e|\vec{E}|x - \left(\frac{e^2}{16\pi\varepsilon x}\right),\ x > 0$. The shape of the potential energy distribution near the metal/vacuum interface, when image force effects are taken into account is illustrated by the lower trance in Fig. 3.2.

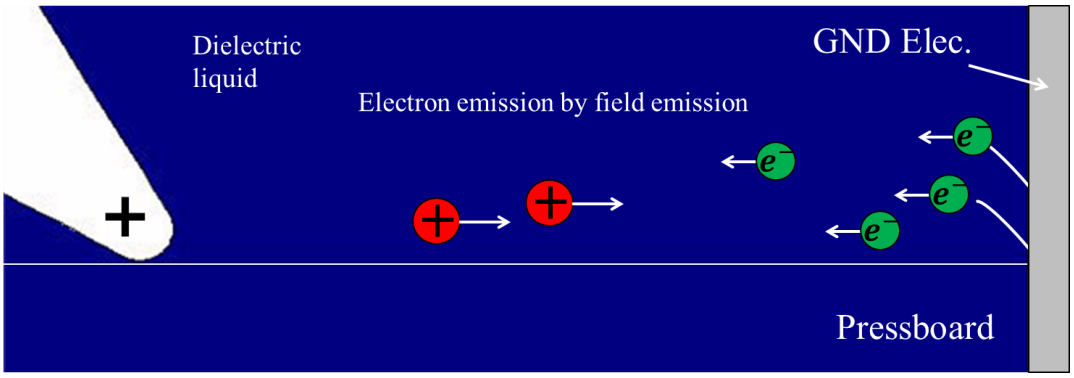

Figure 3.1 Free electron emission from ground electrode under high electric field 1~10× 10^8 V/m

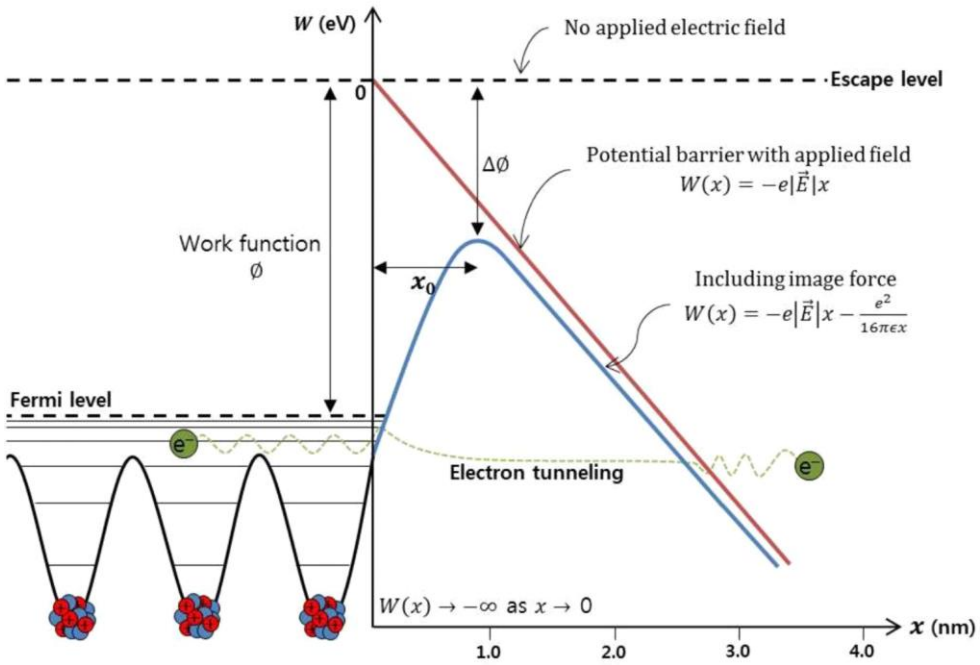

Figure 3.2 Mechanism of field emission from the metal surface [64].

To derive an expression for the emission current let us consider an electron as it leaves the surface in the direction *x* as shown in Fig. 3.2. Electric field can be approximated as that between a point charge and the equipotential planar surface. The field lines here are identical to those existing when an image charge of +e is thought to exist at a normal distance of –x on the other side of the equipotential metal surface. Applying Coulomb's law, the force on the electron in the *x*-direction is given by follows:

$$F(x) = \frac{-e^2}{4\pi\varepsilon_0(2x)^2} = \frac{-e^2}{16\pi\varepsilon_0 x^2} \tag{3.5}$$

The potential energy at any distance *x* is obtained by integrating the above equation from ∞ to *x*.

$$W_{e1} = \frac{-e^2}{16\pi\varepsilon_0 x} \tag{3.6}$$

which gives a parabola shown by curve 1 of Fig. 3.2. The effect of the accelerating external field when applied at right angles to the cathode surface gives the electron a potential energy

$$W_{\mathrm{E}} = -eEx \tag{3.7}$$

which is a straight line shown by Fig. 3.1 (red line). The total energy is then

$$\mathrm{W} = W_{\mathrm{a}} + W_{\mathrm{E}} = -\left(\frac{-e^2}{16\pi\varepsilon_0 x}\right) - eEx \tag{3.8}$$

which shown the resultant blue line (Fig. 3.2). Thus a marked reduction ΔW in the potential barrier is obtained. The maximum reduction at x_m is obtained by differentiating equation (3.8) or

$$\frac{dW}{dx} = \frac{e^2}{16\pi\varepsilon_0 x_{\mathrm{m}}^2} - eE = 0$$

$$x_m = \sqrt{\frac{e}{16\pi\varepsilon_0 E}}$$

Inserting this value into Eqn. (3.8) the lowering in the work function becomes

$$\Delta\mathrm{W} = -\mathrm{e}\sqrt{\frac{eE}{4\pi\varepsilon_0}} \tag{3.9}$$

Hence, the effective value of the work function is

$$W_{eff} = W_{\mathrm{a}} - \sqrt{\frac{eE}{4\pi\varepsilon_0}} \tag{3.10}$$

and the saturation current due to electron emission using Eqn. (3.14) in the presence of field E becomes

$$J_{\mathrm{s}} = AT^2 exp\left[-\frac{e}{kT}\left(W_{\mathrm{a}} - \sqrt{\frac{eE}{4\pi\varepsilon_0}}\right)\right] \tag{3.11}$$

which is known as the Schottky's equation. If the current density in the absence of external field is J_0 (Eqn. (3.14)) then rearranging (3.11)

$$J_s = J_0 \, exp\left[\frac{e}{kT}\left(-\sqrt{\frac{eE}{4\pi\varepsilon_0}}\right)\right] \tag{3.12}$$

To obtain emission current *J* significantly higher than J_0, E must be of the magnitude of 10 MV/cm or higher. In practice a significant field emission current may be observed at lower fields. A few electrons in a metal will have energy slightly above the Fermi level and thus will have a greater probability to penetrate the potential barrier "tunnel effect".

3.2.2 CHARGE INJECTION BY THERMAL ELECTRON EMISSION

In metals at room temperature the conduction electrons will not have sufficient thermal energy to leave the surface. The emission current is related to the temperature of the emitter by the Richardson relation for thermionically emitted saturation current density:

$$J_{\mathrm{TH}} = \frac{4\pi mek^2}{h^3} T^2 exp\left[-\frac{W_a}{kT}\right] \tag{3.13}$$

where *e* and *m* are the electronic charge and mass respectively, *h* is Planck's constant, *k* Boltzmann's constant, *T* the absolute temperature and W_a the surface work function. *A* is Richardson constant ($A = \frac{4\pi mek^2}{h^3}$).

the above expression becomes

$$J_{\mathrm{TH}} = \mathrm{A}T^2 exp\left[-\frac{W_a}{kT}\right] \tag{3.14}$$

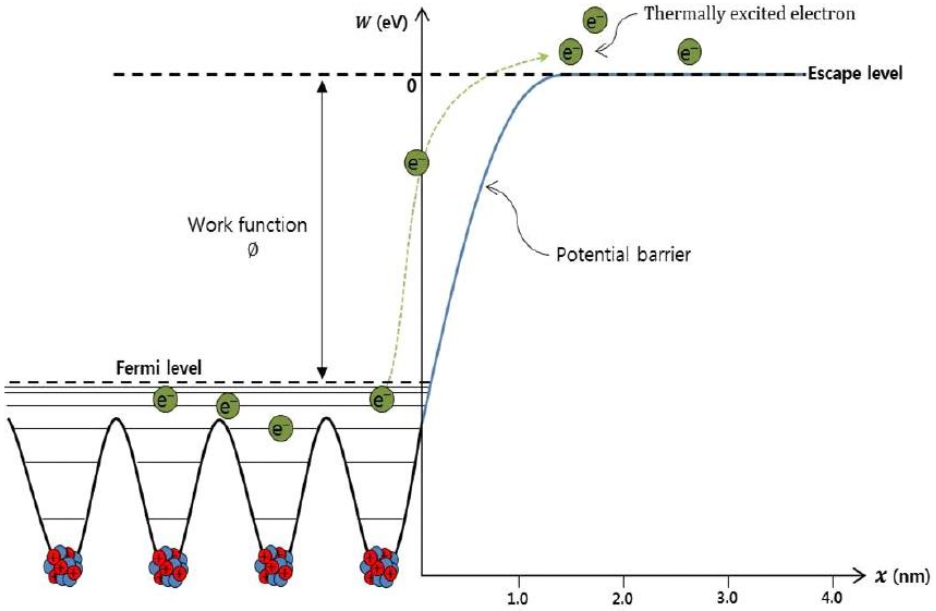

Figure 3.3 Schematic diagram of thermionic emission from the metal surface [64]

3.2.3 MOLECULAR IONIZATION BY ELECTRIC FIELD

Electric field dependent molecular ionization, also known as field ionization, is a direct ionization mechanism, where an extremely high electric field level results in the elevation of a valence band electron in a neutral molecule to the conduction band, thus generating both a free electron and positive ion. This differs from electric field dependent ionic dissociation where the dissociation of a neutral molecule produces a free negative ion and positive ion, which are both relatively large and immobile compared to electron. For field ionization, the asymmetry in the generated carriers mobility values leads to the formation of significant space charge densities in electrically stressed dielectric liquids within the timescales associated with streamer initiation and growth [16]. This process is illustrated graphically in figures 3.4 (a) and (b)

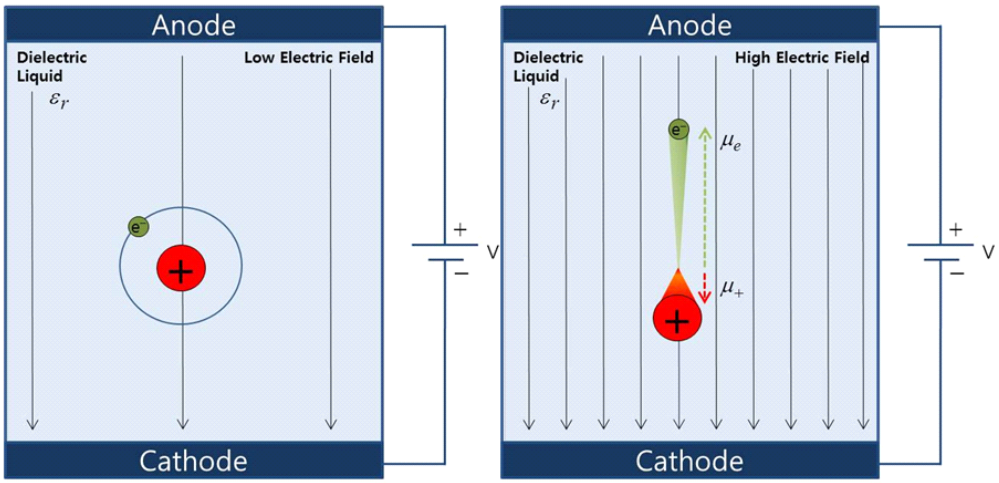

(a) Case of low electric field (b) Case of high electric field

Figure 3.4 Molecular ionization by electric field [64].

In the case of low external electric field (Fig. 3.4 (a)), when the combined force between electron and positive ion is stronger than that of external applied force, the charges are chemically bonded stably in the insulating oil. Therefore, there are a lot of neutral molecules.

Whereas, in high external electric field (Fig. 3.4 (b)) where collisions occur between neutral molecules and free electrons accelerated in the high electric field. The collisions energize a valence electron in the neutral molecule promoting it to the conduction band and generating a positive ion and another free electron [17]

The development of a model that describes the process of field ionization in dielectric liquids, such as transformer oil, is challenging due to the lack of a comprehensive liquid-state theory. Consequently, the literature contains very few publications that propose liquid phase field ionization models. The models that do exist are based on Zener's theory of electron tunneling in solids [17, 65-69].

In their ground breaking work, Devins, Rzad and Schwabe [68] applied the Zener model to dielectric liquids to explain discharge propagation. In this work, the field ionization charge density generation rate source term is

$$G_F\left(\left|\vec{E}\right|\right) = \frac{q^2 n_0 a\left|\vec{E}\right|}{h} exp\left(-\frac{\pi^2 m^* a\Delta^2}{qh^2\left|\vec{E}\right|}\right) \tag{3.15}$$

a is the molecular separation distance, h is Planck's constant, m^* is the effective electron mass, n_0 is the number density of ionizable species, and Δ is the ionization potential. The material parameters for the transformer oil used in Eqn. (3.15) are shown in Table 3.1. The material parameters should be changed

according to the purity and chemical composition of insulating oil, and the material information of pure transformer oil used in this paper has been proved by J. G. Hwang [17, 38, 40]. To apply the ionization ratio by the external electric field to the insulation oil, it is expressed as Eqn. (3.15) by multiplying the ionizable density of electrons and molecules.

$$G_I\left(\left|\vec{E}\right|\right) = e^2 n_0 \gamma\left(\left|\vec{E}\right|\right) = \frac{e^2 n_0 a\left|\vec{E}\right|}{h} exp\left(-\frac{\pi^2 m^* a \Delta^2}{e h^2 \left|\vec{E}\right|}\right) \qquad (3.16)$$

n_0 is the number density of ionizable molecules. Because commonly used dielectric liquids such as transformer oil are very complex liquids there will be a number of individual molecular ionization source terms in play at any one time, with the dominant one being dependent upon the level of the electric field stress. In order to very accurately develop a molecular ionization model for such liquids it is necessary to know the concentrations and ionization potentials of the individual molecules which make up the liquids. This type of information is usually unavailable, particularly for commercially used liquids like transformer oil and so for simulation purposes a reasonable aggregate source term is used [62].

Table. 3.1 Characteristic values of pure transformer oil [1, 17, 38, 67-84]

Parameter	Symbol	Value	Reference
Permittivity of transformer oil	$\varepsilon_{\mathrm{oil}}$	2.2	
Positive ion mobility	μ_{p}	$5 \times 10^{-9}\ m^2 s^{-1} V^{-1}$	[79]
Negative ion mobility	μ_{n}	$5 \times 10^{-9}\ m^2 s^{-1} V^{-1}$	[79]
Electron mobility	μ_{e}	$1 \times 10^{-3}\ m^2 s^{-1} V^{-1}$	[67, 71, 72]
Ion-ion recombination	R_{pn}	9.908× $10^6\ m^3 s^{-1} mol^{-1}$	[73, 83, 84]
Ion-electron recombination	R_{pe}	9.908× $10^6\ m^3 s^{-1} mol^{-1}$	[70, 84]
Electron attachment time	τ_{a}	$1.55 \times 10^{-7}\ s$	[70, 84]
Density of ionisable species	N_0	$0.16603\ \mathrm{mol} \cdot m^{-3}$	
Molecular separation distance	a	$3 \times 10^{-10}\ m$	
Effective electron mass	m^*	9.11×10^{-32} kg	
Molecular ionization energy	Δ	5.12 eV	
Specific heat capacity of oil	C_{p}	$1870\ \mathrm{J} \cdot kg^{-1} \cdot K^{-1}$	
Thermal conductivity of oil	k_{T}	$0.13\ \mathrm{W} \cdot m^{-1} \cdot K^{-1}$	
Mass density of oil	ρ_{oil}	$880\ \mathrm{kg} \cdot m^{-3}$	

3.2.4 DISSOCIATION OF ION BY ELECTRIC FIELD AND TEMPERATURE

Onsager developed a theory which describes how the conductivity of a weak electrolyte is dependent upon the level of electric field stress to which the liquid is subjected [70]. In this theory, highly purified state of transformer oil contains impurities that can undergo chemical reaction leading to space charge generation. The neutral molecule of the impurity can dissociate into positive and negative ions and then free ions can generate electric conductivity by dissociation of oils, and charges having different polarities are recombined into ion pairs as follows [17, 70-79].

$$A^+B^- \underset{k_R}{\overset{k_D}{\rightleftharpoons}} A^+ + B^- \tag{3.17}$$

Equation (3.17) describes that A^+B^- is neutral ion pairs, A^+ and B^- are positive ion and negative ion according to dissociation rate constant, K_D and recombination rate constant, K_R, respectively.

The rate at which neutral ion-pairs dissociate to form free ions and the rate at which free ions recombine to form neutral ion-pairs is controlled by two kinetic rate constants, K_D for dissociation and K_R for recombination. According to Onsager's theory, the value of the dissociation constant K_D, is dependent upon the applied electric field, while the recombination constant K_R, is electric field invariant. The electric field dependence of the dissociation constant results in an increase in the concentration of free ions, and thus the conductivity of the liquid increases as the electric field increases [62].

With the presence of external electric field, the dissociation rate constant K_D has the following form:

$$K_D = K_D^0 f\left(\left|\vec{E}\right|, T\right) \tag{3.18}$$

Where K_d^0 is the zero field dissociation constant (s^{-1}) and $f\left(\left|\vec{E}\right|\right)$ is the electric field dependent function, which relates the increase in the dissociation rate to the electric field level. The electric field dependent function is defined as:

$$f\left(\left|\vec{E}\right|\right) = \frac{I_1(4b)}{2b} \tag{3.19}$$

Where,

$$\mathrm{b} = \sqrt{\frac{q^3\left|\vec{E}\right|}{16\pi\varepsilon_0\varepsilon_r k^2 T^2}} \tag{3.20}$$

where, I_1 is modified Bessel function of the first kind, k is the Boltzmann's constant and T is the absolute temperature (K). Onsager's theory of electric field enhanced ionic dissociation has been used by several authors to describe electrical conduction in non-polar liquids, particularly transformer oil which is often classified as a weak electrolyte due to the unavoidable presence of non-hydrocarbon based impurities in the oil [62, 80-82]. In thermal equilibrium and when not being stressed by an applied electric field, the following relation describes the relative concentrations of neutral ion-pairs and free ions, or free charge carriers in transformer oil:

$$\mathrm{c}K_D^0 = n_{\pm 0}^2 K_R \tag{3.21}$$

where c is the density of neutral ion pairs, $n_{\pm\,0}$ is the equilibrium free ion concentration in the absence of the electric field in the transformer oil. The recombination rate constant, K_r is related to the permittivity and mobility by the Langevin relation as the following [83]:

$$K_R = \frac{e_0}{\varepsilon}(\mu_+ + \mu_-) \tag{3.22}$$

where μ_+ and μ_- are the mobility of free positive ion and negative ion in transformer oil, respectively. In order to develop insight into whether or not electric field enhanced ionic dissociation plays a significant role in the initiation and growth of streamers in transformer oil, it is necessary to characterize the parameter cK_D, as this term represents the free charge carrier source term in the transformer oil. This characterization can be accomplished by using the low field conductivity value of transformer oil. The conductivity of transformer oil is measured to verify the effect of ion dissociation during discharge inception and propagation in insulation oil. The initial concentration of ionic species can be obtained from the medium's conductivity using the following expression [83]:

$$\sigma = \mathrm{e}(\mu_+ n_{+\,0} - \mu_- n_{-\,0}) \tag{3.23}$$

where, $n_{+\,0}$, $n_{-\,0}$ are the equilibrium free ion concentration in the absence of an electric field and oil concentration. σ is conductivity of insulation oil in the absence condition of electric field. Assuming that negative ion and positive ion are at the same energy level, the free ion concentration in the insulation oil without the influence of electric field condition as following:

$$n_{\pm\,0} = \frac{\sigma}{e(\mu_+ + \mu_-)} \tag{3.24}$$

The concentration of the free ions in the absence of the electric field is substituted into the Eqn. (3.18) as following:

$$cK_D^0 = \left(\frac{\sigma}{e(\mu_+ + \mu_-)}\right)^2 K_R \tag{3.25}$$

The complete charge generation mechanism on ion dissociation by the electric field is given by equation (3.23) that is combined with Eqns. (3.25) and (3.18).

$$cK_D = \left(\frac{\sigma}{e(\mu_+ + \mu_-)}\right)^2 K_R \times f\left(|\vec{E}|, T\right) \tag{3.26}$$

The electric field dependent ionic dissociation process, which is described above is a bulk charge generation mechanism, meaning that when modeling the process, the term cK_D represents the generation term in the charge continuity equations for both the positive and negative ions. This is contrast to the case of field emission or Fowler-Nordheim charge injection. Forwler-Nordheim charge injection is a boundary process and so no bulk generation term exists in the continuity equation for the injected electron.

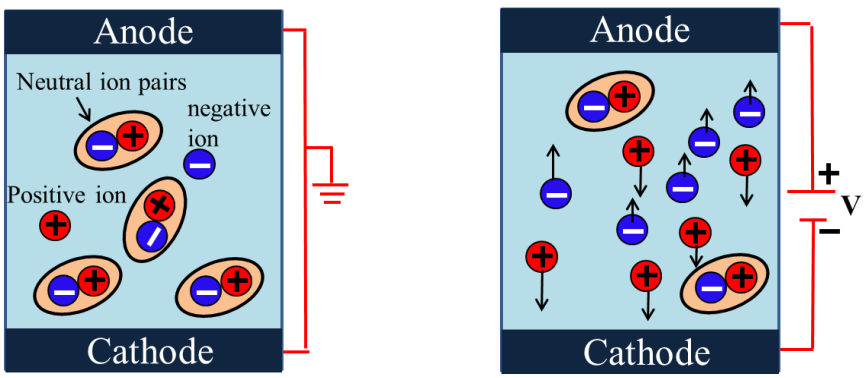

(a) Without external electric field (a) With external electric field

Figure 3.5 Ionic dissociation by electric field [amended from 64]

When there is no external electric field (Fig. 3.5 (a)), the positive ion and the negative ion are in a stable state; there are many neutral ion pairs. Whereas, when the external energy becomes larger than the bonding energy of neutral ion pairs, they are detached from each other as shown in Fig. 3.5 (b). On the other hand, the increase of free ions caused by dissociation increases the conductivity of the fluid [64].

3.3 CARRIER RECOMBINATION

During the formation and growth of a streamer there will exist concentrations of free positive ions and electrons in the dielectric liquid. These free charge carriers are produced due to molecular ionization as discussed in the previous section. The interaction of these free charge carriers with each other and the surrounding media can be assumed to open up the possibility of electron-ion recombination, electron attachment to neutral species, forming negative ions and ion-ion recombination as shown in Fig. 3.6. When developing an electrodynamic model for streamer initiation and growth in dielectric liquids it is important to include, when relevant such processes [62].

By transferring the electron, recombination occurs between positively and negatively charged particles. A photon may be released from this process [83]. The Langevin-Debye relationship is used to model positive ion-negative ion R_{pn} and positive ion-free electron R_{pe} recombination rates in the transformer oil (thus reducing the number of electrons and increasing the number of negative ions in the liquid dielectric) [1, 17 38, 84-86]. According to the Langevin-Debye relationship, the recombination rates can be expressed as

$$R_{pn} = \frac{q(\mu_p + \mu_n)}{\varepsilon} \tag{3.27}$$

$$R_{pe} = \frac{q(\mu_p + \mu_e)}{\varepsilon} \tag{3.28}$$

The ion-electron recombination rate of Eqn. (3.28) is overestimated because the Langevin-Debye relationship is diffusion limited and valid for situations where the electric field levels are low to moderate and the recombining species are of similar physical scale [17, 85].

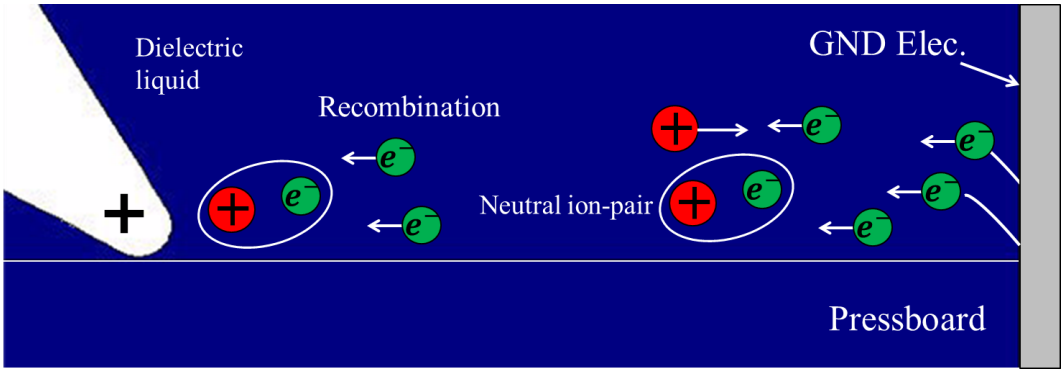

Figure 3.6 Recombination process in mineral oil

3.4 ELECTRON ATTACHMENT

In addition to recombination, electrons also combine with neutral molecules to form negative ions. This process is modeled as an electron attachment time constant. In very pure hydrocarbon liquids, energetic electrons have attenuation lengths on the order of several centimeters, meaning that an electron can be expected to travel for several centimeters in the liquid from the point where it was formed before it attaches to a neutral molecule to form a negative ion [85]. In commercial dielectric liquids, the attenuation length will be shorter due to higher levels of impurities in the liquid [17, 87]. The attachment time constant is simply the quotient of the electron attenuation length and the electron velocity. A representative set of numbers for such a calculation are: An electron attenuation length λ_a of 1 mm, an electron mobility μ_e of 1×10^{-4} $\mathrm{m^2V/s}$ and an electric field strength $\left|\vec{E}\right|$, of 5×10^7 $\mathrm{V/m}$. These numbers give an attachment time τ_a of:

$$\tau_a = \frac{\lambda_a}{\mu_e \left|\vec{E}\right|} = \frac{1 \times 10^{-3}}{5 \times 10^3} = 2 \times 10^{-7}\ (\mathrm{s}) \qquad (3.29)$$

This value for τ_a corresponds well with the attachment time constants used by other authors in the literature [17, 84-87]. Although attachment undoubtedly takes place during streamer growth in dielectric liquids, its impact on the overall streamer propagation process is reasonably small due to the fact that attachment processes take place on a longer time scale than important dynamics such as the separation of positive ions and electrons in the ionization zone at a streamer's tip [87].

3.5 ION AND ELECTRON MOBILITY VALUES

During the course of the research being presented in this thesis, the ion and electron mobility values in transformer oil $\mu_{\pm}$ and μ_e, respectively, are used as input parameters for all electrodynamic simulations. A mobility values of $1 \times 10^{-9}\ \mathrm{m^2/V \cdot s}$ is used for the positive and negative ions in all simulations. This value has been verified experimentally for transformer oil in [82]. It is also in agreement with the theoretical analysis presented in [88]. A mobility value of $1 \times 10^{-4}\ \mathrm{m^2/V \cdot s}$ is used electrons in all simulations. This value corresponds with the data presented in [86] and the electron mobility model described in [89].

3.6 SUMMARY

This chapter discussed the electrodynamic processes associated with the generation and recombination of free charge carriers in transformer oil when the oil is electrically over stressed. Three charge injection and charge generation mechanisms, which are commonly suggested as playing a role in streamer occurrence, development and initial electric field distribution. The dissociation process of dielectric liquids is explained by Onsager theory that highly purified state of transformer oil contains impurities and then mineral oil can undergo chemical reaction leading to space charge generation. The neutral molecule of the impurity can dissociate into positive and negative ions and then free ions can be generated by dissociation of oils.

Sections 3.3 and 3.4 discussed the charge recombination and attachment processes that can take place in transformer oil. The diffusion based Langevin recombination process for the recombination of positive and negative charge carriers was described. When developing an electrodynamic model for streamer initiation and growth in dielectric liquids, it is important process.

The electrohydrodynamics model is directly relevant to numerical simulation model development that has been undertaken as Chapter 3.

CHAPTER 4

Creepage Discharge Characteristics at Oil/pressboard Interface by Nanocomposite Coating Method

4.1 INTRODUCTION

This chapter deals with experimental characterization of creepage discharge to improve the electrical characteristics of oil/pressboard (PB) composite insulation system by solid layer coating method such as epoxy resin, Teflon and silica/epoxy nanocomposite on PB surface under positive standard lightning impulse voltage. Electrode arrangement used in experiment is a rod-plane and needle-bar electrode arrangement in transformer mineral oil. As well known, the PB surface conditions influence partial discharge inception voltage (PDIV) and creepage discharge properties.

Lightning impulse voltage withstanding property is one of important characteristics in power apparatus. In addition, engineers want to predict the discharge initiation, development and propagation in composite insulation system under lightning impulse for upgrading the insulation design of power apparatus. For these reasons, a lot of researchers have recently been devoted to improve the dielectric properties of insulating oil by adding specific functional additives into the oil. However, few studies have been focused on modifications of the insulating paper in order to improve insulating ability.

From the above view point, creepage discharge properties of conventional PB are compared with solid layer coated PB, in terms of discharge propagation length (l_d) and discharge occurrence probability (P_d). As a result, it is found that discharge occurrence probability of solid layer coated PB increases at all applied impulse voltage levels depending on coated material and silica filler loading (S_l) compared with that of conventional PB. The result is interpreted in terms of dielectric property effect, surface modification effect, electron suppression effect by silica/epoxy nanocomposite coating on PB surface.

4.2 EXPERIMENT SETUP

Figures 4.1 (a) and (b) show experimental setup as type 1 side view and top view of electrode system, respectively. The diameter of the rod electrode and plane electrode was 6 and 70 mm, respectively. The rod electrode is placed so that the tip touches the pressboard surface. The position of pressboard and electrode configuration in the experimental system determines the electric field distribution at the oil/pressboard interface. On the other hand, a more directional and intense electric field is created towards the solid surface from localized and inhomogeneous electric field at the edge of the rod electrode compared to other methods. But, the creepage discharge do not always propagate radially in this electrode configuration. For this reason, it is difficult to evaluate the discharge propagation length.

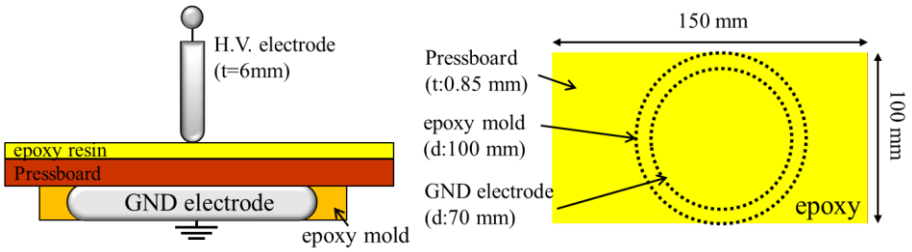

(a) Side view (b) Top view

Figure 4.1 Rod-plane electrode configuration (type 1)

In the case of needle-bar electrode configuration as type 2 (Figs. 4.2 (a) and (b)), the tip radius of the needle electrode was 10 μm and gap distance 50 mm to the bar electrode. To generate the creepage discharge in one direction, we used guide electrode beneath a PB. The needle electrode was placed at an angle of 30 degree from the surface of a specimen with the needle tip touching the pressboard surface. These above two methods have been widely used to study surface discharge phenomena.

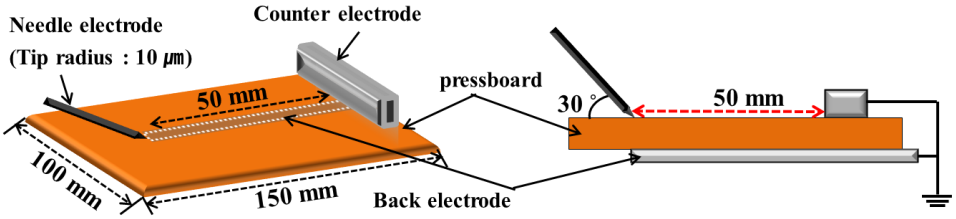

(a) Top view (b) Side view

Figure 4.2 Needle-bar electrode configuration (type 2)

Figures 4.3 (a) to (c) show microscope image of needle electrode before and after impulse experiment and after breakdown. As can be seen in Fig. 4.3 (b), the needle electrode tip is not changed after 400 times impulse voltage, whereas scratches appear nearby needle tip, and the number of scratches and size increased with increasing the number of the applied voltage voltages (average scratch size: 20 μm). But the results revealed that these kinds of scratches nearby the needle tip didn't affect the discharge inception voltage. On the other hand, in Fig. 4.3 (c), the needle tip is mutated after breakdown. The radius of curvature expanded by times 3, affecting the discharge inception voltage. Thus, when the experiment used the needle electrode, it is very important to check the needle electrode tip after experiment. In this work, the needle electrode was checked after every experiment using a microscope to acquire reliable data.

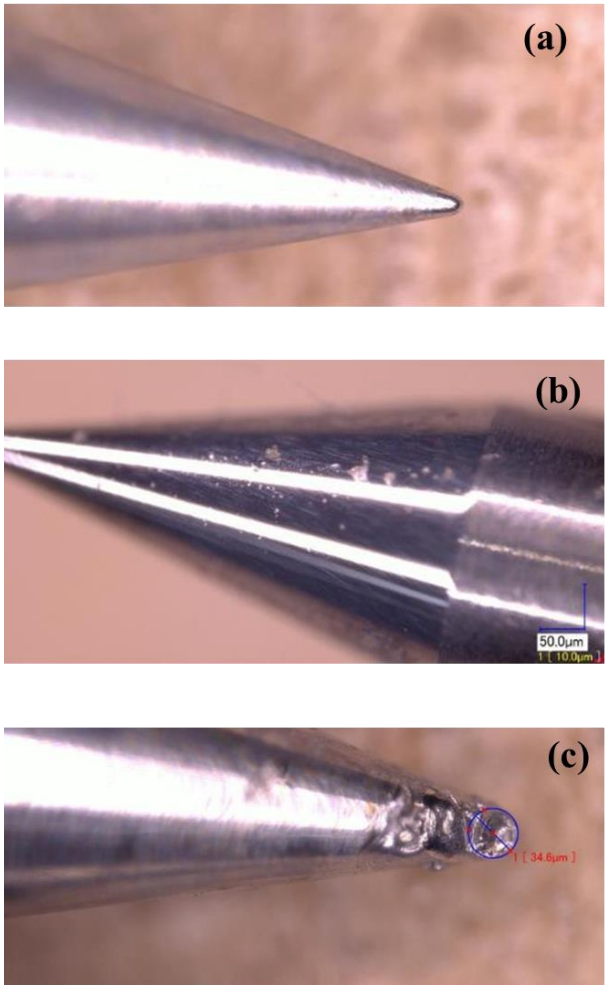

Figure 4.3 Needle electrode (a) before experiment, (b) after experiment and (c) after breakdown

4.3 EXPERIMENTAL PROCEDURE

4.3.1 CREEPAGE DISCHARGE OBSERVATION

Figures 4.4 and 4.5 (a) to (d) show schematic diagram and photograph of the experimental measuring system. Vacuuming was made in the chamber after the test sample was immersed in the insulating oil for three hours to remove moisture and gasses from the insulating oil and fill oil molecules into the PB structure. Discharge image was observed using a digital camera (Fujifilm Finepix S100fs) and usual digital camera equipped with an image intensifier (Hamamatsu C9016-2x series-23). Discharge light emission was also detected with a photomultiplier tube (PMT, Hamamatsu Photonics, H6780-20) to determine PDIV. A 50 Ω resistor was used to obtain the discharge current signal.

A positive standard lightning impulse voltage was applied to the electrode varied from 60 to 100 kV by a step with increment of 20 kV (type 1) and from 20 to 45 kV by a step with increment of 5 kV. The interval time between each voltage level was one minute. The impulse voltage application was repeated 10 times (type 1) and 5 times (type 2) at each voltage level, respectively.

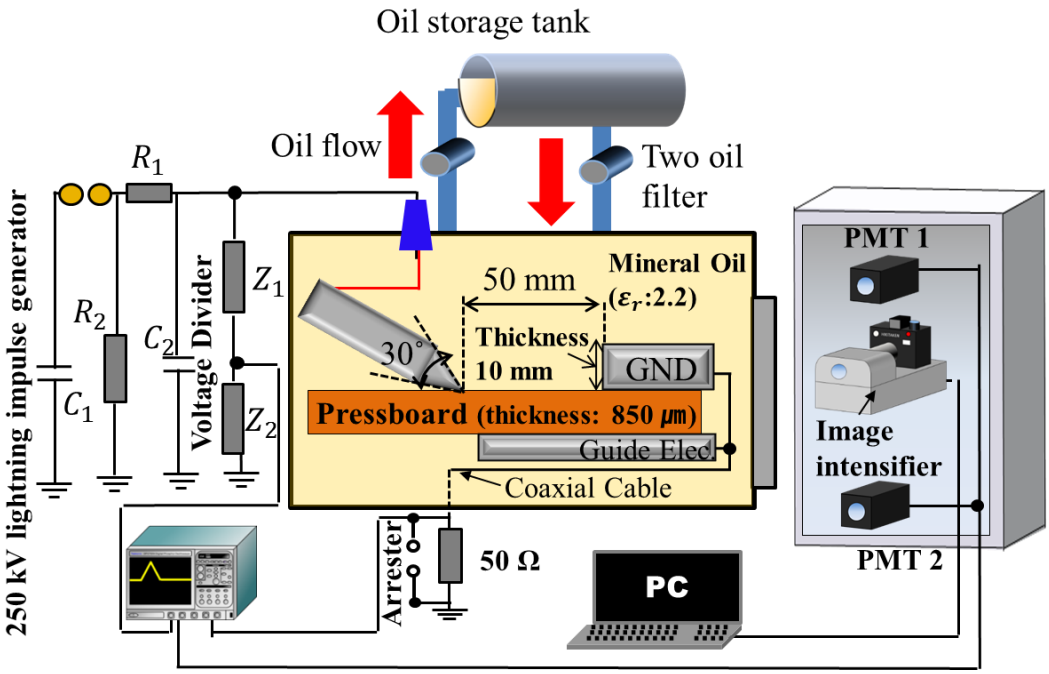

Figure 4.4 Schematic diagram of the experimental setup and measuring system

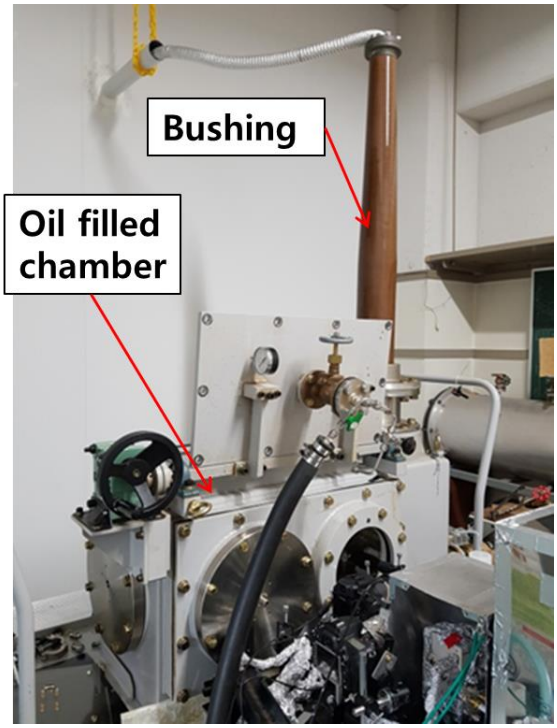

(a) Oil filled chamber

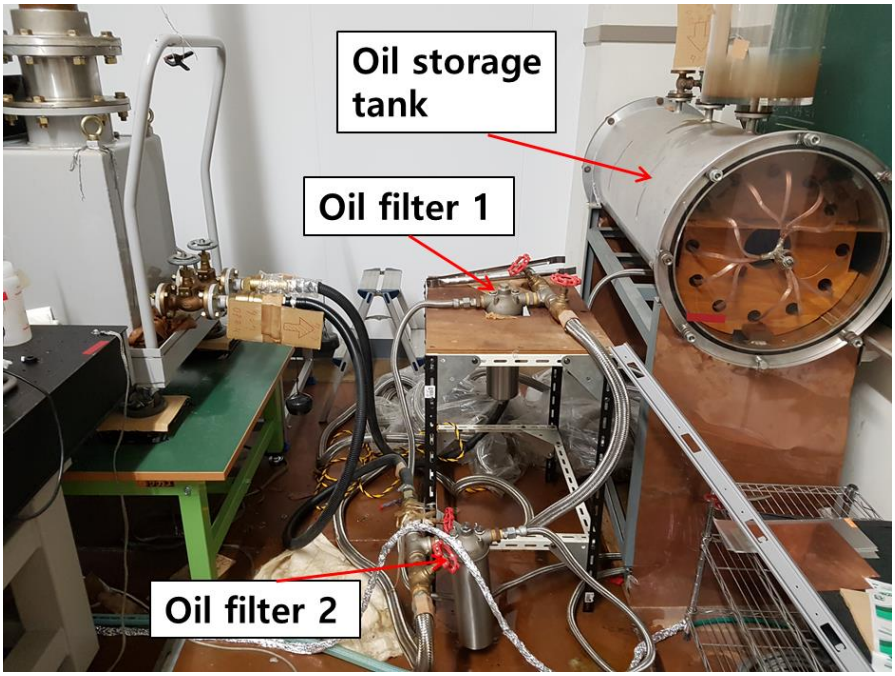

(b) Oil storage tank and two oil filter

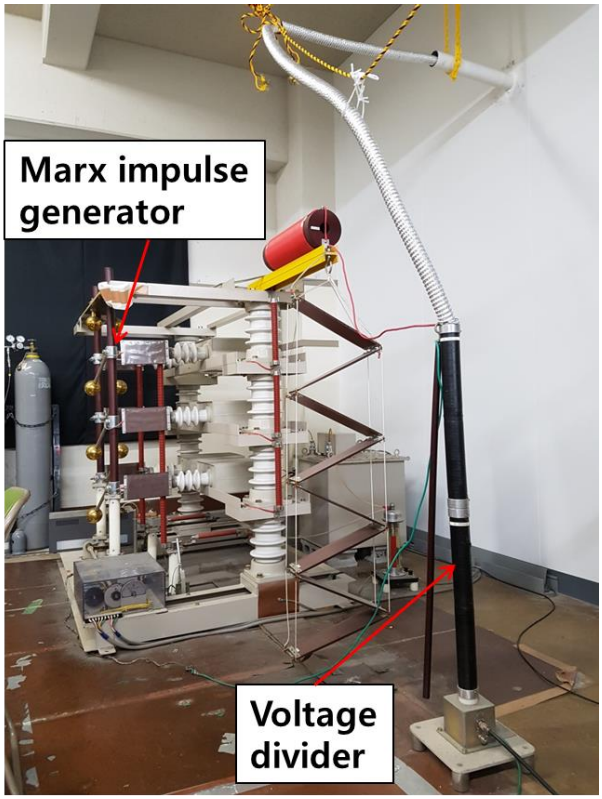

(c) Marx impulse generator and voltage divider

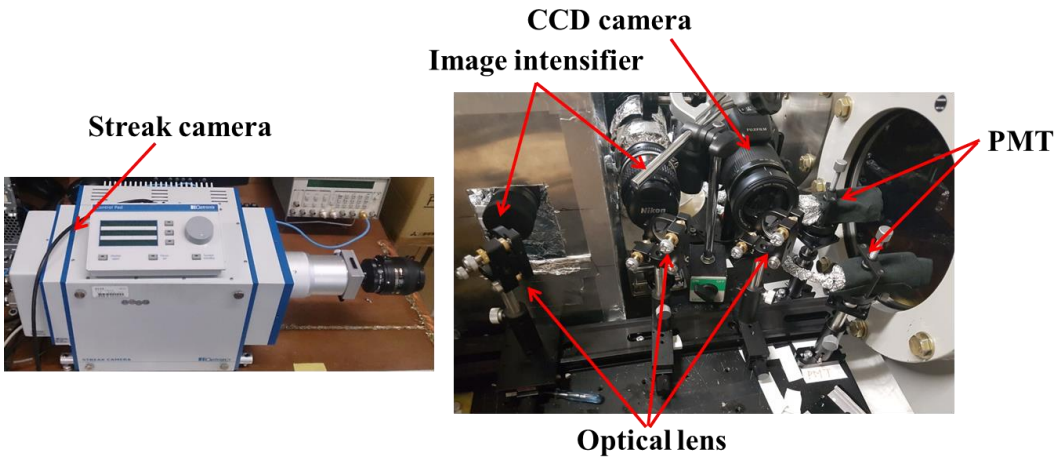

(d) CCD camera, two image intensifier, streak camera, two PMT and three optical lenses

Figure 4.5 Photograph of the experimental system

(a) FINEPIX S100FS

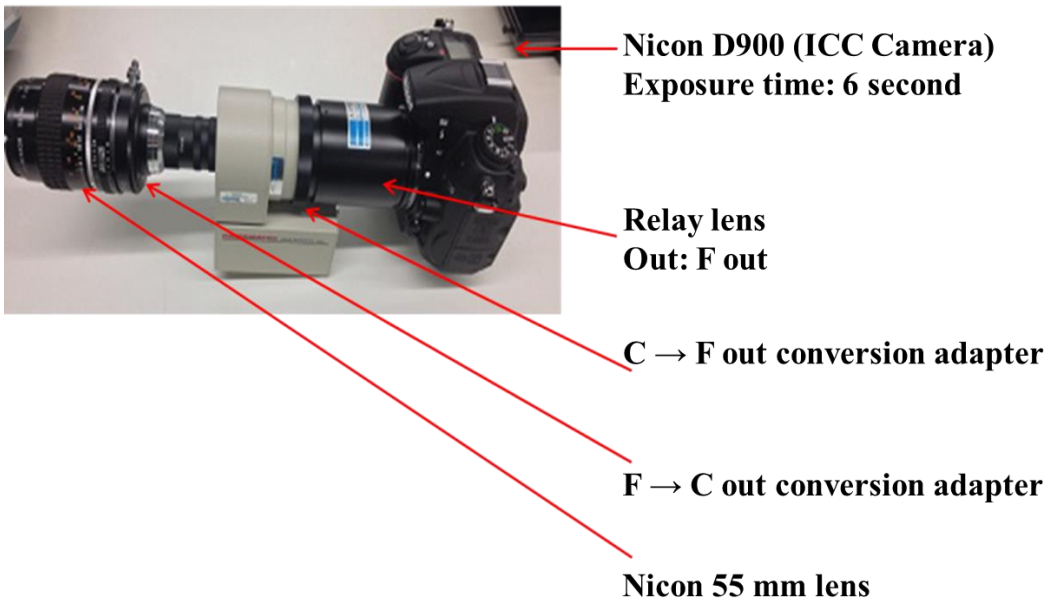

(b) C9016-2X

Figure 4.6 FINEPIX S100FS and image intensifier (I.I)

Table 4.1 Specification of the C9016-2X

Parameter		Type No.	C9016-21 C9546-01 C9547-01	C9016-22 C9546-02 C9547-02	C9016-23 C9546-03 C9547-03	C9016-24 C9546-04 C9547-04	Unit
Photocathode Sensitivity	Luminous Sensitivity (Typ.)		700		230	150	μA/lm
	Radiant Sensitivity[a] (Typ.)	C9016-2x C9546	214		53	47	mA/W
		C9547	192				
	Quantum Efficiency[a] (Typ.)	C9016-2x C9546	50		15	14	%
		C9547	45				
Photocathode	Effective Diameter	C9016-2x C9546	17[b]		17.5[b]		mm
		C9547	25[c]		25[c]		
	Window Material		Borosilicate glass		Synthetic silica		—
	Photocathode Material		GaAsP		Multialkali		—
	Spectral Response		280 to 720		185 to 900		nm
	Peak Wavelength		530		430		
Phosphor Screen	Window Material		FOP				—
	Phosphor Material[b]		P43				—
	Decay Time		See Figure 8				—
Gain	Luminous Gain (Typ.)	C9016-2x	2.2×10^{4}	5.0×10^{6}	1.1×10^{4}	4.0×10^{6}	$(lm/m^2)/lx$
		C9546 C9547	2.0×10^{4}	3.0×10^{6}	1.0×10^{4}	2.4×10^{6}	
	Radiant Emittance Gain[a] (Typ.)	C9016-2x	1.4×10^{4}	3.4×10^{6}	6.8×10^{3}	3.0×10^{6}	$(W/m^2)/(W/m^2)$
		C9546	1.3×10^{4}	2.0×10^{6}	6.2×10^{3}	1.8×10^{6}	
		C9547	1.2×10^{4}	1.9×10^{6}			
Equivalent Background Input (EBI)	Luminous (Typ.)		3×10^{-12}		1×10^{-11}		lm/cm^2
	Radiant[c] (Typ.)		8×10^{-15}		3×10^{-14}		W/cm^2
Limiting Resolution (Typ.)			50	36	57	32	Lp/mm
Image Magnification			1				—
Maximum Input Light Level[b]	Luminous (Typ.)		1.5×10^{-3}	7.0×10^{-6}	5.0×10^{-3}	1.6×10^{-5}	lx
	Radiant[c] (Typ.)		4.0×10^{-10}	1.6×10^{-12}	8.0×10^{-10}	2.4×10^{-12}	W/cm^2
Average of Max. Phosphor Screen Brightness			10				cd/m^2
Power Requirement			100 to 240				V
Power Consumption (Max.)		C9016-2x	4.8				W
		C9546	6	8.4	6	8.4	
		C9547	7.2	10.8	7.2	10.8	
Operating Ambient Temperature			0 to +40				°C
Storage Temperature			-20 to +50				
Operating and Storage Humidity[d]			Below 70				%

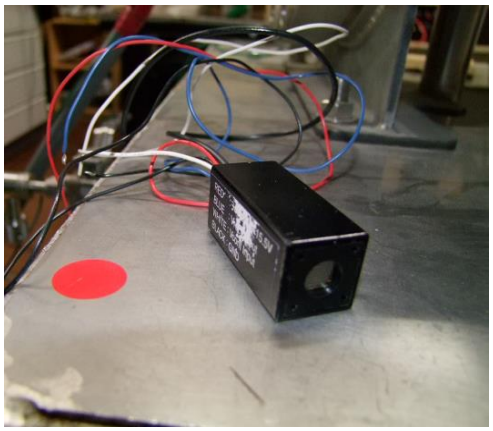

Figure 4.7 Photo multiplier (PMT)

Figure 4.8 Power supply

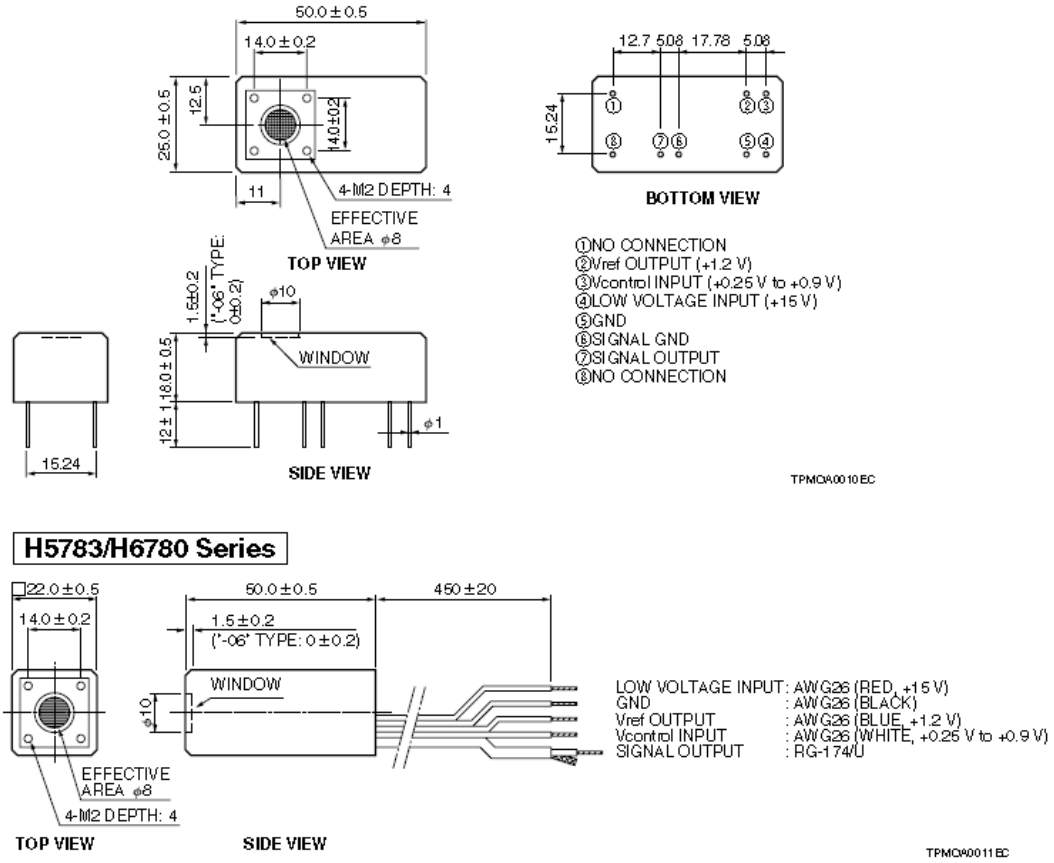

Figure 4.9 Dimensional outlines of PMT

4.3.2 SAMPLE PREPARATION&DIELECTRIC PROPERTY MEASUREMENT

Five kinds of PB samples were used; namely, neat pressboard (NP), dry pressboard (DP), epoxy resin coated pressboard (EP-A and EP-F), Teflon coated pressboard (TP) and pressboard coated by silica/epoxy nanocomposite (SP). Three samples of each specimen were prepared for reproducibility on experiment results. Figure 4.10 shows the schematic diagram to prepare for surface coating on the pressboard surface. In preparing nano silica/epoxy composite, nanoparticles were dispersed in the base epoxy bisphenol A of F type at the proportion of each weight percent using a vacuum mixer. The mass ration of epoxy resin to curing agent is 30:10. EP-A, EP-F and SP specimens were prepared by thinly coating PB surface with bisphenol A type epoxy resin (EP-A), bisphenol F type epoxy resin (EP-F),

silica/bisphenol F type epoxy resin SP, respectively, and then put in a vacuum oven for 30 minute and then being dried using a dry oven for 3 hours at each 70 and 150℃. DP specimen was also dried under the same condition as EP, TP and SP specimen. DP is a reference specimen in this research work. SP specimens with different SiO_2 nano filler contents (0, 0.2, 0.5, 1, 3, 5 and 50wt%) were prepared as shown in Table 4.2. Figures 4.11 (a) and (b) show pressboard samples used in experiment before and after epoxy coating on the one side surface of PB.

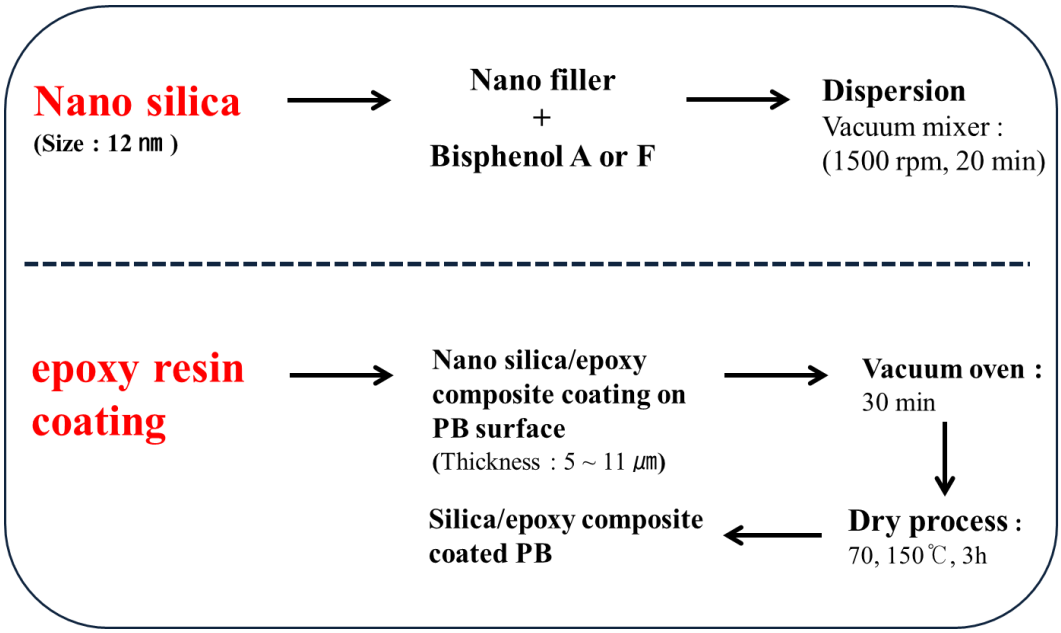

Figure 4.10 Schematic diagrams to prepare for nano silica and epoxy/silica coating on surface of pressboard

Table 4.2 Properties of each specimen

Sample type	Neat PB	Dry PB	Solid layer coating	Teflon Coating	silica/epoxy composites coating
	NP	DP	EP-A, EP-F	TP	SP
					0.2, 0.5, 1, 3, 5, 50 wt% (silica size : 12 nm)
Dry process	Room Temp.	70, 150 ℃ (3h)			

(a) Dry pressboard (DP) (b) Epoxy resin coated PB (EP-F)

Figure 4.11 pressboard samples used in experiment

Figure 4.12 shows the weight and thickness variation of each sample before and after drying process. We confirmed that the average decreasing rate of dried specimen as DP, EP-A, EP-F and SP of weight, thickness and of each specimen decreased by 5.3% and 3%, respectively.

Dielectric properties of each specimen were measured with an impedance analyzer (IWATSU Impedance Analysis PSM3750) at room temperature and frequency from 50 Hz to 2 MHz after the drying process. The number of test samples of each specimen was two. The size and thickness of a sample was 70 mm by 70 mm and 850 μm, respectively. Prior to measurement, gold electrodes with diameter of 50 mm were deposited onto both sides of a sample by Magnetron sputter (MSP-1S) with a thickness of 3 Å for 3 minute to ensure the reproducibility of measurement and improve the contact area between the electrode and the surface of PB. The gold sputtering thickness on the PB surface is 54 nm. The dielectric properties were measured after oil immersion process for 3 hours. Note that measurements of dielectric properties were conducted two times each for two samples with error of 3 %.

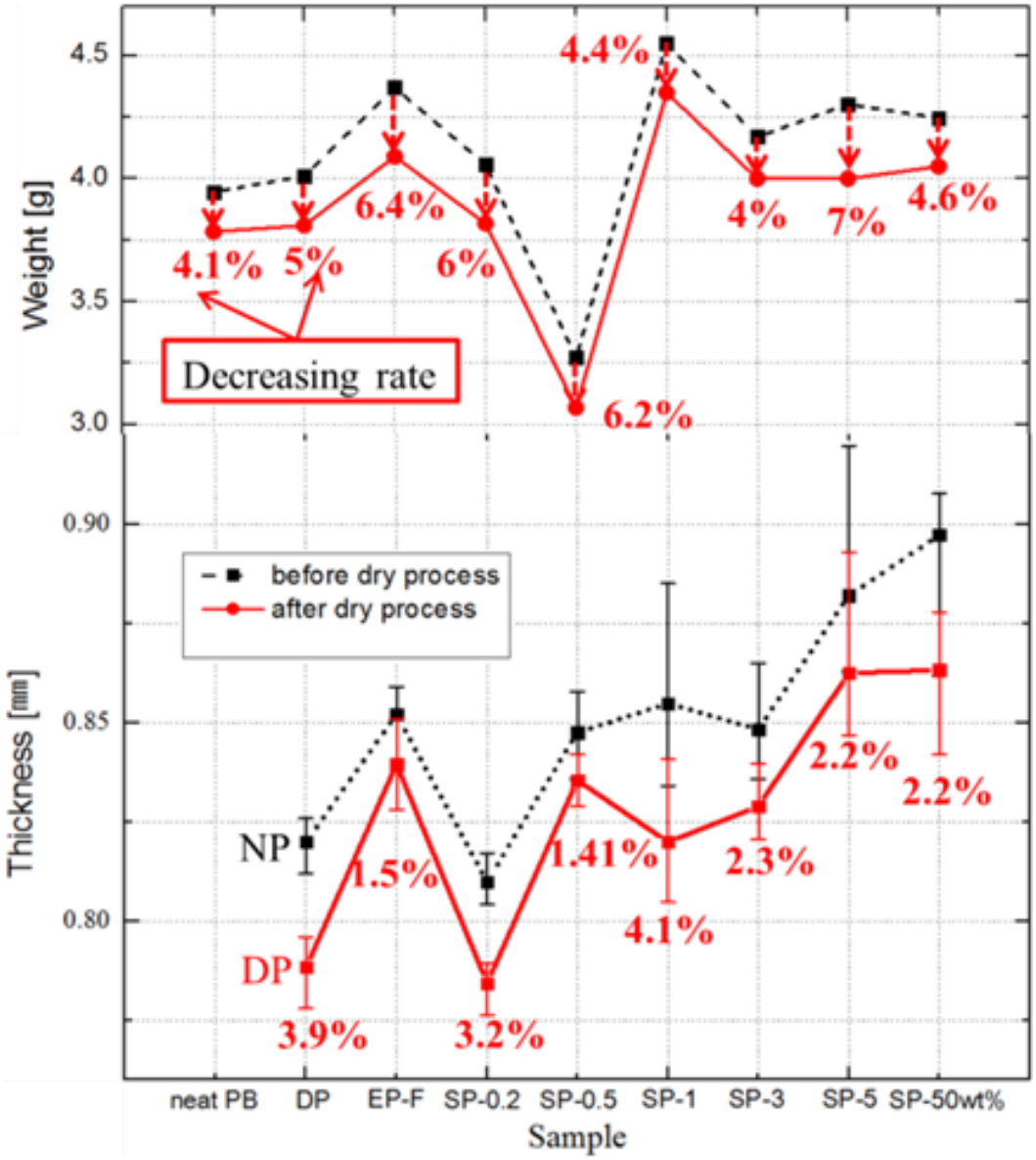

Figure 4.12 Weight and thickness variation of each sample before and after drying process

4.3.3 SURFACE ROUGHNESS AND NANO SILICA DISTRIBUTION STATE

Figure 4.13 shows the surface roughness before and after epoxy resin coating. The result represents an assembly of surface irregularities and constitutes main

surface quality characteristics of each specimen. To characterize the sample surface roughness, the following parameters were used; R_a average surface roughness; and R_z 10 point mean surface roughness. Conventional pressboard have porous, fibrous, protrusions and non-homogenous surface structure. Whereas epoxy resin coated pressboard is smoother than that of conventional PB after new coating method on PB. Figure 4.14 shows R_a and R_z of surface roughness of each type of sample. The surface of NP and DP samples is rougher than that of all the other kinds of the solid layer coating samples (EP-A, EP-F, TP and SP). Therefore, it is found that the solid layer coating provides smoother surface on PB than NP and DP specimen.

Figure 4.15 shown typical SEM image of silica/epoxy nanocomposite. The average thickness of silica/epoxy nanocomposite coating of each sample was 5.4 to 11.9 μm. Note that the thickness of silica/epoxy coating increased with increasing nano particle filler contents. Figure 4.16 shows nano silica dispersion state in base epoxy matrix. As can be seen in Fig. 4.8, low S_l from 0.1 wt% to 5 wt% in the base epoxy matrix exhibit good dispersion of nanoparticles. On the other hand, the nano silica of 50 wt% S_l has formed micro size agglomeration structure in base epoxy resin. In this research, nano silica particles were supplied from Nissan chemical industries. LTD.

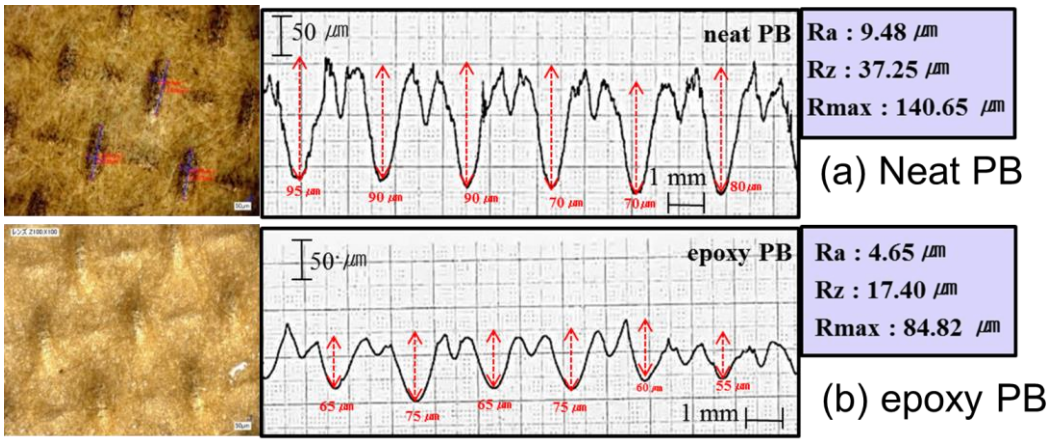

Figure 4.13 Surface roughness before and after epoxy resin coating (a) DP and (b) EP-A

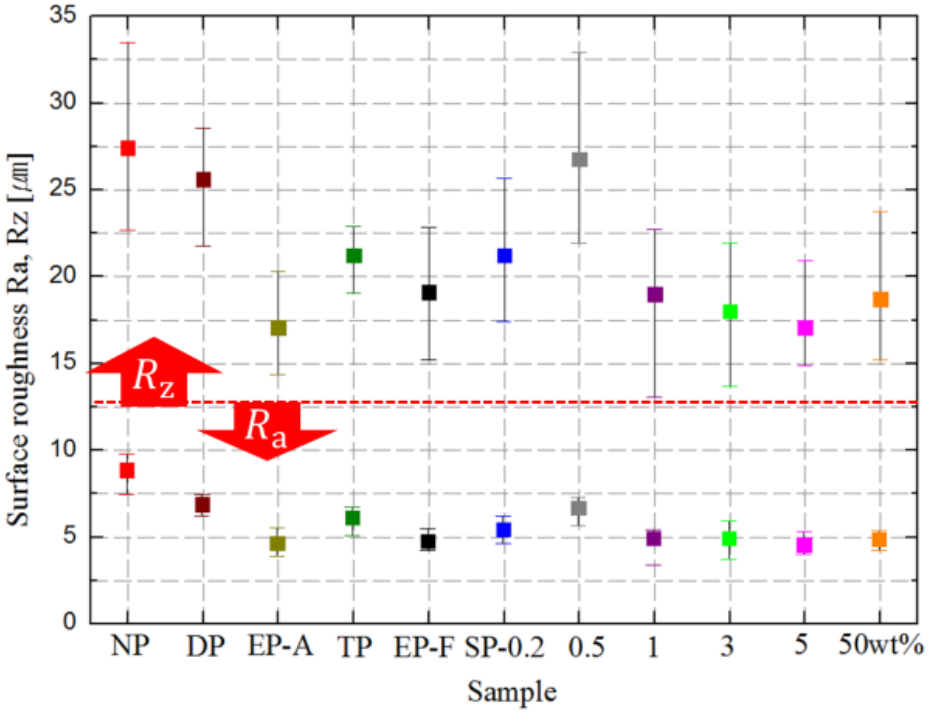

Figure 4.14 Surface roughness of each type of sample measured using a surface roughness tester (bottom: R_a, top: R_z)

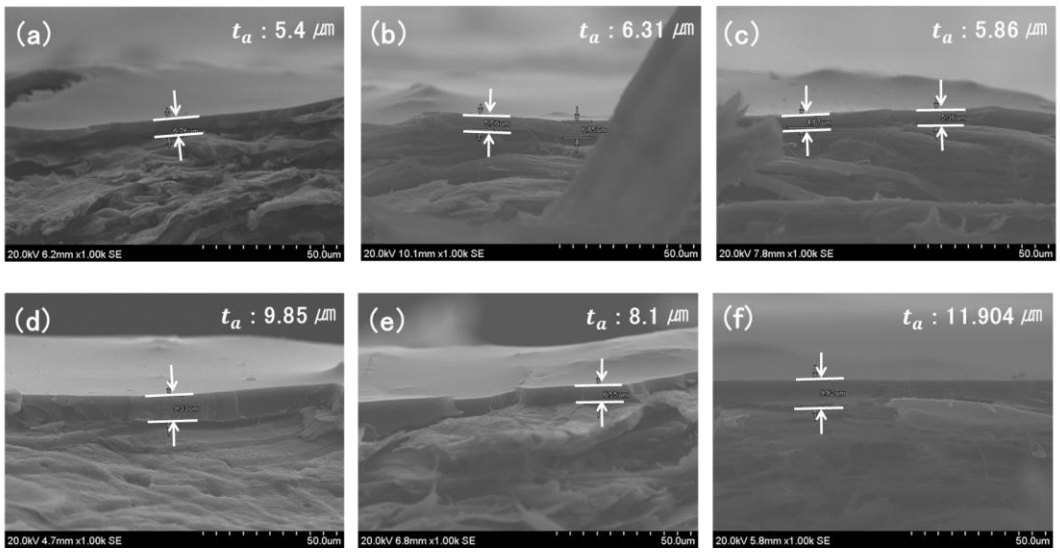

Figure 4.15 SEM image of the epoxy/silica nanocomposite thickness (Cross section view), (a) 0.2wt%, (b) 0.5wt%, (c) 1wt%, (d) 3wt%, (e) 5wt% and (f) 50wt%

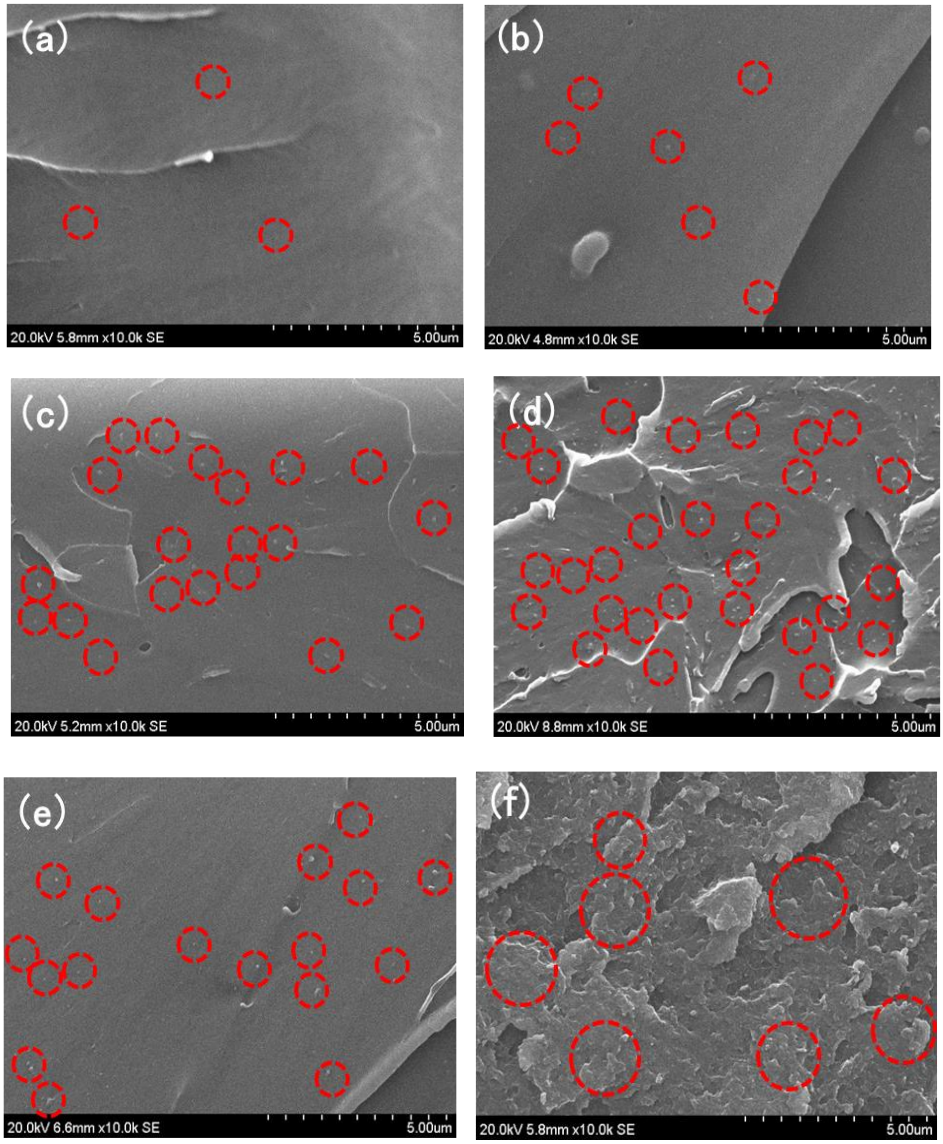

Figure 4.16 SEM image of SiO_2 nanoparticles surrounded by red circle dispersion in base epoxy matrix (Cross section view) (a) 0.2wt%, (b) 0.5wt%, (c) 1wt%, (d) 3wt%, (e) 5wt% and (f) 50wt%

4.3.4 PARTIAL DISCHARGE INCEPTION PROPERTIES

Figures 4.17 (a) and (b) show examples of discharge images and typical waveforms of positive standard lightning impulse voltage and those detected with PMT without and with creepage discharge, respectively. We determined the

partial discharge inception using PMT, image intensifier and discharge current waveform. In general, the luminous sensitivity of PMT (500 [μA/lm]) is higher than that of the image intensifier (230 [μA/lm]) as shown in Table. 4.3. Besides we found that the image intensifier can't catch the light intensity from creepage discharge below 50 pC as shown in Figure 4.18. For this reason, we found that sometime the image intensifier did not perceive the discharge light in spite of PMTs perceived at low apply voltage. Thus, PMT is more reliable tool to decide PDIV that is determined when a waveform is detected from PMT instead of the image intensified camera.

Figures 4.13 (a) and (b) shows general waveforms with/without creepage discharge. In the case of no PD in Fig. 4.17 (a), there is no signal PMT, discharge current and image intensifier image. On the other hand, when the creepage discharge occurred, discharge light emission can be detected clearly by PMTs, current waveform and image intensifier as shown in Fig. 4.17(b).

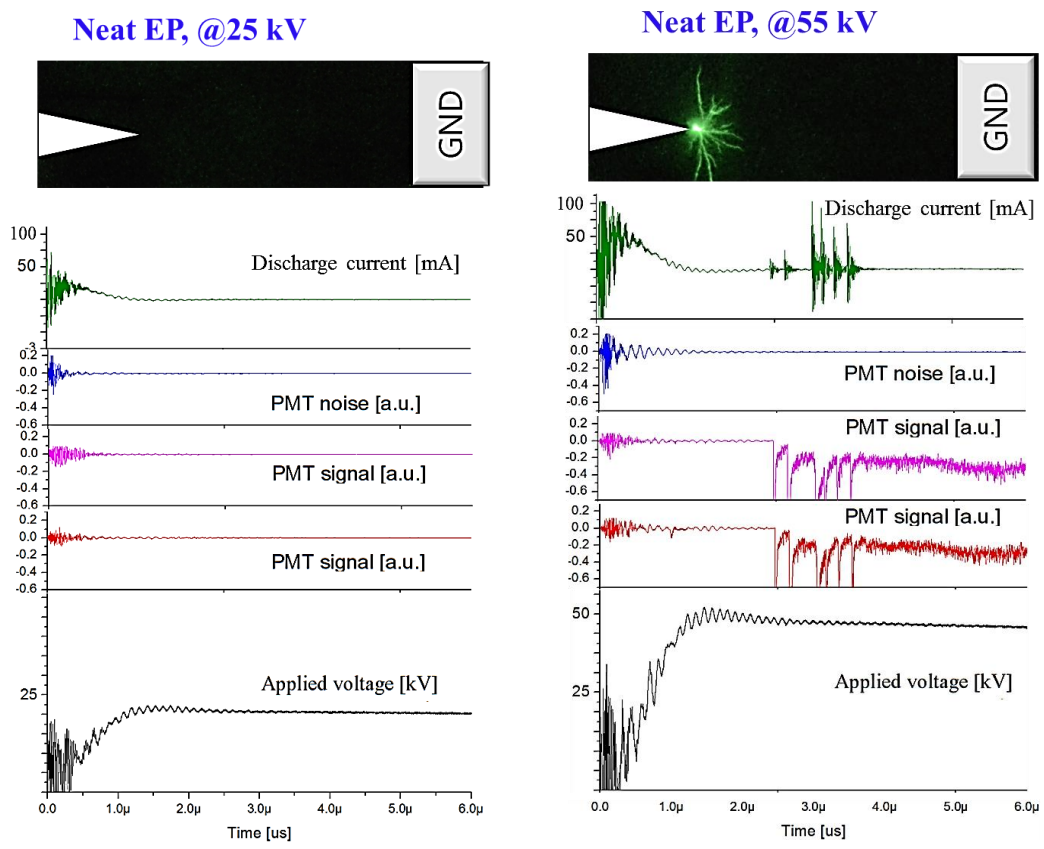

(a) (b)

Figure 4.17 Determination of creepage discharge inception voltage (a) without creepage discharge inception at 25 kV and (b) with creepage discharge inception at 55 kV

Table 4.3 Specification of PMT and image intensifier [90, 91]

Parameter		Unit (μA/lm)
Luminous sensitivity	PMT	500
	I.I	230

PMT: Hamamatsu Photonics, H6780-20
I.I: Hamamatsu C9016-2x, series-23

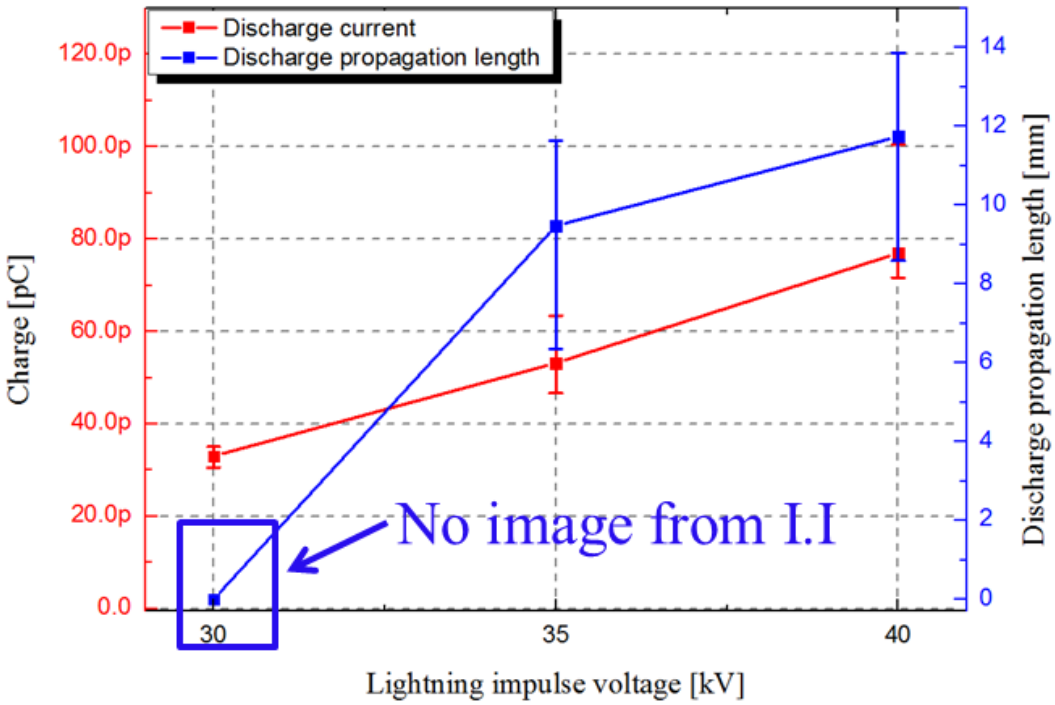

Figure 4.18 Relation between the output of image intensified camera and charge amount in pC as a function of lightning impulse voltage

4.4 RESULTS (ROD-PALNE ELECTRODE)

4.4.1 DIELECTRIC PROPERTIES

Figures 4.19 (a) and (b) show the real frequency dependence of real part ε_r' and imaginary part ε_r'' of the complex relative permittivity for different nano silica filler loading S_l at room temperature. It can be seen in Figures 4.19 (a) that ε_r' decreases stably with increasing frequency from 50 Hz to 2 MHz, whereas the relative dielectric loss ε_r'' increases with increasing as a function of frequency in Fig. 4.19 (b). As can be seen in Fig. 4.20, ε_r' of silica/epoxy nanocomposite coated samples at 100 kHz decreases at 100 kHz corresponding to dominant frequency component that the standard lightning impulse voltage contains.

It is also found that ε_r' of presents firstly decreases and increases with the increase of the S_l, and reaches a minimum at 1wt%. The increase of ε_r' with decrease in frequency is generally known as caused by interfacial polarization at occuring the interface between epoxy and nanoparticles [53-58]. Q. Wang and G. Chen *et al*., [92] has reported same results on decrease ε_r' for silica/epoxy nanocomposite. When fillers are loaded into the epoxy resin, the changes of dielectric properties with the presence of the nano size filler and their loading concentration may be caused by the following reason from Nelson and Forthergill [93]: decrease in the permittivity ε_r' of nano particle/epoxy resin composites is related to the restriction of dipole movement at the interaction zone. For example, the measured real part of the permittivity at 393 K using high permittivity TiO_2 filler ($\approx$ 99) is: 9.99 (base resin), 13.8 (micro-composite, size: 1.5 μm), and 8.49 (nanocomposite, size: 23 nm) at 1 kHz. The nanocomposite has a lower permittivity than the base resin and micro composite. The electrical properties of nanocomposites are mainly determined by the dispersion and nanoparticle filler loading characteristics. The physical and chemical characteristics of the interface can be influenced by these factors, leading to changes in micro scale features such as traps, carrier mobility and free volume [93, 94]. On the other hand, free volume in nano size particle/epoxy composite systems will decrease when nanostructured, and will increase when micro structured. Free volume is demonstrated in experiment and in theory by Nelson and Forthergill. Obviously, free volume plays an important role in the reduction of the permittivity ε_r' [93-97].

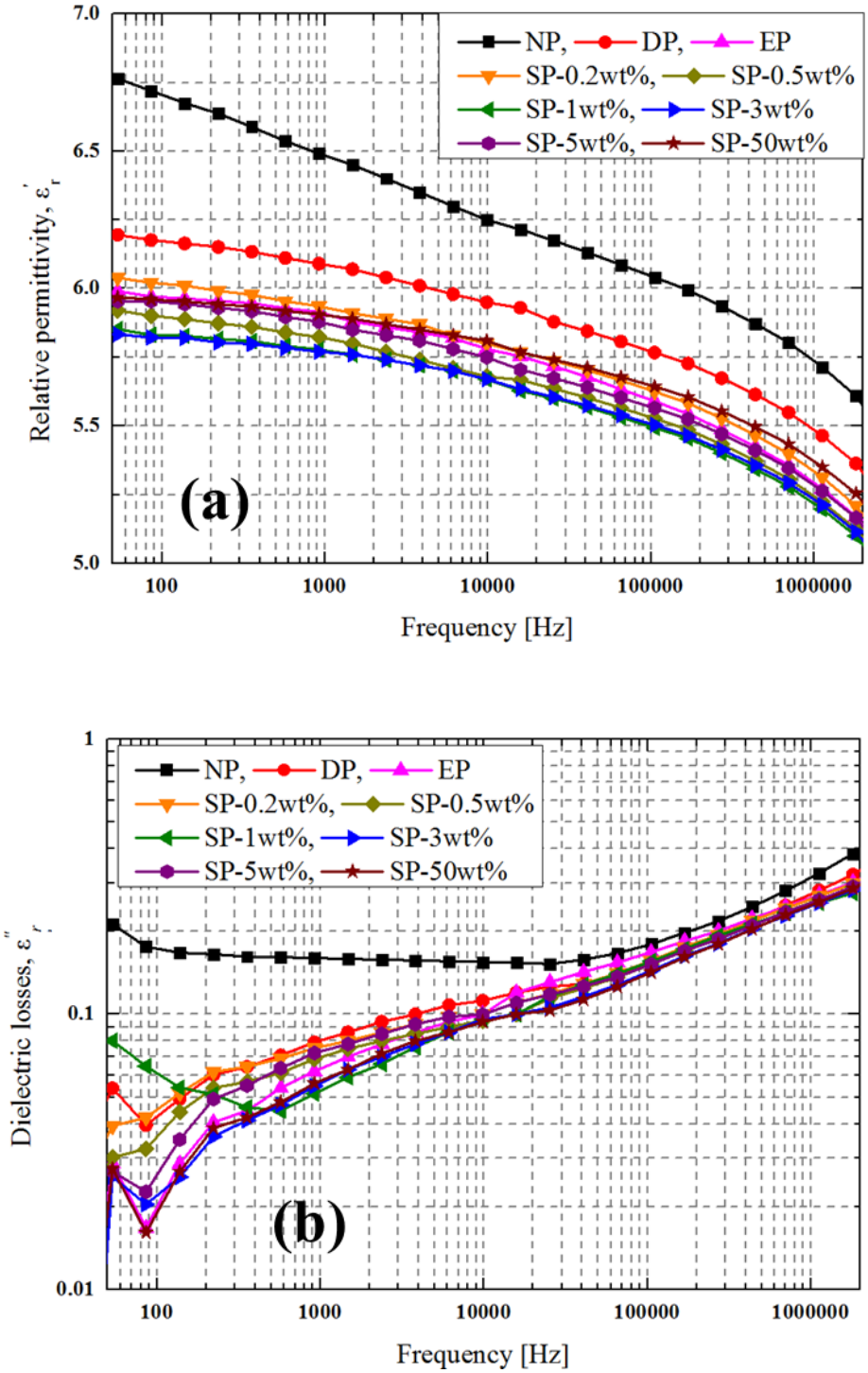

Figure 4.19 Frequency dependence of complex permittivity at room temperature; (a) real part of permittivity of each specimen, (b) dielectric loss

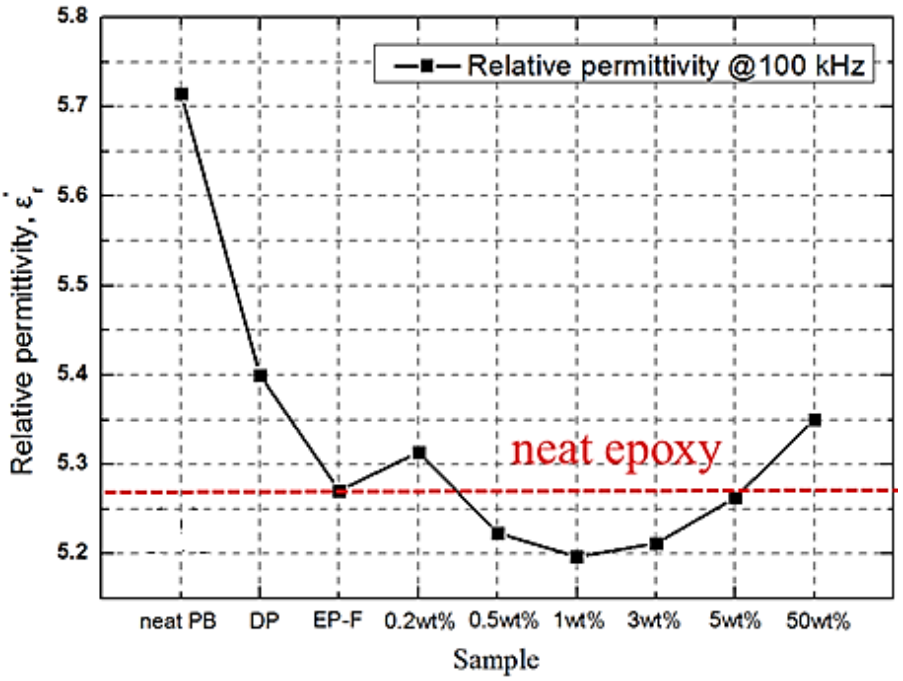

Figure 4.20 Relative permittivity ε_r' at 100 kHz

4.4.2 DISCHARGE PATTERNS AND PDIV

Prior to study discharge patterns under 60, 80 and 100 kV of impulse voltage application, PDIV of each sample was measured first to compare with modified other samples. Figures 4.21 (a) to (f) show discharge image of each sample at 100 kV. White lines and circles in the figures depict the high voltage electrode and ground electrode, respectively. Here, let the discharge propagation length (l_d) be defined as the length from the high voltage electrode to a site of the longest discharge edge part. It should be noted that creepage discharges under a positive lightning impulse voltage do not always propagate radially in this electrode configuration. Such orientation and distribution of branches on the surface of insulator is considered to be due to distortion of the electric field resulting from surface charge accumulated on the insulator [98]. The creepage discharge trend such as discharge light intensity, the number of discharge branches and discharge length is changed according to dry process and surface coated material on the surface of PB. The discharges are composed of ramified branches of streamer propagating on the surface of NP, DP and TP samples, while emitting intense luminous area. Whereas the discharge image in EP-A and EP-F show weak light

spots at all the voltage levels and propagating discharge shows filamentary branches. On the other hand, the discharge pattern of SP-0.2 wt% and SP-5 wt% shows more intense white luminous part at their streamer and branch than that of EP-F samples and propagating discharge shows filamentary branches. Thus, we confirmed that the surface conditions and materials on PB influence creepage discharge properties and tendency.

The total number of discharge branches observed on the surface of each sample was counted using a binary image analysis program (AZO V2.30) as shown in Fig. 4.22. It is seen in these figures that the The discharges are composed of ramified branches of streamer propagating on the surface of NP, DP and TP samples. Note that NP, DP and TP samples have more divided discharge branches from main streamer than EP-F sample as shown in Fig 4.23.

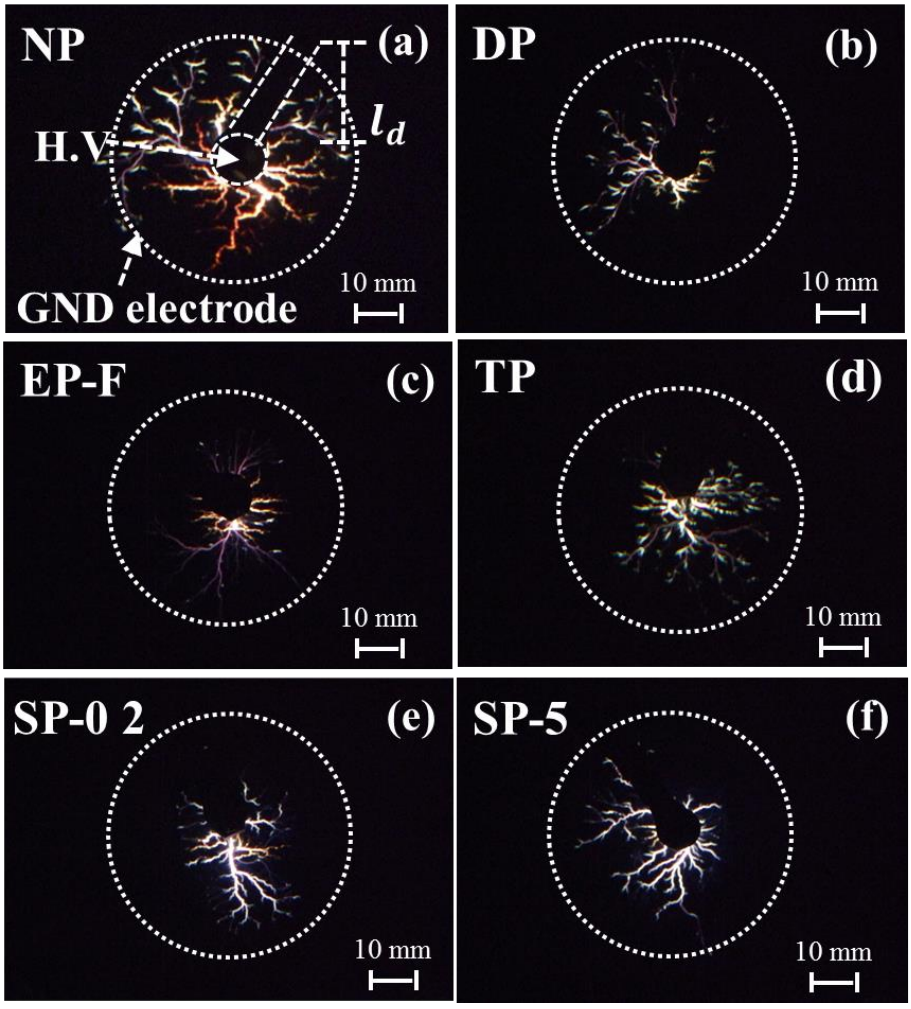

Figure 4.21 Discharge patterns of each sample at 100 kV using rod-plane electrodes in mineral oil

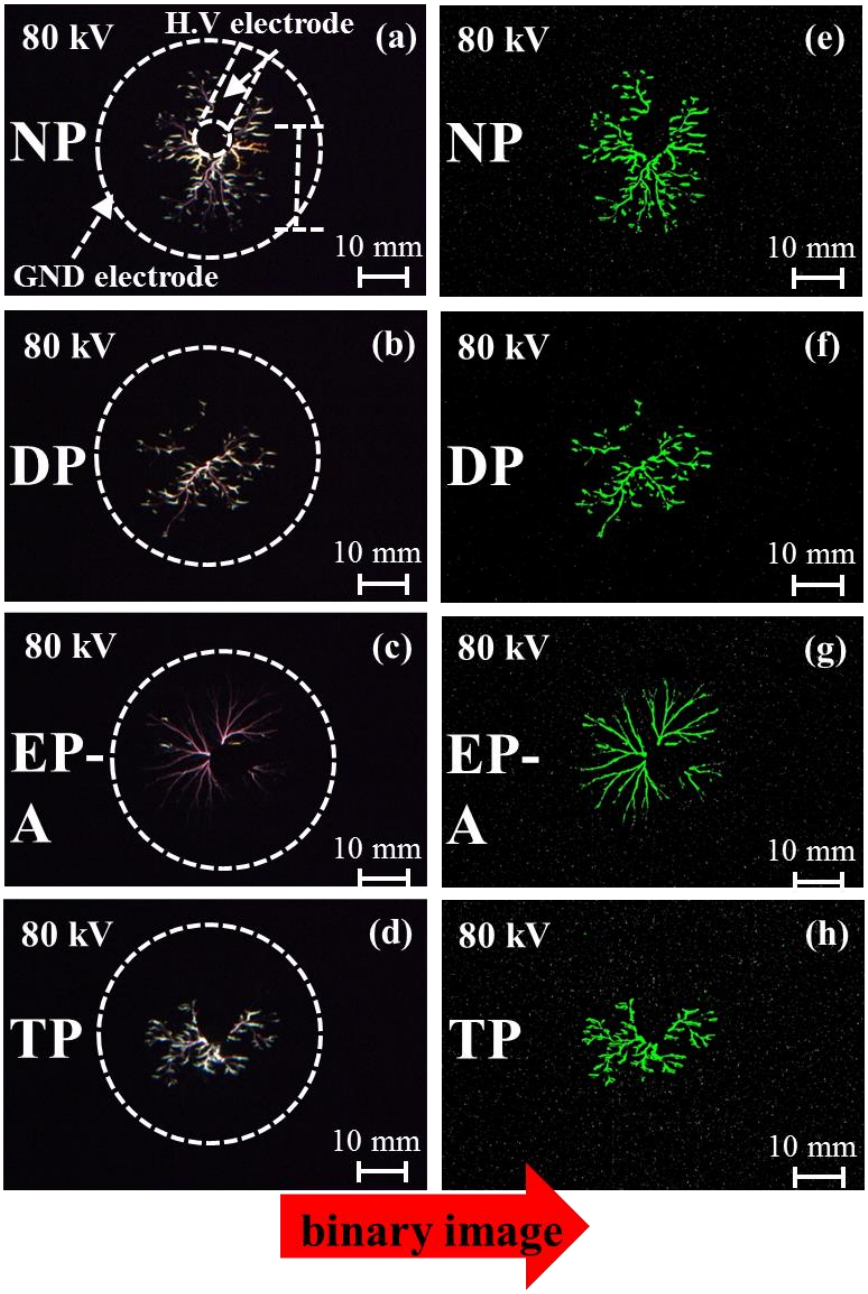

Figure 4.22 Discharge binary images of each sample using image analysis program at 80 kV

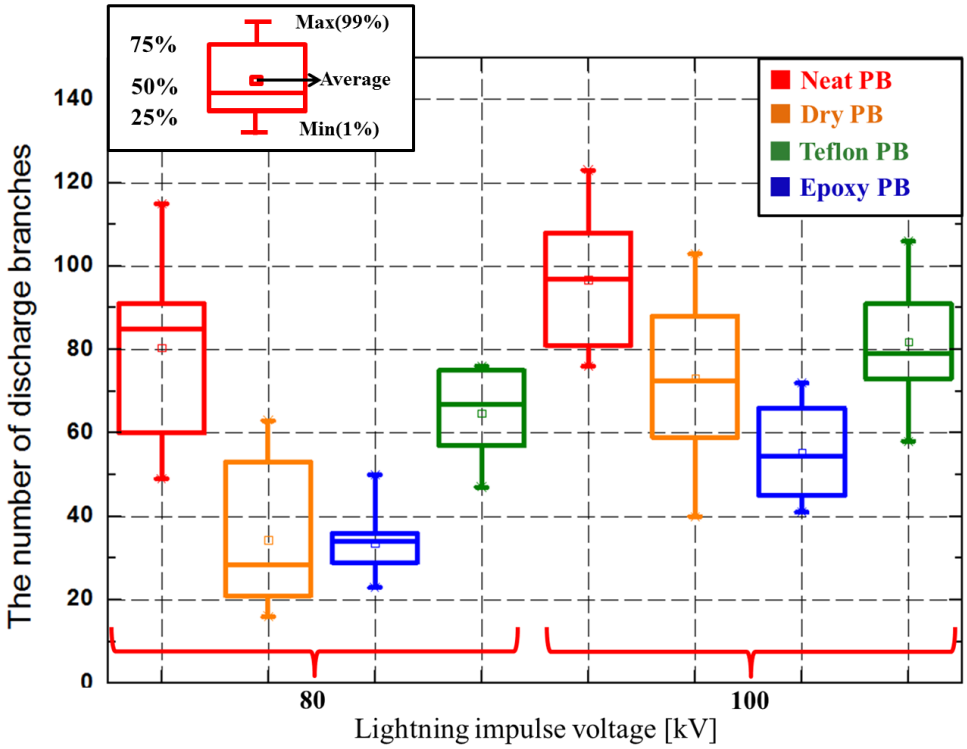

Figure 4.23 The number of discharge branches of each sample at 80 kV and 100 kV

Figure 4.24 shows discharge occurrence probability (P_d) at each voltage level for different kinds of specimen. In NP, the probability (P_d) of 100% of discharge occurrence is observed at each voltage level from 60 to 100 kV. On the other hand, it is seen that P_d at 60, 70 and 100 kV is 33.3, 96.6 and 100 % (DP), 13.3, 66.6 and 100% (EP-A), 10, 33.3 and 80% (EP-F) and 36.6, 56.6 and 100% (TP), respectively. The discharge occurrence probability of DP decreased at only 60 kV. These results indicate that the drying process and the moisture level in PB should affect the discharge inception as well as development process. On the other hand, it should be noticed that P_d of SP (0.2, 0.5, 3 and 5 wt%) are less than 63.5 and 73.3% from 60 to 100 kV, and that P_d of SP with 50 wt% was higher than that of EP-F at all the voltage levels. These results will be discussed in Section 4.6.

Next, let PDIV ratio k_1 can be defined as the ratio of PD occurrence probability of SP to that of EP-F. The ratio k_1 of SP specimen was defined as the voltage of 10% discharge occurrence probability of SP divided by that of EP-F. Figure 4.25 shows the 10% PD occurrence probability ratio k_1 dependent on filler loading of SiO_2 nano fillers under the impulse voltage. As can be seen in Fig. 4.25, the ratio k_1 is larger than one, meaning that discharge occurrence suppression property can be improved with appropriate S_l compared to that of EP-F. The ratio

k_1 presents the highest values at SiO_2 filler loading of SP-0.2wt%, while further increasing S_l results in decrease of k_1.

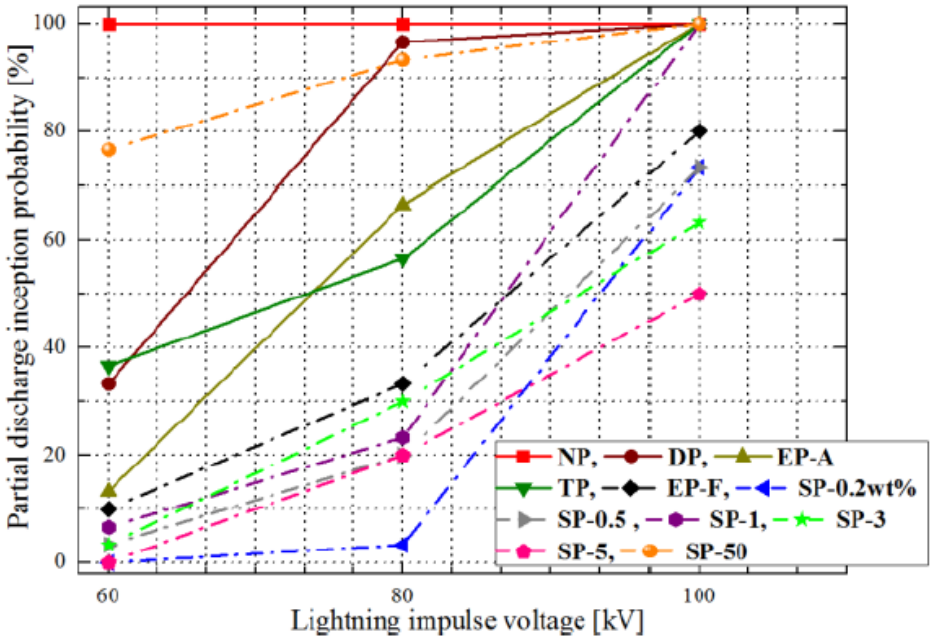

Figure 4.24 Discharge occurrence probability P_d at each voltage level with different coating material

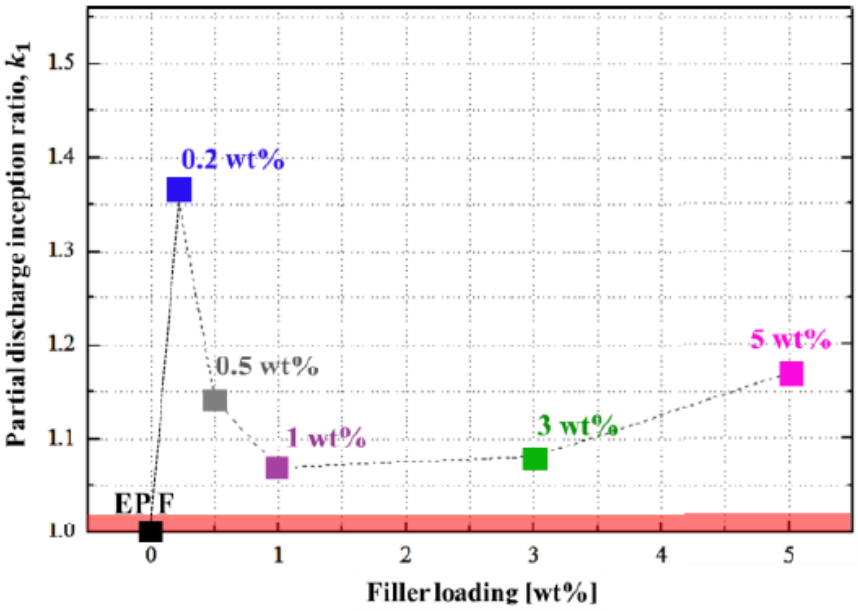

Figure 4.25 PD occurrence probability ratio k_1 against EP-F versus filler loading of nano SiO_2, where k_1 is defined as the voltage of 10% discharge occurrence probability of SP divided by that of EP-F.

4.4.3 DISCHARGE PROPAGATION LENGTH

Figures 4.26 and 4.27 show the discharge propagation length l_d of each type of specimen with different SiO_2 nano filler loading, respectively, at all the voltage levels. It is evident from the two figures that l_d for each sample increases as the applied impulse voltage increases from 60 to 100 kV. Note that the average discharge propagation length l_{dave} of the solid layer coating samples EP-A, EP-F, TP and DP is shorter than that of NP sample at all the voltage levels. On the other hand, it should be noticed that l_{dave} of PS-0.2, 0.5 and 5 wt% is shorter than that of the other samples at all the voltage levels. These results indicate that the solid layer coating of epoxy, Teflon and nano silica/epoxy composites on PB should affect not only the discharge inception but also the development process as well. That might be influenced by dry process and surface modification. These detailed results will be discussed in Section 4.6 together with the results of the needle-bar electrode system.

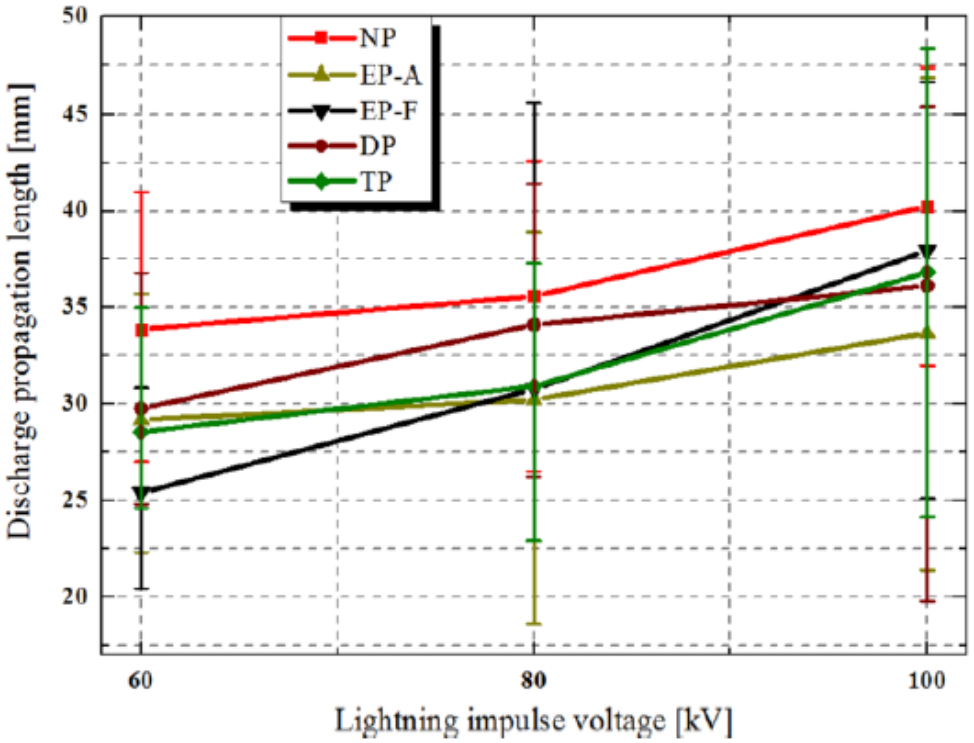

Figure 4.26 Discharge propagation length l_d at each lightning impulse voltage (NP, DP, EP-A, EP-F and TP)

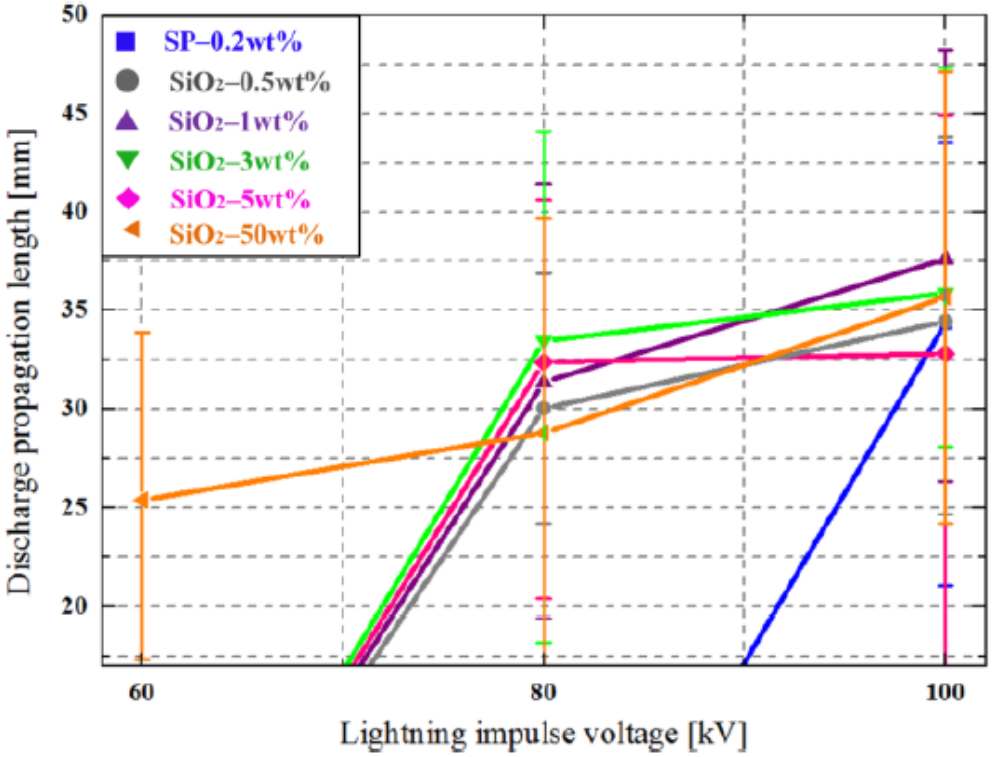

Figure 4.27 Discharge propagation length l_d of SP specimens at each lightning impulse voltage

4.5 RESULTS AND DISCUSSION(NEEDLE-BAR ELECTRODE)

4.5.1 DISCHARGE PATTERNS AND PDIV

Figures 4.28 (a) to (e) show creepage discharge image of each sample NP, DP, EP-A, SP-0.2 wt% and SP-3 wt% at 45 kV using the needle-bar electrode system, respectively. White triangles in the figures depict the high voltage electrode. The measuring method of discharge propagation length (l_d) is the same with Section 4.3.2. The discharges are composed of ramified branches of streamer propagating on the surface of NP and DP samples, while emitting intense luminous area appears at the end part of their branch tip and streamer. Note that NP and DP samples have more discharge branches than EP-A, EP-F and SP specimens and

this phenomenon is similar with the results obtained by the rod-plane electrode system. Figure 4.29 shows discharge light intensity as a function of the applied impulse voltage V_i of each kind of sample. The discharge light intensity of EP-A, EP-F and SP specimen shows weak discharge light intensity at all the voltage levels than that of NP and DP. Propagating discharge of EP-A, EP-F and SP samples shows filamentary branches.

Figure 4.30 shows discharge occurrence probability (P_d) at each voltage level V_i for different kinds of specimen. Each specimen was tested 3 times at least under the same test conditions. In NP, the probability (P_d) of 100% of discharge occurrence is observed at each voltage level from 25 to 45 kV. On the other hand, it is seen that P_d at 20, 25 and 30 kV is 66.6, 86.6 and 100% for DP, 53.3, 73.3 and 86.6% for EP-A and 26.6, 53.3 and 73.3% for EP-F, respectively. These results indicate that the drying process and moisture level in PB affect both the discharge inception and development processes. On the other hand, it should be noticed that P_d of 0.2 and 3 wt% at V_i 40 and 45 kV is 100%. These results indicate that the SiO_2/epoxy composite on the surface of PB should improve the discharge inception voltage.

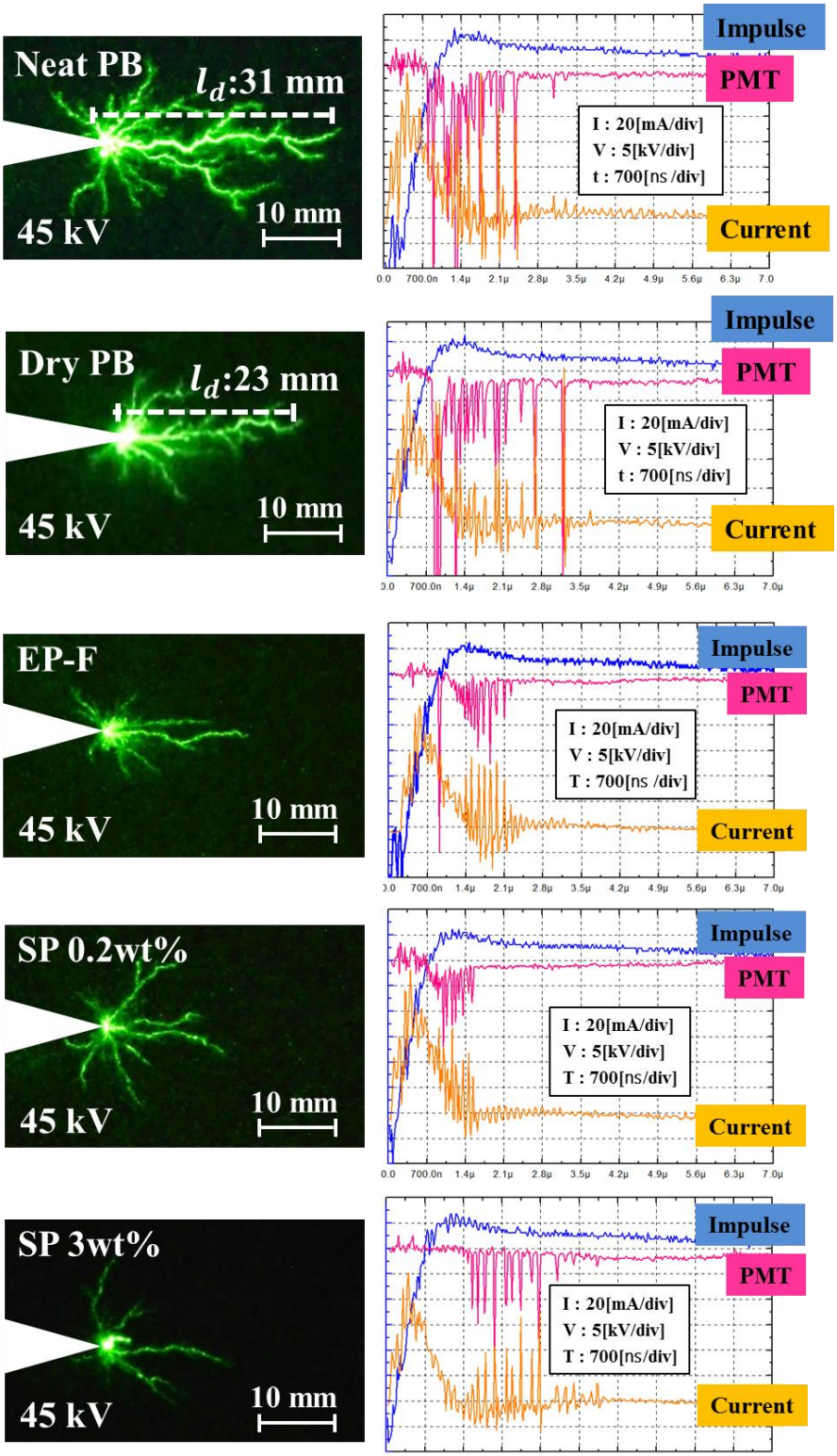

Figure 4.28 Discharge patterns of (a) NP, (b) DP, (c) EP-F, (d) SP-0.2wt% and (e) SP-3wt% at V_i 45 kV

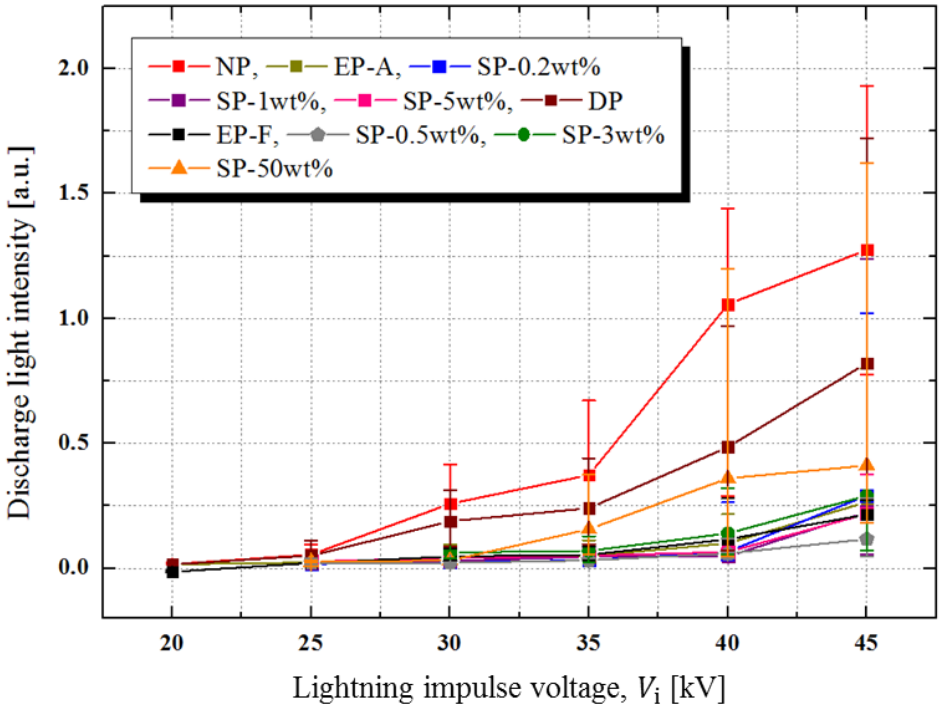

Figure 4.29 Discharge light intensity from PMTs waveforms as a function of V_i for different kinds of specimen

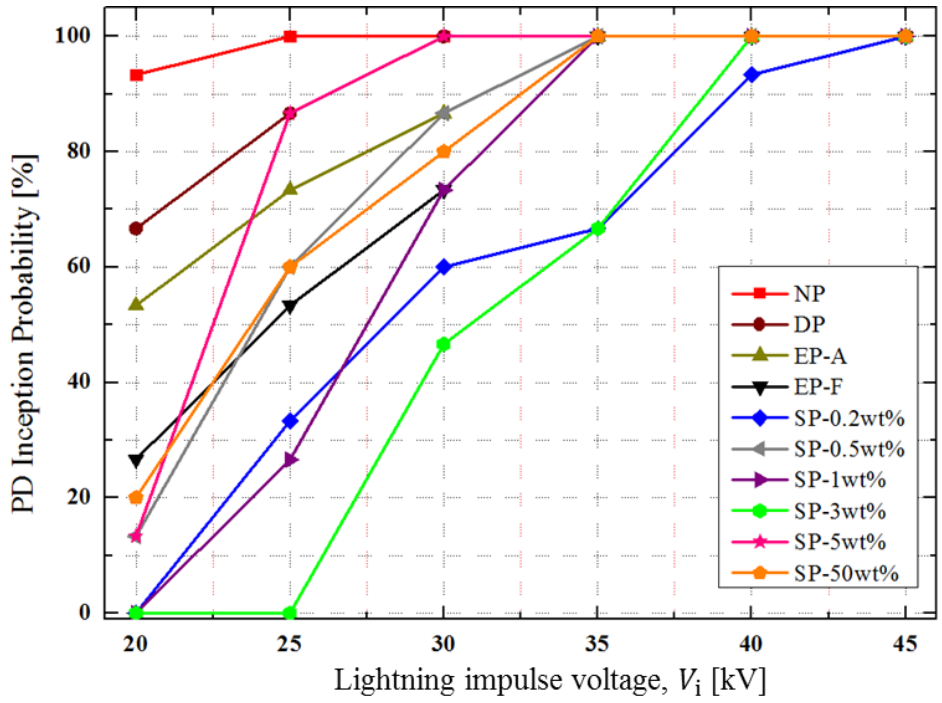

Figure 4.30 Discharge occurrence probability at each voltage level for different kinds of specimen

Figure 4.31 shows ε_r' and 30% discharge occurrence probability ratio k_2, which is defined as V_i giving 30% P_d of EP-F divided by that giving 30% P_d of nano silica/epoxy composite coated PB. The ratio k_2 dependent on the filler loading of silica nano fillers under the V_i. As seen in Figure 4.31 the ratio k_2 is larger than one. Meaning that insulation performance against the creepage discharge generation can be improved with appropriate filler loadings compared to that of NP. Note that k_2 presents the highest value 1.4 at silica filler loading of 3 wt%, while decreases with further increasing nano silica filler loading above 5 wt%. High filler loading sample with 50 wt% of the filler shows still a high ratio k_2 than that of EP-F. Moreover, ε_r' firstly decreases and increases with the increase of the filler loading, and reaches a minimum at 3 wt%. It can be concluded that the reduction of ε_r' corresponds to the improved P_d of SP specimens.

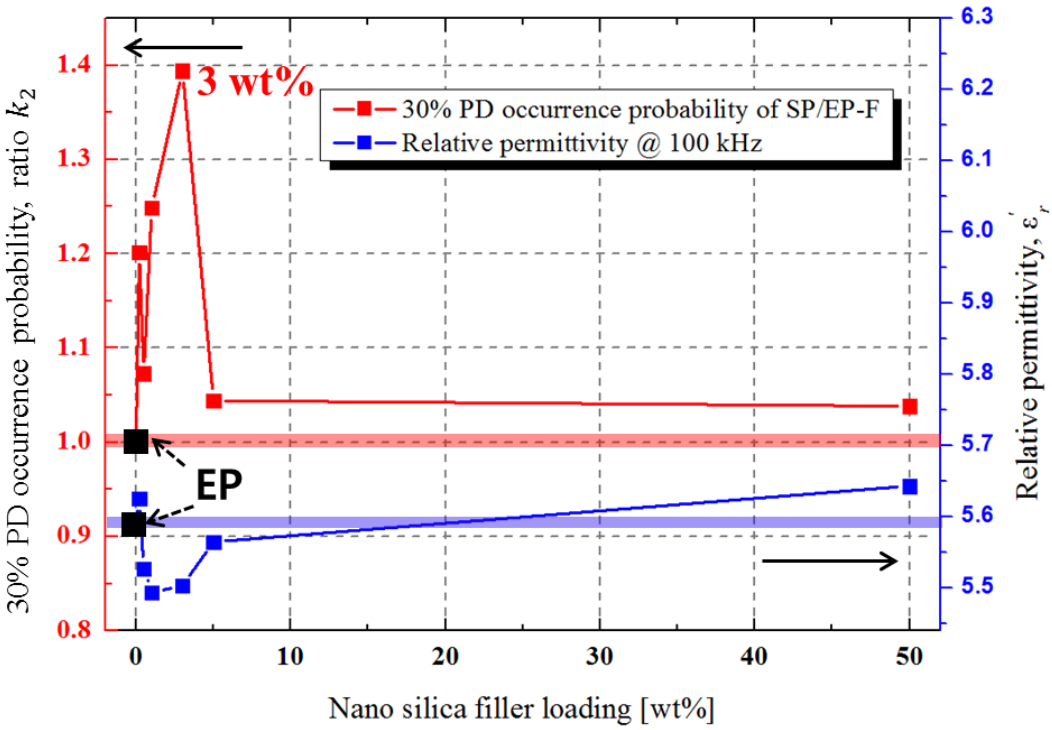

Figure 4.31 The ratio k_2 of 30% discharge occurrence probability P_d of nano silica filler loaded to that of EP coated NP and relative permittivity ε_r' at 100 kHz as a function of nano silica filler loading for epoxy/silica nanocomposite coated PB

Many researchers conveyed the similar conclusions on the effect of nano filler loading on the performance of vacuum surface flashover and breakdown properties, and proposed a variety of models and interpretations. Yu Chen *et al*. investigated the vacuum surface flashover characteristic of nano size Al_2O_3/epoxy nanocomposite. The flashover voltage shows the highest values at Al_2O_3 filler loading of 3 wt%. The experimental results were explained in terms of the effects of different roles of shallow and deep traps introduced by the nano filler loading [56]. Shengtao Li *et al*. also investigated the surface flashover and breakdown voltages of TiO_2/epoxy nanocomposite in SF_6 gas. The optimal filler loading of TiO_2 for the normalized flashover voltage k_1 was 1 wt% [53-55]. On the other hand, the present study reveals that the PD occurrence probability of SP-0.2 wt% SiO_2 added epoxy composite insulation (SP) is improved to be 1.3 times as much as that of EP-F. The decreasing PD occurrence probability with the nano filler loading can be explained in two ways as follows; 1) SiO_2/epoxy nano composites coating on PB suppresses emission of trapped electron from the surface of PB in the discharge inception process, and 2) the discharge inception voltage possibly depends on the surface roughness as well as the filler loadings. More detailed discussion will be made in Section 4.6

4.5.2 DISCAHRGE PROPAGATION LENGTH

Figures 4.32 and 4.33 show the discharge propagation length l_d of each sample at all the voltage levels. It is evident from the figure that l_d for each sample increases as the applied V_i increases from 20 to 45 kV. Note that the average propagation length l_{dave} of DP, EP-A, EP-F and SP samples at all V_i is shorter than that of NP samples by 42%, 64% and 70%, respectively. Figure 4.34 shows relation between discharge propagation length and relative permittivity. Discharge propagation length ratio k_3 be defined as 45 kV giving l_d of neat EP divided by that giving l_d of silica/epoxy nanocomposite. As seen in Fig. 4.34, discharge propagation length ratio k_3 is larger than one, meaning that the insulation performance against the creepage discharge propagation can be improved with appropriate S_l compared to that of EP. Note that k_3 presents increases and decreases with the increase of the S_l above 3 wt%, respectively. It can be concluded that the low S_l improved l_d. But note that once discharge occurred, l_d of each sample is becomes the same at each voltage level, besides scattering of the data overlaps each other, meaning no appreciable effect of the filler loading on l_d in oil condition. These results will be discussed in Section 4.6.

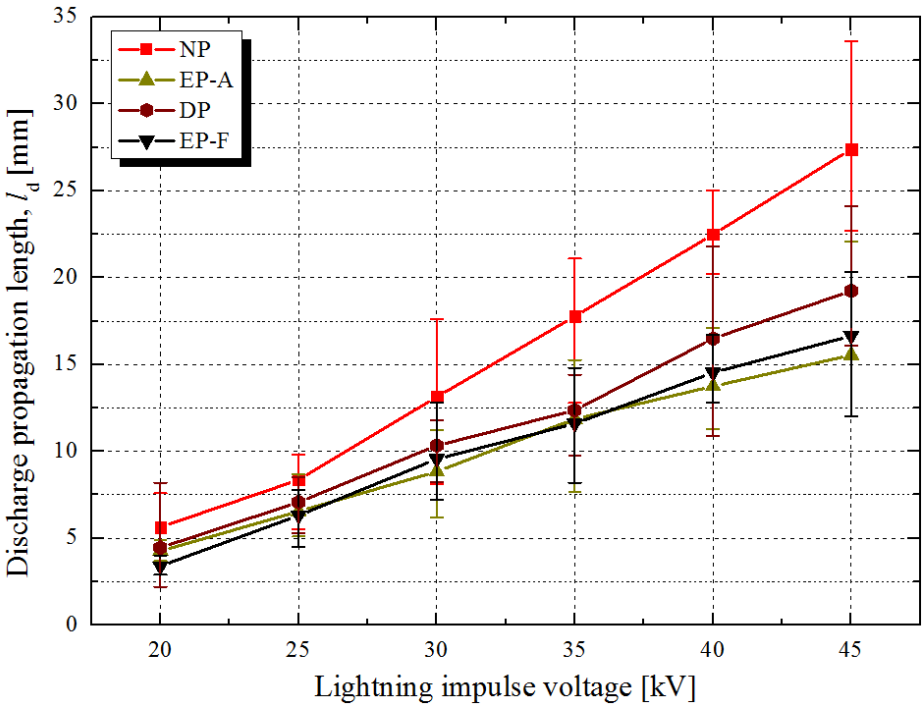

Figure 4.32 Discharge propagation length l_d of NP, DP, EP-A and EP-F as a function of V_i

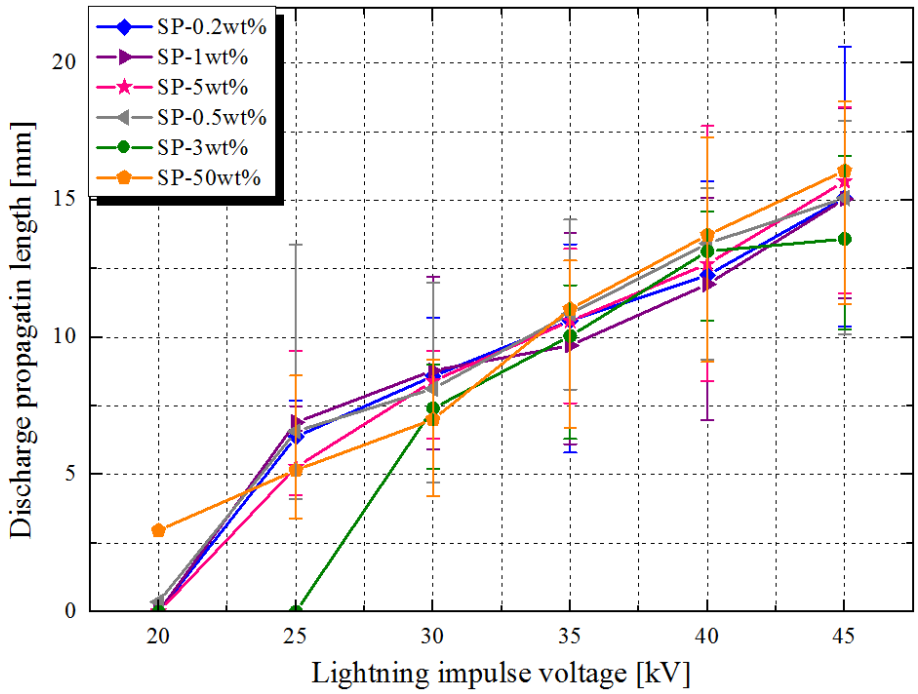

Figure 4.33 Discharge propagation length l_d of SP specimens as a function of V_i for the needle-bar electrode system

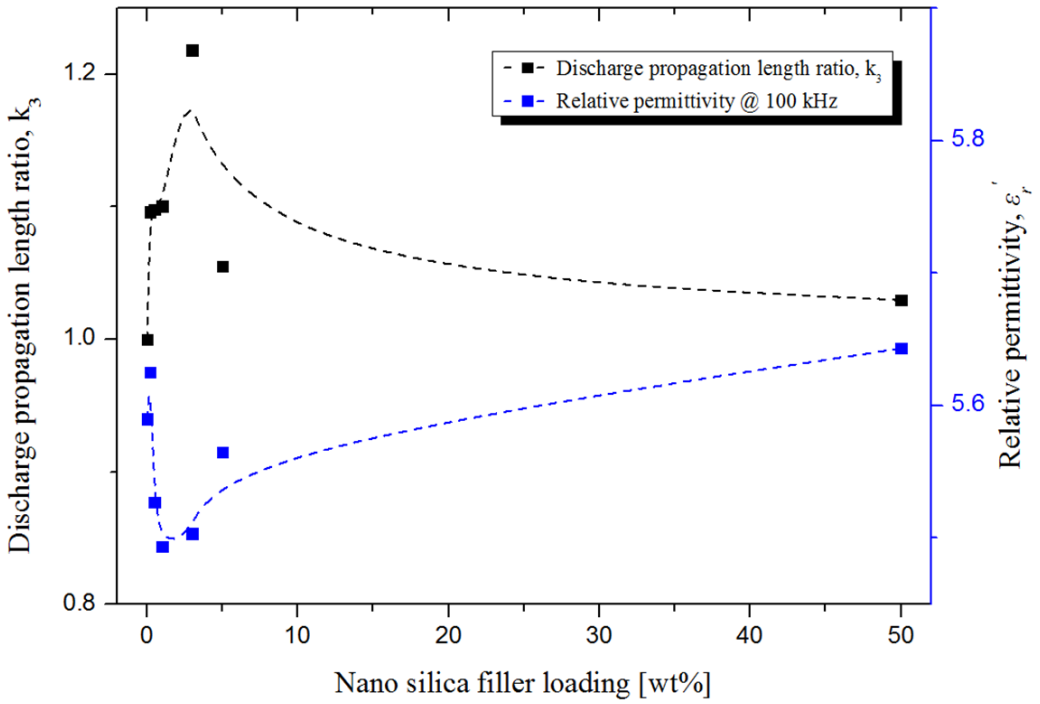

Figure 4.34 The relationship between average discharge propagation length l_{dave} ratio k_3 and permittivity ε_r' of SP with different silica filler loading at 45 kV

4.6 DISCUSSION (EFFECT OF SOLID LAYER COATING)

The effect of the solid layer coating on P_d and l_d is discussed. The following three factors are possibly considered to explain the experimental results on P_d and l_d, respectively:

1) Drying of water content in neat PB and decrease in ε_r' by silica/epoxy nanocomposite coating
2) Surface modification effect by solid layer coating
3) Silica/epoxy composites coating suppressing the electron emission from the surface of PB

4.6.1 DRY EFFECT AND PERMITTIVITY EFFECT

Note that cellulose paper placed on a factory floor is said to be able to hold 4-8% moisture in the relative humidity of 30 to 70% in winter and summer, respectively as shown in Fig. 4.35 [9]. Besides, PB cellulose fibres form microcapillaries, which contain insulation oil, gaseous residues and water molecules.

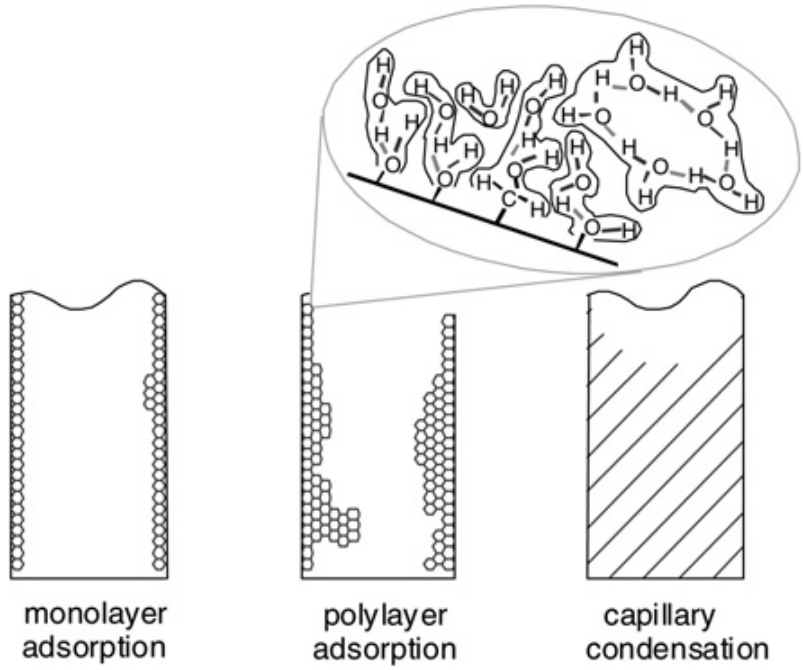

Figure 4.35 Bonds of water molecules in a PB microcapillary [98]

Insulation paper consists of a compound of cellulose fibres linked by hydrogen and Van-der-Waals bonds. Water is absorbed in the amorphous structures of cellulose, in the pores of the cell walls and in the polyose-lignin-gel (remains from wood) [98]. Cellulose fibre form microcapillaries, which contain insulation oil, gaseous residues in the wet state water. For low water content, the molecules are bound by strong bonds forming a monolayer. When water content (more than 1-2 % moisture relative to weight) increases, only relatively weak Van-der-Waals bonds and capillary forces hold water molecules in the cellulose compound as shown in Fig. 4.31 [9, 97].

In general, discharge inception voltage is dependent on the inherent capacitance of solid insulation as well as surface roughness, impurities between interface of composite insulation and type of materials etc. According to an empirical formula given in Eqn. (4.1) with increasing the inherent capacitance of solid insulation, the electric field of triple junction increases. On the other hand,

creepage discharge is more likely to occur and then propagate along the surface of PB with increase in the C [pF/mm^2] of solid insulation, because the electrostatic energy stored in the C increases [99, 101]. We confirmed that the weight, thickness after dry process and C after epoxy/silica nanocomposite coating decreased by 5.3%, 3% and 14%, respectively. Equation 4.1 and figure 4.36 show relation between capacitance and estimated discharge inception voltage.

$$V = \mathrm{K}C^{-n} \tag{4.1}$$

C is the specific capacitance of pressboard [pF/mm^2]; V is applied voltage [kV]; K and n are constant (estimated n: 0.77)

Estimated discharge inception voltage after dried process and surface coating on PB from Eqn. 4.1 increases with decreasing specific capacitance as shown in Fig. 4.32. Besides, in rod-plane electrode results, P_d of DP decreased by 66.7% at only 60 kV and l_d also decreased by and 12.1, 4.2 and 10.2% at each V_i as shown in Fig. 4.24, 4.26, 4.30 and 4.32. It is because the capacitance decreases, resulting in less discharge development according to Eqn 4.1. Thus, it can be said that the moisture level in PB affects the discharge inception and development as well.

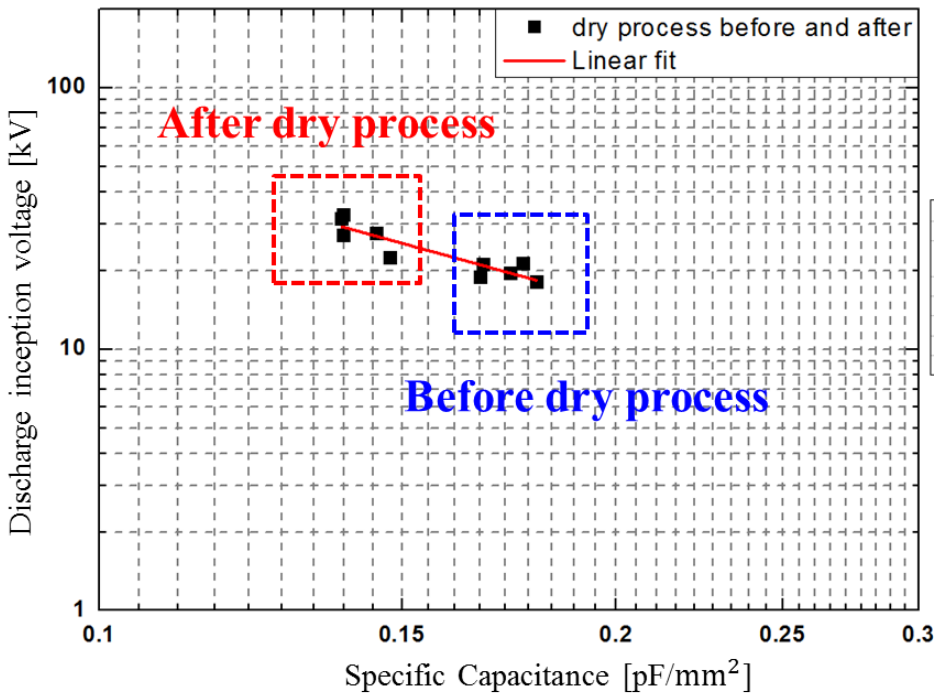

Figure 4.36 Relation between estimated discharge inception voltage and the specific capacitance before and after dry process of pressboard at 70 and 150℃ for 3 hours, respectively

4.6.2 SURFACE MODIFICATION EFFECT

The second possible reason for P_d and l_d is a surface modification effect by the solid layer coating on PB. The surface of NP and DP exhibits numerous protrusions of cellulose fibrous as shown in Fig. 4.37 [98, 101], whereas the surface protrusions of EP-A, F and SP samples were covered with epoxy resin. For that reason, there are no protrusions on the surface of coated PB using a microscope as shown in Fig. 4.37. We estimated the electric field distribution with presence of protrusions around the high voltage electrode using COMSOL Multiphysics 2D MODEL as well as surface roughness measurement results as shown in Fig. 4.38.

The generalized hydrodynamic drift-diffusion equations combined with Poisson's equation were employed in dielectric liquids. The detailed analysis method using COMSOL MULTIPHYSICS will be dealt in Chapter 6.

Figure 4.39 shows the simulation results, the electric field is disturbed with the presence of protrusions around the needle electrode simultaneously with discharge inception over 1×10^8 V/m, and then the creepage discharge is likely to propagate toward protrusion tip along the pressboard surface. Concentrated electric field in protrusion tip is more likely to increase with increasing time than in protrusion pole part as shown in Fig. 4.40. Thus, in the case of NP and DP, it might be possible that the electric field concentration occurs at the protrusion tip and it could be starting point of a creepage discharge inception.

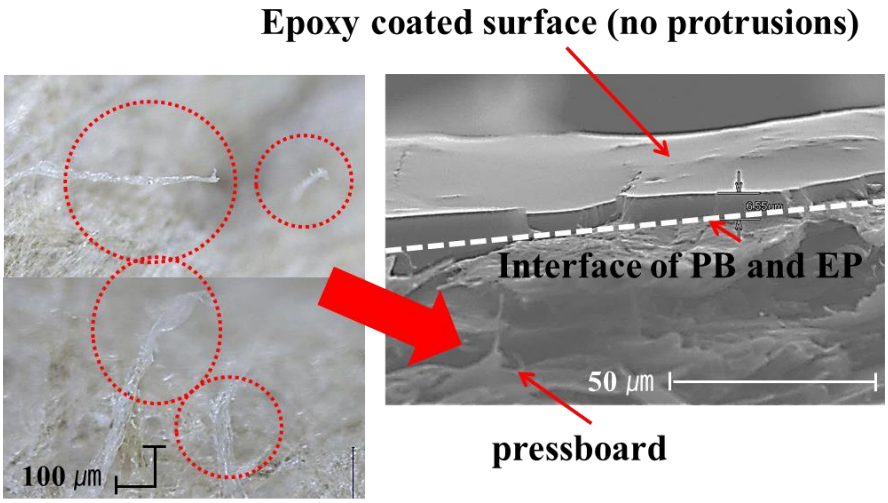

Figure 4.37 Surface protrusions on the surface of conventional pressboard (DP) using microscope and scanning electron microscope image

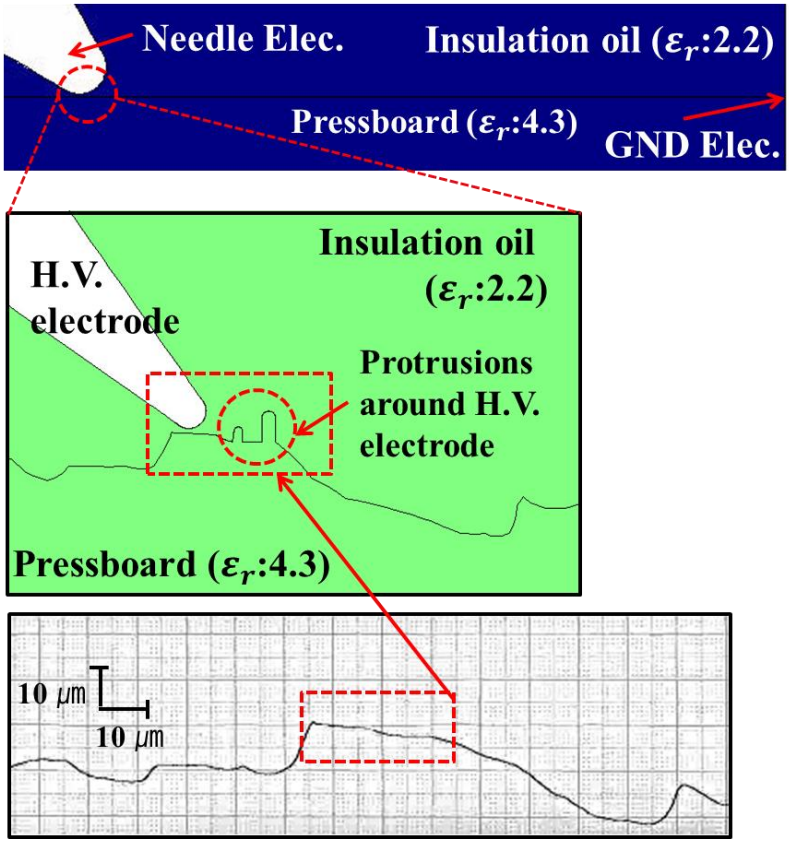

Figure 4.38 Analysis model with presence of protrusions on the surface of PB with surface roughness measured in DP

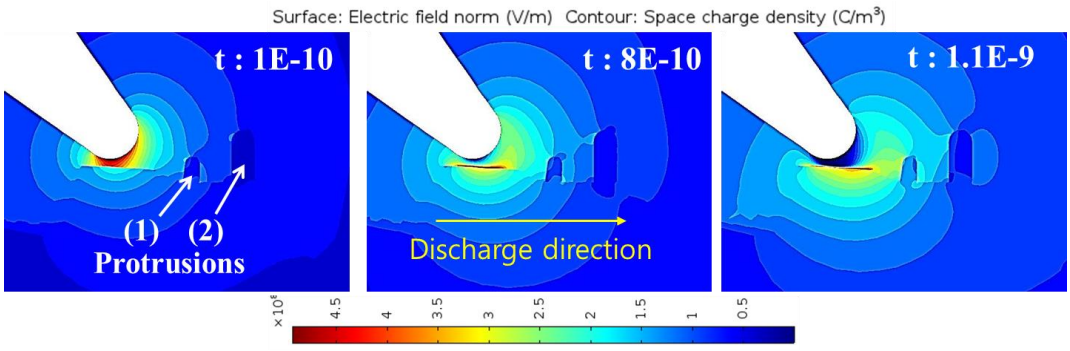

Figure 4.39 The calculated electric field distribution with presence of a protrusion on the surface of PB around the high voltage needle electrode

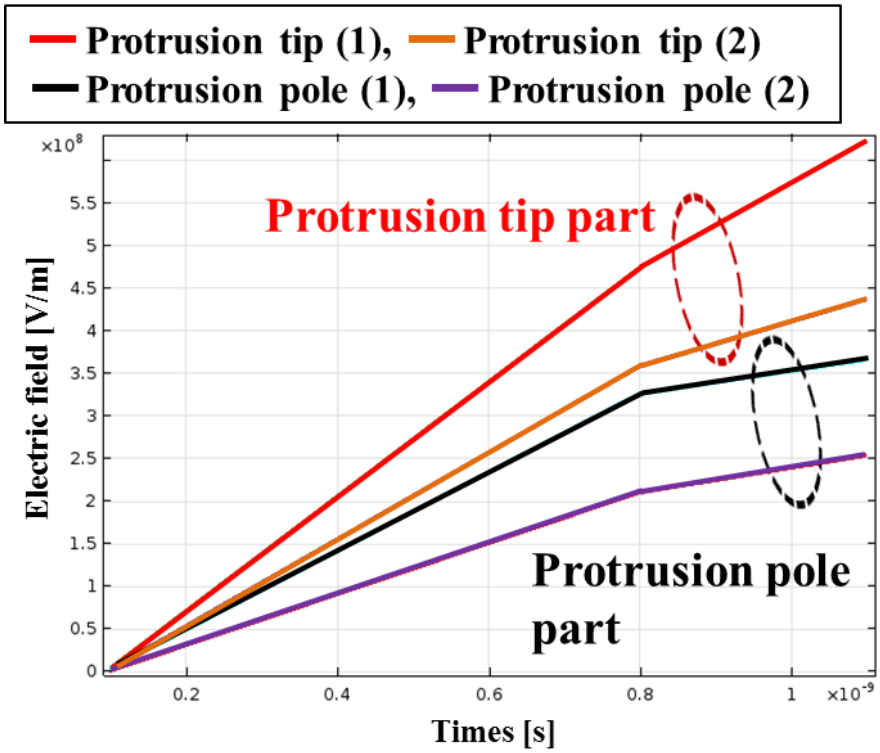

Figure 4.40 The electric field results of protrusion tip parts and pole parts

4.6.3 ELECTRON SUPPRESSION EFFECT

The third possible reason for P_d and l_d is that epoxy/silica nano composites coating may suppress initial electron emission contributing to creepage discharge inception and propagation from the surface of PB, resulting in the decrease of the P_d at all the V_i as well as the decrease in l_d as well.

Let us propose a surface flashover model in the nanocomposite coating PB as illustrated in Fig. 4.41. In general, oil immersed PB form microcapillaries which contain insulation oil. Porosity of PB causes oil to penetrate into the PB bulk. The free charges such as positive ion, negative ion and electron are generated from oil immersed PB bulk due to molecular ionization and ionic dissociation under a high electric field [32]. During creepage discharge process, charge carriers emitted from electron avalanches could excite the electron from the surface of PB, and newly generated electrons can play a role as the seed of new electron avalanches and some of these secondary electrons will again strike the surface of PB, producing tertiary electron [103]. Then, the creepage discharge is more likely to incept and then can more readily creep along the surface of PB. Deep electron

traps introduced by the epoxy/nanoparticle composites coating can restrain the emission of the internal secondary electrons and initial electron inside the surface layer of PB, and the discharge inception voltage can be possibly increased. Namely, the epoxy/silica nanocomposites coating on PB suppresses the electron emission and thus extraction of electrons from the surface layer of epoxy/silica nanocomposites in the discharge inception and propagation process.

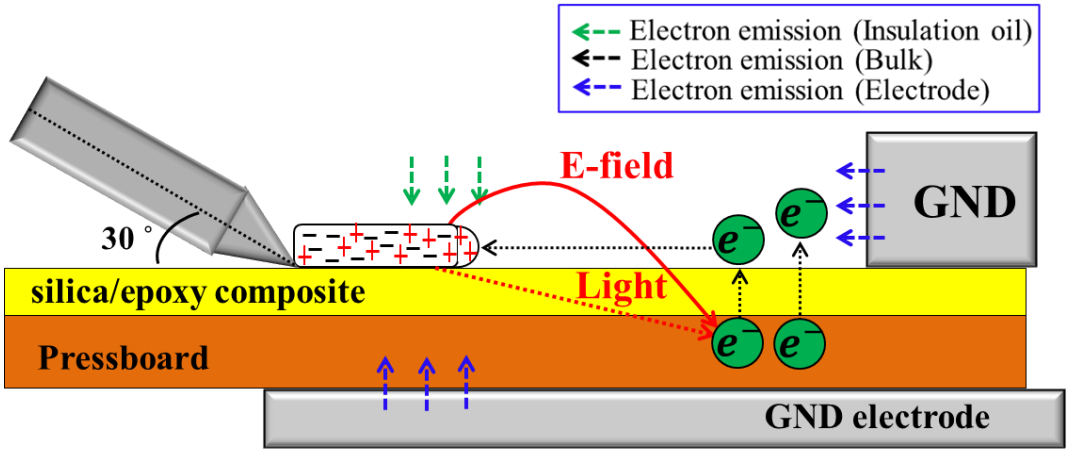

Figure 4.41 Surface discharge conceptual model in oil/PB composite insulation system

4.7 SUMMARY

Chapter 4 focused on surface modifications of the insulating paper by solid layer coating method to discuss the effect of the solid layer coating at the oil/PB composite insulation system on the suppression on both creepage discharge inception and propagation. The creepage discharge behaviour at the oil/pressboard interface have been discussed with different silica filler loadings, coating materials and electrode configurations.

The research work reveals that the new coating method on the PB surface can indeed affect the creepage discharge behaviour as well as dielectric properties.

The experimental results are summarized as follows:

1. ε_r' decreases with the increase of the S_l, while further increasing S_l results in increase ε_r'.

2. Silica/epoxy nanocomposite coated PB shows lower P_d and smaller l_d with low silica filler loading up to 3 wt% than that of conventional PB, and should improve the insulation performance of PB/oil insulation system.
3. Three possibly considered mechanism are proposed to explain the results on the effect of the coating method on P_d and l_d as follows:

    1) Drying of water content in neat PB decrease in ε_r' by silica/epoxy nanocomposite coating
    2) Surface modification effect by solid layer coating
    3) Silica/epoxy composites coating suppressing the electron emission from the surface of PB

CHAPTER 5

Creepage Discharge Characteristics of Silica/Epoxy Nanocomposite Plate

5.1 EXPERIMENT

5.1.1 ELECTRODE SETUP

Figures 5.1 (a) and (b) show side view and top views of electrode system, respectively. The tip radius of the needle electrode was 10 μm and gap distance was 50 mm to the bar electrode. The needle electrode was touched at an angle of 30 degree from the surface of silica/epoxy nanocomposite. There is no back electrode at the bottom place of the specimen to consider only the surface effect of specimens on creepage discharge.

The whole electrode system was placed in a mineral oil immersed chamber as shown in Fig. 5.2. Vacuuming was made in the chamber for 2 hours to reduce gasses that influence to PDIV of the oil/solid composite insulation system. Discharge image was observed using a digital camera (Fujifilm Finepix S100fs) and a digital camera equipped with an image intensifier (Hamamatsu C9016-2x). Discharge light emission was also detected with a photomultiplier tube (PMT, Hamamatsu Photonics, H6780~4) to determine PDIV. A 50 Ω resistor was used to obtain the discharge current signal.

A positive standard lightning impulse voltage was applied to the needle electrode varied from 25 kV (PDIV of neat epoxy) to 75 kV by a step with increment of 5 kV. The interval time between each voltage level was one minute. The impulse voltage application was repeated 5 times at each voltage level.

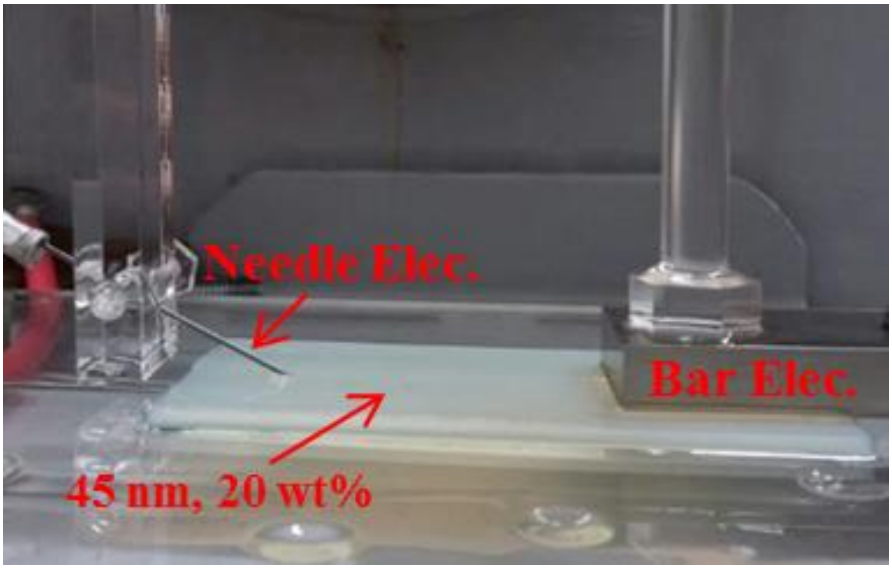

(a) Side view

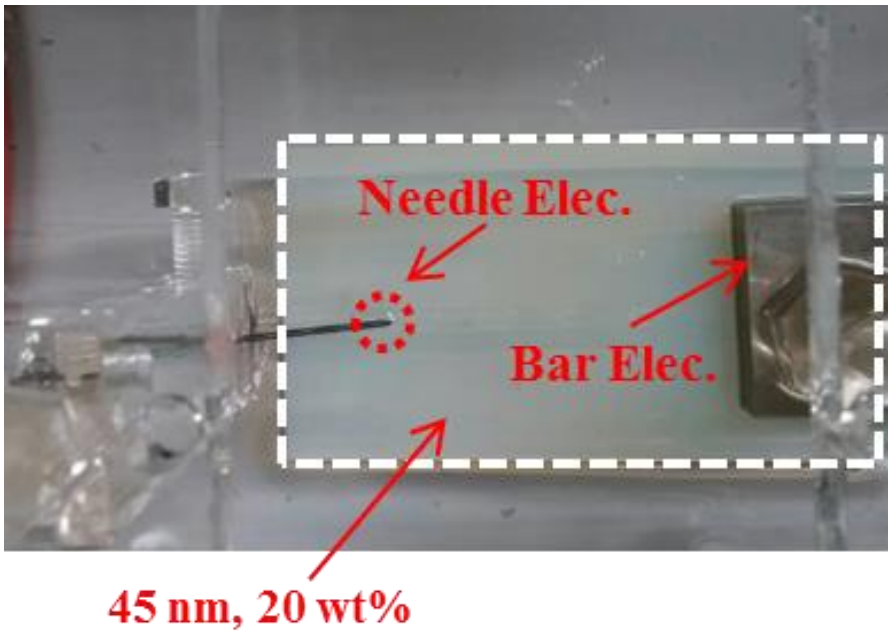

(b) Top view

Figure 5.1 Needle-bar electrode configurations with nano silica/epoxy composite plate

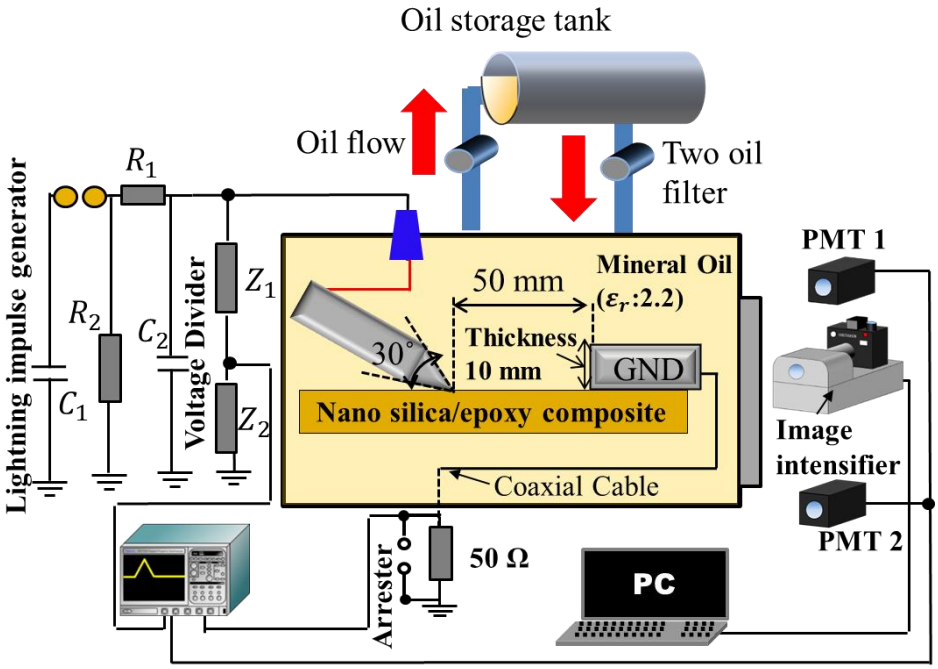

Figure 5.2 Diagram of experimental setup to measure and observe PDIV and creepage discharge properties in oil and SiO_2/epoxy composite insulation system

5.1.2 SAMPLE PREPARATION

Table 5.1 lists prepared silica/epoxy nanocomposite with different filler loading (0.1, 0.5, 1, 3, 5, 10, 20, 45 wt%) of 45 nm and particle size (12, 22, 45, 80, 130, 500 nm and 13 μm) as shown in Table 5.1.

Figures 5.3 and 5.4 show photos and SEM images of prepared with different nano S_i. All samples were supplied from Nissan chemical industries., LTD. The size of each sample for creepage discharge measurement and dielectric property is 70 mm by 100 mm and 3 mm, 70 mm by 70 mm and 1 mm, respectively. Figures 5.3 and 5.4 shows SEM image of both surface layer and middle layer of 12, 22, 45 and 80 nm silica fillers to investigate the nano silica state of dispersion in the base epoxy matrix. To observe nano silica state of dispersion, samples with pretreated by Platinum vapor deposition and protective film laminated using focused ion beam (FIB) with accelerating voltage 1.0 kV. The observation of the particle dispersion state was investigated by Nissan Chemical Co. Ltd. As can be seen in Figs. 5.3 and 5.4, white circles in the figures show nano silica particles dispersed in base epoxy. All the silica/epoxy nanocomposite specimens seem to exhibit good dispersion of nanoparticles in both surface layer and middle layer.

Table 5.1 Properties of prepared nano silica/EP composites

Sample name	Silica size	Silica purity	Manufacturing method	Surface treatment	Filler loading, x wt% (weight percent)
N·EP (EP)	Neat epoxy	-	-	-	-
EP12-3, 10	12 nm	normal	A	A	3, 10 wt%
EP 22-3, 10	22 nm	normal	A	A	3, 10 wt%
EP 45-x	45 nm	normal	B	A	0.1, 0.5, 1, 3, 5, 10, 20, 45 wt%
EP 80-3, 10	80 nm	normal	A	B	3, 10 wt%
EP 500-3	500 nm	normal	Other company product	A	3 wt%
EP 13000-3	13 μm	normal	Other company product	A	3 wt%

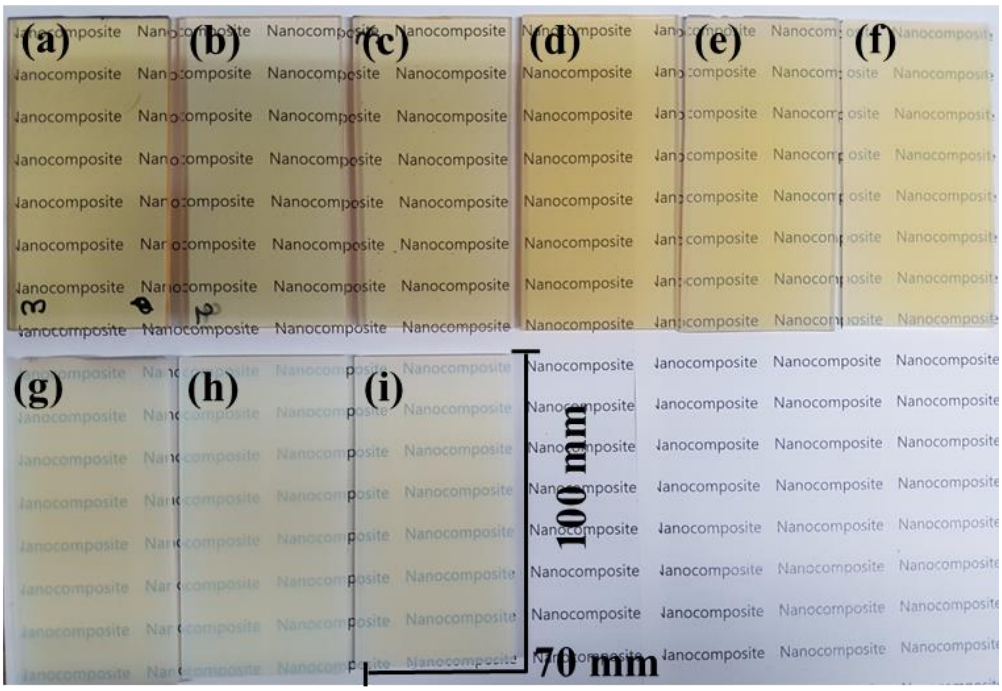

Figure 5.3 Photos of samples with different nano silica filler loading and neat epoxy (a) neat epoxy (b) 0.1wt%, (c) 0.5wt%, (d) 1wt%, (e) 3wt%, (f) 5wt%, (g) 10wt%, (h) 20wt% and (i) 45wt%

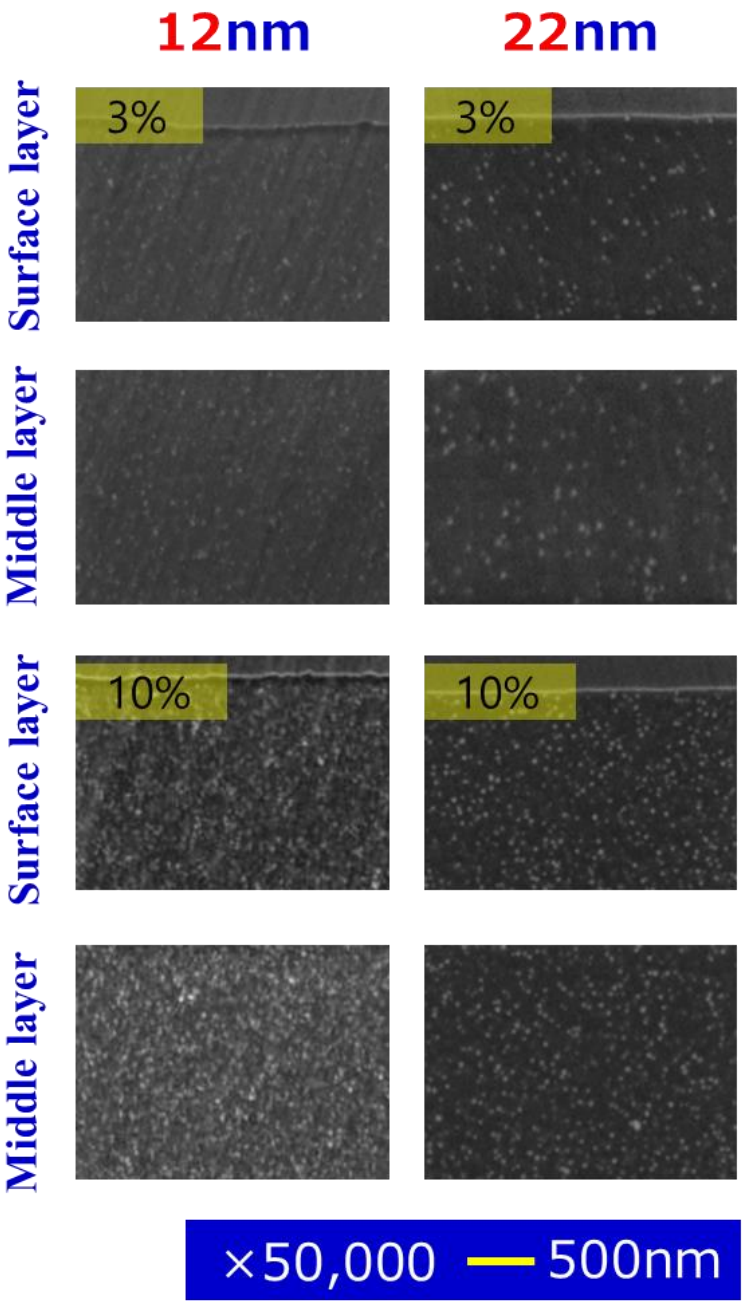

Figure 5.4 SEM images of surface and middle layer of nano silica/EP composites with different nano silica

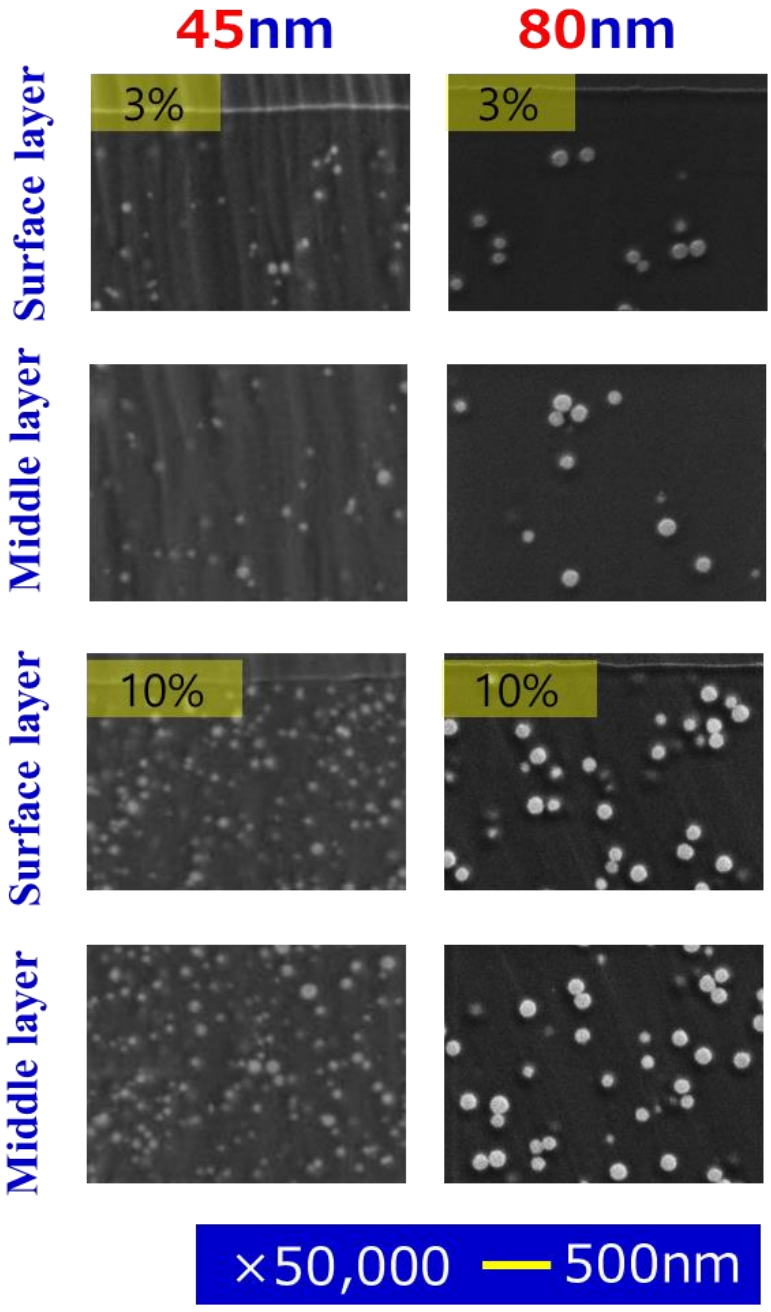

Figure 5.5 SEM images of surface and middle layer of nano silica/EP composites with different nano silica

5.1.3 DIELECTRIC PROPERTY MEASUREMENT

Before dielectric property measurement, all the samples were dried for 1 hour at 100℃ to remove the moisture effect. Figures 5.6 (a) and (b) show the weight and thickness before and after the drying process of silica/epoxy nanocomposite. As you can see in the figures, the weight decreases after the dry process and then increases after 24 hours at room temperature. But there is no variation of thickness before and after the dry process.

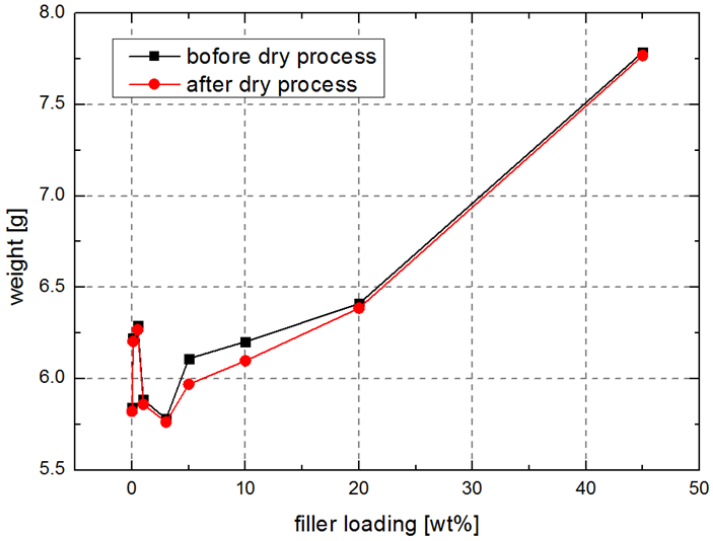

(a) Weight variation before and after dry process of sample with different filler loading

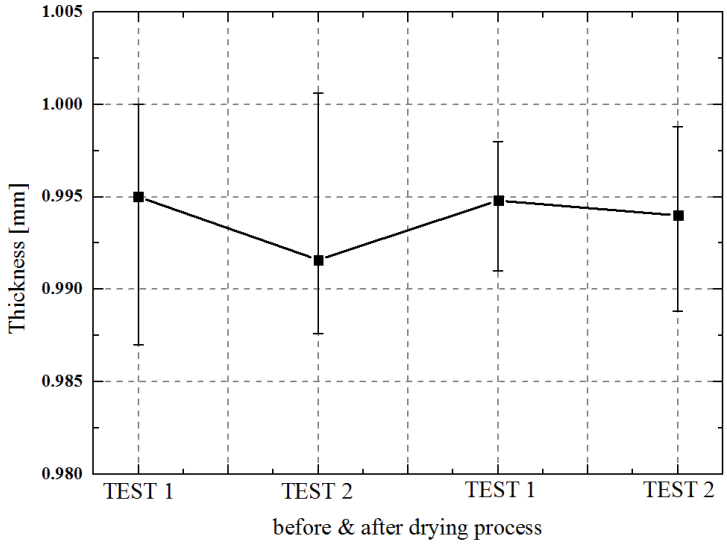

(b) Thickness variation before and after dry process

Figure 5.6 The variation of weight and thickness of 5wt% silica/epoxy nanocomposite before and after drying process at 100℃ for 1 hour

Dielectric properties of each specimen were measured with an impedance analyzer (IWATSU Impedance Analysis PSM3750) at room temperature and frequency from 50 Hz to 2 MHz after dry process. The number of test samples of each specimen was two. The size and thickness of a sample was 70 mm by 70 mm and 1mm, respectively. Prior to measurement, gold electrodes with diameter of 50 mm were deposited onto both sides of a sample by Magnetron Sputter (MSP-1S) to ensure the reproducibility of measurement and improve the contact area between the electrode and the surface of epoxy plate. Gold electrode on the surface of sample is sputtered for 3 minute with a thickness of 3 Å/sec and then we confirmed that the thickness of sputtering on the surface of epoxy/silica nanocomposite plate is 54 nm using a thickness gauge as shown in Fig. 5.7. Note that measurements of dielectric properties were conducted two times each for two samples with error of 2 %.

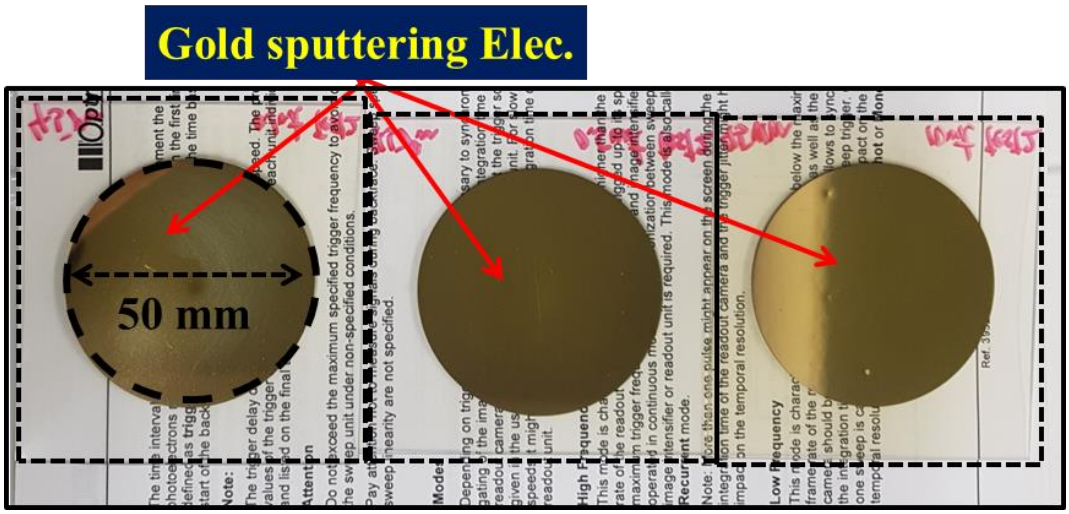

Figure 5.7 Silica/epoxy nanocomposites for dielectric property measurement

5.2 RESULTS AND DISCUSSION

5.2.1 DIELECTRIC PROPERTIES

Figures 5.8 (a) to (b) show frequency dependence of real part (permittivity ε_r') and imaginary part (dielectric loss ε_r'') of the complex dielectric constant ε_r^* for EP with different nano silica filler loadings at room temperature. It can be seen in Figure that ε_r' decreases stably with increasing frequency from 50 Hz to 2 MHz.

As can be seen in Fig. 5.9, ε_r' increases with increase in the filler loading at 100 kHz corresponding to dominant frequency component that standard lightning impulse voltage contains. It is also obvious from Fig. 5.9 that ε_r' decreases with decreasing the filler loading below 1 wt%, and reaches a minimum at 0.1 and 0.5 wt%, while further increasing nano S_l results in increased ε_r' above 3 wt%. This reduction in ε_r' was discussed in Chapter 4. As can be seen in Fig. 5.8 (b), ε_r'' decreases with increasing frequency from 50 Hz to 2 MHz, while no significant difference appears in ε_r'' under 20 wt% loading at 100 kHz.

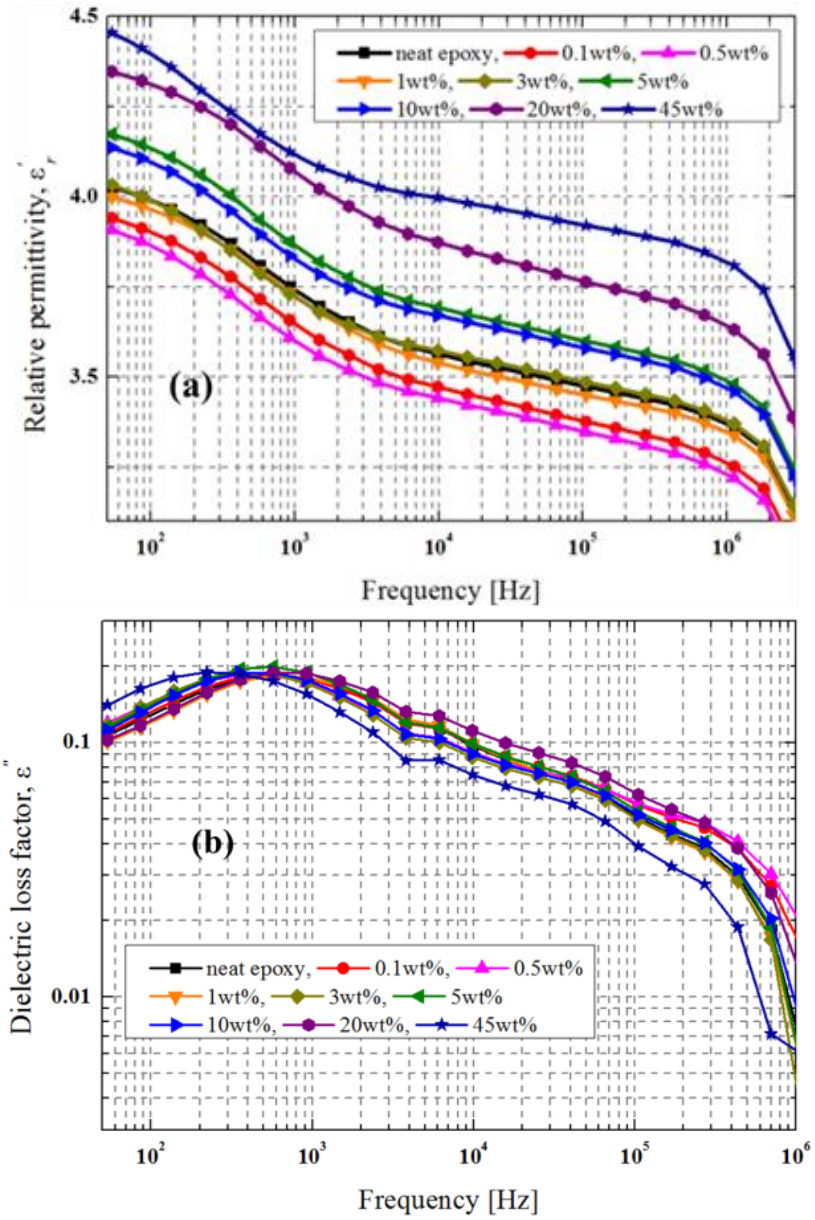

Figure 5.8 Frequency dependence of complex permittivity at room temperature; (a) real part of permittivity of each specimen, (b) dielectric loss

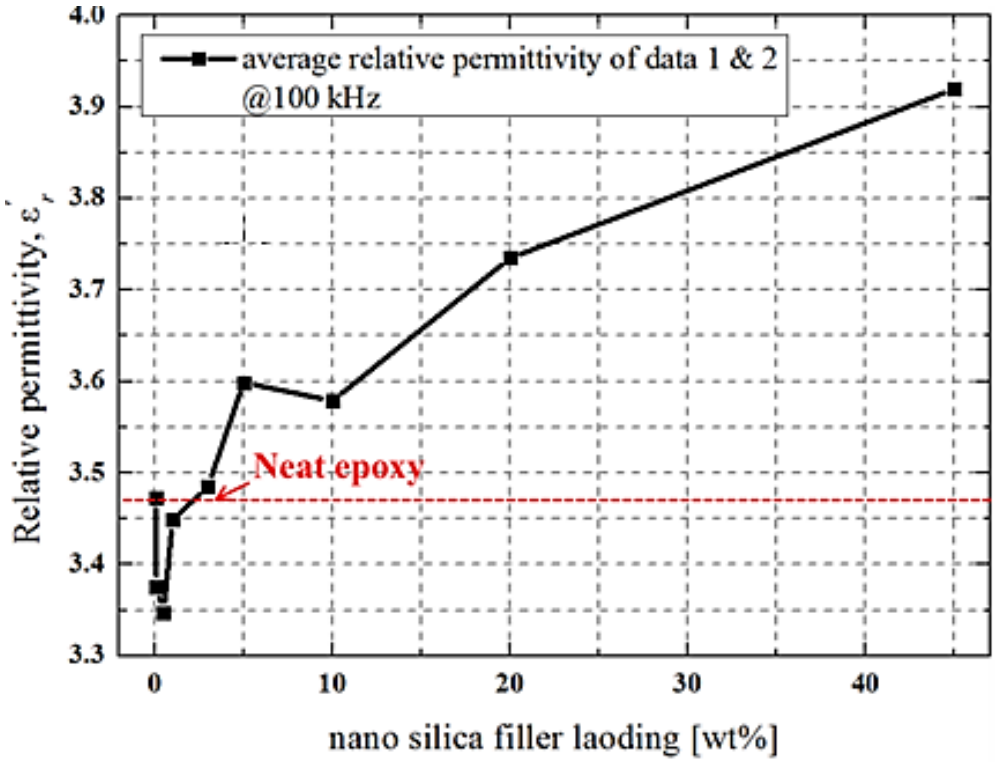

Figure 5.9 Relative permittivity at 100 kHz with different nano silica filler loading

Figures 5.10 (a) to (b) and 5.11 (a) to (b) show frequency dependence of real part (permittivity ε_r') and imaginary part (dielectric loss ε_r'') of the complex dielectric constant ε_r^* for EP with different nano silica size of 3 wt% and 10 wt%, respectively at room temperature. It can be seen in Figure that ε_r' decreases stably with increasing frequency. As can be seen in Fig. 5.11 (a) and 5.12 (a), ε_r' increases with increase in the filler size at 100 kHz corresponding to dominant frequency component that standard lightning impulse voltage contains. It is also obvious from Fig. 5.11 (a) and 5.12 (a) that ε_r' decreases with decreasing the filler size below 22 nm, while further increasing nano silica filler size results in increased ε_r' above 22 nm with keeping the filler loading constant. As can be seen in Fig. 5.10 (b) and 5.11 (b), ε_r'' increases with increasing frequency, while no significant difference appears in ε_r'' under 20 wt% loading at 100 kHz.

Santanu Singha and M. Joy Thomas et al., [104] have reported dielectric property with different particle size. Micro size particle/epoxy composites show a higher permittivity value than the nanocomposites. They suggest the reason on the high permittivity value in micro composites probably due to the fact that there is no restriction in the mobility of epoxy chains with micro fillers [104]. Toshikatsu Tanaka et al., [105-107] have reported electron traps existing inside core quantum dots (QDs), shell and interface in a core-shell structure embedded in polymer

matrix. The QDs model has formed polymer matrix, shell insulator and core quantum dot. Following Eqn. 5.1 shows polarizability in core-shell system [105-107].

$$\alpha = 4\pi r_2^3 \frac{(\varepsilon_2 - \varepsilon_m)(\varepsilon_1 - 2\varepsilon_2) + \rho(\varepsilon_1 - \varepsilon_2)(\varepsilon_m - 2\varepsilon_2)}{(\varepsilon_2 + 2\varepsilon_m)(\varepsilon_1 + 2\varepsilon_2) + 2\rho(\varepsilon_2 - \varepsilon_m)(\varepsilon_1 - \varepsilon_2)} \quad (5.1)$$

where core with permittivity and shell radius is ε_1 and r_1, shell with permittivity , fraction of the total particle volume occupied by the core and thickness is ε_2, $\rho = (r_1/r_2)^3$ and (r_2-r_1), respectively.

Eqn 5.1 can be explained in terms of increase in ε_r' with filler loading and size. On the other hand, α and ε_r' are proportional to each other. The α increase with increase nano filler size, relation between polarizability and ε_r' shows follows:

$$\varepsilon_r' = \varepsilon_0 + \chi$$

where ε_r' is permittivity [F/m], ε_0 is space permittivity [F/m] and χ is polarizability.

$\rho = (r1/r2)^3$ is the fraction of the total particle volume occupied by the core. A core-shell nanoparticle can be approximated as an effective homogeneous sphere with an equivalent permittivity given by the Eqn. 5.2. The ε_c increase with increase nanoparticle size from Eqn. 5.2.

$$\varepsilon_c = \varepsilon_2 \frac{\varepsilon_1(1 + 2\rho) + 2\varepsilon_2(1 - \rho)}{\varepsilon_1(1 - \rho) + \varepsilon_2(2 + \rho)} \quad (5.2)$$

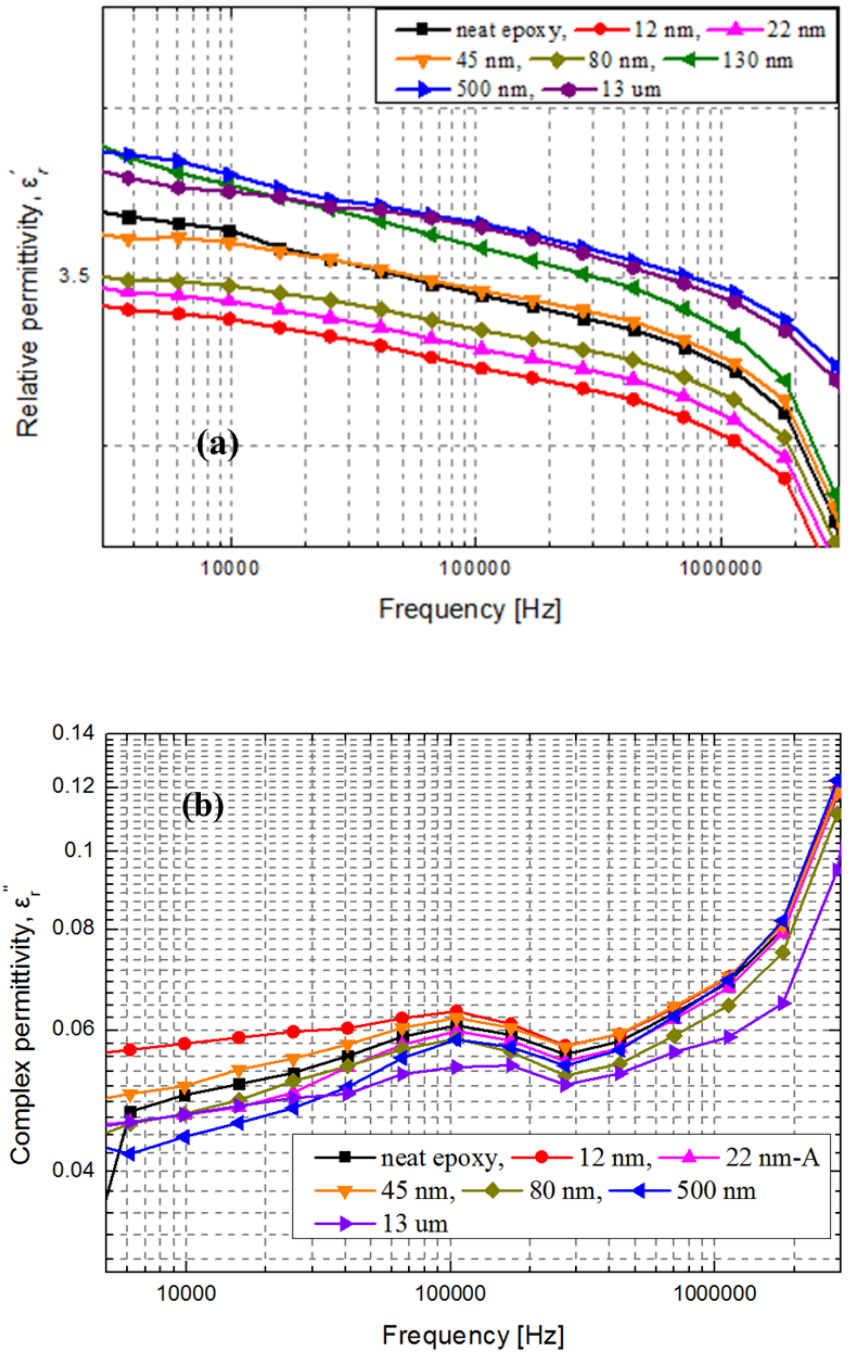

Figure 5.10 Frequency dependence of complex permittivity at room temperature with different nano silica sizes with keeping the filler loading 3 wt%; (a) real part of permittivity of each specimen, (b) dielectric loss

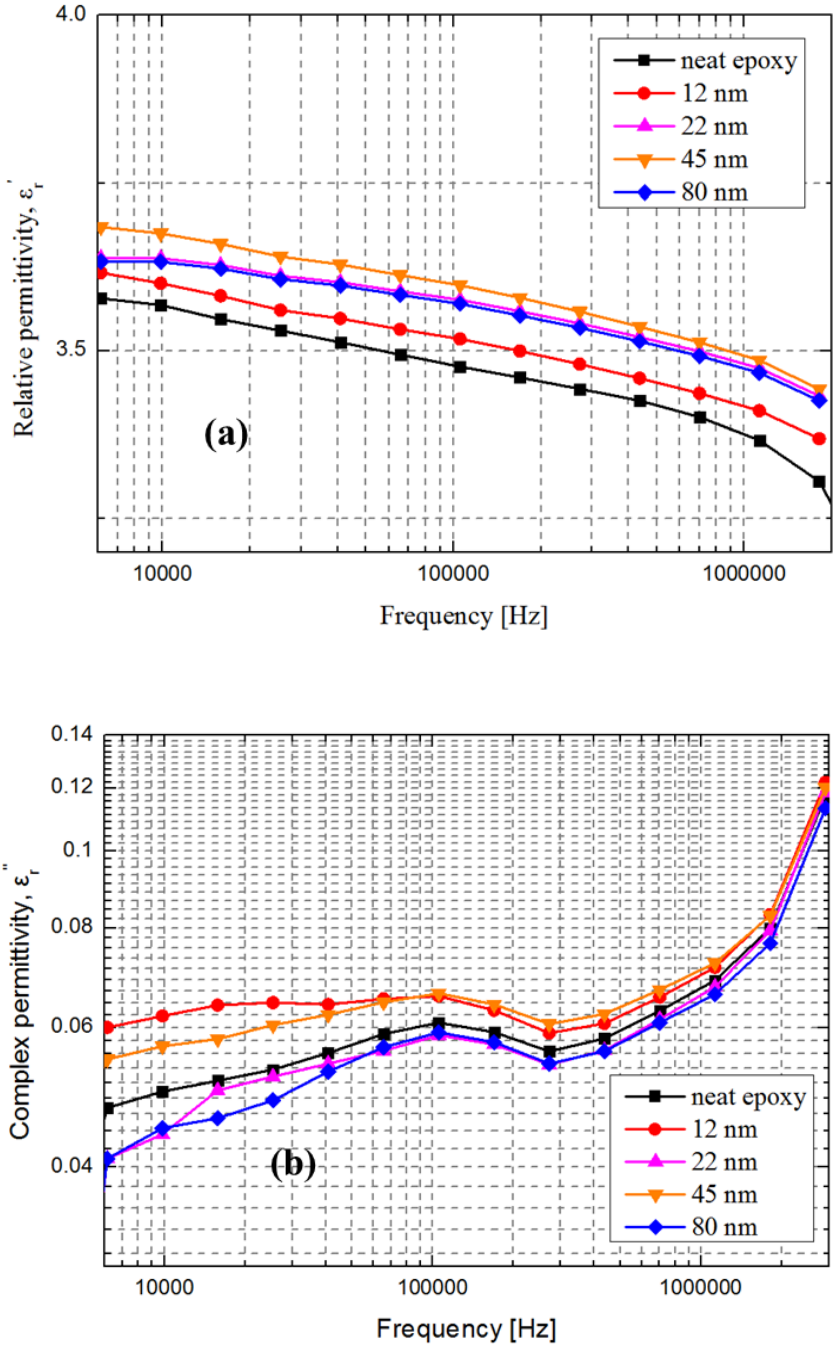

Figure 5.11 Frequency dependence of complex permittivity at room temperature with different nano silica size with 10 wt%; (a) real part of permittivity of each specimen, (b) dielectric loss

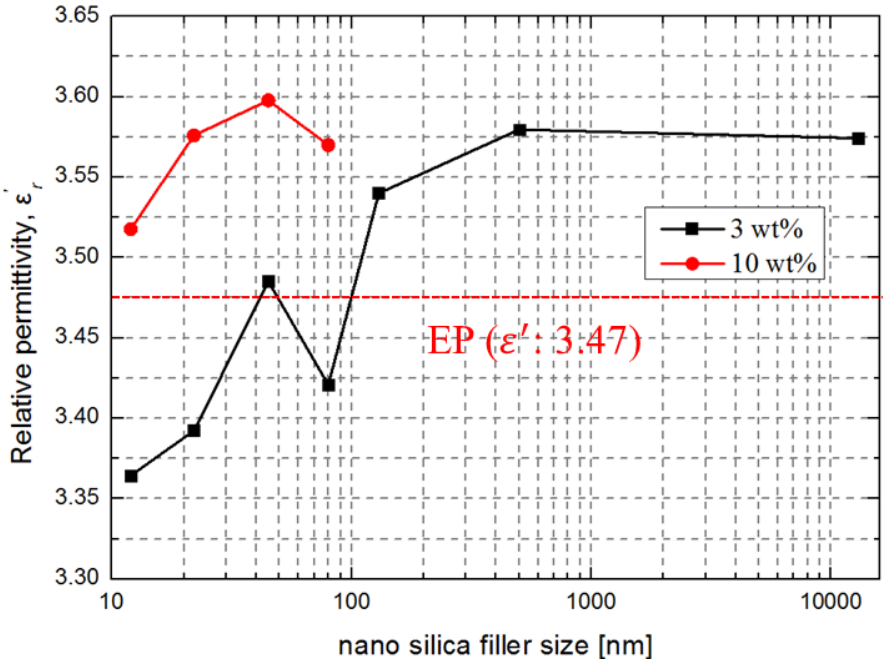

Figure 5.12 Relative permittivity at 100 kHz as a function of nano silica size for different filler loading

5.2.2 DISCHARGE PATTERNS AND DISCAHRGE OCCURRENCE PROBABILITY

Figures 5.13 (a) and (b) show creepage discharge image of EP and EP 45-1 wt% at 75 kV as well as waveforms of two PMT signals, current and impulse voltage. The decision way of PDIV is same with that given in Chapter 4. Note that white triangles in the figures depict the high voltage electrode. Here, let the discharge final length l_d be defined as the length from the high voltage electrode to a site of a longest discharge edge part. Discharge streamer in neat EP exhibits more intense luminous from the needle tip and higher peak current than that of EP 45-1 wt% at all the voltage levels as observed from PMT signal and current waveform.

Prior to study creepage discharge pattern under 25-75 kV of impulse voltage application, PDIV of neat EP was measured to be 30 kV. Three specimens were used to confirm reproducibility at least under the same conditions. Creepage discharges of all the samples were found to occur intermittently and randomly at a given V_a. Figure 5.14 shows discharge occurrence probability (P_d) as a function of V_i with different S_l. As can be seen in the Figure, P_d of 100% is observed over 45 kV for neat EP, while EP 45-45 wt% exhibits higher P_d than neat EP at 30 kV.

Next, let 50% creepage discharge occurrence ratio k_4 be defined as V_i giving 50% P_d of neat EP divided by that giving 50% P_d of silica/epoxy nanocomposite.

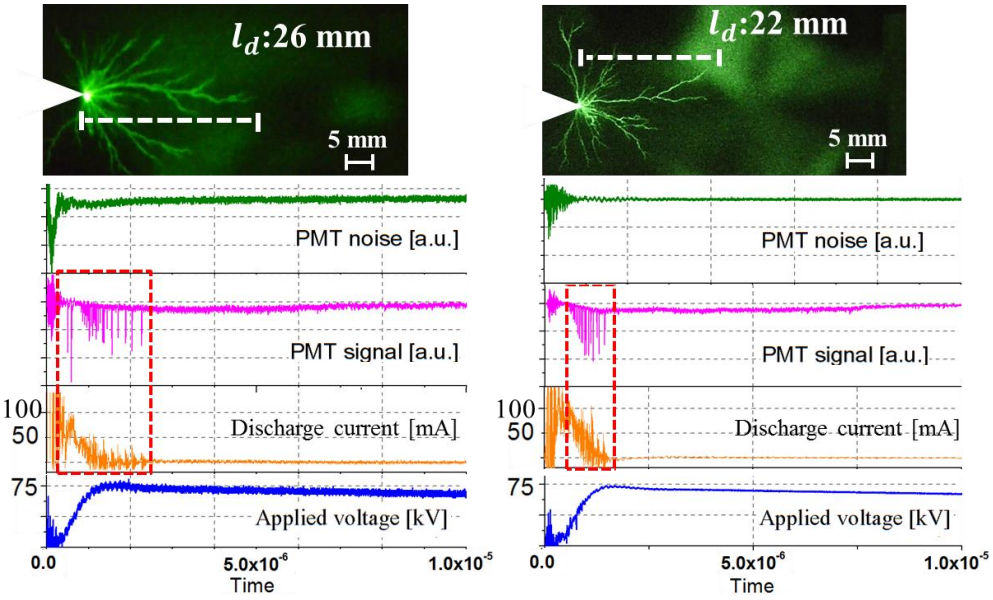

(a) Neat epoxy discharge image (b) SP-1wt% discharge image

Figure 5.13 Discharge image of neat EP and SP 45-1wt% at 75 kV

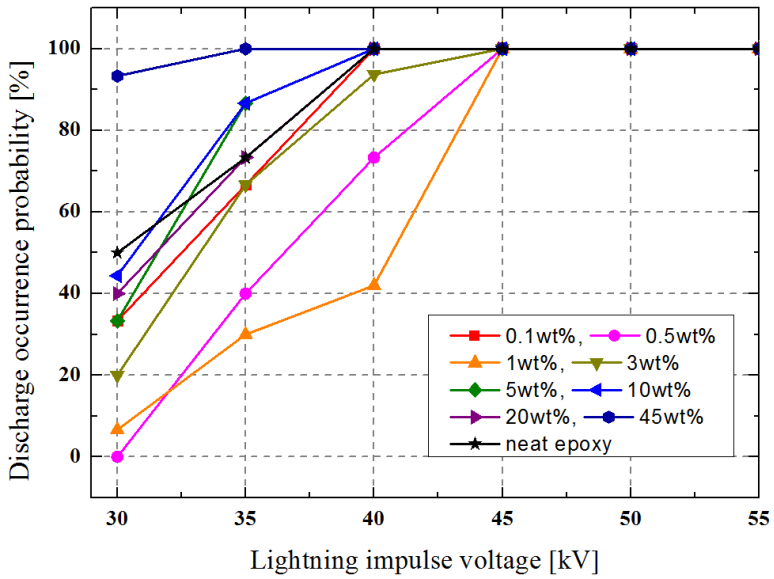

Figure 5.14 Discharge occurrence probability at each voltage level with different nano silica filler loading

Figure 5.15 shows the relationship between ε_r' and 50% discharge occurrence probability ratio k_4. As seen in figure, the ratio k_4 is larger than one, meaning that the insulation performance against the creepage discharge generation can be improved with appropriate S_l compared to that of neat EP. Note that k_4 presents the highest value 1.33 at S_l of 1 wt%, while further decreases with increasing nano S_l above 3 wt%. ε_r' presents firstly decreases and increases with the increase of the S_l, and reaches a minimum at 0.5 wt%. It can be concluded that the appropriate low S_l improved P_d of silica/epoxy nanocomposite specimens.

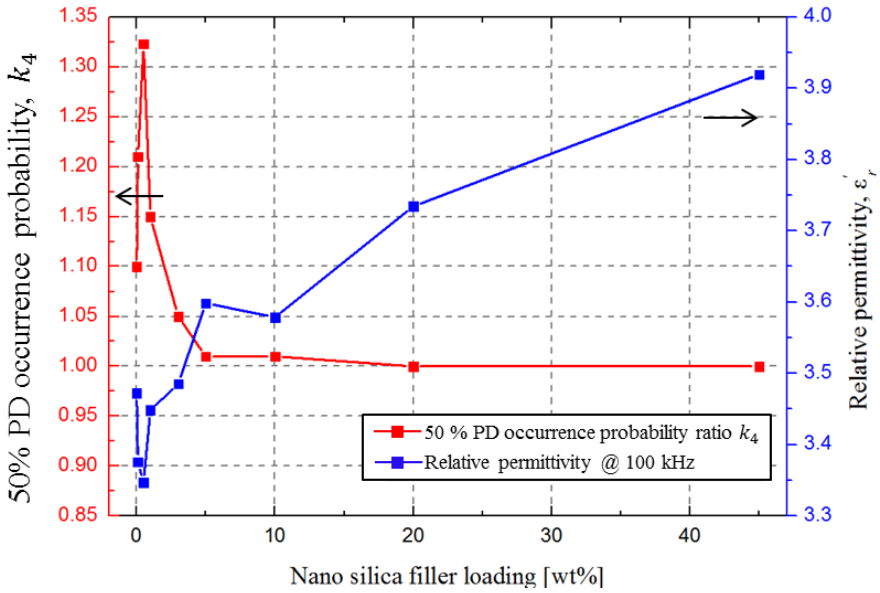

Figure 5.15 The relationship between discharge occurrence probability P_d and permittivity ε_r'

Figure 5.16 shows P_d as a function of V_i for different nano silica size with keeping the filler loading constant. As can be seen in Figure, EP with big size nano particles (130, 500 nm and 13 μm) exhibits higher P_d than neat EP and EP with small size particles at all the V_i, whereas EP with small size particles as low as 80 nm and 3 wt% show that creepage discharge occurrence can be improved. Figure 5.17 shows the relationship between ε_r' and 50% P_d. Note that 50% PD occurrence probability ratio k_4 presents the highest value 1.25 at nano silica size of 22 nm, while ratio k_4 decreases with increasing nano silica size.

Shengtao Li *et al.*, [94] have reported surface flashover performance under impulse voltage in vacuum with nanoparticles (NPs) and micro size particles (MPs) in terms of shallow and deep traps. MPs show contrary behavior and MPs causes a serious low flashover voltage, whereas small amounts (up to 3 wt%) of NPs improve flashover performance by over 58% compared with neat polystyrene.

MPs can introduce shallow traps while NPs introduce deep traps. The deep traps are crucial in improving flashover performance by trapping the charge carriers and thereby weakening secondary electron multiplication processes. In Fig. 5.17, nano size particle 22 nm can be improved P_d by over 28% and 43% compared with neat EP and 13 um size particle, respectively. This result shows similar trend with reference [94]. Thus, it might be possible that the nano size particle improve creepage discharge inception process, meaning that charge carriers are suppressed by deep trap from emitted secondary electron of the surface of epoxy/silica nanocompsoites.

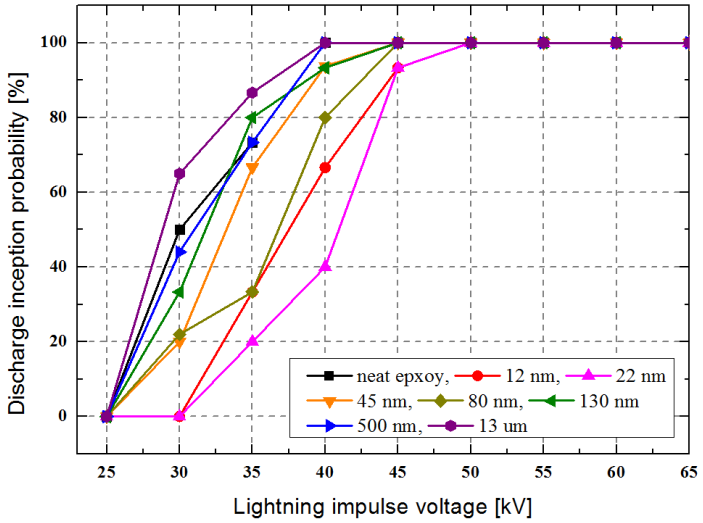

Figure 5.16 Discharge occurrence probability 3 wt% at each voltage level with different nano silica size

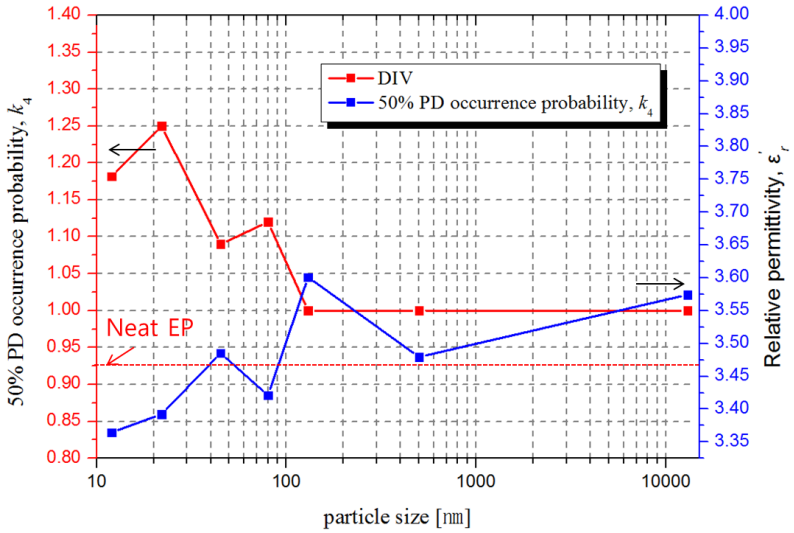

Figure 5.17 The relationship between discharge occurrence probability P_d and permittivity ε_r' of 3 wt%

5.2.3 DISCHARGE PROPAGATION LENGTH

Figures 5.18 to 5.22 show the discharge propagation length l_d at V_i and ratio k_5 of each kind of sample with different filler loading and size at 75 kV. It is evident from Figs. 5.18 to 5.22 that l_d for each kind of sample increases as the applied voltage V_i increases from 30 to 75 kV. Note that the average discharge propagation length l_{dave} of nano silica/epoxy composite samples at all the voltage levels is shorter than that of neat EP samples. Figs 5.19 and 5.21 show the l_{dave} ratio k_5 at 75 kV. Ratio k_5 be defined as 75 kV giving l_d of neat EP divided by that giving l_d of silica/epoxy nanocomposite. As seen in figure, the ratio k_5 is larger than one, meaning that the insulation performance against the creepage discharge propagation can be improved with appropriate S_l and filler size compared to that of neat EP. Note that k_5 presents increases and decreases with the increase of the S_l and filler size above 3 wt% and 80 nm, respectively. It can be concluded that the low S_l and EP with small size particles improved l_d. But as mentioned in chapter 4, once discharge occurred, l_d of each sample is becoming the same at each voltage levels, besides scattering of the data overlaps each other, meaning no appreciable effect of the filler loading on l_d appears under the present condition.

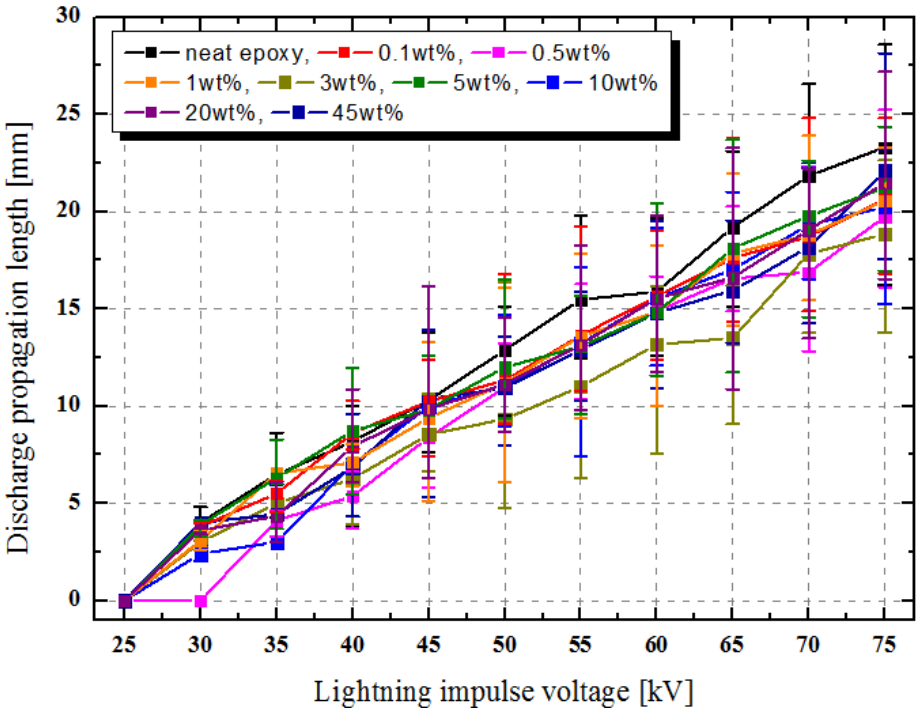

Figure 5.18 Discharge propagation length of EP with different silica filler loading as a function of V_i with keeping the 45 nm filler size

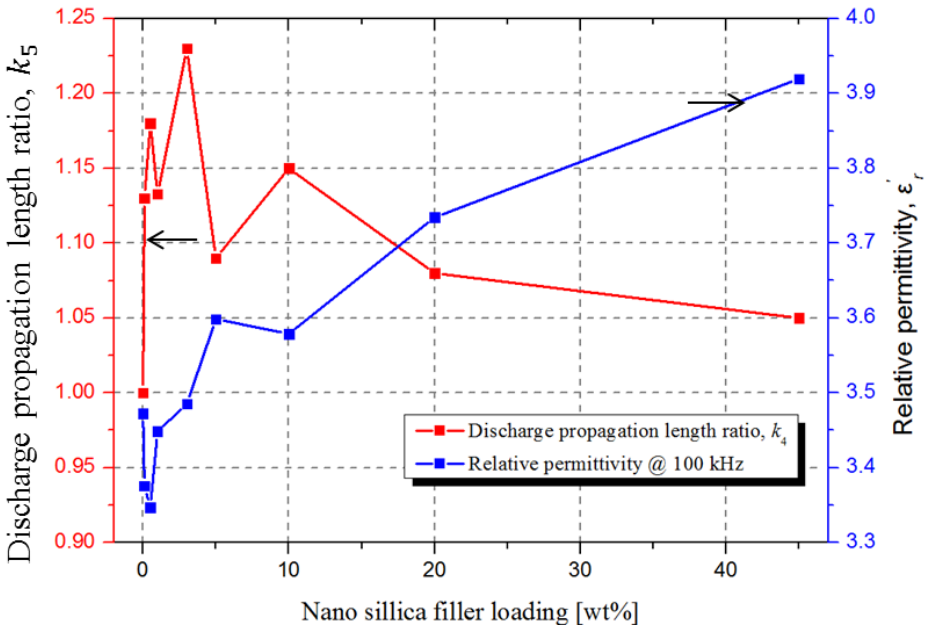

Figure 5.19 The relationship between average discharge propagation length l_{dave} and permittivity ε_r' of EP as a function of silica filler loading at 75 kV

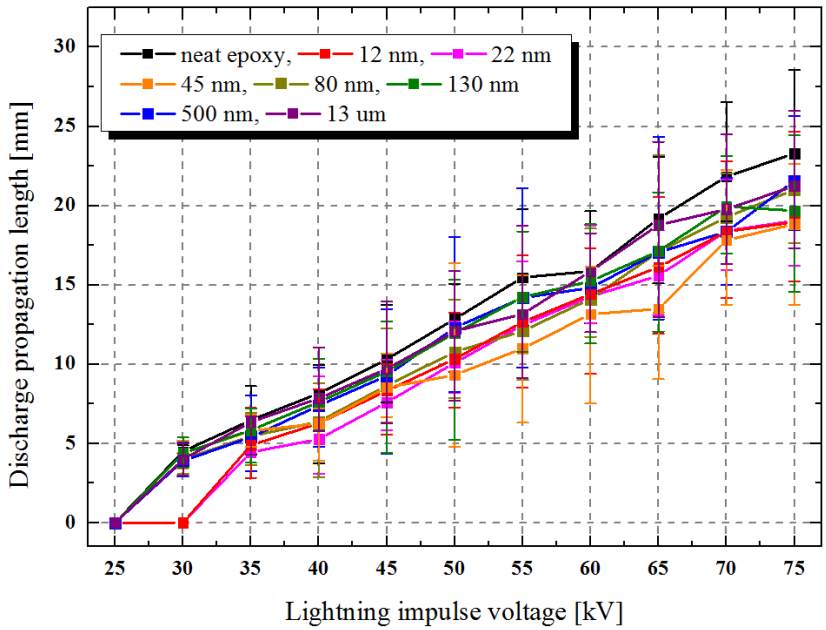

Figure 5.20 Discharge propagation length l_d of EP with different silica filler size as a function of V_i with keeping the 3 wt% filler loading

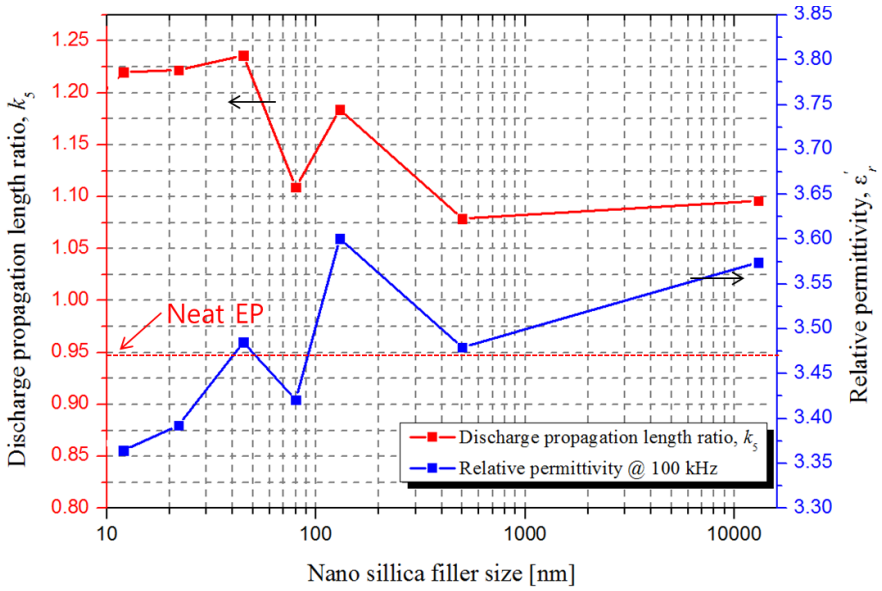

Figure 5.21 The relationship between average discharge propagation length l_{dave} and permittivity ε_r' of EP as a function of silica filler size at 75 kV with keeping the 3 wt% filler loading

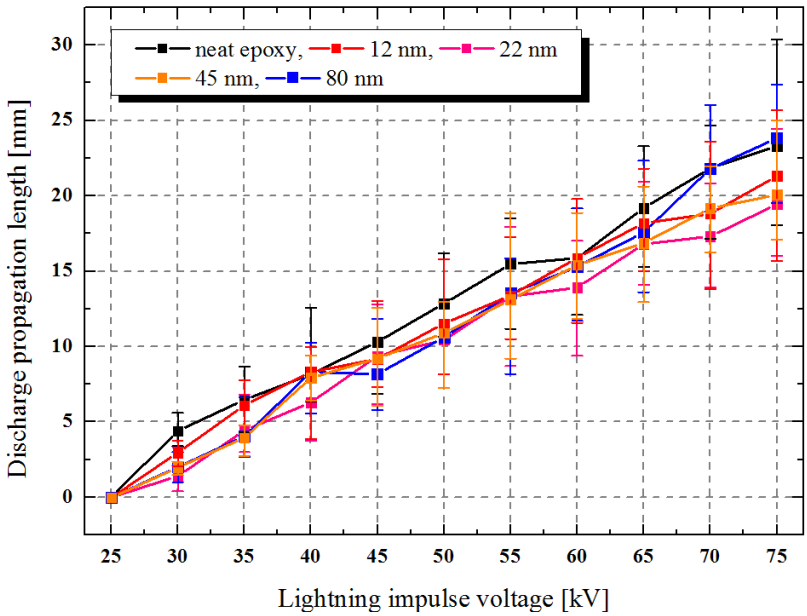

Figure 5.22 Discharge propagation length l_d of EP with different silica filler size as a function of lightning impulse voltage with keeping the 10 wt% filler loading

5.2.4 DISCUSSION

Next, the effect of nano silica on PDIV is discussed. The following two reasons are possibly considered to explain the experimental results of the effect of nano silica loading on the discharge occurrence probability of EP as shown in Figs. 5.15 and 5.16:

1) Relative permittivity reduction effect by introducing nano size silica particle in base epoxy
2) Silica/epoxy nanocomposites are more likely to suppress the electron emission from the surface layer of nanocomposite.

In view of the tradition dielectric theory, it is well known that particles introduce defects into epoxy resin and such defects act as the charge accumulation centers, enhancing the local electric field. This causes a decrease in PDIV and BDV which is confirmed in microcomposites. When the size of the particles in reduced to nanometer level, the situation is totally different [56, 84, 108-112]. For instance, the electric strength and surface flashover voltage increase in particle/epoxy nanocomposites with appropriate filler loading. These characteristics are associated with the nanoparticle/epoxy interaction zone. However, the structure and properties of the interaction zone are influenced by many factors such as the surface modification of particles, dispersion and type of particles, the physical characteristics of epoxy resin etc. [55].

The electric field distribution at triple junction (mineral oil, pressboard and electrode) is influenced by the relative permittivity of silica/epoxy nancomposite. On the other hand, low permittivity may weaken the electric field distortion near the triple junction and thereby improve the creepage discharge performance. Following Eqns. 5.1 and 5.2 show random arranged model related with $\varepsilon_{\mathrm{r}}'$ dependent filler loading and consider a core-shell system, respectively.

$$\varepsilon_a^k = \left(\frac{V_p}{100}\right) * \varepsilon_p^k + \left(1 - \frac{V_p}{100}\right) * \varepsilon_m^k \tag{5.1}$$

where $\varepsilon_{\mathrm{a}}^k$ is $\varepsilon_{\mathrm{r}}'$ of composites, $\varepsilon_{\mathrm{p}}^k$ is $\varepsilon_{\mathrm{r}}'$ of nano filler, $\varepsilon_{\mathrm{m}}^k$ is $\varepsilon_{\mathrm{r}}'$ of matrix, V_{p} is nano filler loading and *k* is parallel circuit (k=1), series circuit (k=-1) and random arranged (k=1/3).

$$\alpha = 4\pi r_2^3 \frac{(\varepsilon_2 - \varepsilon_m)(\varepsilon_1 - 2\varepsilon_2) + \rho(\varepsilon_1 - \varepsilon_2)(\varepsilon_m - 2\varepsilon_2)}{(\varepsilon_2 + 2\varepsilon_m)(\varepsilon_1 + 2\varepsilon_2) + 2\rho(\varepsilon_2 - \varepsilon_m)(\varepsilon_1 - \varepsilon_2)} \tag{5.2}$$

where core with permittivity and shell radius is ε_1 and r_1, shell with permittivity and fraction of the total particle volume occupied by the core is ε_1 and (r_2-r_1), $\rho = (r_1/r_2)^3$ and α is polarizability.

The effect of decrease in ε_r' with filler loading and size can not be explained, but, it can be explained in terms of increase in ε_r' with filler loading and size. The ε_r' reduction effect with low nano filler loading is discussed in Chapter 4. In the case of Eqn. 5.2, the α increase with increase nano filler size, the relation between polarizability and ε_r' shows follows:

$$\varepsilon_r' = \varepsilon_0 + \chi$$

where ε_r' is permittivity [F/m], ε_0 is space permittivity [F/m] and χ is polarizability.

Figure 5.23 shows calculated value of ε_r' for epoxy/silica nanocomposite by random arranged model as following Eqn. 5.3.

$$\varepsilon_a^k = \left(\frac{V_p}{100}\right) * \varepsilon_p^k + \left(1 - \frac{V_p}{100}\right) * \varepsilon_m^k \qquad (5.3)$$

where ε_a^k is relative permittivity of epoxy/silica nanocomposite, ε_p^k is relative permittivity of nano filler (ε_r': 5.5), ε_m^k is relative permittivity of matrix (ε_r': 3.46) and *k* is parallel circuit (*k*=1), series circuit (*k*=-1) and random arranged (*k*=1/3). The results revealed that the calculated value by random arranged model is good agreement with experimental measured results and the ε_r' increase with increasing nano silica filler loading. On the other hand, low filler loading firstly decreases different from calculated results. This reduction part with low filler loading considered nanoparticle effect on ε_r' as mentioned in Chapter 4.

Figure 5.24 shows *E-d* characteristics of small gap between high voltage electrode and composites surface. The present dielectric property results reveal that the relative permittivity of low filler loading and small size particle decreased, reducing the electric field concentration between oil and solid interface as can be seen in Fig. 5.24. Therefore, the flashover performance in composite insulation system is superior at low filler loading and small particle size in terms of ε_r', as shown in Fig. 5.15 and 5.16. But there is need to explain on detailed mechanism for influence according to different particle size.

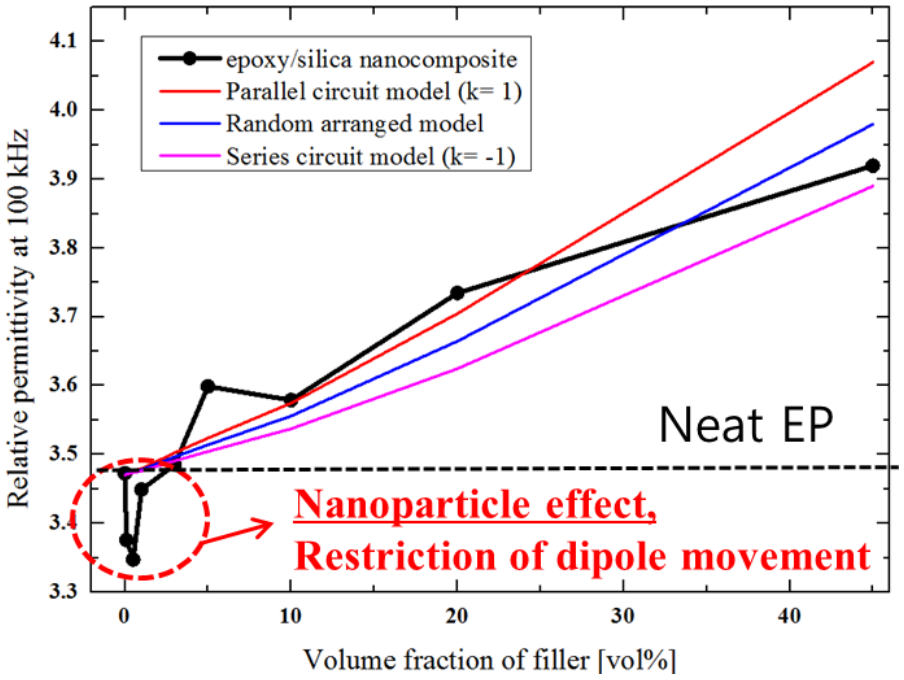

Figure 5.23 Calculated value of relative permittivity for epoxy/silica nanocomposite with different silica filler loading (relative permittivity of matrix and filler = 3.46 and 5.5)

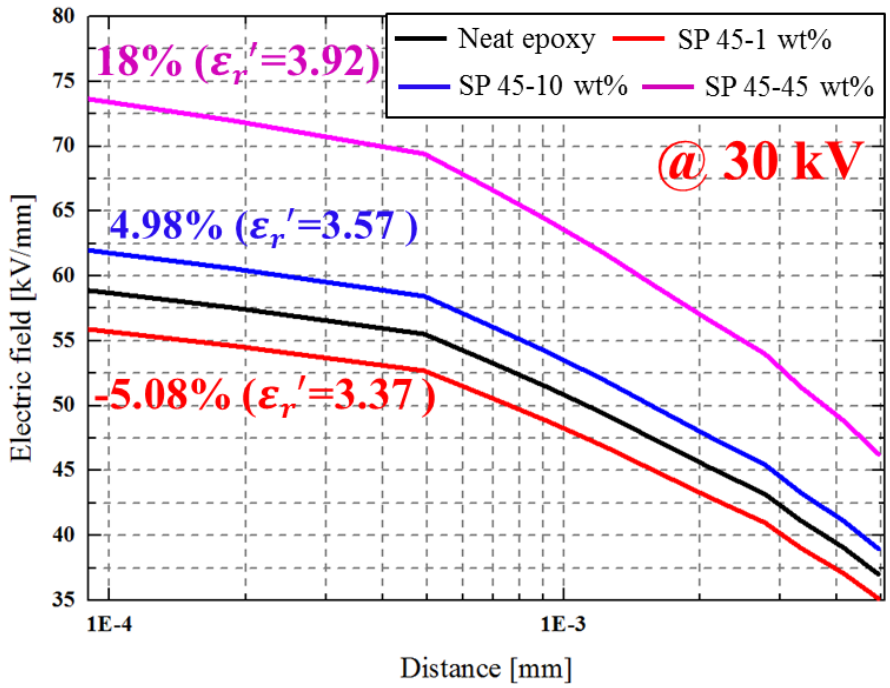

Figure 5.23 *E-d* characteristics of each sample with different nano silica filler loading

Second possible discussion is that nano silica/epoxy composites may suppress electron emission contributing to discharge initiation from the surface layer of nanocomposites, resulting in the decrease of P_d at all the V_i. Li shengtao et al., conducted thermally stimulated current (TSC) and pulsed electroacoustic method (PEA) measurements in vacuum condition. They indicate that deep electron trap level with increase in its density is introduced by nanofillers, leading to decrease in the charge carrier mobility as a result of enhancement of flashover voltage [84, 113]. Yu Chen et al., investigated the vacuum surface flashover characteristics of nano Al_2O_3/epoxy composite [114, 115]. The experimental results were explained in terms of different effects of shallow and deep traps. To the vacuum flashover process; i.e. deep electron traps can restrain the emission of internal secondary electrons inside the surface layer of material, and the surface flashover voltage can be possibly increased by enhancing the density of deeper traps.

With the above considerations taken into account, let us propose a surface flashover model in the epoxy/silica nanocomposites as illustrated in Fig. 5.25. Ionized free electron emitted from mineral oil under high electric field, besides free electrons are emitted from surface layer of epoxy/silica nanocomposites, and newly generated electrons can play a role as the seed of new electron avalanches. Then, the discharge is more likely to incept and creep along the interface between oil and PB. The epoxy/silica nanocomposites suppresses the electron emission from surface layer and thus extraction of electrons from the surface of nanocomposites on the discharge inception and propagation process.

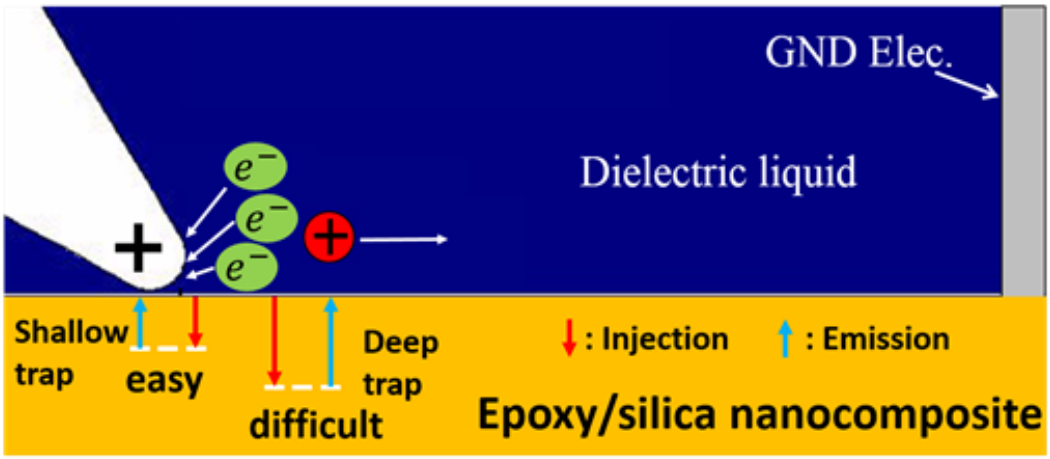

Figure 5.25 Surface flashover conceptual model in mineral oil

5.3 SUMMARY

Chapter 5 focused on surface flashover inception and propagation of the silica/epoxy nanocomposite with different silica filler loading and particle size to verify the nano silica effect in mineral oil under positive standard lightning impulse voltage.

The experimental results are summarized as follows:

1. Creepage discharge inception process is influenced by nanoparticle filler loading in base epoxy resin, the nano filler content of 1 wt% produces the best insulation performance in terms of discharge occurrence probability.
2. Creepage discharge inception is also affected by nano silica size, the nano filler size of 22 nm, 3 wt% produces the best insulation performance in mineral oil
3. The nano filler loading and filler size gives does not give appreciable effect on discharge propagation length under the present condition.
4. To explain our experimental results, we suggested two possibly considered mechanism on the effect of the coating method on P_d as follows:

    1) Relative permittivity reduction effect by introducing nano size silica particle in base epoxy
    2) Silica/epoxy nanocomposites are more likely to suppress the electron emission from the surface layer of nanocomposite.

Above two mechanisms are generally considered in surface discharge and surface flashover phenomenon in SF_6 gas, further work is needed on creepage discharge behavior and electrical properties such as streamer velocity, surface conductivity and resistivity, respectively.

CHAPTER 6

Creepage Discharge Modelling Approach

6.1 INTRODUCTION

An empirical study of creepage discharge behavior at the oil-pressboard interface using a needle-bar electrode experiment has been presented in Chapters 4 and 5.

A lot of researchers have investigated to understand the creepage discharge behavior in one insulation system such as oil, gas and air condition using COMSOL Multiphysics, because it is very difficult to analysis in composite insulation system. On the other hand, some researchers considered the solid insulation as ideal case, assuming that the conduction current in solid insulation for zero space charge. Besides COMSOL Multiphysics have a lot of limitations for electric field analysis, although they efforts to fit simulation results to experimental ones. Thus, these problems still remain challenge.

For this reason, we investigated the creepage discharge behavior in oil/pressboard composite insulation at 5 mm short electrode gap. The composite insulation model is developed by considering the effective barrier height by Poole-Frenkel model and relative permittivity of pressboard. Newly considered parameters are as follows:

1. The introduction of Poole-Frenkel conduction model for solid insulation
2. The introduction of effective barrier height for solid insulation
3. The introduction of dissociation for liquid insulation

The simulation results on Poole-Frenkel model, Effective barrier height and permittivity of solid insulation are discussed in Section 6.4.2-6.4.3.

6.2 GOVERNING EQUATIONS IN OIL

6.2.1 HYDRODYNAMIC DIFFUSION-DRIFT MODEL

The general expression of governing equations that contain the physics to model streamer development are based on the hydrodynamic diffusion-drift model for positive ion (ρ_+), negative ion (ρ_-) and electron (ρ_e) charge densities which are coupled through Gauss's Law given in Eqn 3.5. The thermal diffusion equation (3.6) is included to model temperature variations by the electric field and Joule heating during the creepage discharge as follows [17, 32, 33, 35-38, 65-67, 116-120]:

$$-\nabla \cdot (\varepsilon_r \nabla \mathrm{V}) = \rho_+ + \rho_- + \rho_e \tag{6.1}$$

$$\frac{\partial \rho_+}{\partial \mathrm{t}} + \nabla \cdot \left(\rho_+ \mu_+ \vec{E}\right) = G_I(|E|) + G_D(|E|, T) + \frac{\rho_+ \rho_- R_{\pm}}{q} + \frac{\rho_+ \rho_- R_{+,e}}{q} \tag{6.2}$$

$$\frac{\partial \rho_-}{\partial \mathrm{t}} + \nabla \cdot (\rho_- \mu_- \vec{E}) = -G_D(|E|, T) - \frac{\rho_+ \rho_- R_{\pm}}{q} + \frac{\rho_e}{\tau_a} \tag{6.3}$$

$$\frac{\partial \rho_e}{\partial \mathrm{t}} + \nabla \cdot (-D_e \nabla_{\rho e} \rho_e \mu_e \vec{E}) = -G_I(|E|) - \frac{\rho_+ \rho_- R_{+,e}}{q} - \frac{\rho_e}{\tau_a} \tag{6.4}$$

$$\frac{\partial \mathrm{T}}{\partial \mathrm{t}} + \mathbf{v} \cdot \nabla T = \frac{1}{\rho_l c_v} \left(k_T \nabla^2 T + \vec{E} \cdot \vec{J}\right) \tag{6.5}$$

In also (6.1) - (6.5), the parameters μ_+, μ_- and μ_e are the mobilities of the positive ions (1×10^{-9} m^2.V $\cdot$ s [17, 65]), negative ions (1×10^{-9} m^2.V $\cdot$ s [17, 65]) and electrons (1×10^{-4} m^2.V $\cdot$ s [17, 66, 67]), respectively, ρ_+, ρ_-, ρ_e are positive ions, negative ions and electrons, respectively; ε_r is the relative permittivity of a material; E is the total electric field intensity due to the applied voltage and space charge distributions; T is the temperature; q is the electronic charge; k_T thermal conductivity (0.13 W/m·K); c_v specific heat (1.7×10^3 J/kg $\cdot$ K); J_+, J_-, J_e are current density of positive ion, negative ion and electron, respectively; $G_I(|E|)$ is the molecular ionization; $G_D(|E|, T)$ is the ionic dissociation source term; R is the recombination rate; τ_a is the electron attachment time constant; v is oil's velocity.

The governing equations for solid insulation are composed of Gauss' law, the conduction current equation for zero space charge.

$$-\nabla \cdot \left(\varepsilon_r \nabla \vec{E}\right) = 0 \tag{6.6}$$

$$\nabla \cdot \vec{J} = 0 \tag{6.7}$$

where ε_r is relative permittivity of solid insulation; $\vec{E}$ and $\vec{J}$ are electric field within a solid insulation and current density of the solid insulation that is following equation (6.8) using Ohm's law.

$$\vec{J} = \sigma \vec{E} \tag{6.8}$$

where σ is the electrical conductivity of the solid insulation, In this simulation, σ is negligible such that $\sigma = 0$, i.e. the displacement current density is only considered.

Ohm's integration method is a calculating the total current through the surface integral of the physical quantity across the discharge space. This represents the total current flowing into integration space as following Eqn. 6.9.

$$\mathrm{I} = \int_S \left(\overrightarrow{J_c} + \frac{\partial \vec{D}}{\partial t}\right) \cdot d\vec{a} \tag{6.9}$$

where $\vec{D}$ is applied voltage and space charge distribution by total flux density and $\vec{a}$ is the surface integration on the electrode or discharge space.

6.2.2 CHARGE EMISSION FROM ELECTRODE AND SOLID INSULATION SURFACE

To consider the electron emission for the surface of solid insulation and for ground electrode and back electrode, the charge generation in PB bulk is assumed to be given by a dominant process among candidates of Poole-Frenke (P-F) emission from PB surface to dielectric liquid, and field emission from the metal electrode to dielectric liquid expressed in equations as follows:

$$J_{FE} = \frac{e^3\left|\vec{E}\right|^2}{8\pi h\Phi_{\mathrm{D}}}\exp\left(-\frac{8\pi\sqrt{2m}\Phi_{\mathrm{D}}^{\frac{3}{2}}}{3he\left|\vec{E}\right|}\right) \tag{6.10}$$

$$J_{TH} = AT^2 exp\left(-\frac{e\Phi_{\mathrm{D}}}{kT}\right) \tag{6.11}$$

$$J_{PF} = AE^2 exp\left(\frac{\beta_{PF}\sqrt{E} - \emptyset}{kT}\right) \tag{6.12}$$

$$A = \frac{4\pi q k^2 m^*}{h^3}$$

where J_{FE} is emitted current density due to the influence of the applied electric field; J_{TH} is emitted current density due to the influence of thermal; $J_{\mathrm{PF}}$is emitted current density from solid insulation bulk; e is the magnitude of electronic charge ($1.602 \times 10^{-9}\ C$); $\left|\vec{E}\right|$ is the local electric field; h is Planck's constant; k is Boltzmann's constant; m is free electron mass; $\mathrm{A} = 1.2 \times 10^6\ \mathrm{A/(m^2K^2)}$ is Richardson's constant; Φ_{D} is effective barrier height.

We confirmed that the relation between each current density ($J_{\mathrm{FE}}, J_{\mathrm{TH}}, J_{\mathrm{PF}}$) and electric field. The result revealed that the J_{FE} increases with increasing electric field linearly. Whereas J_{PF} shows non-linear relation and high current density than that of J_{FE} after 70 kV/mm as shown in Fig 6.1. On the other hand, current density by temperature variation showed no significant change (about 1E-51 $\mathrm{A/m^2}$). Thus we considered J_{FE} and J_{PF} from electrode and PB surface, respectively.

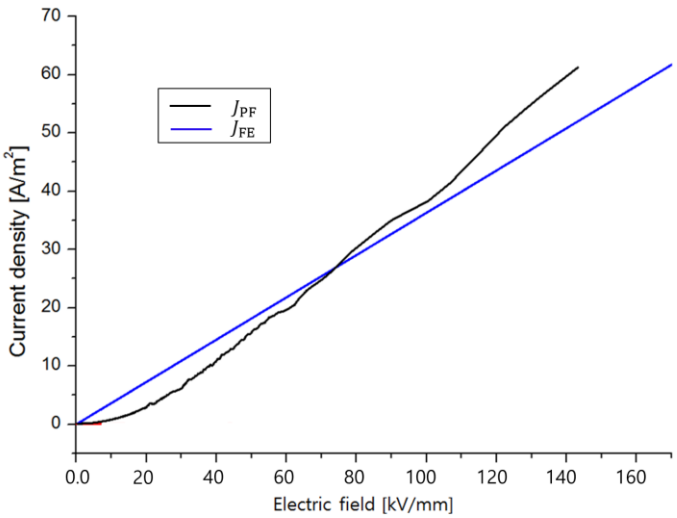

Figure 6.1 Relation between each current density (J_{FE}, J_{PF}) and electric field

$\Phi_D = \phi_w - \chi$, when ϕ_w is the work function of the metal electrode and χ is the electron affinity of the dielectric material in simulation, it is assumed that Φ_D formed at the interface between the ground electrode and oil and between the pressboard and oil is 4.5 eV and 4.91 eV, respectively. Note that the work function of tungsten is 4.5 eV, which is assumed to be barrier height in calculation of J_{FE} into the oil. On the other hand, quantum chemical calculation of molecule consists of pressboard provides that the vacuum level is located by 1.34 eV below the lowest unoccupied molecular orbital (LUMO), and the work function is 4.91 eV from Fermi level to vacuum level as shown in Fig. 6.2, 6.3 and 6.4. The reason for taking Φ_D as 4.91 eV arises from the assumption that the carrier located at the Fermi level can be free into the oil by exceed the energy equivalent to the barrier, i.e. the energy difference between the vacuum level and Fermi level.

Here, it is assumed that the electron emission by electric field emission and thermal electron emission is used as boundary conditions. It is also assumed that the electrode surface and liquid insulation are as ideal surface condition and pure liquid except for impurities and bubbles in liquid, respectively.

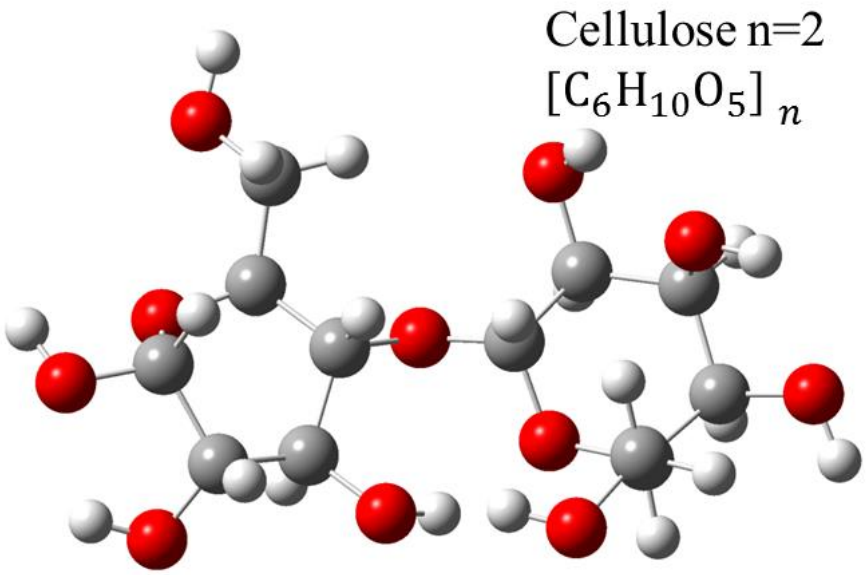

Figure 6.2 Molecule structure of cellulose paper $[C_6H_{10}O_5]$

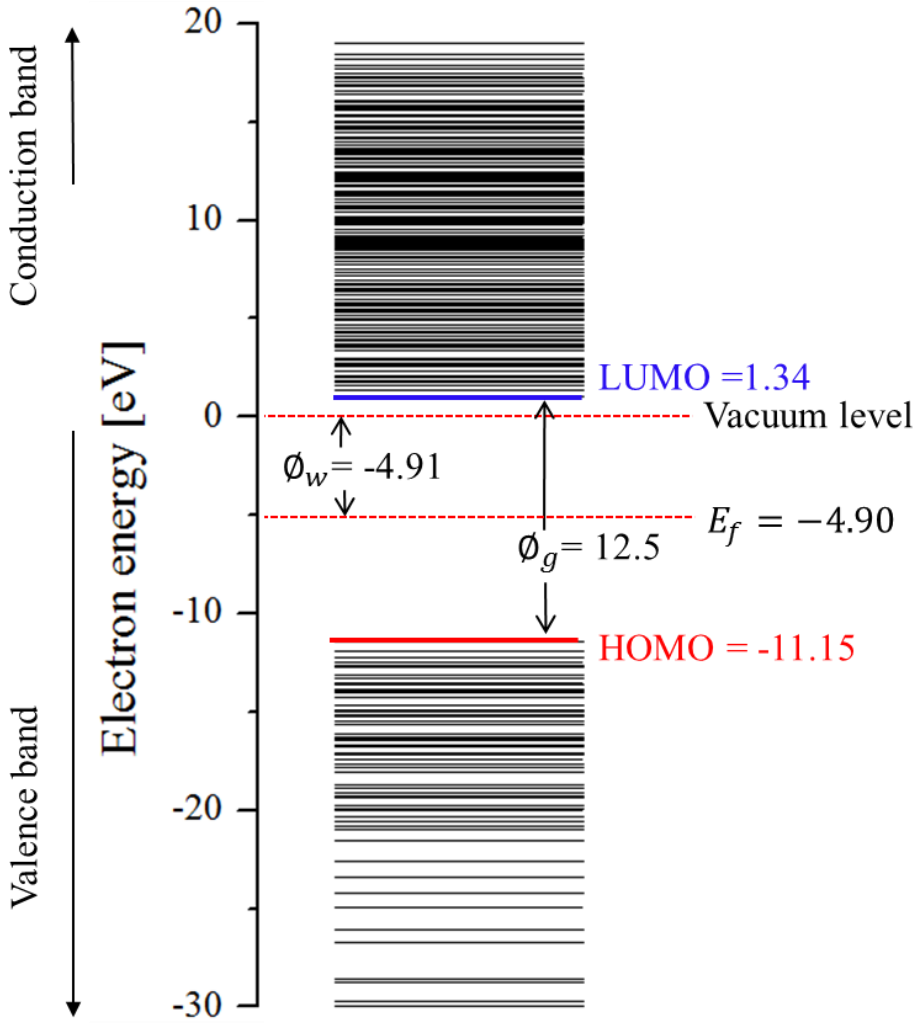

Figure 6.3 Quantum chemical calculation of molecule consists of PB

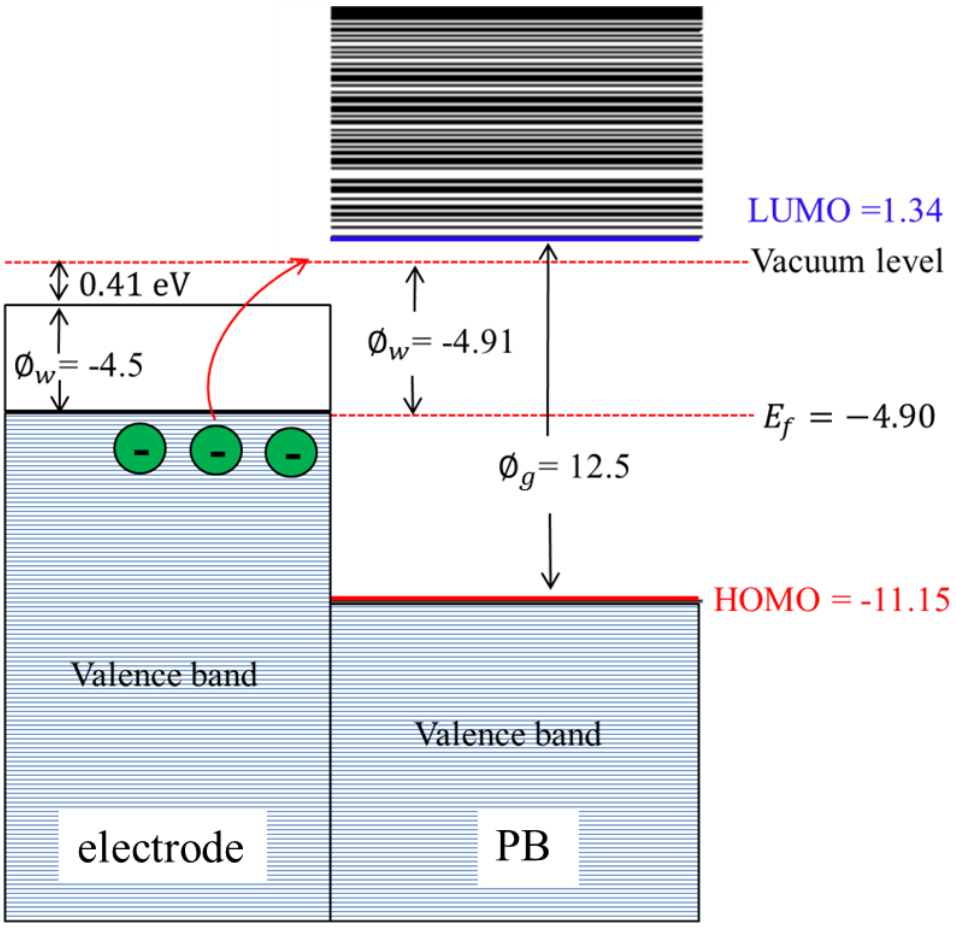

Figure 6.4 Conceptual model of quantum chemical calculation of PB

6.2.3 LIGHTNING IMPULSE VOLTAGE

To simulate the creepage discharge behavior under standard lightning impulse voltage, we used a source of lightning voltage with $1.2/50\ \mu s$ as shown in Fig. 6.5. A convenient analytical representation of the pulse waveform is the double-exponential expression used here as

$$\mathrm{V(t)} = V_1[\mathrm{Exp}(-t/\tau_2) - \mathrm{Exp}(-t/\tau_1)] \qquad (6.12)$$

with $\tau_2 = 1.443T_{\mathrm{t}}$, $\tau_2 = 0.2T_{\mathrm{f}}$, $V_1 = V_m \mathrm{exp}(T_{\mathrm{f}}/1.443T_t)$

where T_{f} and T_{t} are virtual front time, virtual time of half voltage

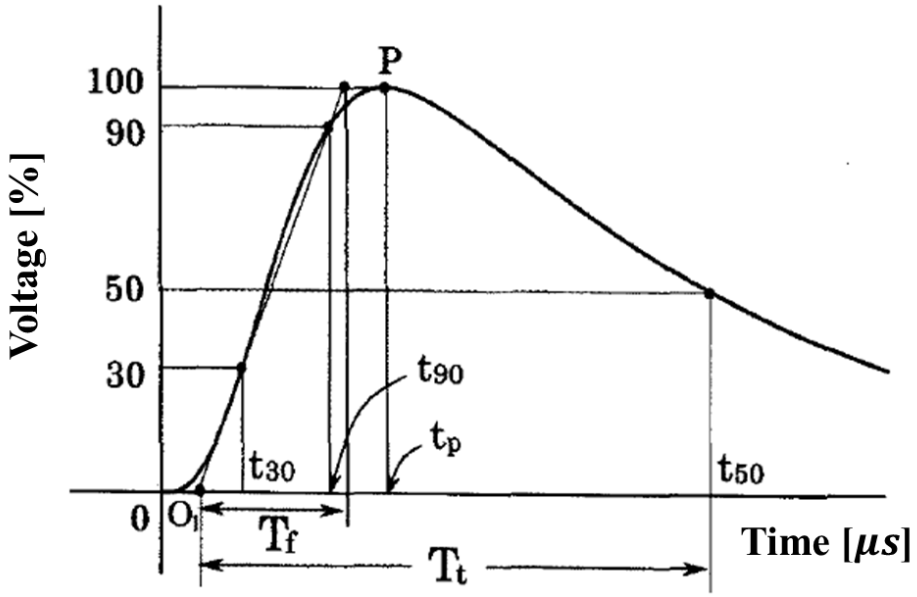

Figure 6.5 Waveform of standard lightning impulse voltage for numerical simulation. The rising time, T_f is 1.2 μs and the 50% of falling time, T_t is 50 μs. (amended from [120])

6.3 NEEDLE-BAR GEOMETRY

Figures 6.6 and 6.7 show needle-bar electrode system and needle-bar geometry in COMSOL Multiphysics, respectively. The distance between the needle electrode and bar is 5 mm in simulation. The radius of curvature of needle electrode is 10 μm. The applied voltage to the needle electrode is 25 kV standard lightning impulse voltage. Streamer development as well as the related physics parameters for the needle-bar electrode model was solved using equations (6.1) - (6.11). Experiment was also performed under the same conditions with the simulation model.

Many studies of streamers in transformer oil are conducted under a non-uniform geometry such as needle-sphere or needle plane electrode geometries [17, 62, 118]. The non-uniform geometries generate a highly divergent electric field distribution, thereby localizing all high field activity, such as streamer initiation, near the needle electrode tip [17]. Application of the 100 kV impulse voltage to the needle electrode creates a non-uniform electric field distribution with a large field enhancement near the sharp needle tip, causing ionization to initiate streamers.

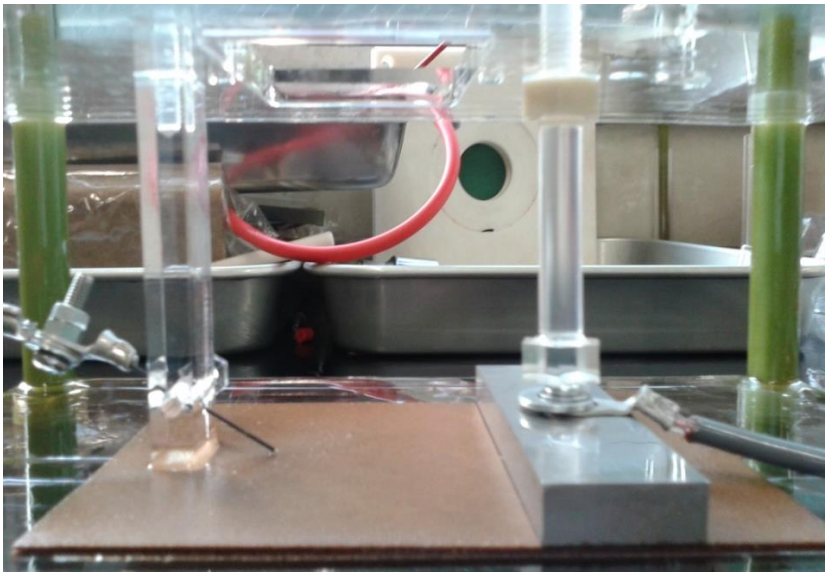

Figure 6.6 Needle-bar electrode system with PB immersed in oil

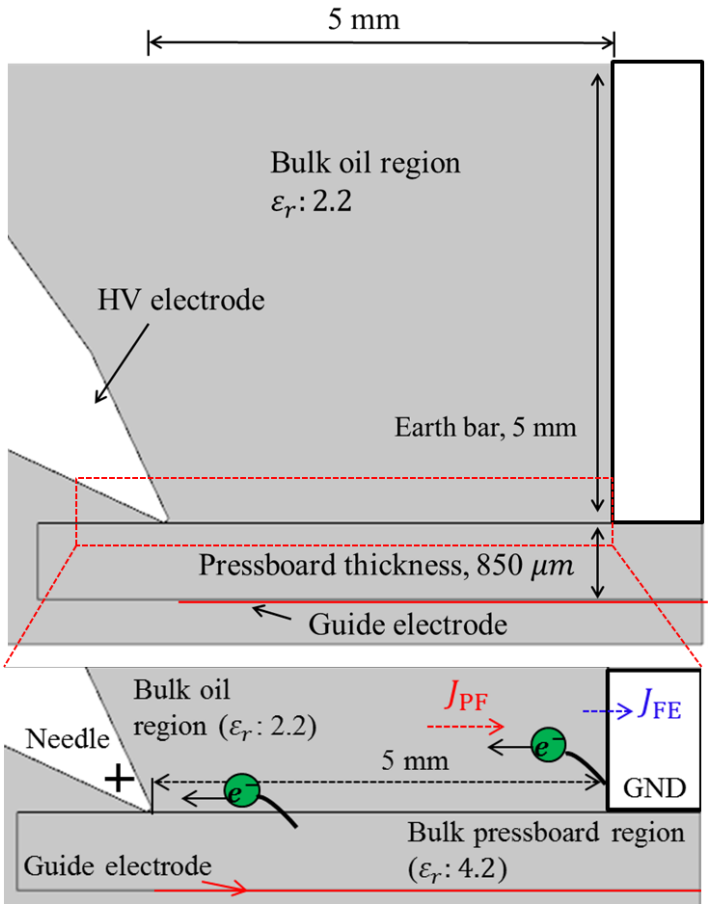

Figure 6.7 Computer- aided design representation of the needle-bar electrode geometry used for streamer simulation and conceptual model of electron emission from ground and PB bulk

6.4 SIMULATION RESULTS

6.4.1 CREEPAGE DISCHARGE UNDER HIGH ELECTRIC FIELD

Figure 6.8 shows result of numerical model to simulate the positive streamer propagation at mineral oil and pressboard interface at 100 kV. The characteristics of the electric field dynamics and the charge density dynamics is dependent molecular ionization model correlate well. As shown in Fig. 6.9, the full ionization model simulation results show the development of an electric field wave, which propagates from the needle electrode's tip towards to the bar electrode. The initial process of analysis, high electric field region is formed around needle electrode according to electric field distribution, and then creepage discharge propagate along oil/pressboard interface at electric field level 5.5×10^8 V/m. The results on electric potential indicate that electric potential drops in the electric field wave's tail (the streamer channel). The potential drop in the electric field wave's tail given by these results ranges from 3 to 5×10^7 [V/m]. Potential drops of this level are an order of magnitude greater than 2 to 4×10^6 [V/m] range for the average drop in the tail of a streamer, which is stated as being appropriate for the potential drop in a streamer in transformer oil [123, 124].

Figure 6.10 shows space charge density and electron density. The space charge peak value is the same with electron density and electric field peak value as a function of time, meaning that the space charge is concentrated, where the peak of the electric field is formed. The free electron move to the needle electrode at a high speed than ions, and the ion charge carriers with relatively slow speed remain in space and then leading to ionization, dissociation, recombination and electron attachment. In this reason, the level of electron free charge carrier density decreases as a function of time as shown in Fig. 6.10. Figures 6.11 and 6.12 show temperature variation at the needle electrode tip by discharge energy and temperature distribution as a function of time step, meaning that the movement of the free charge generated by field ionization due to the electric field contributes to Joule heating that increases the temperature. We found that the high temperature distribution is formed at creepage discharge streamer head and needle electrode tip as shown in Fig. 6.12. These results are consistent with other reference works [17, 40, 62]. Figs. 6.13 (a) and (b) show discharge from in simulation result and experimental results. Discharge current for simulation is current derived from the integration of current density during the creepage discharge propagation. The result revealed that the peak value of simulation calculated discharge current is around 0.68 A, which is greater than the peak of experimental measured discharge current about 0.43 A.

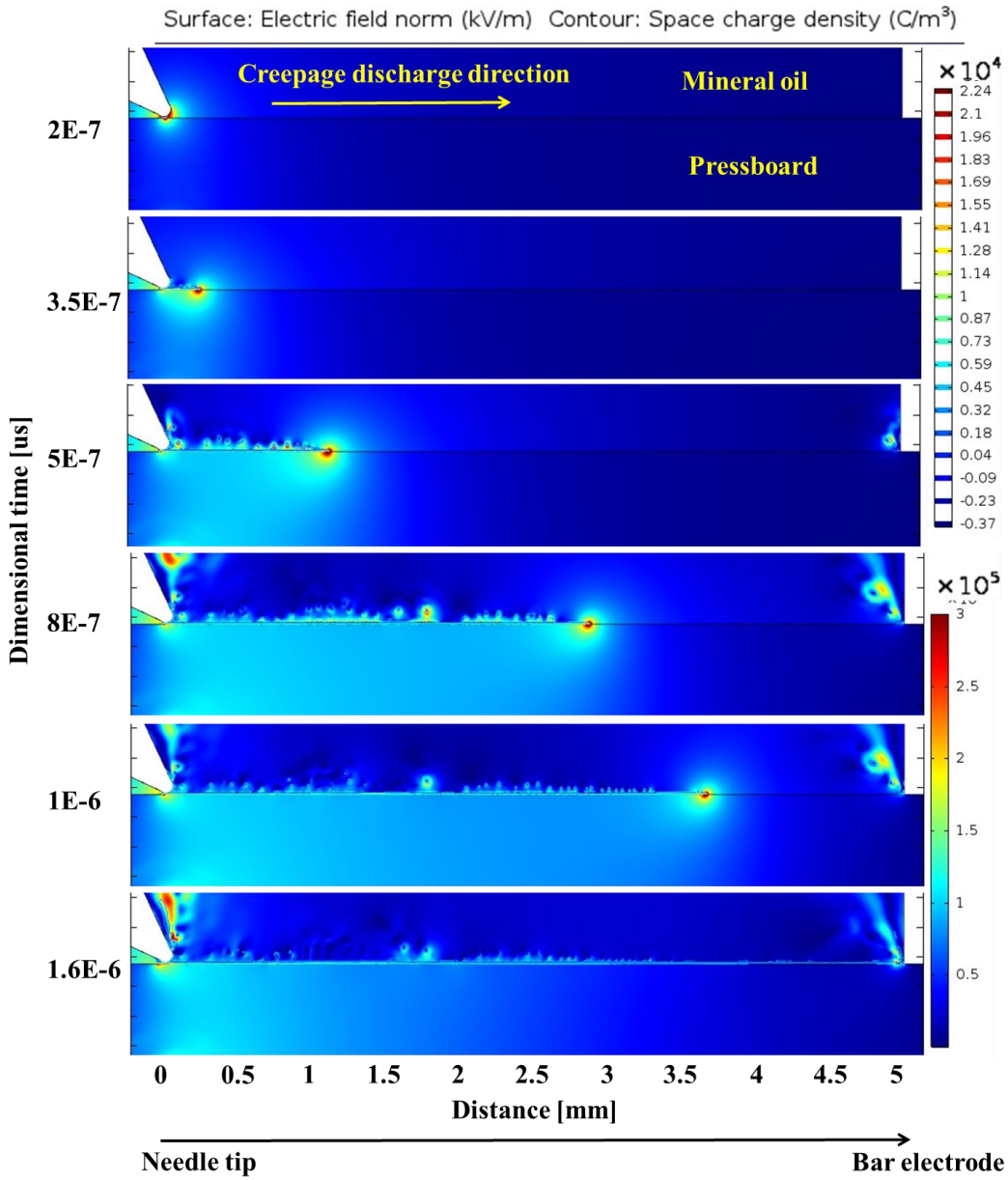

Figure 6.8 Electric field wave propagation as a function of time at 25 kV

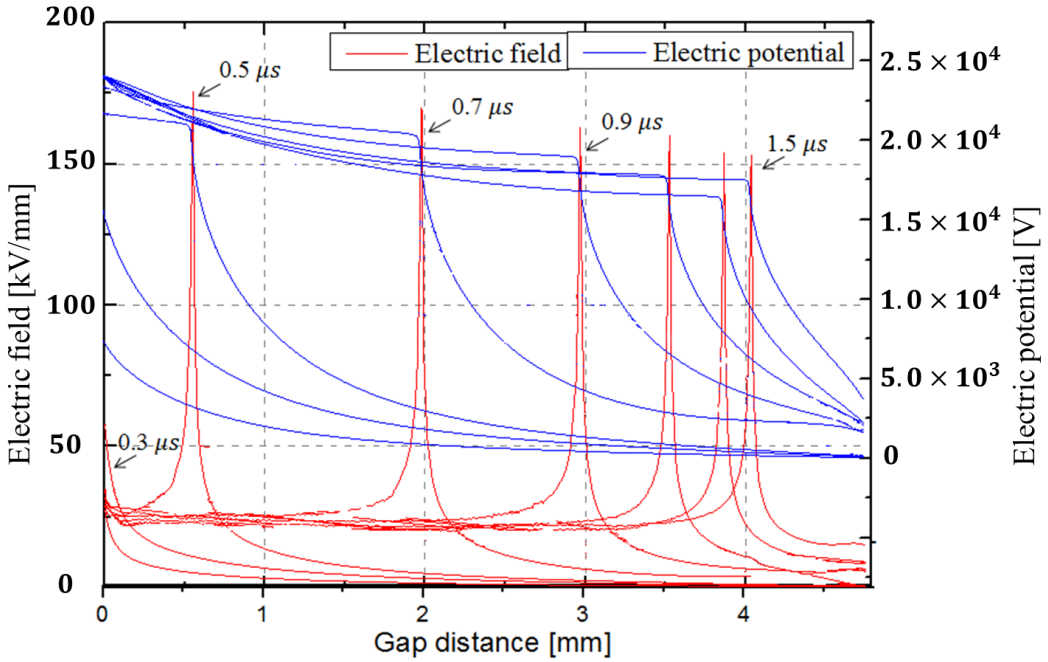

Figure 6.9 Electric field distribution and electric potential as a function of time steps

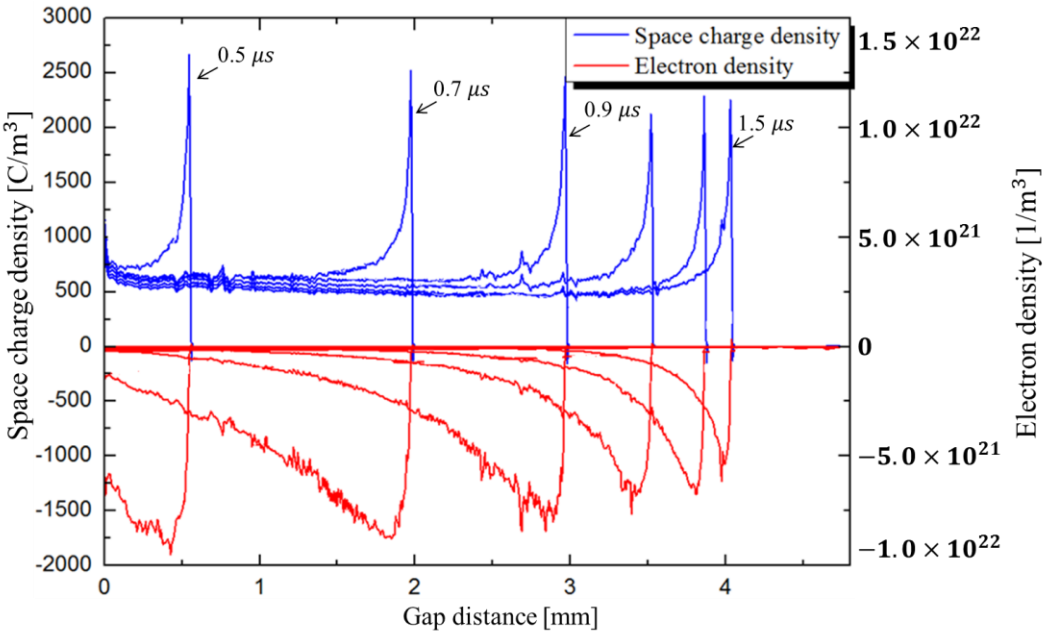

Figure 6.10 Electron and space charge density distribution as a function of time steps

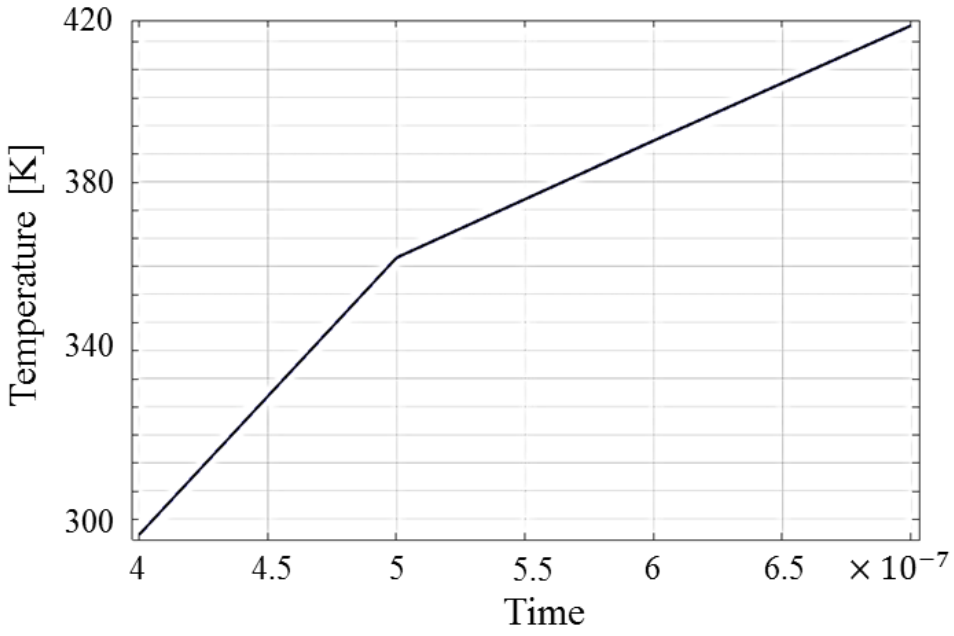

Figure 6.11 Temperature rise as a function of time at the needle tip

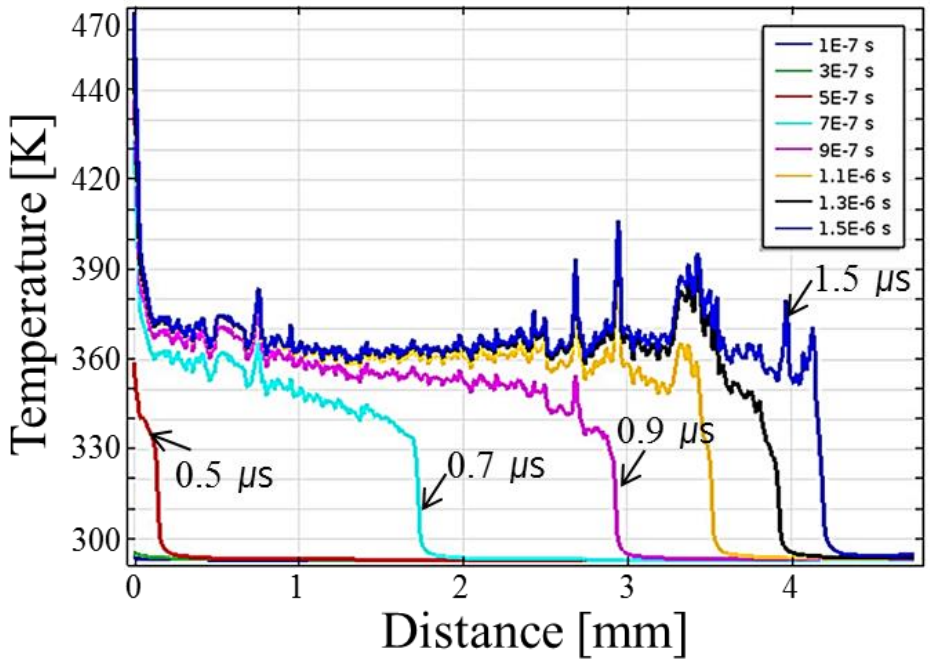

Figure 6.12Temerature distribution as a function of time step

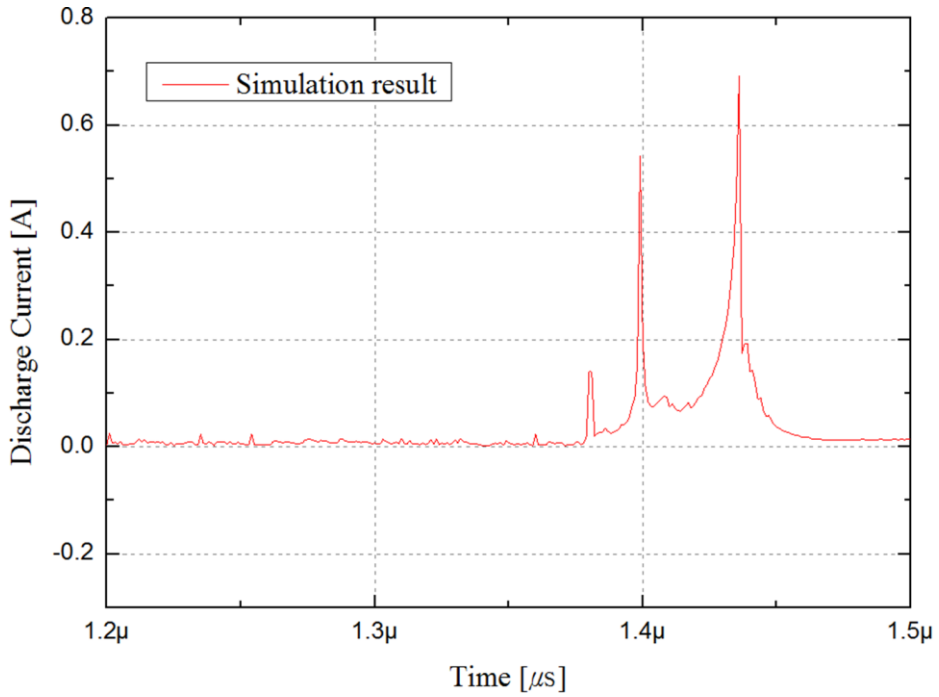

(a) Simulation calculated discharge current by Ohm's integration method

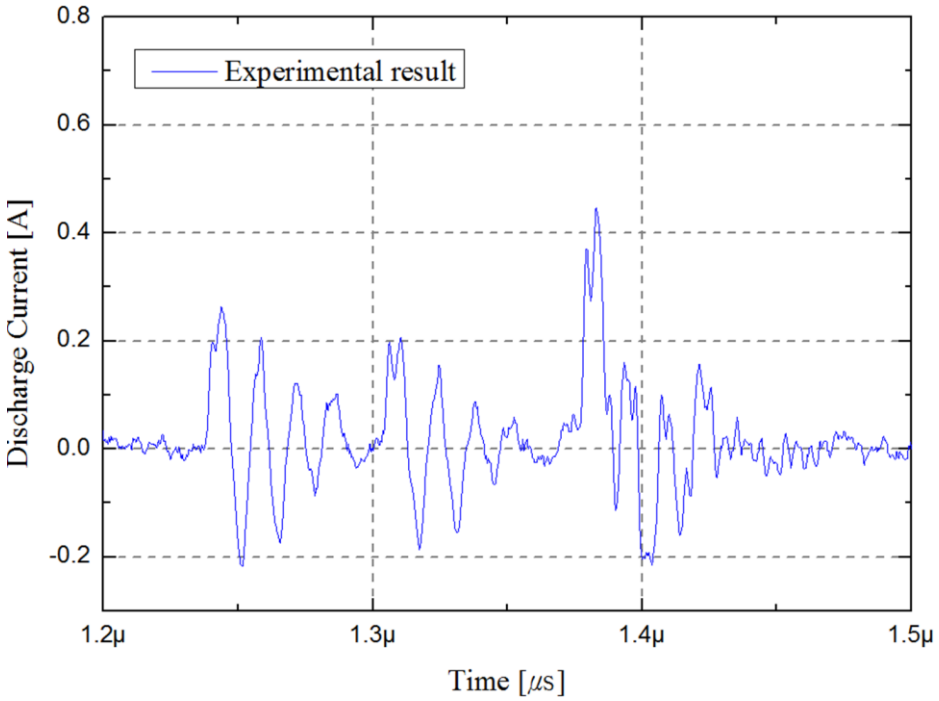

(b) Experimental measured discharge current

Figure 6.13 Discharge current derived from the integration of current density during the creepage discharge propagation on the surface PB at 25 kV

6.4.2 POOLE-FRENKEL MODEL FOR SOLID INSULATION DEPENDENT ON EFFECTIVE BARRIER HEIGHT

The experiment results revealed that the BDV is 25 kV at 5 mm gap distance, BD time is 7 μs. The numerical results on breakdown time (t_{bd}) and discharge velocity (v) with considering P-F model are compared without consideration of the surface charge generation. The results revealed that the P-F model shows fast streamer propagation (v: 3.28 μs, t_{bd}: 1.52 μs) with Φ_{D} 4.9 than the case without consideration of P-F model (v: 3.12 μs, t_{bd}: 1.6 μs) and BDV of both model is 25 kV.

Lei Zhou and Michael R. Zachariah *et al.*, [124] reported substantial changes of work function with nanoparticle size dependent. They results show the work function significant decreasing trend from 4.31 to 4.26 eV as mobility size increases from 15 to 80 nm. Besides, work function of agglomeration nanoparticle also decreasing with increasing aggregate of nanoparticles. Low work function is able to inject charges into the conduction band. On the contrary, higher work function does not exhibit efficient charge transfer.

J. K. Nelson *et al.*, [115] reported the above similar results by silica/XLPE nanocomposites, as a result of a change in the work function and activation energies of nanocomposites by nano size silica and silica surface modification.

Above viewpoint, the creepage discharge characteristics are investigated dependent on effective barrier height (Φ_{D}) of solid insulation. The insulation of Φ_{D} is given 4.9, 5.9, 8.9 and 12 eV assuming PB in simulation and permittivity of each case is same.

Figure 6.14 shows the discharge velocity and breakdown time dependent on Φ_{D} of solid insulation at 100 kV. The result revealed that the discharge propagation velocity and BDV time are influenced by Φ_{D} of solid insulation from in our simulation results. The breakdown time increases with increasing Φ_{D} of solid insulation, besides streamer velocity also decreased. Low Φ_{D} has been shown to dramatically affect streamer propagation and leading to breakdown.

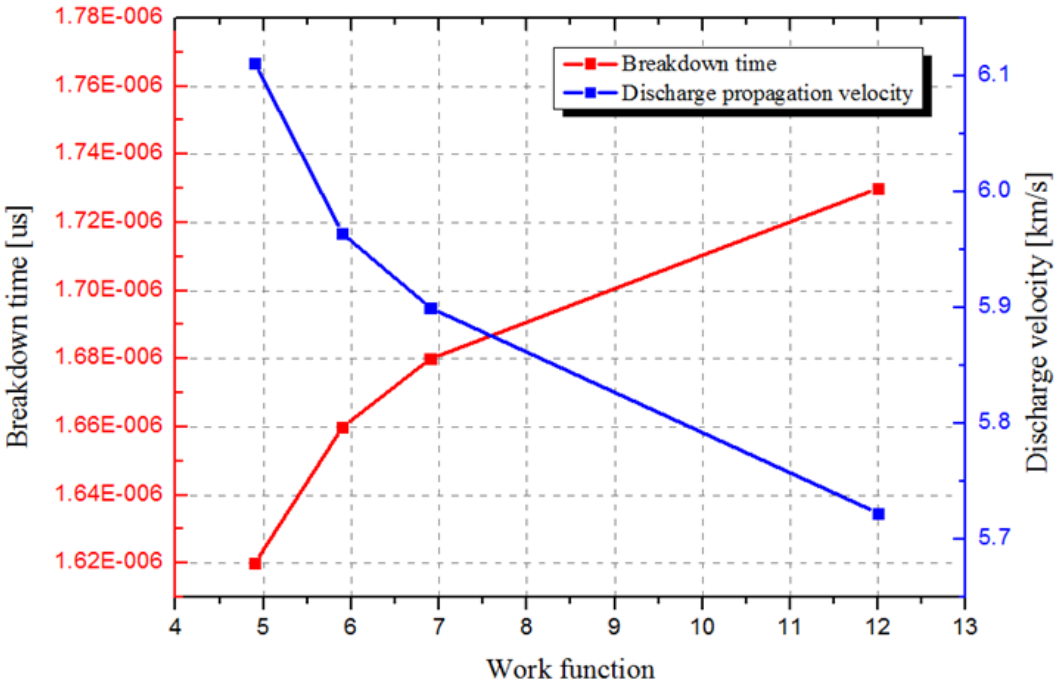

Figure 6.14 Discharge velocity and breakdown time dependent on Φ_D of solid insulation under 100 kV lighting impulse voltage

6.4.3 CREEPAGE DISCHARGE VELOCITY AND BDV DEPENDENT ON PERMITTIVITY EFFECT

Figure 6.15 shows creepage discharge propagation velocity and BDV to confirm the effect of creepage discharge characteristic depending on permittivity at oil/pressboard interface. The results revealed that the breakdown time decreases with increasing permittivity of solid insulation, besides streamer velocity also increased. The effect of permittivity differences between oil and solid insulation on streamer propagation has been well documented in the literature extensively. For example, researchers report that low permittivity insulating solid such as polyethylene and polypropylene, which have relative permittivity of ~2.3 almost matching that of oil, result in high flashover voltages for impulse and AC voltage [126]. The greater the relative permittivity of a material, the greater the polarization charge that develops in a region where there is a local imbalance of dipoles. This polarization charge is a source of electric field that affects electrodynamics in a system such as a composite liquid-solid insulation structure

[17, 127]. High permittivity has been shown to dramatically affect streamer propagation and breakdown time, such that streamers in the oil are attracted towards the pressboard surface [17, 121, 128]. The result of discharge velocity is accords with reference papers [46, 128].

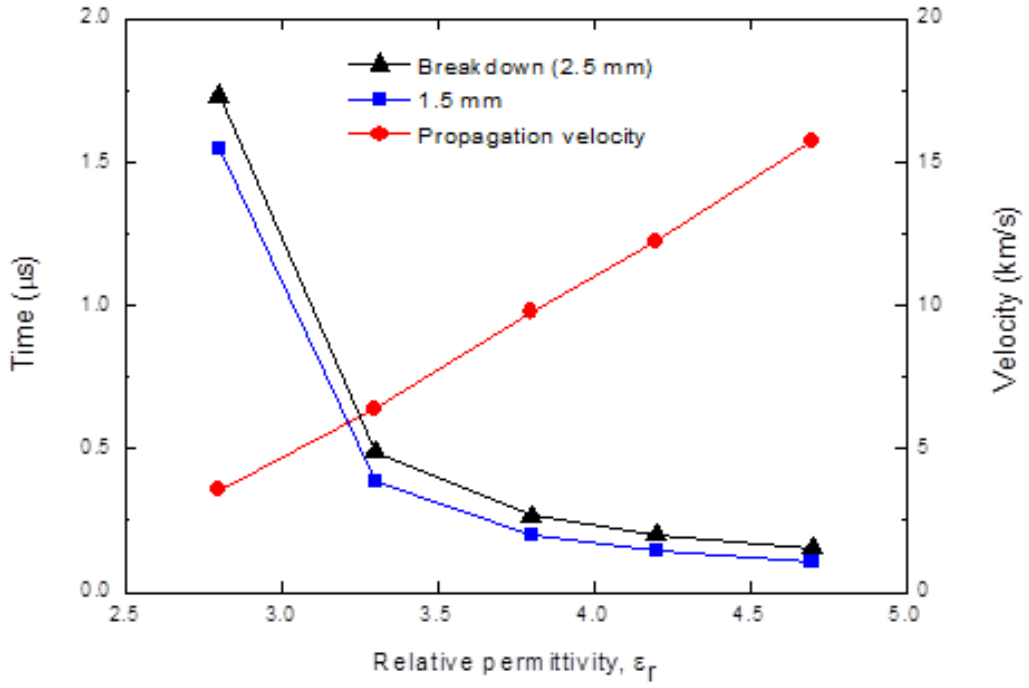

Figure 6.15 Creepage discharge propagation velocity and BDV with different ε_r' [127]

6.5 SUMMARY

A composite insulation model has been developed using an FEA software package to verify the effect of nano silica with considering Poole-Frenkel model for solid insulation, besides we considered the effective barrier height and relative permittivity variation of solid insulation at the oil-pressboard interface under positive standard lightning impulse voltage.

The results of this research work investigated the possibility of the numerical and experimental approaches used to modeling creepage discharge in dielectric liquid with a solid insulator with the needle-bar electrode configuration. A fully coupled finite element model was developed. The numerical results were found to

be in good agreement with the experimental results in terms of BD time and BDV. The BD time of simulated creepage discharge shows similar order with experimental results. Further work is needed on physical parameters such as charge generation and conduction mechanism of each dielectric as well as PB parameters such as surface roughness.

CHAPTER 7

CONCLUSIONS AND FURTHER WORK

7.1 CONCLUSIONS

To study the creepage discharge behaviour in composite insulation system, we considered the experiment and simulation analysis. In experiment, a creepage discharge using a rod-plane electrode and needle-bar electrode configuration has been developed to study the creepage discharge characteristics compared with conventional pressboard at the oil/pressboard interface. We have focused on surface modifications of the insulating paper by solid layer coating method to improve the insulation property. Five different pressboard samples, i.e. neat PB, dry PB, epoxy coated PB, Teflon coated PB and epoxy/silica nanocomposite coated PB have been tested to verify the nano silica effect on discharge inception and discharge propagation with different surface condition. The research work reveals that the new coating method on the PB surface can indeed affect the creepage discharge behaviour as well as dielectric properties. We suggested three possibly considered mechanism to explain the experimental results on the effect of the coating method on improvement of P_d and l_d.

1) Drying of water content in neat PB and decrease in ε_r' by silica/epoxy nanocomposite coating
2) Surface modification effect by solid layer coating
3) Silica/epoxy composites coating suppressing the electron emission from the surface of PB

The dominant mechanism to explain the results on P_d is silica/epoxy composites coating effect (3), but the mechanisms (1) and (2) are enough to explain the results on l_d than that of (3).

To verify the effect of nano silica particles on discharge inception and propagation, creepage discharge behaviour have been tested with different filler loading and nano particle size. The results suggest that creepage discharge

inception process is influenced by appropriate nanoparticle filler loading and filler size in base epoxy resin, the low silica filler loading and small size produces the best insulation performance. To explain our experimental results, we suggested two possibly considered mechanism on the effect of the coating method on P_d as follows:

1) Relative permittivity reduction effect by introducing nano size silica particle
2) Silica/epoxy nanocomposites are more likely to suppress the electron emission from the surface layer of nanocomposite.

Above two mechanisms all contributed to the discharge inception process, further work is needed on creepage discharge behavior and electrical properties such as streamer velocity, surface conductivity and resistivity, respectively.

The work presented in this thesis has also made a significant contribution to the development of a computational simulation model of surface discharge at the oil/pressboard interface. A 2-D axial symmetry model has been developed using COMSOL Multiphysics, an FEA software package. In general, the electric field dependent molecular ionization mechanism plays an important role in the discharge inception and propagation at the oil-pressboard interface. On the other hand, the composite insulation model is developed by considering Poole-Frenkel model for solid insulation. The numerical results were found to be in good agreement with the experimental results in terms of BD time and BDV. The BD time of simulated creepage discharge shows similar order with experimental results.

7.2 FURTHER WORK

For further work, experiments on the nano silica effect of creepage discharge compare with conventional pressboard under AC voltage, switching impulse waveforms as well as negative impulse voltage should be performed. To investigate the applicability of pressboard by epoxy/silica nanocomposite in oil filled transformer, long term life test and degradation behaviour at oil/pressboard composite insulation system should be performed.

The experiment of the epoxy/silica nanocomposite plate under different condition such as SF6 gas and air condition to compare with mineral oil results

and to verify the nanoparticle effect under AC voltage or/and impulse polarity should be performed.

Further computational work to study the creepage discharge behavior due to negative streamer should also be considered. Besides, the comparison with experiment and simulation results should be performed. But there is needed some parameters such as electron, positive and negative ion mobility by electric field or/and temperature, besides further work is needed on physical parameters of pressboard such as surface roughness of conventional pressboard should be considered.

APPENDIX A

List of Publications

A.1 Refereed Conference Papers

The following papers have been peer reviewed and presented at International Conferences:
(No. 6 and 7 are scheduled to present a paper at International Conference on Dielectric Liquids at Manchester Univ. in 2017)

1. Kyunghoon Jang, Shigeyoshi Yoshida, Masahiro Kozako and Masayuki Hikita, "Effect of Thin Solid Layer Coating on Creepage Discharge Characteristics in Oil/Pressboard Composite Insulation System", *Proceeding of Electrical Insulation and Dielectric Phenomena (CEIDP), IEEE Conference* (4-pages), pp. 832-835, 2015

2. Kyunghoon Jang, Takao Akahoshi, Masahiro Kozako and Masayuki Hikita, "Impulse Creepage Discharge Properties of Solid Coated Pressboard/Oil Composite Insulation with Rod-Plane Electrode System", *Proceeding of Korea-Japan Joint Symposium*, (4-pages), pp.11-14, 2015

3. Kyunghoon Jang, Takao Akahoshi, Masahiro Kozako and Masayuki Hikita, "Nano SiO_2/Epoxy Coating Effect on Creepage Discharge Characteristics in Oil/Pressboard Composite Insulation System", *International Conference on Dielectric (ICD)*, (4-pages), Vol. 1, pp.394-397, 2016

4. Takao Akahoshi, Kyunghoon Jang, Masahiro Kozako and Masayuki Hikita, "Effect of Discharge Trace Formation on Creepage Discharge Characteristics in Oil/Pressboard Composite Insulation system under Impulse Voltage Application" *International Conference on Dielectric (ICD)*, (4-pages), Vol. 1, pp.342-345, 2016

5. Kyunghoon Jang, Takao Akahoshi, Masahiro Kozako and Masayuki Hikita, "Dependence of Silica Nano Filler added to Epoxy Resin on Creepage Discharge Properties in Mineral Oil", *International Work on High Voltage Engineering IWHV*, (4-pages), pp.73-76, 2016

6. Masaki Kurachi, Kyunghoon Jang, Takao Akahoshi, Masahiro Kozako and Masayuki Hikita, "Dielectric Properties and Creepage Discharge of Epoxy/silica Nanocomposite in Mineral oil", *International Conference on Dielectric Liquids*, June, 2017

7. Soichiro Kainaga, Shigeyoshi Yoshida, Takahiro Umemoto, Manabu Yoshimura and Takao Tsurimoto (Mitsubishi Electric Corporation), Takao Akahoshi, Kyunghoon Jang, Masaki Kurachi, Masahiro Kozako and Masayuki Hikita (Kyushu Institute of Technology), "Effect of Discharge Trace on Creeping Discharge Characteristics in Oil/Pressboard Composite Insulation System under Impulse Voltage Application", *International Conference on Dielectric Liquids*, June, 2017

8. Choi Jin-Hyun, Kim Su-Hun, Jang Kyunghoon, Hikita Masayuki, Lee Se-Hee, "Finite Element Analysis for Surface Discharge Due to Interfacial Polarization at the Oil-Nanocomposite Interface", *21st International Conference on the Computation of Electromagnetic Fields, June 18-22, 2017*

A.2 Peer Reviewed Journal Papers

1. Kyunghoon Jang, Takao Akahoshi, Masahiro Kozako and Masayuki Hikita, "Impulse Creepage Discharge Properties of Solid Coated Pressboard/Oil Composite Insulation with Rod-Plane Electrode System", *IEEJ Transaction on Fundamentals and Materials* (A), 2017

2. Takao Akahoshi, Kyunghoon Jang, Masahiro Kozako and Masayuki Hikita, "Effect of White discharge Trace on Impulse Creeping Discharge Characteristics in Oil/Pressboard Composite Insulation System", *IEEJ Transaction on Fundamentals and Materials* (A), 2017

A.3 Refereed Domestic Conference Papers

1. Shigeyoshi Yoshida, Kyunghoon Jang, Masahiro Kozako, Masayuki Hikita, "Lightning Impulse Creepage Discharge Characteristics in Oil with Presence of Pressboard Barrier", *Kyushu branch annual conference*, pp.4, 2014

2. Kyunghoon Jang, Shigeyoshi Yoshida, Masahiro Kozako and Masayuki Hikita, "Effect of Epoxy Resin Coating on Creepage Discharge Properties of Oil/Pressboard Composite Insulation System", *Domestic Annual Conference*, no.1-138, 2015

3. Takao Akahoshi, Kyunghoon Jang, Masahiro Kozako, Masayuki Hikita, "Characteristics of Creepage Discharge Propagation after Formation of White Discharge Trace under Impulse Voltage Application in Oil/Pressboard Composite Insulation System", *The Institute of Electrical Engineers of Japan*, pp.234-239, 2015

4. Kyunghoon Jang, Takao Akahoshi, Masahiro Kozako and Masayuki Hikita, "Impulse Creepage Discharge Properties of Solid Coated Pressboard/Oil Composite Insulation with Needle-Bar Electrode System", *Domestic Annual Conference*, no.1-170, 2016

5. Takao Akahoshi, Kyunghoon Jang, Masahiro Kozako, Masayuki Hikita, "State Change of White discharge Trace by Pressure in Oil/Pressboard Composite Insulation System", *Domestic Annual Conference*, no.1-169, 2016

6. Takao Akahoshi, Kyunghoon Jang, Masahiro Kozako, Masayuki Hikita, "Effect of White Discharge Trace on Impulse Creeping Discharge Characteristics in Oil/Pressboard Composite Insulation system", *Fundamentals and Materials Society IEE Japan*, pp.234-239, no.5-E-a2-3, 2016

7. Kyunghoon Jang, Takao Akahoshi, Masahiro Kozako and Masayuki Hikita", Creepage Discharge and Dielectric Characteristics of Nano Silica/Epoxy Composite Coated Pressboard in Mineral Oil", *Annual Conference in Korea*, pp.49-50, 2016

8. Jin-Hyung Choi, Kyunghoon Jang, Takao Akahoshi, Masayuki Hikita, Se-Hee Lee, "Finite Element Analysis using Surface Charge on Liquid-Solid Interface in Insulating Liquid", *Annual Conference in Korea* , pp.118-119, 2016

8. Takao Akahoshi, Masaki Kurachi, Kyunghoon Jang, Masahiro Kozako, Masayuki Hikita, "Characteristics of discharge on Oil Gap Subdivided by Barrier PBs in the Oil.PB Composite Insulation System under Lightning Impulse Voltage Application", *The Institute of Electrical Engineers of Japan*, 2016

9. Jang Kyunghoon, Takao Akahoshi, Masaki Kurachi, Masahiro Kozako, Masayuki Hikita, "Numerical Model Analysis on Creepage Discharge Behavior at the Oil/Pressboard Interface", *Domestic Annual Conference*, 2017

10. Masaki Kurachi, Kyunghoon Jang, Takao Akahoshi, Masahiro Kozako, Masayuki Hikita, “Impulse Creepage Discharge Inception Voltage of Epoxy Silica Nanocomposite in Mineral Oil” *Domestic Annual Conference*, 2017

11. Takao Akahoshi, Masaki Kurachi, Kyunghoon Jang, Masahiro Kozako, Masayuki Hikita, “Impulse Creeping Discharge Characteristics in Oil/Pressboard Composite Insulation system after Formation of the White Trace”, *Domestic Annual Conference*, 2017

A.4 Patent

1. “沿面放電の発生を抑制する方法” with Nissan Chemical Industries., LTD

Number:10778 Patent application: 2016-132011 (Proof)
Submission date:2016.07.01

【Patent certificate】
【Document name】
【Number】10778
【Recipient】Commissioner of the patent and trademark office
【International patent classification】C01B 33/145
【Inventor】
【Address】千葉県袖ヶ浦市北袖１１番１　日産化学工業株式会社材料科学研究所内
【Name】末村尚彦
【Inventor】
【Address】千葉県袖ヶ浦市北袖１１番１　日産化学工業株式会社材料科学研究所内
【Name】石田智久
【Inventor】
【Address】福岡県北九州市戸畑区仙水町１番１号国立大学法人九州工業大学内
【Name】小迫雅裕
【Inventor】
【Address】福岡県北九州市戸畑区仙水町１番１号国立大学法人九州工業大学内
【Name】匹田政幸
【Inventor】

【Address】福岡県北九州市戸畑区仙水町１番１号国立大学法人九州工業大学内
【Name】チャン　ギョンフン
【Inventor】
【Address】福岡県北九州市戸畑区仙水町１番１号国立大学法人九州工業大学内
【Name】赤星卓勇
【An applicant for a patent】
【Identification number】000003986
【The name or title】日産化学工業株式会社
【An applicant for a patent】
【Identification number】504174135
【The name or title】国立大学法人九州工業大学
【Agent】
【Identification number】100101236
【Patent attorney】
【The name or title】栗原浩之
【Erected agent】
【Identification number】100166914
【Patent attorney】
【The name or title】山▲崎▼ 雄一郎
【Patent attorney fee】
【予納台帳番号】042309
【Amount of payment】14,000円
【List of submission】
【物件名】明細書1
【物件名】特許請求の範囲1
【物件名】要約書1
【物件名】図面１
【Comprehensive mandate number】1212778
【Document name】明細書
【Title of invention】沿面放電の発生を抑制する方法
【Technical field】
【０００１】
本発明は、高電圧（電力）機器の絶縁材料の沿面放電発生を抑制する技術に関する。
【背景技術】
【０００２】
高電圧（電力）機器において、固体絶縁材料の表面は高電圧により沿面放電が起きやすい箇所である。ここで表面とは、液体／固体、気体／固体、真空／固体などの異質の界面を意味する。この場合、沿面放電は固体中で

はなく、液体、気体、真空中のいずれかで発
生する。
【０００３】
従来、樹脂表面の沿面放電を抑制する技術としては、沿面放電が生じる可能性のある固
体絶縁材料の誘電率制御による電界緩和（この場合、液体・気体・真空の誘電率に合わせるべく、固体の低誘電率化を行うこと）、誘電率の空間的な傾斜分布による電界緩和、導電率の非線形性による電界緩和、表面の凹凸による沿面距離の増加、などが報告されている。つまり、沿面放電を防止する対策としては、電界緩和あるいは物理的な沿面距離を取る方策しか実施されていない。
【先行技術文献】
【特許文献】
【０００４】
【特許文献１】特開２０１２－１１０２０６号公報
【特許文献２】特開２０１６－０３１８４５号公報
【発明の概要】
【発明が解決しようとする課題】
【０００５】
本発明は、固体絶縁材料である樹脂硬化体自体の電界緩和（即ち樹脂の低誘電率化）に頼ることなく、樹脂硬化体の表面の沿面放電の発生を抑制する方法を確立することを課題
とする。
【課題を解決するための手段】
【０００６】
本発明は、固体絶縁材料である樹脂中にナノサイズの無機微粒子を分散させたナノコンポジット絶縁材料を用いることで、樹脂表面の沿面放電の発生を抑制するという知見に基づいて完成されたものである。
【０００７】
上記目的を達成する本発明は、ナノサイズの無機微粒子を樹脂中に分散させて樹脂硬化体の表面の沿面放電の発生を抑制することを特徴とする、沿面放電の発生を抑制する方法
にある。
【０００８】
ここで、無機微粒子としては、シリカ、アルミナ、チタニア、ジルコニア、酸化亜鉛、酸化錫、酸化アンチモン、酸化鉄、酸化マグネシウム、又はこれらを主成分とする複合酸化物微粒子を用いることができる。
【０００９】
ナノサイズの粒子とは、一般的には、ナノメートル（ｎｍ）オーダーの大きさを持つ粒子のことで、一般的には１～数百ｎｍの大きさの粒子をいうが、本発明では、平均粒子径が１～４００ｎｍのものとする。なお、平均

粒子径は、後述するとおり、比表面積による
ものとする。
【００１０】
本発明で用いる無機微粒子は、その平均粒子径が５～２００ｎｍであるのが好ましい。樹脂としては、エポキシ樹脂などの一般的な熱硬化性樹脂を用いる。ナノコンポジットにおける無機微粒子の添加率は０．１～５０質量%である。
【発明の効果】
【００１１】
本発明を用いることで、固体絶縁材料の電界緩和や物理的な沿面距離増加を施さずとも、樹脂硬化体の固体表面の沿面放電発生電圧を向上することができ、ＧＩＳ（ガス絶縁開閉装置）の 絶縁スペーサや油入り変圧器のプレスボード用コーティング樹脂等へ好適に利用さ
れうる。
【図面の簡単な説明】
【００１２】
【図１】沿面放電の測定系の概略構成を示す図である。
【発明を実施するための形態】
【００１３】
本発明に用いられる絶縁樹脂としては、例えば、エポキシ樹脂、ポリイミド樹脂、ポリアミドイミド樹脂、シリコーン等の熱硬化性樹脂が挙げられる。また、ポリエチレン、ポリプロピレン等の熱可塑性樹脂も挙げられる。
【００１４】
本発明に用いられるエポキシ樹脂としては特に限定されるものではないが、ビスフェノールＡ型エポキシ樹脂、ビスフェノールＦ型エポキシ樹脂、脂環式エポキシ樹脂等が挙げられる。通常、これらエポキシ樹脂と硬化剤等を組み合わせて配合された後、注型・熱硬化して所望の形状に成形される。
【００１５】
本発明に用いるエポキシ樹脂の硬化剤としては、フェノール樹脂、アミン類、ポリアミド樹脂、イミダゾール類、ポリメルカプタン、酸無水物等が挙げられる。
【００１６】
フェノール樹脂としては、例えばフェノールノボラック樹脂、クレゾールノボラック樹脂等が挙げられる。
【００１７】
アミン類としては、例えばピペリジン、Ｎ，Ｎ－ジメチルピペラジン、トリエチレンジアミン、２，４，６－トリス（ジメチルアミノメチル）フェノール、ベンジルジメチルアミン、２－（ジメチルアミノメチル）フェノール、ジエチレントリアミン、トリエチレンテトラミン、テトラエチレンペンタミン、ジエチルアミノプロピルアミン、Ｎ－アミノエチルピペラジン、ジ（１－メチル－２－アミノシクロヘキシル）メタン、メンセンジア

ミン、イソフオロンジアミン、ジアミノジシクロヘキシルメタン、１，３－ジアミノメチルシクロヘキサン、キシレンジアミン、メタフェニレンジアミン、ジアミノジフェニルメタン、ジアミノジフェニルスルホン等が挙げられる。これらの中で液状であるジエチレントリアミン、トリエチレンテトラミン、テトラエチレンペンタミン、ジエチルアミノプロピルアミン、Ｎ－アミノエチルピペラジン、ジ（１－メチル－２－アミノシクロヘキシル）メタン、メンセンジアミン、イソフオロンジアミン、ジアミノジシクロヘキシルメタン等は好ましく用いることができる。

【００１８】

ポリアミド樹脂としては、ダイマー酸とポリアミンの縮合により生成するもので、分子中に一級アミンと二級アミンを有するポリアミドアミンである。

【００１９】

イミダゾール類としては、２－メチルイミダゾール、２－エチル－４－メチルイミダゾール、１－シアノエチル－２－ウンデシルイミダゾリウムトリメリテート、エポキシイミダゾールアダクト等が挙げられる。

【００２０】

ポリメルカプタンは、例えばポリプロピレングリコール鎖の末端にメルカプタン基が存在するものや、ポリエチレングリコール鎖の末端にメルカプタン基が存在するものであり、液状のものが好ましい。

【００２１】

本発明に用いる酸無水物としては一分子中に複数のカルボキシル基を有する化合物の無水物が好ましい。これらの酸無水物としては、無水フタル酸、無水トリメリット酸、無水ピロメリット酸、無水ベンゾフェノンテトラカルボン酸、エチレングリコールビストリメリテート、グリセロールトリストリメリテート、無水マレイン酸、テトラヒドロ無水フタル酸、メチルテトラヒドロ無水フタル酸、エンドメチレンテトラヒドロ無水フタル酸、メチルエンドメチレンテトラヒドロ無水フタル酸、メチルブテニルテトラヒドロ無水フタル酸、ドデセニル無水コハク酸、ヘキサヒドロ無水フタル酸、メチルヘキサヒドロ無水フタル酸、無水コハク酸、メチルシクロヘキセンジカルボン酸無水物、クロレンド酸無水物等
が挙げられる。

【００２２】

これらの中でも常温、常圧で液状であるメチルテトラヒドロ無水フタル酸、メチルエンドメチレンテトラヒドロ無水フタル酸、メチルブテニルテトラヒドロ無水フタル酸、ドデセニル無水コハク酸、メチルヘキサヒドロ無水フタル酸が好ましい。これら液状の酸無水物は粘度が２５℃での測定で１０ｍＰａｓ～１０００ｍＰａｓ程度である。

【００２３】

また、上記硬化物を得る際、適宜、硬化促進剤が併用されても良い。硬化促進剤としてはトリフェニルホスフィンやトリブチルホスフィンなどの有

機リン化合物、エチルトリフェニルホスフォニウムブロマイド、メチルトリフェニルホスホニウムリン酸ジエチル等の第４級ホスフォニウム塩、１，８－ジアザビシクロ（５，４，０）ウンデカン－７－エン、１，８－ジアザビシクロ（５，４，０）ウンデカン－７－エンとオクチル酸の塩、オクチル酸亜鉛、テトラブチルアンモニウムブロミド等の第４級アンモニウム塩、ジメチルベンジルアミン等の３級アミン等が挙げられる。これらの硬化促進剤は、硬化剤１質量部に
対して、０．００１～０．１質量部の割合で含有することができる。

【００２４】

本発明に用いられるナノサイズの無機微粒子としては、絶縁性や分散性の観点から、金属酸化物微粒子が好ましい。金属酸化物微粒子の好ましい例としては、シリカ、アルミナ、チタニア、ジルコニア、酸化亜鉛、酸化錫、酸化アンチモン、酸化鉄、酸化マグネシウム又はこれらを主成分とする複合酸化物微粒子が挙げられる。このうち、シリカは誘電率が４程度と低く、熱膨張率も低いため、本発明に用いられる無機微粒子として好適に用いられる。

【００２５】

本発明に用いられるシリカは、粒子形態のシリカであり、平均粒子径が２００ｎｍ以下、例えば５ｎｍ～２００ｎｍ、好ましくは１０ｎｍ～１００ｎｍであり、より樹脂の沿面放電を抑制する観点から、好ましくは２０ｎｍ～８０ｎｍである。粒子径が２００ｎｍよりも大きい、または５ｎｍよりも小さいと、沿面放電抑制効果が小さくなる。

【００２６】

本発明に用いられるシリカ粒子の平均粒子径とは、窒素吸着法により測定された比表面積値から算出される平均粒子径値である。

【００２７】

特に本発明では、上記平均粒子径の値を有するコロイダルシリカを好適に使用でき、該コロイダルシリカとしては、シリカゾルを用いることができる。シリカゾルとしては、ケイ酸ナトリウム水溶液を原料として公知の方法により製造される水性シリカゾル及び該水性シリカゾルの分散媒である水を有機溶媒に置換して得られるオルガノシリカゾルを原料として使用する事が出来る。また、メチルシリケートやエチルシリケート等のアルコキシシランを、アルコール等の有機溶媒中で触媒（例えば、アンモニア、有機アミン化合物、水酸化ナトリウム等のアルカリ触媒）の存在下において加水分解し、縮合して得られるシリカゾル、又はそのシリカゾルを他の有機溶媒に溶媒置換したオルガノシリカゾルも原料として用いることができる。

【００２８】

上述のオルガノシリカゾルにおける有機溶媒の例としては、アルコール類、エーテル類、ケトン類、エステル類、アミド類、炭化水素類、ニトリル類等が挙げられる。

【００２９】
アルコール類としては、メタノール、エタノール、１－プロパノール、２－プロパノール、１－ブタノール、イソブチルアルコール、２－ブタノール、エチレングリコール、グリセリン、プリピレングリコール、トリエチレングリコール、ポリエチレングリコール、ベンジルアルコール、１，５－ペンタンジオール、ジアセトンアルコール等が挙げられる
。
【００３０】
エーテル類としては、ジエチルエーテル、ジブチルエーテル、テトラヒドロフラン、ジオキサン、エチレングリコールモノメチルエーテル、エチレングリコールモノプロピルエーテル、プロピレングリコールモノメチルエーテル、プロピレングリコールモノエチルエーテル、ジエチレングリコールモノメチルエーテル、ジエチレングリコールモノエチルエーテル、ジエチレングリコールモノブチルエーテル等が挙げられる。
【００３１】
ケトン類としては、アセトン、メチルエチルケトン、２－ペンタノン、３－ペンタノン、メチルイソブチルケトン、２－ヘプタノン、シクロヘキサノン等が挙げられる。
【００３２】
エステル類としては、ギ酸エチル、酢酸メチル、酢酸エチル、酢酸プロピル、酢酸ブチル、エチレングリコールモノエチルエーテルアセタート、エチレングリコールモノブチルエーテルアセタート、プロピレングリコールモノメチルエーテルアセタート等が挙げられ
る。
【００３３】
アミド類としては、アセトアミド、Ｎ，Ｎ－ジメチルホルムアミド、Ｎ，Ｎ－ジメチルアセトアミド、Ｎ－メチルピロリドン等が挙げられる。
【００３４】
炭化水素類としては、ｎ－ヘキサン、シクロヘキサン、ベンゼン、トルエン、キシレン、ソルベントナフサ、スチレン等があげられ、更にハロゲン化炭化水素類としてはジクロロメタン、トリクロロエチレン等が挙げられる。
【００３５】
ニトリル類としては、アセトニトリル、グルタロニトリル、メトキシアセトニトリル、プロピオニトリル、ベンゾニトリル等が挙げられる。
【００３６】
上記オルガノシリカゾルの市販品の例としては、例えば商品名ＭＡ－ＳＴ－Ｓ（メタノール分散シリカゾル、日産化学工業（株）製）、商品名ＭＴ－ＳＴ（メタノール分散シリカゾル、日産化学工業（株）製）、商品名ＭＡ－ＳＴ－ＵＰ（メタノール分散シリカゾル、日産化学工業（株）製）、商品名ＭＡ－ＳＴ－Ｍ（メタノール分散シリカゾル、日産化学工業（株）

製）、商品名ＭＡ－ＳＴ－Ｌ（メタノール分散シリカゾル、日産化学工業（株）製）、商品名ＩＰＡ－ＳＴ－Ｓ（イソプロパノール分散シリカゾル、日産化学工業（株）製）、商品名ＩＰＡ－ＳＴ（イソプロパノール分散シリカゾル、日産化学工業（株）製）、商品名ＩＰＡ－ＳＴ－ＵＰ（イソプロパノール分散シリカゾル、日産化学工業（株）製）、商品名ＩＰＡ－ＳＴ－Ｌ（イソプロパノール分散シリカゾル、日産化学工業（株）製）、商品名ＩＰＡ－ＳＴ－ＺＬ（イソプロパノール分散シリカゾル、日産化学工業（株）製）、商品名ＮＰＣ－ＳＴ－３０（ｎ－プロピルセロソルブ分散シリカゾル、日産化学工業（株）製）、商品名ＰＧＭ－ＳＴ（１－メトキシ－２－プロパノール分散シリカゾル、日産化学工業（株）製）、商品名ＤＭＡＣ－ＳＴ（ジメチルアセトアミド分散シリカゾル、日産化学工業（株）製）、商品名ＸＢＡ－ＳＴ（キシレン・ｎ－ブタノール混合溶媒分散シリカゾル、日産化学工業（株）製）、商品名ＥＡＣ－ＳＴ（酢酸エチル分散シリカゾル、日産化学工業（株）製）、商品名ＰＭＡ－ＳＴ（プロピレングリコールモノメチルエーテルアセテート分散シリカゾル、日産化学工業（株）製）、商品名ＭＥＫ－ＳＴ（メチルエチルケトン分散シリカゾル、日産化学工業（株）製）、商品名ＭＥＫ－ＳＴ－ＵＰ（メチルエチルケトン分散シリカゾル、日産化学工業（株）製）、商品名ＭＥＫ－ＳＴ－Ｌ（メチルエチルケトン分散シリカゾル、日産化学工業（株）製）及び商品名ＭＩＢＫ－ＳＴ（メチルイソブチルケトン分散シリカゾル、日産化学工業（株）製）等を挙げることができるが、これらに限定されない。

【００３７】

本発明に使用されるシリカ粒子の表面は疎水化処理されていても良い。疎水化処理剤としては、シラザン、シロキサン又はアルコキシシラン及びその部分加水分
解物若しくはその重合した２量体～５量体のオリゴマーが挙げられる。

【００３８】

シラザンとしては、例えばヘキサメチルジシラザン、及びヘキサエチルジシラザンが挙げられる。

【００３９】

シロキサンとしては、例えばヘキサメチルジシロキサン、１，３－ジブチルテトラメチルジシロキサン、１，３－ジフェニルテトラメチルジシロキサン、１，３－ジビニルテトラメチルジシロキサン、ヘキサエチルジシロキサン及び３－グリシドキシプロピルペンタメチルジシロキサンが挙げられる。

【００４０】

アルコキシシランとしては、例えばトリメチルメトキシシラン、トリメチルエトキシシラン、トリメチルプロポキシシラン、フェニルジメチルメトキシシラン、クロロプロピルジメチルメトキシシラン、ジメチルジメトキシシラン、メチルトリメトキシシラン、テトラメトキシシラン、テトラエトキシシラン、テトラプロポキシシラン、テトラブトキシシラン、エチル

トリメトキシシラン、ジメチルジエトキシシラン、プロピルトリエトキシシラン、ｎ－ブチルトリメトキシシラン、ｎ－ヘキシルトリメトキシシラン、ｎ－オクチルトリエトキシシラン、ｎ－オクチルメチルジエトキシシラン、ｎ－オクタデシルトリメトキシシラン、フェニルトリメトキシシラン、フェニルメチルジメトキシシラン、フェネチルトリメトキシシラン、ドデシルトリメトキシシラン、ｎ－オクタデシルトリエトキシシラン、フェニルトリメトキシシラン、ジフェニルジメトキシシラン、ビニルトリメトキシシラン、ビニルトリエトキシシラン、ビニルトリス（βメトキシエトキシ）シラン、γ－メタアクリルオキシプロピルトリメトキシシラン、γ－アクリルオキシプロピルトリメトキシシラン、γ－（メタアクリルオキシプロピル）メチルジメトキシシラン、γ－メタアクリルオキシプロピルメチルジエトキシシラン、γ－メタアクリルオキシプロピルトリエトキシシラン、β－（３，４－エポキシシクロヘキシル）エチルトリメトキシシラン、γ－グリシドキシプロピルトリメトキシシラン、γ－グリシドキシプロピルメチルジエトキシシラン、γ－グリシドキシプロピルトリエトキシシラン、Ｎ－β（アミノエチル）γ－（アミノプロピル）メチルジメトキシシラン、Ｎ－β（アミノエチル）γ－（アミノプロピル）トリメトキシシラン、Ｎ－β（アミノエチル）γ－（アミノプロピル）トリエトキシシラン、γ－アミノプロピルトリメトキシシラン、γ－アミノプロピルトリエトキシシラン、Ｎ－フェニル－γ－アミノプロピルトリメトキシシラン、γ－メルカプトプロピルトリメトキシシラン、３－イソシアネートプロピルトリエトキシシラン、トリフルオロプ
ロピルトリメトキシシラン、ヘプタデカトリフルオロプロピルトリメトキシシラン、ｎ－デシルトリメトキシシラン、ジメトキシジエトキシシラン、ビス（トリエトキシシリル）エタン及びヘキサエトキシジシロキサンが挙げられる。

【００４１】

本発明における樹脂中のナノシリカの配合量としては、例えば０．１～５０質量％であり、好ましくは0.2～30質量％であり、より樹脂の沿面放電を抑制する観点から、好ましくは0.5～20質量％、より好ましくは1～１５質量％である。

【００４２】

ナノシリカの配合量が５０質量％よりも多いと樹脂硬化物の誘電率が上昇し、放電抑制効果が小さくなる。また、ナノシリカの配合量が０．１質量％よりも少ないとシリカを添加した効果が小さくなり、樹脂の放電抑制効果が得られない。

【００４３】

上述のオルガノシリカゾルを、例えばエポキシ樹脂と混合して脱溶媒することで、ナノシリカが分散したエポキシ樹脂を得ることが出来る。この樹脂に適宜、硬化剤を添加して、注型・加熱等によって硬化反応を行い、所望の絶縁樹脂成型物が得られる。

【実施例】
【００４４】
（材料の準備）
ビスフェノールＡジグリシジルエーテルＪＥＲ８２８（三菱化学（株）製、エポキシ価１８５ｇ／ｅｑ．）に、平均粒子径１２～５００ｎｍのシリカ粒子を分散させたエポキシモノマー分散シリカゾルをシリカ濃度３０．５質量%となるよう調整した。平均粒子径５００ｎｍのシリカ粒子には、アドマファインＳＯ－Ｃ２（アドマテックス（株）製）を用いた。平均粒子径は、シリカの３００℃乾燥粉末の比表面積を比表面積測定装置モノソーブ（登録商標）ＭＳ－１６（ユアサアイオニクス（株）製）を用いて測定し、平均粒子径（ｎｍ）＝２７２０／比表面積（m^2／g）の換算式により算出した。
【００４５】
【表１】

	粒子径(nm)	エポキシ樹脂	SiO2(%)
モノマーゾル1	12	ビスフェノールA型	30.5
モノマーゾル2	22	ビスフェノールA型	30.5
モノマーゾル3	45	ビスフェノールA型	30.5
モノマーゾル4	80	ビスフェノールA型	30.5
モノマーゾル5	500	ビスフェノールA型	30.5

【００４６】
実施例１～実施例１０表１で準備したエポキシモノマー分散シリカゾルと、酸無水物（リカシッドMH－７００、新日本理化（株）製）、反応促進剤（ジメチルベンジルアミン、東京化成）を表２に記載の配合比で混合しエポキシ樹脂硬化用組成物を得た。得られたエポキシ樹脂硬化用組成物を注型板（離型フィルムＰＬ＃４００（フタムラ化学（株）製）で被覆されたガラス板３ｍｍ厚）に流し込み、７０℃で２時間、９０℃で２時間、１５０℃で８時間の硬化条件で加熱処理を行い、エポキシ樹脂硬化体を得た。
【００４７】
【表２】

	モノマーゾル(g)		エポキシ樹脂(g)	酸無水物(g)	促進剤(g)	SiO2(%)
実施例1	モノマーゾル1	5.0	23.6	21.7	0.3	3
実施例2	モノマーゾル2	5.0	23.4	21.6	0.3	3
実施例3	モノマーゾル2	16.5	13.6	19.9	0.2	10
実施例4	モノマーゾル3	1.7	26.6	22.4	0.3	1
実施例5	モノマーゾル3	5.0	23.5	21.7	0.3	3
実施例6	モノマーゾル3	8.3	20.8	21.3	0.3	5
実施例7	モノマーゾル3	16.5	13.5	20.0	0.2	10
実施例8	モノマーゾル3	32.5	0.0	17.9	0.2	20
実施例9	モノマーゾル4	5.0	23.7	21.9	0.3	3
実施例10	モノマーゾル4	16.5	13.5	20.0	0.2	10
比較例1	なし	0.0	55.0	44.4	0.6	0
比較例2	モノマーゾル5	5.0	23.6	21.9	0.3	3

【００４８】
（沿面放電の測定方法）
沿面放電の測定系の概略構成を図１に示す。この装置は、各印加電圧時の時間波形及び発光像を取得し、沿面放電発生確率を算出するものである。
【００４９】
試料１としては、実施例１～１０で作製したエポキシ樹脂硬化体を用いた。試料１の厚さは、３ｍｍである。
【００５０】
図１に示すように、試料１の表面に針電極２と、平板電極３とをギャップ長ｇ＝５０ｍｍで配置した。これらの試料１及び針電極２と平板電極３との電極系は、試験容器４内に配置した。試験容器４内に鉱油５を充填し、試料１及び電極系を鉱油５内に配置した。
【００５１】
針電極２の直径は１ｍｍで、先端曲率半径は１０μｍであり、試料１の表面に対してθ＝３０°傾けて配置した。針電極２をインパルス電圧発生装置６に接続し、平板電極３は５０Ωの抵抗を介して接地した。針電極２に、分圧器７を介して、正極性標準雷インパル電圧（１．２μｓ／５０μｓ）を、３５ｋＶ～７５ｋＶまで、５ｋＶステップで、印加間隔１分間で印加し、沿面放電の発生をイメージインテンシファイア付きのＣＣＤカメラ８を用いて確認した。試料１の数は３枚、試験回数は各電圧で５回実施し、計１５回の実験で沿面放電発生確率を算出した。
【００５２】
また、試料１の比誘電率は誘電率計測器を用いて評価した。
【００５３】
試料条件、試料の比誘電率の測定結果、および沿面放電試験結果を表３に示した。表３からシリカ微粒子の充填率が増加すると比誘電率が増加する傾向がわかる。一方で、シリカ微粒子の粒径が５００ｎｍの試料以外は放電発生確率が低下し、放電発生電圧が増加することがわかる。また、放電発生確率が１００％に到達する電圧も、粒径が５００ｎｍの試料以外は５～１５ｋＶ上昇した。つまり、本提案の手法を用いることで、樹脂の比誘電率はほぼ不変あるいは増加するにも関わらず、樹脂表面の沿面放電の発生を抑制できるこ
とになる。
【００５４】
【表３】

	シリカ粒子径 [nm]	シリカ添加率 [wt%]	比誘電率 (@100 kHz)	35kVにおける 放電発生確率[%]	放電発生確率が 100%の電圧[kV]
実施例1	12	3	3.46	33	50
実施例2	22	3	3.50	20	50
実施例3		10	3.58	33	45
実施例4	45	1	3.48	7	50
実施例5		3	3.51	0	50
実施例6		5	3.56	33	55
実施例7		10	3.59	0	55
実施例8		20	3.75	40	50
実施例9	80	3	3.53	33	45
実施例10		10	3.60	55	50
比較例1	シリカなし	0	3.47	73	40
比較例2	500	3	3.58	73	40

平均粒子径１３０ｎｍのシリカ粒子を分散させたエポキシモノマー分散シリカゾルをシリカ濃度３０．５質量%となるよう調整した。

【表４】

	粒子径	エポキシ樹脂	SiO2(%)
モノマーゾル6	130nm	ビスフェノールA型	30.5

実施例１～１０と同様の条件で、下記組成にて実施例１１及び比較例３の硬化物を作成した。

【表５】

	モノマーゾル(g)		エポキシ樹脂(g)	酸無水物(g)	促進剤(g)	SiO2(%)
実施例11	モノマーゾル3	0.81	26.3	21.7	0.3	0.5
比較例3	モノマーゾル6	5.0	23.5	21.7	0.3	3.0

上記と同様の装置を用い、沿面放電の発生を光電子増倍管９を用いて確認した。光電子増倍管９は、信号用９ａと、ノイズ用９ｂとを用いた。

【表６】

	シリカ粒子径 [nm]	シリカ添加率 [wt%]	比誘電率 (@100 kHz)	35kVにおける 放電発生確率[%]	放電発生確率が 100%の電圧[kV]
実施例1	12	3	3.46	31	50
実施例2	22	3	3.50	20	50
実施例11	45	0.5	3.35	40	45
実施例4		1	3.48	30	45
実施例9	80	3	3.53	31	45
比較例1	シリカなし	0	3.47	71	40
比較例2	500	3	3.58	71	40
比較例3	130	3	3.59	80	45

試料条件、試料の比誘電率の測定結果、および沿面放電試験結果を表４に示した。シリカ微粒子の粒径が１３０ｎｍ以上の試料以外は放電発生確率が低下し、放電発生電圧が増加することがわかる。また、放電発生確率が１００%に到達する電圧も、粒径が５００ｎｍ以上の試料以外は５～１０ｋＶ上昇した。つまり、本提案の手法を用いることで、

樹脂の比誘電率はほぼ不変あるいは増加するにも関わらず、樹脂表面の沿面放電の発生を抑制できることになる。

【産業上の利用可能性】
【００５５】
本発明によって、本発明を用いることで、固体絶縁材料の電界緩和や物理的な沿面距離増加を施さずとも、固体表面の沿面放電発生電圧を向上することができ、GIS(ガス絶縁開閉装置)の 絶縁スペーサや油入り変圧器のプレスボード用コーティング樹脂等へ好適に利用されうる。
【符号の説明】
【００５６】
１ 試料
２ 針電極
３ 平板電極
４ 試験容器
５ 鉱油
６ インパルス電圧発生装置
７ 分圧器
８ カメラ
９ 光電子増倍管
９ａ 信号用
９ｂ ノイズ用

【書類名】特許請求の範囲
【請求項１】
ナノサイズの無機微粒子を樹脂中に分散させて樹脂硬化体の表面の沿面放電の発生を抑制することを特徴とする、沿面放電の発生を抑制する方法
【請求項２】
前記無機微粒子がシリカであることを特徴とする、請求項１に記載の方法。
【請求項３】
前記樹脂が熱硬化性樹脂である請求項１又は２に記載の方法。
【請求項４】
前記無機微粒子の添加率が０．１～５０質量%である請求項１～３のいずれか一項に記載の方法
【請求項５】
前記無機微粒子の平均粒子径が５～２００ｎｍである請求項１～４のいずれか一項に記載の方法。
【書類名】要約書
【要約】
【課題】固体絶縁材料である樹脂自体の電界緩和（即ち樹脂の低誘電率化）に頼ることなく、樹脂表面の沿面放電の発生を抑制する手法を確立するこ

と。
【解決手段】ナノサイズの無機微粒子を樹脂中に分散させて樹脂硬化体の表面の沿面放
電の発生を抑制することを特徴とする、樹脂表面の沿面放電の発生を抑制する方法による。
【選択図】なし
【書類名】図面
【図１】

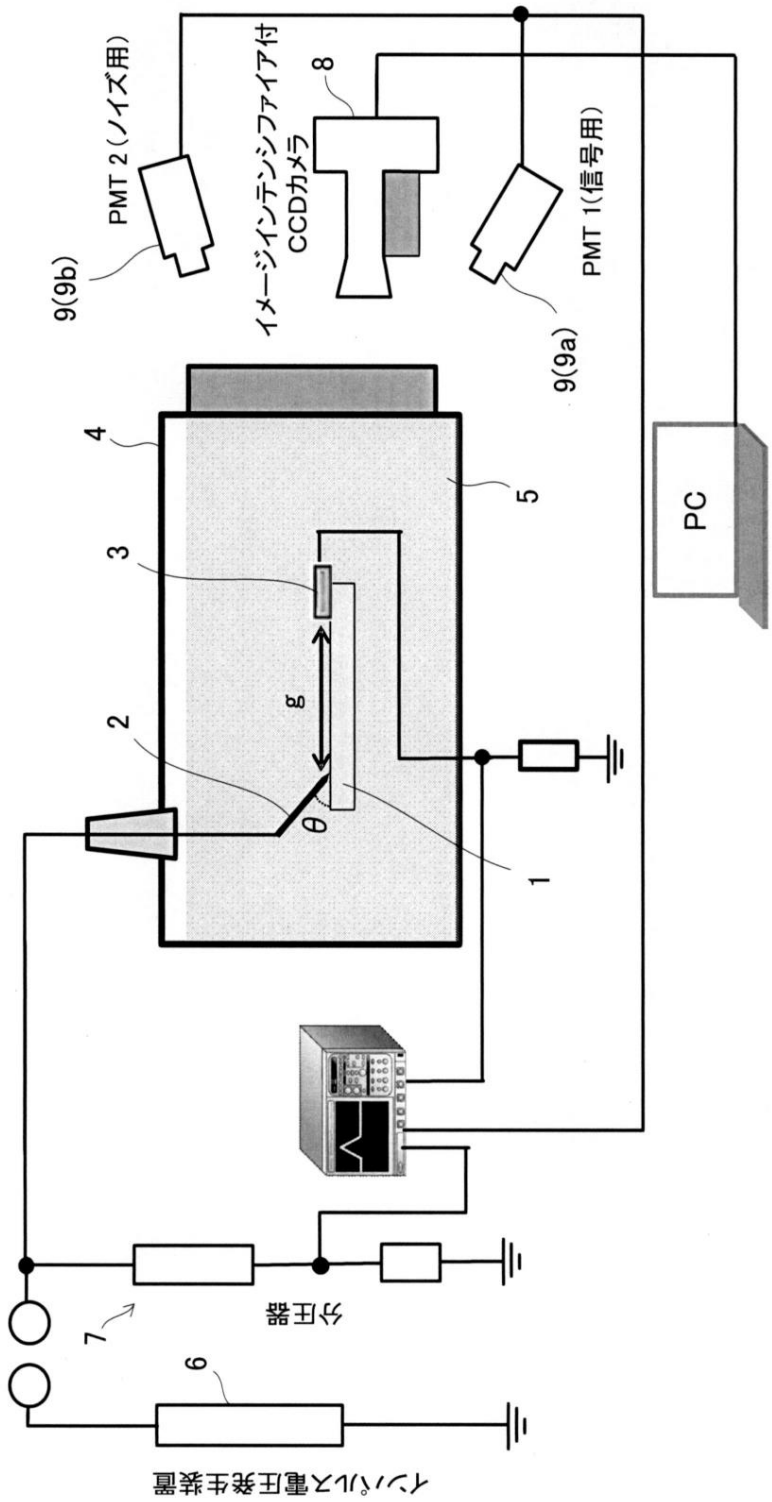
PMT 2（ノイズ用）
9(9b)
イメージインテンシファイア付
CCDカメラ
8
PMT 1(信号用)
9(9a)
4
5
PC
3
g
2
θ
1
分圧器
7
9
インパルス電圧発生装置

APPENDIX B

B.1 Experiment at 5 mm Short Gap at 25 kV

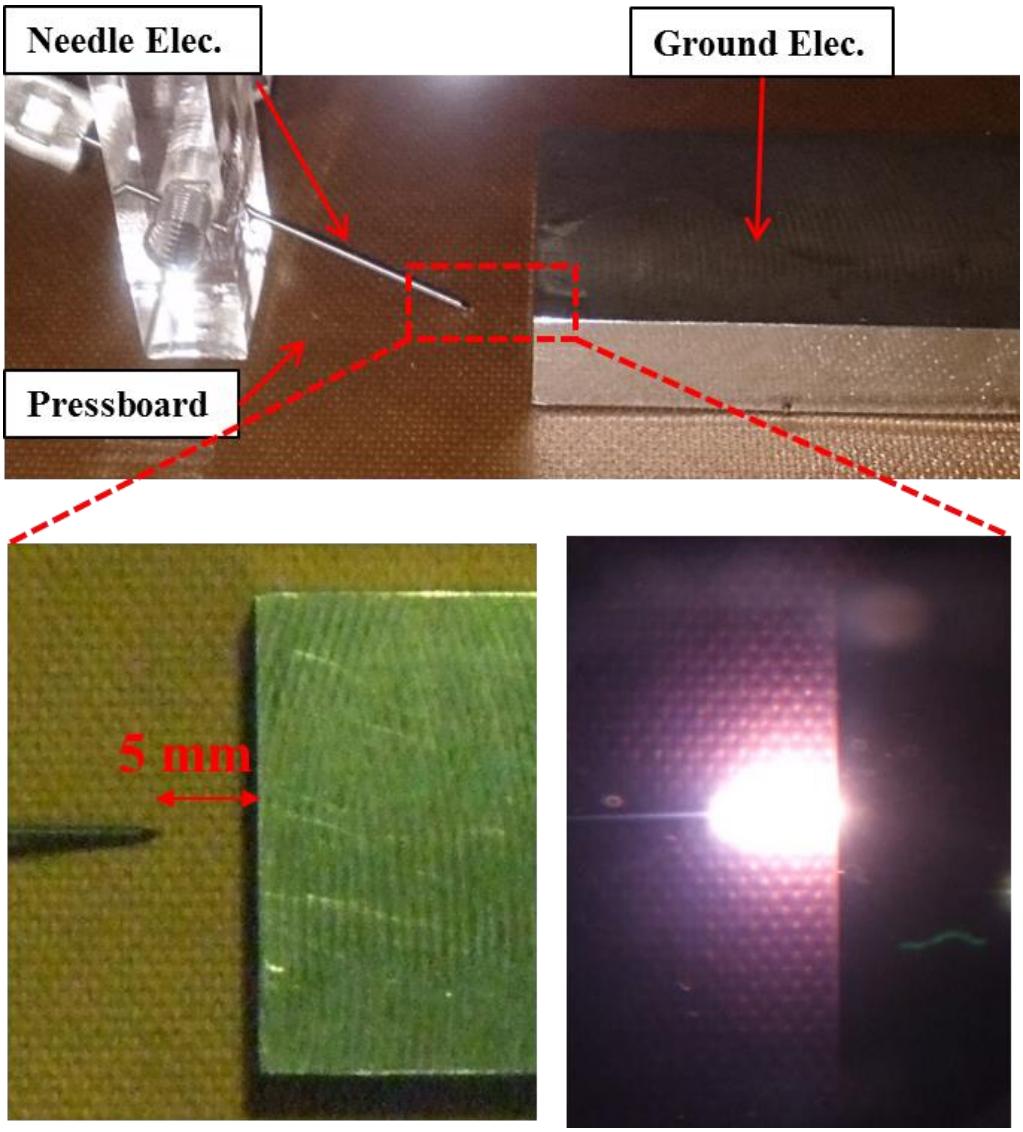

Figure B1. Experimental setup at 5mm gap distance in mineral oil

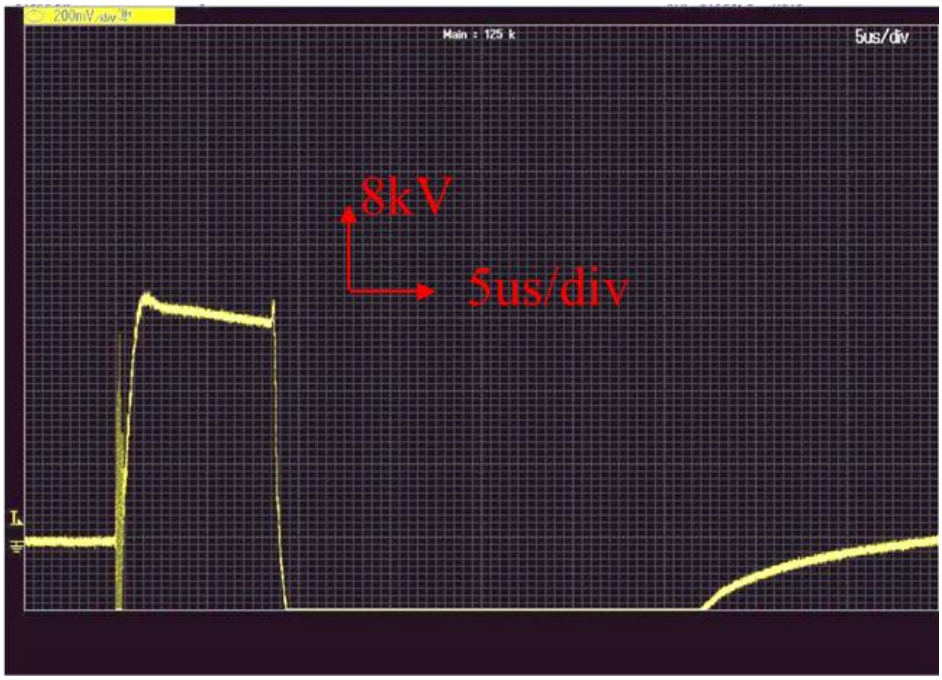

Figure B2. Experimental waveform of OSC

B.2 Snapshots of Electric Field Distribution using Rod-Plane Electrode Configuration

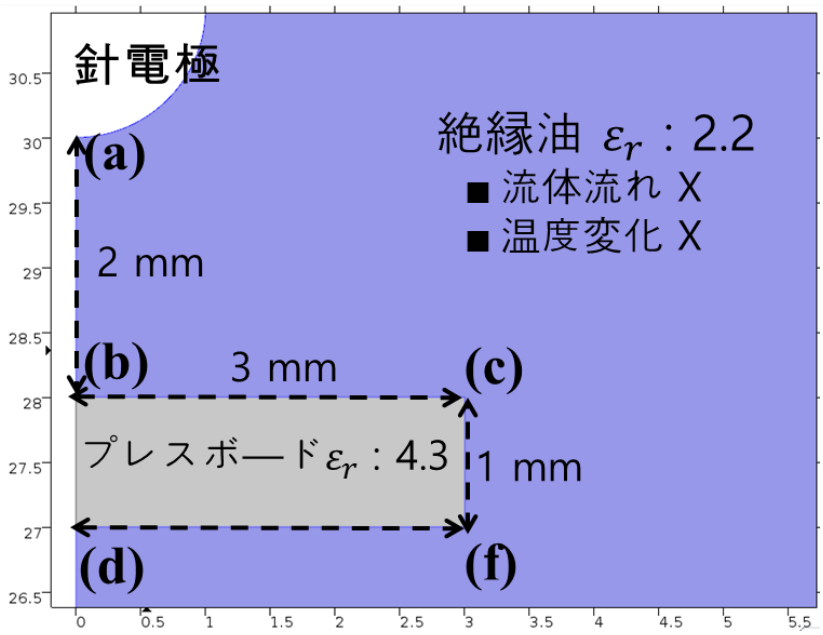

Figure B3. Simulation model of rod-plane electrode configuration

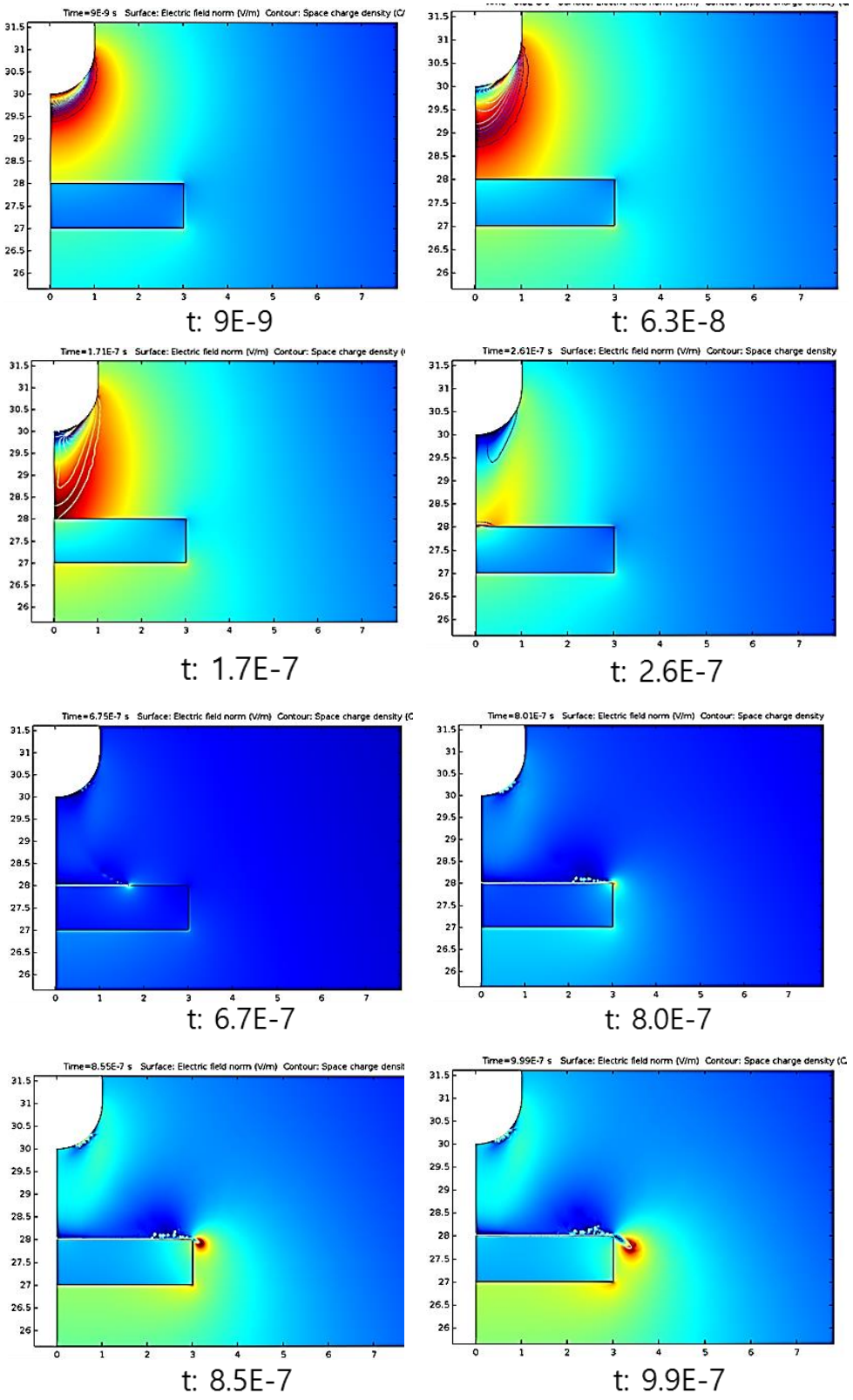

Figure B4. Simulation results of rod-plane electrode configuration under positive lightning impulse voltage

APPENDIX C

COMSOL Multiphysics

C.1 How to setup FEM mesh for simulation

Figure C1 shows distribution of FEM mesh on the needle-bar electrodes. In general, mesh is a crucial step in obtaining a reliable simulation result. Dense mesh size is formed to produce accurate simulation results for complicated Multiphysics finite element analysis combined with multiple systems, while calculation needs a lot of analysis time. In some cases, calculation is not possible due to a lack of system resources. On the other hand, if the mesh size is not densely formed to obtain the analysis result within a short time, accurate calculation results can't be obtained. In such problems, the sharp geometries as needle electrode requires a fine mesh in these regions. In addition, discharge dynamics often take place in a small volume with respect to the entire simulation space. A fine mesh is hence needed to resolve the solution at such region. Thus, a proper mesh size is required to reflect the Multiphysics analysis of interested region as shown in Fig. C1.

There are two types of mesh element that can be used in COMSOL: triangular and quadrilateral elements. Triangular meshing was preferred since it meshes sharp electrodes more efficiently. COMSOL also offers a tool to specify the size of mesh elements along boundaries and subdomains ensuring better accuracy at regions of interest. However, investigations revealed that the element type does not affect the simulation results significantly. All the simulation results are compared with Kyungpook University's simulation results of Professor Se-Hee Lee to verify our results [36, 37, 64, 114, 121].

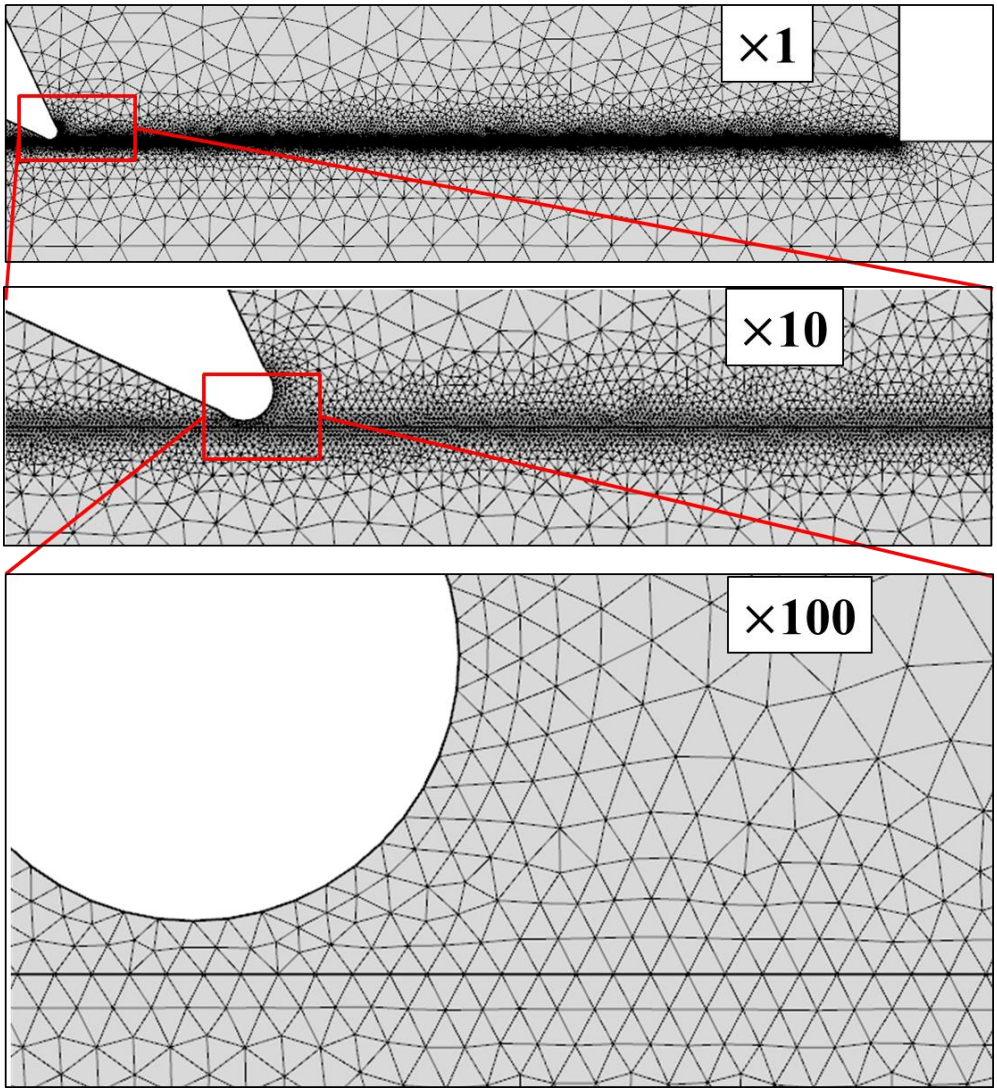

Figure C1 Distribution of FEM mesh on the needle-bar electrode

REFERENCES

[1] Hidayat Zainuddin, "Study of Surface Discharge Behaviour at the Oil-pressboard Interface", *Thesis for the degree of Doctor of Philosophy*, university of southampton, 2013.

[2] Forensic Science newsletter, 2005, http://www.forensic.cc/newsletter/transformer-failures

[3] P. Przybylek, Z. Nadolny and H. Moscicka-Grzesiak, "Bubble Effect as a Consequence of dielectric Losses in Cellulose Insulation", *IEEE Transactions on Dielectrics and Electrical Insulation*, Vol. 17, no. 3, 2010

[4] A. J. Kachler, I. Hohlein, "Aging of Cellulose at Transformer Service Temperatures. Part 1: Influence of Type of Oil and Air on the Degree of Polymerization of Pressboard, Dissolved Gases, and Furanic Compounds in Oil", *Feature article*, Vol. 21, Issue 2, 2005

[5] S. V. Kulkarni and S. A. Khaparde, "Transformer Engineering Design and Practice", *CRC Press*, pp. 496, 2004.

[6] V. Sokolov, Z. Berler and V. Rashkes, "Effective methods of assessment of insulation system conditions in power transformer: a view based on practical experience", *Proceedings of the Electrical Insulation Conference and Electrical Manufacturing & Coil Winding Conference*, USA, pp. 659-667, papers (39), 1999

[7] Yangchun Cheng, Jinqing Wei, Chongzhi Zhao and Haoyong Song, "Experimental Research on Creepage Discharge Between oil-impregnated Pressboard Layers", *Proc. 17th Conference CEFC*, pp. 1-10, 2009

[8] CIGRE Working Group 12.18: Life Management of Transformers, "Guidelines for life management techniques for power transformers", *Draft Final Report Rev*. 2, 22, 2002

[9] Thomas A. Prevost and T. V. Oommen, "Cellulose Insulation in Oil-Filled Power Transformers: Part 1-History and Development", *IEEE Electrical Insulation Magazine*, Vol. 22, Issue: 1, 2006

[10] J. A. Lapworth and A. Wilson, "Transformer Internal Over-Voltages Caused by Remote Energisation", *IEEE PES Power Africa Conference and Exposition*, pp. 1-6, 2007

[11] DU Yue-fan, LV Yu-zhen, WANG Fo-chi, Ki Xiao-xin and Li Cheng-rong, "Effect of TiO2 Nanoparticles on the Breakdown Strength of Transformer Oil", *IEEE International Symposium on Electrical Insulation (ISEI)*,6-9 June, 2010

[12] LV Yu-zhen, Le-feng Wang, Xiao-xin Li, Yue-fan Du, Jian-quan Zhou and Cheng-rong Li, "Experimental Investigation of Breakdown Strength of

Mineral Oil-Based Nanofluids", *IEEE International Conference on Dielectric Liquids,* pp. 1-3, 2011

[13] R. Hollertz, L. Wagberg and Claire Pitois, "Novel Cellulose Nanomaterials", *IEEE International Conference on Liquid Dielectrics*, Bled, Slovenia, pp.1-4, 2014

[14] Rebecca Hollertz, David Ariza, Claire Pitois and Lars Wagberg, "Dielectric Response of Kraft Paper from Fibres Modified by Silica Nanoparticles", *Annual Report Conference on Electrical Insulation and Dielectric Phenomena*, pp.459-462, 2015

[15] Min Chen, Limin Wu, Shuxue Zhou and bo You, "A Method for the Fabrication of Monodisperse Hollow Silica Spheres", *Advanced materials*, Vol. 18, pp. 801-806, 2006

[16] Ruijin Liao, Fuzhou Zhang, Yuan Yuan, Tuan Liu and Chao Tang, "Preparation and Electrical Properties of Insulation Paper Composed of SiO2 Hollow Spheres", *MDPI open access Journal*, Vol. 5, pp. 2943-2951, 2012

[17] Jae-Won George Hwang, "Elucidating the Mechanisms Behind Pre-Breakdown Phenomena in Transformer Oil Systems", *Thesis for the degree of Doctor of Philosophy, Massachusetts Institute of technology*, 2010

[18] A. Kara, O. Kalenderli and K. Mardikyan, "Effect of Dielectric Barriers to the Electric Field of Rod-Plane Air Gap", *proceedings of the COMSOL users Conference*, 2006

[19] R. Hanaoka, T. Kohrin, T. Miyagawa and T. Nishi, " Creepage Discharge Characteristics over Solid-Liquid Interfaces with Grounded Side Electrode", *International Conference on Conduction and Breakdowns in Dielectric Liquids*, pp.308-315, Vol. 9, 2002

[20] Fri Murdiya, Ryoichi Hanaoka, Hideki Akiyama and Katsunori Miyagi, "Creeping Discharge Developing on Vegetable-Based Oil/Pressboard Interface under AC Voltage", *IEEE Trans. Dielectr. Electr. Insul.,* Vol. 21, pp.2102-2110, 2014

[21] F. Murdiya, R. Hanaoka, R. Hashi and K. Miyagi, "Properties of Creeping Streamer Progressed Dielectric Barrier with Narrow Gap in PFAE Oil", *Journal of Energy and Power Engineering*, Vol. 7, pp.1-4, 2013

[22] Fri Murdiya, "Research on Creeping Discharge Phenomena in Insulation Oils-Vegetable based Oils as Substitute of Mineral Oil", *Thesis for the degree of Doctor of Philosophy, UNIVERSITY OF KANAZAWA*, 2015

[23] M. J. Heathcote, *J & P Transformer Book, 12th ed., Butterworth-Heinemann*, 1998

[24] R. Bartnikas, "Engineering Dielectrics, Volume 3: electrical Insulating Liquids", *American Society for Testing and Materials*, 1994

[25] J. Bidlack, M. Malone and B. Russel, "Molecular Structure and Component Integration of Secondary Cell Walls in Plants", *Proc. Okla. Acad. Sci*., Vol. 72, pp.51-56, 1992

[26] P. M. Mitchinson, "Surface Tracking in the Interphase Region of Large Trasnformer", *Ph,D. thesis, University of Southamton*, 2008

[27] "The Effect of Moisture on the Breakdown Voltage of Transformer Oil" www.vaisala.com

[28] M. C. Silva, "Characterization of three non-product materials from a bleached eucalyptus kraft pulp mill, in view of valorizing them as a source of cellulose fibres", *Industrial Crops and Products*, Vol. 27, Issue 3, pp.288-295, 2008

[29] T. V. Oommen and Thomas A. Prevost, "Cellulose Insulation in Oil-Filled Power Transformers: Part 2-Maintaining Insulation Integrity and Life, *IEEE Electrical Insulation Magazine,* Vol. 22, issue: 2, 2006

[30] K. Giese, "The Effects of Cellulose Insulation Quality on Electrical Intrinsic Strength", *IEEE Electrical Insulation Magazine,* Vol. 10, pp.38-42, Issue 5, 1994

[31] Y. Suzuki and M. Takagi, "Oil Impregnation in Transformer Boards Theoretical Analysis of Changes in Impregnation Depth", *IEEE Transactions on Electrical Insulation*, Vol. EI-19, 1984

[32] H. Zainuddin, P. L. Lewin and P. M. Mitchinson, "Modeling the Inter-phase Region of High Voltage Transformers", *IEEE International Conference on Dielectric Liquids*, pp.1-4, 2011

[33] Ho-Young Lee and Se-Hee Lee, "Numerical Analysis for Surface Discharge on Solid Insulation in the Dielectric Liquid and Experimental Validation", *Korea-Japan Joint Symposium*, 2015

[34] F. M. Clark, "Insulating Materials for Design and Engineering Practice", *John Wiley & Sons, Inc*., 1962

[35] J. Dai, Z. D. Wang and P. Jarman, "Moisture and ageing effect on the creepage discharge characteristics at the oil/transformer-board interface under divergent field", *Annual report conference on electrical insulation and dielectric phenomena (CEIDP),* pp. 662-665, 2008

[36] Ho-Young Lee, Jae-Seung Jung, Hong-Kyu Kim and Se-Hee Lee, "Numerical and Experimental Validation of Discharge Current with Generalized Energy Method and Integral Ohm's Law in Transformer Oil", *OEEE Transactions on Magnetics*, Vol. 50, no. 2, 2014

[37] Ho-Young Lee and Se-Hee Lee, "Finite Element Analysis of Positive Streamer Propagation with Lightning Impulse Voltage", *International Conference on Electrical Machines and Systems (ICEMS)*, pp.1836-1839, 2010

[38] Hwang. J. G. et al., "Modeling streamers in transformer oil: The transitional fast 3rd mode streamer", *Properties and Applications of Dielectric Materials (ICPADM*), pp.573-578, 2009

[39] Jadidian, Jouya, Markus Zahn, Nils Lavesson and Karl Borg, "Surface Flashover Breakdown Mechanisms on Liquid Immersed Dielectrics", *Applied Physics Letters 100,* no. 17, 2012

[40] Francis O'Sullivan, J. George Hwang and Markus Zahn, "A Model for the Initiation and Propagation of Positive Streamers in Transformer Oil", *IEEE International symposium on Electrical Insulation (ISEI),* pp.210-214, 2008

[41] R. Liu, C. Tornkvbist, V. Chandramouli, O. Girlanda and L. A. A. Pettersson, "Ester fluids as alternative for mineral oil: the difference in streamer velocity and pre breakdown voltages", *Annual Report conference on Electrical Insulation and Dielectric Phenomena CEIDP*, pages 543-548, 2009

[42] X. Yi and Z. D. Wang, "The Influences of Solid Surface on the Propagation of Creepage Discharge in Insulating Liquids", *IEEE Transaction on Dielectric and Electrical Insulation*, Vol. 22, no. 1, 2015

[43] M. Akyuz, L. Gao and V. Cooray, "Positive Streamer Discharges along Insulating Surface", *IEEE Transaction on Dielectric and Electrical Insulation*, Vol. 8, no. 6, 2001

[44] P. M. Mitchinson, P. L. Lewin, G. Chen and P. N. Jarman, "A new approach to the study of surface discharge on the oil-pressboard interface", *IEEE International Conference on Dielectric Liquid (ICDL),* pp.1-4, 2008

[45] A. Beroual, "Pre-breakdown Mechanisms in Dielectric Liquids and Predicting Models", *Electrical Insulation Conference (EIC),* pp.117-128, 2016

[46] O. Lesaint and G. Massala, "Positive Streamer Propagation in Large Oil Gaps: Experimental characterization of propagation modes", *IEEE Transactions on Dielectric and Electrical Insulation*, Vol. 5, no. 3, 1998

[47] Q. Liu and Z. D. Wang, "Streamer Characteristic and Breakdown in Syhnthetic and Natural Ester Transformer Liquids under Standard Lightning Impulse Voltage", *IEEE Transactions on Dielectrics and Electrical Insulation*, Vol. 18, no. 1, 2011

[48] O. Lesaint and G. Massala, "Transition to fast streamers in mineral oil in the presence of insulating solids", *IEEE International Symposium on Electrical Insulation*, Mntreal, Quebec, Canada, June 16-19, pp.737-740, 1996

[49] Lars Lundgaard, Dag Linhjjell and Gunnar Berg, "Propagation of Positive and Negative Streamers in Oil with and without Pressboard Interfaces", *IEEE Transactions on Dielectrics and Electrical Insulation,* Vol. 5, no. 3, 1998

[50] Y. Kamata, E. Ohe, K. Endoh, S. Furukawa, "Development of Low-permittivity Pressboard and its Evaluation for Insulation of Oil-immersed EHV Power Transformers", *IEEE Transactions on Electrical Insulation*, Vol. 26, no. 4, 1991

[51] David Ariza, Marley Becerra, Rebecca Hollertz and Claire Pitois, "On the initiation of negative streamers at mineral oil-solid interfaces", *Annual Report Conference on Electrical Insulation and Dielectric Phenomena (CEIDP*), pp.563-565, 2015

[52] David Ariza, Marley Becerra, Rebecca Hollertz and Claire Pitois, "Propagation of negative streamers along mineral oil-solid interfaces", *Annual Report Conference on Electrical Insulation and Dielectric Phenomena (CEIDP)*", pp.566-569, 2015

[53] Weiwang Wang and Shengtao Li, "Impulse and DC surface flashover of LDPE/TiO2 nanocomposites in Vacuum", *International Conference on Condition Monitoring and Diagnosis*, pp.497-500, 2016

[54] MaBO, Daomin Min, Jiasheng Ru, Shaoming Pan, Huang Yin, Yuanwei Zhu and Shengtao Li, "Investigating the Influence of Temperature and DC Electric Field on the Electric Conduction of Oil Impregnated Paper Insulation", *International Conference on Condition Monitoring and Diagnosis*, pp.514-517, 2016

[55] Shengtao Li, Weiwang Wang, Fengyan Ni and Guilai Yin, "Surface Flashover in Vacuum and Bulk Breakdown in Polystyrene Nanocomposites", *Conference Proceedings of ISEIM*, pp.486-490, 2011

[56] Yu Chen, Yonghong Cheng, Kai Wu, J. Leith Nelson, "Flashover Characteristic of Epoxy Composites Filled with Different Micro Inorganic Oxide Particles under Nanosecond Pulse in Vacuum", *IEEE Transactions on Plasma Science*, vol. 37, Issue 1, pp. 195-203, 2008

[57] Y. H. Cheng, Y. Chen, P. J. Tang, K. Wu, L. Shao, Q. Chen, "Study on the Vacuum Surface Flashover Characteristics of Epoxy Composites with Different Fillers under Steep High Voltage Impulse", *International Conference on Solid Dielectrics*, Winchester, UK, pp.349-352, 2007

[58] Yu Chen, "Flashover Characteristic of Epoxy Composite Filled with Different Micro-Inorganic Oxide Particles under Nanosecond Pulse in Vacuum", *IEEE Transactions on Plasma Science*, Vol. 37, no. 1, 2009

[59] Kenneth Wechsler and Michael Riccitiello, "Electric Breakdown of a Parallel Solid and Liquid Dielectric System", *AIEE Electrical Insulation Committee, paper* 61-245, 1960

[60] K. Weehsler and M. Riccitiello, "Electric Breakdown of a Parallel Solid and Liquid Dielectric System", AIEE Trans. Part 3, *Power Application System*, Vol. 80, pp. 365-368, 1961

[61] Jadidian, Jouya, Markus Zahn, Nils Lavesson, Ola Widlund and Karl Borg, "Surface Flashover Breakdown Mechanisms on Liquid Immersed Dielectrics", *Applied Physics Letters* 100, no. 17, 2012

[62] Francis M. O'Sullivan, "A Model for the Initiation and Propagation of Electrical Streamers in Transformer Oil and Transformer Oil Based Nanofluids" *Doctor of Philosophy, Massachusetts institute of technology*, 2006

[63] R. H. Fowler and L. Nordheim, "Electron Emission in Intense Electric Field", *Proc. Roy. Soc. A, Vol. 119, no. 78*1, pp. 173-181, 1928

[64] Ho-Young Lee, "Multiphysics Analysis of Electrical Discharge and ELectrogydrodynamics in Dielectric Liquid", *Thesis for the degree of Doctor of Philosophy, Kyungpook National University*, 2014

[65] Uno G*ä*fvert, Albert Jaksts, Christer T*ö*rnkvist and Lars Walfridsson, "Electrical Field Distribution in Transformer Oil", *IEEE Transactions on Electrical Insulation*, Vol. 27, no.3, 1992

[66] Werner F. Schmidt, "Electronic Conduction Processes in Dielectric Liquids", *IEEE Transactions on Electrical Insulation*, Vol. 19, no. 5, 1984

[67] A. O. Allen, "Drift Mobilities and Conduction Band Energies of Excess Electrons in Dielectric Liquids, NSRDS-NBS, 1976

[68] J. C. Devins, S. J. Rzad and R. J. Schwabe, "Breakdown and prebreakdown phenomena in liquids", *J. Appl. Phys*., 1981

[69] C. Zener, "A theory of the electrical breakdown of solid dielectrics", Proc. Roy. Soc. A, 1934

[70] J. Qian, "Analysis of Polarity Effects in the Electrical Breakdown of Liquids", *J. Phys. D. Appl*., Vol. 39, pp. 359-369, 2006

[71] H. Akiyama, "Streamer discharges in liquids and their application", *IEEE Transaction Dielectric Insulation*, Vol. 7, pp.646-653, Issue 5, 2000

[72] W. F. Schmidt, "Electronic Conduction Processes in Dielectric Liquids", *IEEE Trans. Electr. Insul.*, pp.389-418, Issue 5, 1984

[73] A. Denat, B. Gosse and J. P. Gosse, "Electrical Conduction of Solutions of an ionic Surfactant in Hydrocarbons", *IEEE International Conference on dielectric Liquids*, Vol. 12, pp.197-205, 1981

[74] L. Onsager, "Deviations from Ohm's Law in Weak electrolytes", *J. Chem, Phys*., Vol. 2, pp. 599-615, 1934

[75] L. Onsager, "Deviations from Ohm's Law in Weak Electrolytes", *J. Chem. Phys*., Vol. 2, pp. 599-615, 1934

[76] H. Zainuddin, P. L. Lewin and P. M. Mitchinson, "Modeling the Inter-phase Region of High Voltage Transformer", *IEEE International Conference on Dielectric Liquids*, pp.1-4, 2011

[77] P. M. Mitchinson, P. L. Lewin, B. D. Strawbridge and P. Jarman, "Tracking and surface discharge at the oil-pressboard interface", *IEEE Electrical Insulation Magazine*, Vol. 26, pp. 35-41, 2010

[78] G. G. Touchard, T. W. Patzek and C. J. Kadke, "A physicochemical explanation for flow electrification in low-conductivity liquids in contact with a corroding wall", *IEEE Transactions on Industry Applications*, Vol. 32, pp. 1015-1057, 1996

[79] A. P. Washabaugh and M. Zahn, "A chemical reaction based boundary condition for flow electrification", *IEEE Transactions on Dielectrics and Electrical Insulation*, Vol. 4, pp. 688-709, 1997

[80] A. Alj, A. Denat, J. P. Gosse and B. Gosse, "Greation of Charge Carriers in Nonpolar Liquids", *IEEE Transaction Electrical Insulation*, Vol. EI-20, pp. 221-231, 1985

[81] F. Pontiga and A. Castellanos, "Electrical Conduction of Electrolyte Solutions in Non-polar Liquids", *IEEE Transaction Indus. Appl.*, Vol. 32, no. 4, 1996

[82] U. Gafvert, A. Jaksts, C. Tornkvist and L. Walfridsson, "Electrical Field Distribution in Transformer Oil", *IEEE Transaction Electrical Insulation*, Vol. 22, pp. 647-660, 1992

[83] J. M. Cabaleiro, T. Paillat and O. Moreau, "Modelling of static development and dynamic behavior of the electrical double layer at oil-pressboard interface", *Electrostatics Joint Conference*, 2009

[84] Trung Nam Tran, "Surface Discharge Dynamics: Theory, Experiment and Simulation", *Ph.D. thesis, University of Southamton*, 2010

[85] U. Gafvert, A. Jakes, C. Tornkvist and L. Walfridsson, "Electrical field distribution in transformer oil", IEEE Transaction Electrical Insulation, Vol. 22, pp. 647-660, 1992

[86] W. F. Schmidt, "Liquid State Electronics of Insulating Liquids", CRC Press, 1997

[87] F. M. O'Sullivan, "A model for the initiation and propagation of electrical streamers in transformer oil and transformer oil based nanofluids", *Ph.D. thesis, Massachusetts Institute of Technology*, 2007

[88] I. Adamczewski, "Ionization, Conductivity and Breakdown in Dielectric Liqudis", *Tay-lor & Francis*, pp. 185-228, 1996

[89] A. Mozumder, " Electron Mobility on Liquid Hydrocarbons: Application of the Quasi-Ballistic Model", Chem. Phys. Letts., no. 233, pp. 167-172, 1995

[90] Photomultiplier Tube datasheet has been download from: www.datasheetcatalog.com

[91] Image Intensifier units datasheet has been download from: www.datasheetcatalog.com

[92] Q. Wang and G. Chen, "Effect of nanofillers on the dielectric properties of epoxy nanocomposite", *Advances in Materials Research*, Vol. 1, No. 1, 2012

[93] J. Keith Nelson, "Dielectric Polymer Nanocomposites", Chapter 7, pp. 216-220, 2010

[94] Toshikatsu Tanaka and Alun S. Vaughan, "Tailoring of Nanocomposite Dielectrics", from fundamentals to devices and application Chapter 9, 2016

[95] Toshikatsu Tanaka and Masahiro Kozako, "Proposal of a Multi-core Model for Polymer Nanocomposite Dielectrics", *IEEE Transaction on Dielectric and Electrical Isulation*, Vol. 12, no. 4, Issue 1, 2005

[96] J. K. Nelson and Y. Hu, "The impact of nanocomposite formulations on electrical voltage endurance", *International Conference on Solid Dielectric*, Toulouse, France, pp.832-835, Vol. 2, 2004

[97] F. Sadaoui and A. Beroual, "DC Creeping Discharges over Insulating Surface in Different Gases and Mixtures", *IEEE Transaction Dielectric Electric Insulation*, Vol. 21, no. 5, 2014

[98] M. Koch, S. Tenbohlen, "Evolution of bubbles in oil-paper insulation influenced by material quality and ageing", *Published in IET Electric Power Application*, Vol. 5, Issue 1, pp.168-174, 2010

[99] Kyunghoon Jang, Takao Akahoshi, Masahiro Kozako and Masayuki Hikita, "Nano SiO2/Epoxy Coating Effect on Creepage Discharge Characteristics in Oil/Pressboard Composite Insulation System", *International Conference on Dielectric (ICD)*, pp.394-397, 2016

[100] Y. Yokoi and Y. Suzuki, "Empirical Formula and Polarity Effect of the Impulse Surface Discharge in Air", IEEJ, Vol.90, no.4

[101] Hitoshi Okubo, "High Electric Field Theory", Ohmasha, 2013

[102] Kyunghoon Jang, Takao Akahoshi, Masahiro Kozako and Masayuki Hikita, "Impulse Creepage Discharge Properties of Solid Coated Pressboard/Oil Composite Insulation with Rod-plane Electrode System", *Conference on Electrical Insulation & Dielectric Phenomena (CEIDP)*, pp.832-835, 2015

[103] T. Tanaka, "Analysis of electric Charge Accumulation in Polymeric Insulation by Quantum Chemical Calculation,", Annual Meeting of The Institute of Engineers of Japan, 2015

[104] Santanu Singha and M. Joy Thomas, "Dielectric Properties of Epoxy Nanocomposite", *IEEE Trnasactions on Dielectric Electrical Insulation*, Vol. 15, no. 1, 2008

[105] Toshikatsu Tanak, "Analysis of Nano-fillers as Quantum Dots", *The papers of Technical Meeting on Dielectric and electrical Insulation, IEEJ*, pp. 33-38, 2016

[106] T. Tanaka, "A Novel Concept for Electronic Transport in Nanoscale Spaces Formed by Islandic Multi-cored Nanoparticles", *IEEE International Conference on Dielectric* (ICD), vol. 1, pp.23-26, 2016

[107] T. Tanaka, "A Quantum Dot Model for Permittivity of Polymer Nanocomposites", IEEE Conference on electrical Insulation and Dielectric Phenomena (CEIDP), pp. 40-43, 2016

[108] Yong-Hong Cheng, Zeng Bin Wang and Kai Wu, "Pulsed Vacuum Surface Flashover Characteristics of TiO2/Epoxy Nano-Micro Composites", *IEEE Transaction on Plasma Science*, Vol. 40, no. 1, 2012

[109] Shengtao Lo, Guilai Yin, Suna Bai and Jianying Li, "A New Potential Barrier Model in Epoxy Resin Nanodielectrics", *IEEE Transactions on Dielectric and Electrical Insualtion*, Vol. 18, no. 5, 2011

[110] Shengtao Li, Guilai Yin, G. Ghen, Jianying Li, Suna Bai, "Short-term Breakdown and Long-term Failure in Nanodielectrics: A Review, *IEEE Transactions on Dielectric and Electrical Insulation*, Vol. 17, no. 5, 2010

[111] Hulya Kirkici, Mert Serkan and Kalyan Koppisetty, "Nano/Micro Dielectric Surface Flashover in Partial Vacuum", *IEEE Transactions on Dielectric and Electrical Insulation*, Vol. 14, no. 4, 2007

[112] Yujie Hy, Robert C. Smith, J. Keith Nelson and Kinda S. Schadler, "Some mechanistic understanding of the impulse strength of nanocomposite", *Annual Report Conference on Electrical Insulation and Dielectric Phenomena (CEIDP)*, pp.31-34, 2006

[113] Shengtao Li, Guilai Yin, "Surface Flashover in Vacuum and Bulk Breakdown in Polystyrene Nanocomposites", IEEE Trans. Dielectr. Insul., pp.486-490, 2011

[114] Y. Chen, Y. Cheng, "Vacuum flashover properties of epoxy composite coating filled with different micro/nanometer inorganic oxide particles under nanosecond pulse", Prog. Natural Sci., vol. 18, 2008

[115] Mihir Roy, J. Keith Nelson and R. K. MacCrone, "Candidate mechanisms controlling the electrical characteristics of silica/XLPE nano dielectrics", *Journal of Materials Science*, Vol. 42, Issue 11, pp. 3789-3799, 2007

[116] Francis O'Sullivan, J. George Hwang and Markus Zahn, "A Model for the Initiation and Propagation of Positive Streamers in Transformer Oil", *IEEE International Symposium on Electrical Insulation (ISEI)*, pp.210-214, 2008

[117] Olivier Ducasse, Liberis Papageorghiou, Olivier Eichwald, Nicols Spyrou and Mohammed Yousfi", Critical Analysis on Two-Dimensional Point to Plane Streamer Simulations using the Finite Element and Finite Volume Methods", *IEEE Transactions on Plasma Science*, Vol. 35, no. 5, 2007

[118] Jouya Jadidian, "Charge Transport and Breakdown Physics in Liquid/Solid Insulation System", *Doctor of Philosophy*, *Massachusetts Institute of Technology*, 2013

[119] Se-Hee Lee, Se-Yeon Lee, Young-Ki Chung and Il-Han Park, "Finite Element Analysis of Corona Discharge Onset in Air with Artificial Diffusion Scheme and under Fowler-Nordheim Electron Emission", *IEEE Transaction on Magnetics*, Vol. 43, no. 4, 2007

[120] Shuji Sato, Koji Kato, Tomoaki Ito and Sumiko Sakaguchi, "Double-Exponential Parameter Determination for the Lightning Impulse Voltage", IEEJ, Vol. 120-A, no. 11, 2000 (In Japaness)

[121] COMSOL AB., COMSOL Multiphysics Modeling Guide, 2008

[122] Y. V. Torshin, "On the Existence of Leader Discharges in Mineral Oil", *IEEE Transaction dielectric Electrical Insulation*, Vol. 2, no. 1, 1995

[123] Y. V. Torshin, "Prediction of Breakdown Voltage of Transformer Oil from Predischarge Phenomena", *IEEE Trnasaction Dielectric Electrical Insulation*, Vol. 10, no. 6, 2003

[124] Lei Zhou and Michael R. Zachariah, "Size resolved particle work function measurement of free nanoparticles: Aggregates vs. spheres", *Chemical Physics Letters*, Vol. 525-526, pp.77-81, 2012

[125] M. U. Anker, "Effect of Test Geometry, Permittivity Matching and Metal Particles on the Flashover Voltage of Oil/solid Interfaces", *IEEE Transaction Power App*. System, Vol. PER-3, Issue 12, pp.33-33, 1983

[126] S. Ingebrigtsen, H. S. Smalo and L. E. Lundgaard, "Effects of electron attaching and electron releasing additives on streamers in liquid cyclohexane", *IEEE Transaction Dielectric Electrical Insulation*, Vol. 16, Issue 6, pp.1524-1535, 2009

[127] Jin-Hyun Choi, Kyunghoon Jang, Takao Akahoshi and Se-Hee Lee, "Finite Element Analysis using Surface Charge on Liquid-Solid Interface in Insulating Liquid", Annual Conference, 2016 (in Korean)

[128] G. Massala and O. Lesaint, "Positive streamer propagation in large oil gaps: Electrical properties of streamers," *IEEE Tran. Diel. Elec. Insu.*, vol. 5, no. 3, pp. 371-381, 1998.